THE UNIVERSITY OF MANITOBA

FACULTY OF GRADUATE STUDIES

*****

COPYRIGHT PERMISSION PAGE

Optical and Microwave Remote Sensing of Wheat and Canola

BY

Klaus Hochheim

A Thesis/Practicum submitted to the Faculty of Graduate Studies of The University of Manitoba in partial fulfillment of the requirements of the degree of Doctor of Philosophy

Optical and Microwave Remote Sensing of Wheat and Canola

By

Klaus Hochheim

A Thesis

Submitted to the Faculty of Graduate Studies

in Partial Fulfillment of the Requirements

for the Degree of

Doctor of Philosophy

Department of Geography

University of Manitoba

Winnipeg, Manitoba

2003

Abstract

The primary focus of this research is the evaluation of RADARSAT-1 (5.3 GHz HH) data to: 1) understand the nature of seasonal backscatter from wheat and canola; and 2) determine the extent to which RADARSAT can discriminate variations in biomass at the field scale. This research is necessary because managers, scientists and agricultural producers locally require better information on production related parameters and regionally need to assess the impacts of climate variability on the grain and oil seed producing regions of the Great Plains.

In support of the first objective, detailed vertically stratified seasonal representations of wheat and canola representing low and high biomass canopies were generated. These data were used to develop an adaptive multi-layer (4 layer) volumetric moisture model parameterized for wheat and canola to gain an understanding of the nature of RADARSAT-1 backscatter. The model generates a measure referred to as the TMc (total effective volumetric moisture) that is correlated to RADARSAT-1 backscatter.

The model results for wheat were highly correlated to backscatter (r^2= 0.67- 0.97). The results suggest a relatively high extinction coefficient for high biomass wheat canopies. The seasonal backscatter over wheat is bimodal, with the green leafy portion of the canopy driving early season backscatter, and heads driving the end of season backscatter.

The early season model results for canola were less promising (r^2 = 0.46) suggesting the need to integrate a scattering model based on leaf geometry early in the growing season. Later in the season, when pods dominated the canopy, the volumetric model worked much better (r^2 = 0.94). The seasonal backscatter profile for canola was very distinct from wheat.

Early season backscatter was driven by the leafy portion of the canopy, maximum backscatter as associated with the reproductive period (pod development).

Results associated with objective 2 showed that RADARSAT-1 has a potential to map biomass variation for wheat at the booting and heading stage, and later in the year as the crop senesces. Backscatter is inversely related to biomass (as defined by the normalized difference vegetation index (NDVI)) at the booting to heading stage, and positively correlated at the hard dough stage. The NDVI data and ground confirmation data support the premise that many of the parameters determining the optical reflectance are also directly and indirectly related to factors driving microwave backscatter.

Acknowledgments

Thanks to Mr. D. Orchard and Mr. Don Hill for providing access to their fields, to Keith Mills of Westco for providing yield monitor data and extensive soil sample data, and to the Manitoba Remote Sensing Centre for providing additional RADARSAT-1 data in 1998 through the Manitoba RADARSAT-1 Announcement of Opportunity. A special thanks to Wendy Kulzer for her assistance in gathering and processing the ground confirmation data; I couldn't have done it without you. Thanks also to Dr. Ron Brown (CCRS) for financial support and to the RADARSAT-1 ADRO program for data and logistical support. NSERC and CEOS supported this research with grants to Dr. David G. Barber.

Table of Contents

List of Figures

List of Tables

Chapter 1: Introduction, Science Rationale and Objectives

1.1 Introduction

Remote sensing techniques exploit variations in reflectance, absorption and transmission of electromagnetic energy (EME) over Earth surface features to extract information about a resource. The focus of this research is to investigate the interaction of optical (0.4 -1.1 μm) and microwave (cm) EME over wheat and canola canopies for extracting crop assessment information.

Remote sensing within the agricultural context is being exploited in a number of ways. For example, organizations such as Statistics Canada (Korporal et al., 1989; Reichart and Caissy, 2002), the Canadian Wheat Board (CWB) (Bullock, 1992; Hochheim and Barber, 1998) and the United States Department of Agriculture (USDA) (Doraiswamy et al., 1994) use optical satellite data as a supplementary tool for assessing crop condition and yield potential. The information obtained is generally used to provide early season estimates of yield potential at regional and global scales and is key in developing market strategies.

Internationally, remote sensing data is used by organizations such as the United States Agency for International Development (USAID) and the United Nations Food and Agricultural Organization (UN/FAO) to operationally monitor biomass in Africa, the Near East and southwest Asia. ARTEMIS (Africa Real Time Environmental Monitoring Using Imaging Satellites) is an environmental monitoring program of the UN/FAO. The information generated by this program on growing conditions is utilized for the FAO

Global Information and Early Warning System (GIEWS) and Emergency Centre for Locust Operations (ECLO) (Griguolo and Mazzant, 1996).

On more local scales, remote sensing techniques are being assessed for use in precision crop management; a technology based farm management system that seeks to identify, analyze and manage variability within fields for optimum profitability and sustainability of the land resource. Remote sensing serves as a valuable tool to map broad soil classes, in-field variations of LAI (leaf area index) and biomass, percent cover, crop phenology, plant disease, weeds and yield potential (Moran et al., 1997, Brisco et al., 1998, McNairn et al., 2002, Miller et al., 2002).

The above applications almost exclusively rely on optical data. For regional scale applications the National Oceanic and Atmospheric Administration (NOAA), Advanced Very High Resolution Radiometer (AVHRR) and the Moderate Resolution Imaging Spectroradiometer (MODIS) data are extensively exploited; for the precision farming applications, higher resolution satellites such as SPOT, Landsat, IKONOS and IRS are used. The timely acquisition of cloud free optical data is often problematic in studying the dynamic phenomena of crop growth and development. With the launching of synthetic aperture radar (SAR) satellites in the 1990s, including the launch of RADARSAT-1 opportunities exist to obtain high resolution data at weekly intervals unencumbered by variations in atmospheric conditions, cloud contamination or day/night considerations. The current challenge is to determine the extent to which SAR data can be exploited for crop condition assessment at local and regional scales.

1.2 Science Rationale

The focus of this research is to investigate the use of optical data and temporal microwave data for crop condition assessment. Of particular interest is the evaluation of RADARSAT-1 (5.3 GHz, HH polarized) data for monitoring the growth and development of wheat and canola. This work is important since the understanding of the seasonal backscatter (σ^{o}(dB)) over these crops is poor and hence RADARSAT-1's potential to provide crop assessment information.

Wheat and canola were chosen as these crops account for 65% of the major grains grown in western Canada. Wheat accounts for 50% of production whereas canola accounts for 15%. The other grains (35%) include pulses, barley, oats, rye, and flax. The crops also provide an interesting contrast in terms of canopy architecture (i.e., the size and distribution of component parts within the canopy) therefore providing an opportunity to evaluate the capabilities and limitations of RADARSAT-1 data to effectively monitor crop condition as a function of crop type.

Crop condition, as expressed by crop growth and development is intimately linked to the aerial and root zone environment (soil fertility, soil moisture and air temperature etc.) which in turn affects green leaf area (LA) and green leaf duration (LD). Crop yield is a function of leaf area at the beginning of the reproductive stage and final yield is related to the duration of LAI (Wiegand et al., 1991). The successful use of optical or microwave remote data for crop condition assessment is therefore directly linked to the ability to monitor these two parameters temporally.

To effectively evaluate canopy reflectance and microwave backscatter, requires an understanding of the factors affecting leaf and canopy reflectance and microwave backscatter supported by detailed ground confirmation data coincident with each satellite pass. Parameters significant to optical data include measures of green biomass and LAI; for active microwave data, factors include the dielectric properties (volumetric moisture) of the component parts of a canopy their geometry (size and orientation), crop height, soil roughness and volumetric moisture, and row orientation and spacing.

1.3 Objectives

The overarching objective of this research is to investigate the interaction of electromagnetic energy in the optical (0.4-1.1 μm) and microwave (5.3 GHz HH pol.) portion of the electromagnetic spectrum (EMS) as related to the seasonal evolution of wheat and canola in order to assess crop condition and potential productivity.

Specific objectives include:

1) Obtaining a weekly vertically stratified physical characterization of the wheat and canola. This type of parameterization is generally lacking in the literature but is important as it relates to modeling of microwave backscatter.
2) Developing an adaptive multi-layer volumetric moisture model to assess the nature of RADARSAT-1 backscatter over wheat and canola.
3) Assessing the ability of RADARSAT-1 data to discriminate within field variability in wheat and canola fields. Ground confirmation data together with

optical data are used in a supporting role to aid in the interpretation of the microwave backscatter response.

1.4 Thesis Outline

The optical and microwave characterization of the seasonal evolution of a crop canopy is directly related to the physical characteristics of the canopy, which are a function of growth and development (phenological stage). The growth and development of a canopy are, in turn, a function of numerous environmental factors. Chapter 2 briefly reviews the growth stages of wheat and canola (Section 2.1.1) and is followed by a discussion of environmental factors affecting temporal growth and development of crops specifically temperature, moisture and N-fertilization, and their effect on biomass accumulation and partitioning (Section 2.1.2). These sections are of particular relevance vis-à-vis Chapter 5 and 6 where the nature of within field variation is examined. Subsequent sections review how interacts of optical (Section 2.2) and microwave (Section 2.3) portions of the electromagnetic spectrum with seasonally evolving canopies, including a brief review of factors external to crop condition that affect canopy reflectance and microwave backscatter.

Chapters 3 and 4 provide a detailed physical multi-layered characterization of wheat and canola in terms of the areal ($m^2 \cdot m^{-2}$) distribution of component parts within the canopy as well as the distribution of water ($gm \cdot cm^{-3}$) amongst the component parts of the canopy. Based on the detailed physical data an adaptive multi-layer volumetric moisture model is introduced which is used to examine the nature of microwave backscatter from RADARSAT-1 for wheat and canola respectively.

Chapters 5 and 6 examine RADARSAT-1 backscatter trends per day of year (DOY) over wheat and canola fields so as to determine the extent to which these data can be used to map within and between field variations. Optical data and ground confirmation data (soil texture, organic matter, yield monitor and biomass data) are used to aid the assessment of RADARSAT-1 capabilities.

Chapter 7 provides an overall summary of results and recommendations for further study.

Chapter 2: Background and Review of Pertinent Literature

2.1 Introduction

The optical reflectance and microwave backscatter are linked directly to the physical properties of a canopy. The significance of any one or combination of canopy parameters is a function of the electromagnetic frequency used to monitor the canopy.

Section 2.1.1 reviews the phenological development of wheat and canola. Section 2.1.2 reviews some of the dominant factors affecting crop growth and development with special attention to the impacts of each factor on biomass accumulation and partitioning. Section 2.2 briefly reviews the optical properties of leaves and canopies and their significance in crop condition assessment. Finally, Section 2.3 discusses the nature of microwave backscatter from crop canopies.

2.2 The Physical Evolution of Wheat and Canola Canopies.

In terms of remote sensing the amount and duration of green biomass are key attributes with respect to the EM interaction when assessing the potential productivity of an agricultural surface. The objectives of this section are: 1) to briefly review the growth and development stages of wheat and canola; and 2) to highlight the effect of temperature, moisture and fertilization on dry matter accumulation and partitioning.

2.2.1 Crop Development and Growth

2.2.1.1 Phenological Development of Wheat

A number of growth scales have been suggested over the years to describe the development of wheat from germination, to emergence through tillering, jointing, heading and maturity. Among the more popular scales for cereal grains are the Feekes, Zadoks and Haun scales (Large, 1954; Zadoks et al., 1974; Haun, 1973, Appendix A). The Zadoks scale has gained more prominence due to its increased detail relative to the other approaches. Figure 2.1 shows some of the key developmental stages of wheat.

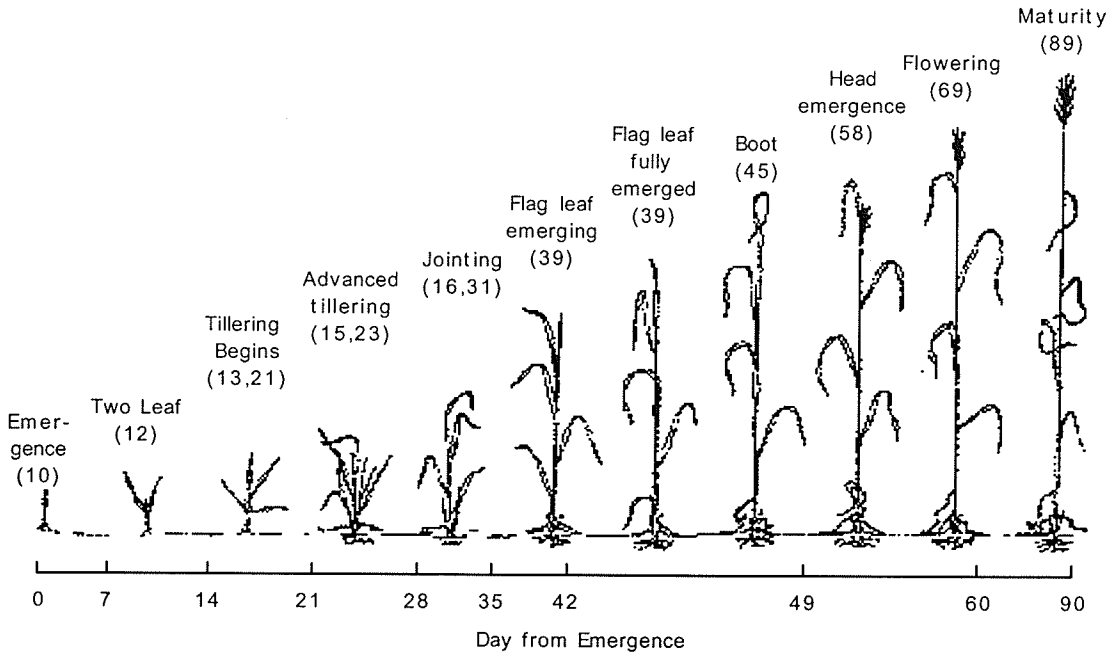

Figure 2.1 The developmental stages of wheat, Zadoks scale (Adapted from Hay and Walker, 1989).

Plant emergence typically occurs 7-14 days after seeding. The rate of emergence is largely a function of early season soil moisture and temperature (Anderson et al., 1985; Gauer et al., 1982). Wheat leaves are produced at a rate of about one every 4 to 5 days to a total of eight or nine leaves, with the last leaf being termed a flag leaf. Tillering occurs in close association with the appearance of leaves on the main stem. At tillering, plants can compensate for low plant populations or take advantage of good growing conditions. Under typical field conditions for spring wheat in Western Canada, a plant may produce three tillers in addition to the main shoot. Tillers which establish early, i.e., at 4-5th leaf stage, are likely to reach maturity. Tillers which form later are likely to abort without producing grain (Anderson et al., 1985). During tillering, the initiation of heads on the main shoot and tillers begins. At this stage the head is microscopic. The parts that will become the floral structures and kernels are already being formed. When head formation is complete, the stem begins elongating (jointing). Just prior to jointing total plant biomass is dominated by green leaves (Figure 2.2).

Stem elongation is usually initiated by the fourth internode. This is followed in sequence by the internodes above it. The last stem segment to elongate is the peduncle, which accounts for a large proportion of the total stem length. During the stem elongation phase head growth is rapid. This is a period where development phases of the main stem and remaining productive tillers are brought into closer synchronization prior to heading.

The booting stage is the period just prior to heading where the flag leaf sheath encloses the growing head. As the peduncle continues to elongate the head is pushed out of the flag leaf sheath; the plant is now "headed".

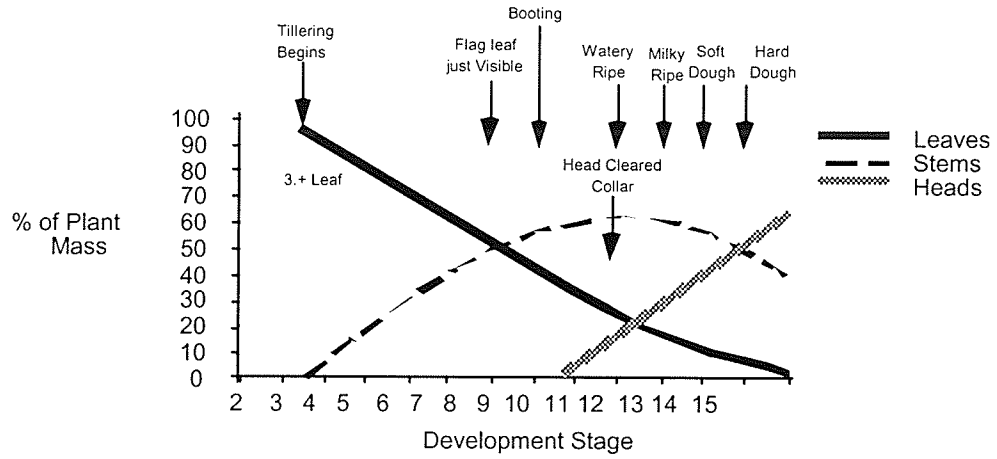

Figure 2.2 Distribution of wheat biomass in relation to plant development stage (After Bauer et al., 1987).

Within a few days after heading, flowering (pollination) begins. Flowering is usually noted by extrusion of the anthers from each floret. The flowering period for an individual head may last approximately 4 days. The canopy reaches its maximum green leaf area during the late boot to flowering stage (Nelson et al., 1995).

Following pollination the embryo and endosperm begin to form. Grain development occurs over a number of distinct phases: 1) watery ripe to the milk stage; 2) soft dough; and 3) hard dough. During the water ripe stage the kernel rapidly increases in size and the kernel's length and width are established but does not accumulate much biomass (Anderson et al., 1985). When the kernel is squeezed, a clear fluid emerges. During the watery ripe stage the lower leaves in the canopy start to senesce. At the milk dough stage, a milk-like fluid can be squeezed out of the kernel and the embryo is fully formed. Lower leaves continue to senesce rapidly as nutrients in the lower leaves are being redistributed to the upper canopy/heads. At the soft dough stage the kernel has a doughy consistency, and stage dry matter accumulation in the head is at a maximum (water concentration in the

kernel ~75 %). At the end of the hard dough stage the kernel has achieved physiological maturity (water concentration 30-40 %). The glumes and the peduncle are no longer green and little green colour remains on the plant. At the kernel hard stage the wheat plant is completely yellow and water concentration in the kernel is ~ 20-25% (Nelson et al., 1995).

2.2.1.2 Phenological Development of Canola

Canola is an oilseed grown throughout much of western Canada, largely confined to the sub-humid climatic region of the prairies. This crop matures at a similar rate to wheat. Development stages of canola are presented in Figure 2.3 and Table A-2 (Appendix A).

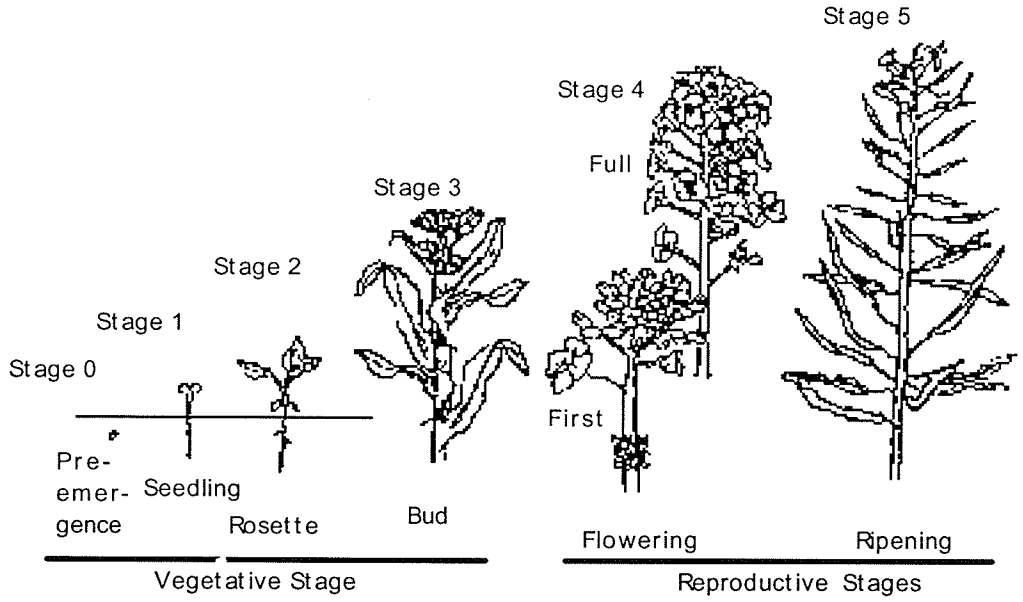

Figure 2.3 The development of canola (Thomas, 1984).

Upon emergence (4-10 days after seeding) the seedling consists of a 1.5 - 2.5 cm stem and two small cotyledons (seed leaves). Four to eight days after emergence the first true leaves develop. A rosette pattern is established whereby the lower older leaves tend to be

the largest; the smaller younger developing leaves developing in the centre. At the rosette stage stem length has not increased whereas stem thickness has. The budding stage coincides with bolting or stem elongation. The initial buds form at the centre of the rosette and rises as the stem bolts. As the stem bolts the remaining leaves unfold. Secondary branches develop from the axils of some of the upper and lower leaves. Each of these secondary stems develops leaves and flower bud clusters. During the budding stage and just before flowering, the main stem reaches 30-60% of its maximum length and total dry matter (Thomas, 1984), Figure 2.4b.

Maximum leaf area is reached at flowering (Figure 2.4a). At this stage, leaf area duration, especially beyond the onset of flowering, significantly impacts pod set and early seed growth. Flowering begins on the main stem with 3-5 flowers opening per day. Duration of flowering is 14-21 days. Only about 40-50 percent of the flowers produced develop reproductive pods which are retained to harvest (Thomas, 1984). By mid-flower, lower pods have started to elongate, leaf area has been significantly reduced, and stems have become the dominant food supply for plant growth. Towards the end of the flowering period canola seed accounts for approximately 15-35 % of total dry matter. About 35 to 45 days after flower opening, seed filling is complete. At this stage seeds in the lower pods have turned green, most of the leaves have senesced, and pod walls have become the major food producers although the stem is still an important source.

Seed filling is followed by senescence at time when stems and pods yellow and dry down. Seed moisture is lost at ~ 2-3 % per day depending on growing conditions.

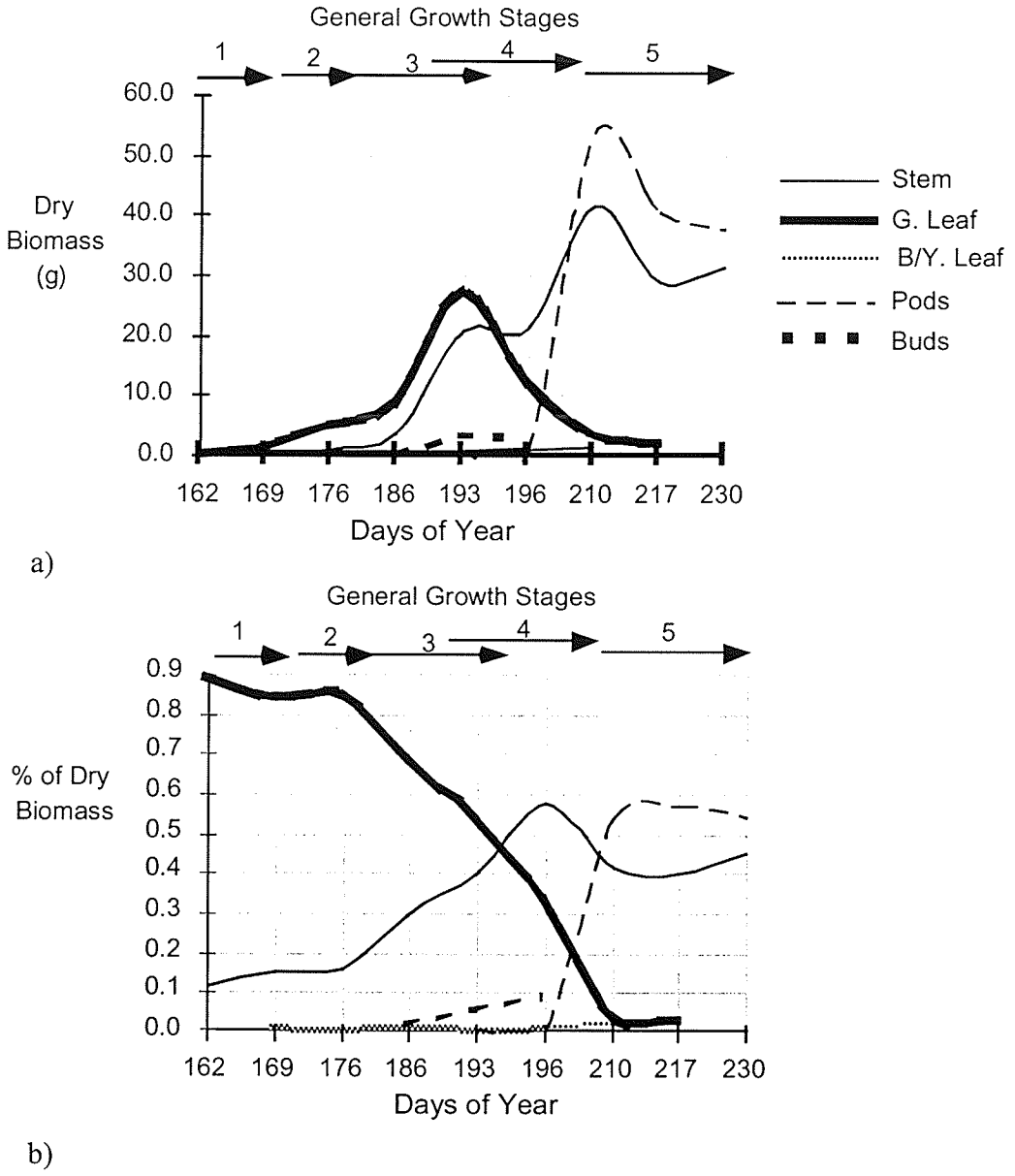

Figure 2.4 a) Seasonal distribution of dry biomass (g) for canola (B. Napus), and b) percent distribution of dry biomass for canola (B. Napus), Miami MB, 1997.

2.2.2 Factors Affecting Crop Growth and Development

There are a multitude of factors affecting crop growth and development. The intention here is to provide a brief overview of three key factors, namely temperature, moisture and N- fertilization, and indicate how they affect the rate of leaf production, the rate of leaf expansion and duration of leaf expansion with its consequent effect on yield.

The growth of any crop is a process whereby solar energy is converted into chemical energy to produce biomass. This involves three processes which occur in sequence:

1) the interception of incident energy by the leaf canopy;
2) the conversion of the intercepted energy to chemical potential energy (expressed as plant dry matter); and
3) the partitioning of the dry matter produced between harvested parts and the remaining plant (Hay and Walker, 1989).

2.2.2.1 Temperature

Provided the plants are not limited by water or nutrient stress, temperature is the sole control over the rate of leaf production and leaf area expansion (Hay and Walker, 1989). Plant functions such as evapotranspiration, photosynthesis, water and nutrient absorption and transportation, and various biological and chemical processes are regulated by temperature. Generally chemical reactions double with each 10°C increase (Thomas, 1984). For wheat and canola the base temperature (below which little significant growth occurs) is 5°C (Bauer et al., 1984; Morrison et al., 1989).

The phenological development of crops is typically modeled using growing degree days (GDDs). The average heat accumulated during a day is computed by adding the maximum and minimum daily temperatures and dividing the total by two. The base temperature is subtracted from this total to obtain the number of GDDs for a given day. Depending on the crop type and variety, the accumulated GDDs required to reach maturity varies. On average, spring wheat and argentine canola (*B. napus*) require 1040 GDDs, polish canola (*B. rapa*) requires 850 GDD's (Thomas, 1984).

2.2.2.1.1 Wheat

Campbell and Davidson (1989) subjected wheat plants to several temperature treatments under non-limiting conditions. Plants subjected to the higher temperatures (27°C daytime versus 12°C night time (T27/12)) matured 12% faster than the T22/12 treatment, reducing the effective grain filling period by 5 days, with a consequent loss in head weight of 25% (Figure 2.5). At the lower temperature treatment resulted in taller plants, greater green leaf area and higher total photosynthetic area (TPA) allowing photosynthesis to extend to the milk dough stage (Figure 2.5) thus increasing yield. High temperature tends to increase tillering early in the growing season, but is not a factor in tiller viability at maturity.

2.2.2.1.2 Canola

Many of the relationships between temperature and growth shown for wheat apply directly to canola. Seedlings generally prefer mild temperatures up to flowering as

excessive heat or cold tends to reduce photosynthesis and, therefore, leaf expansion and dry matter production. Both low and high temperatures can affect canola during the flower stage: low temperatures tend to delay the onset of flowering, high temperatures at flowering tend to reduce the time from flowering to maturity, thereby reducing potential dry matter accumulation. High temperatures during flowering also reduce the time the flower is receptive to pollen, the duration of pollen release and its viability. This results in a decrease in pods, seeds per pod and hence yield. Very hot weather combined with drought during the flowering period can lead to dramatic yield losses should conditions persist (Thomas, 1984).

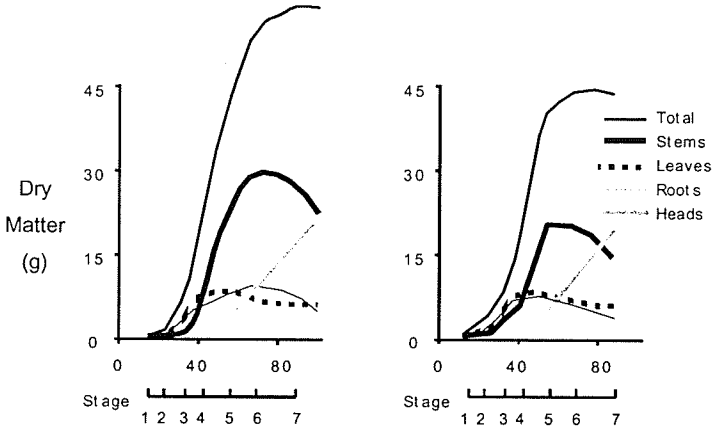

Figure 2.5 The effect of temperature on dry matter partitioning for spring wheat, a) T22/12 (Day/night temperature, °C); b) T27/12 (Crop stages: 1 - three leaf; 2- four tiller; 3-one node visible; 4- last leaf visible (LLV); 5- Anthesis; 6- milk dough; 7- maturity), (Adapted from Campbell and Davidson, 1979).

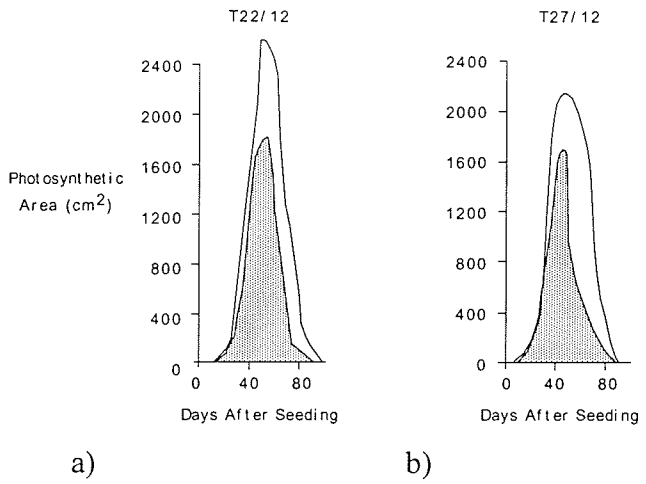

Figure 2.6 The effect of temperature treatments on total photosynthetic area of spring wheat: a) T22/12 (Day/night temperature, ^{o}C); b) T27/12. (Adapted from Campbell and Davidson, 1979).

2.2.2.2 Moisture

Water is an essential factor in plant growth and the dominant factor in the development of canopy leaf area (Hay and Walker, 1989; Raddatz et al., 1994). Too much or too little moisture results in a progressive decline in the rates of cell and leaf expansion resulting in lower leaf area and green leaf duration (Hay and Walker, 1989) thus limiting total dry matter accumulation and yield potential. The rate and duration of rainfall, its timing within the growing season, and the ability of soil to absorb, store, and make available water are all factors that potentially limit crop growth and yield potential. Soil parameters which influence the amount of water a given soil can supply growing plants, include soil texture, structure and organic matter (OM) content (Bradley, 1974).

2.2.2.2.1 Wheat

The impact of moisture stress on photosynthetic area depends on the timing and duration of a stress event. When applied to the period of tillering to LLV (last leaf visible), the period of maximum vegetative growth, the most pronounced effects of moisture stress are decreases in photosynthetically active leaf area, stem growth and root accumulation (Figure 2.7). When stress is applied later (LLV - AN (anthesis)) the effect on leaf growth is less, as most of the growth has already occurred. Stress during this latter period tends to reduce stem and head elongation. Yield was most severely impacted when moisture stress was applied during the grain filling period. Stress when applied during the earlier vegetative period had significant impact as well but was less detrimental (Campbell, et al., 1981; Asrar et al., 1985).

Generally, stress applied to young tissue provides the greatest check on plant growth, but when removed young tissue tends to recover. Older tissue will not recover after stress is removed and the plant will senesce rapidly.

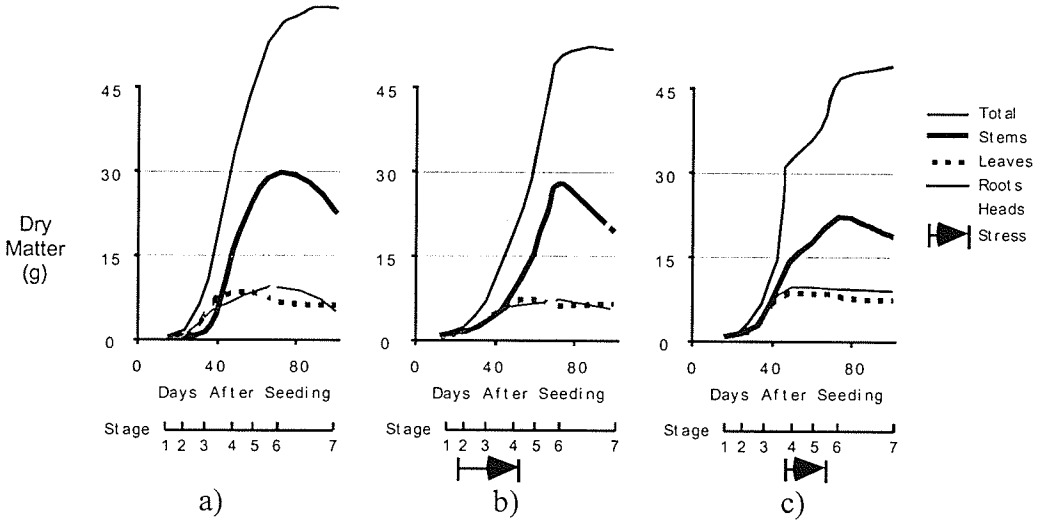

Figure 2.7 The effect of moisture stress on dry matter accumulation of spring wheat, a) non-stressed, b) stress applied from tillering to LLV, c) stress applied from LLV to AN (Crop stages: 1 - three leaf; 2 - four tiller; 3 - one node visible; 4 - last leaf visible (LLV); 5 - Anthesis; 6 - milk dough; 7 - maturity). (Adapted from Campbell and Davidson, 1979).

2.2.2.2.2 Canola

Adequate moisture tends to increase leaf area and duration of green leaf area, lengthens the flowering period, increases the number of branches per plant, the number of flowers that form pods, the number of seeds per pod, seed weight and seed yield. Early stress affects leaf area and growth. Recovery from early stress events is possible with timely precipitation but not without some impact on final yield. Moisture stress during flowering

to ripening results in significant yield decreases. Average effects of moisture stress on yield components are summarized in Table 2.1.

Table 2.1The effect of moisture availability on plant productivity (Thomas, 1984).

Water Use	(mm)	# branches per plant	# of pods per plant	# Seeds per pod	1000 Seed Wt (g)	Yield (kg/ha)
Rain fed	210	3.5	48	15.2	3.09	922
Low Irr.	282	3.9	54	18.8	3.22	1537
High Irr.	369	4	61	20.3	3.48	2463

2.2.2.3 Nitrogen Fertilization

Growth and development of crops such as wheat and canola can be adversely affected by deficiencies or excesses of any one of a number of key nutrients. Given optimum levels of phosphorous (P), potassium (K), and other macro- and micro-nutrients, nitrogen (N) is by far the most important nutrient controlling canopy development (Hay and Walker, 1989). Nitrogen is an essential constituent of cell walls, cytoplasmic proteins, nucleic acids and chlorophyll in addition to many other components. It therefore plays an important role in the rate of leaf expansion, final leaf size and longevity, and tiller or branch formation and survival (Hay and Walker, 1989).

2.2.2.3.1 Wheat

Dry weight accumulation is proportional to applied N. High N tends to increase photosynthetic leaf area (LA) and total photosynthetic area (Figure 2.8). Increased LA and duration of green leaf area increased crop yield even in the presence of moisture stress

(Figure 2.9). At low N (58kg/ha) the effect of moisture stress on spring wheat yield was low, highlighting the effect of N as a limiting factor.

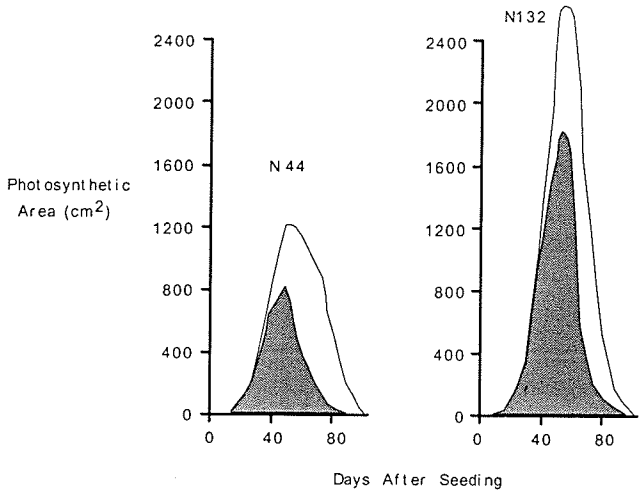

Figure 2.8 Photosynthetic area of spring wheat as a function of N (Adapted from Campbell and Davidson, 1979).

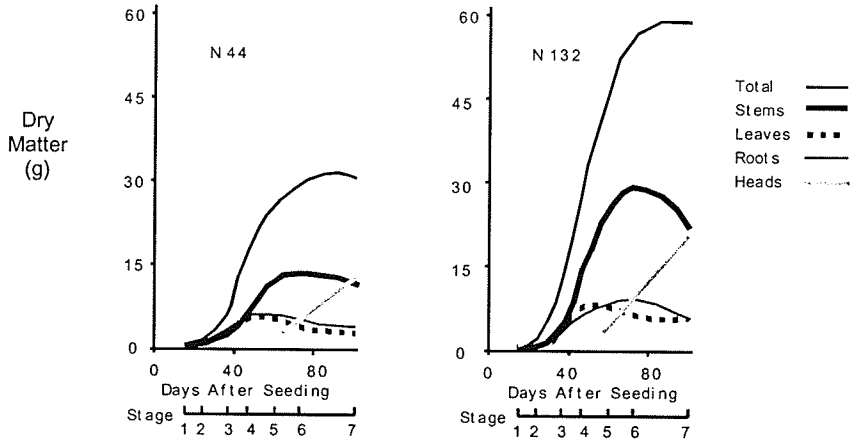

Figure 2.9 The effect of N and moisture stress on yield of spring wheat (after Campbell et al., 1981).

2.2.2.3.2 Canola

The effect of nitrogen fertilization on canola in the absence of stress is increased growth, as expressed by increased stem length, number of flowering branches, total plant biomass, the magnitude and duration of leaf area, and the number of and weight of pods and seeds (Figure 2.10). (Thomas, 1984; Allen and Morgen, 1972).

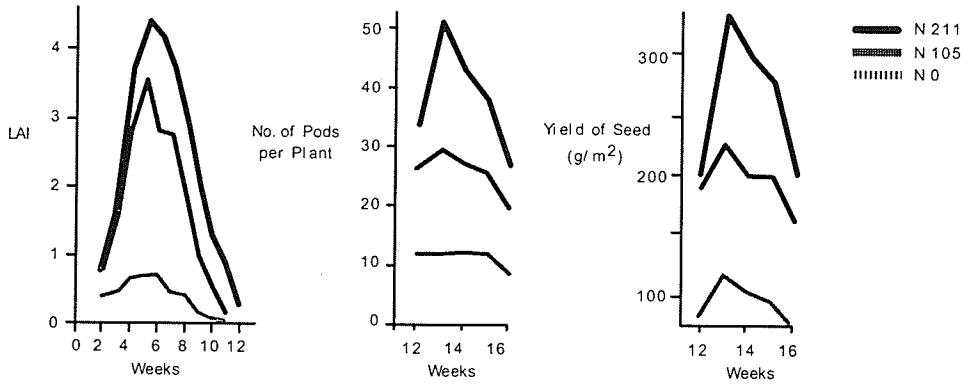

Figure 2.10 The effect of N-fertilization treatments (kg/ha)?on, a) Leaf area index (LAI), b) Number of pods per plant, and c) Yield of seed (g/m^2) for spring seeded canola. (Adapted from Allen and Morgen, 1972).

2.2.3 Summary

Based on the review thus far the following summary is provided regarding the growth and development of wheat and canola.

- The growth and development of wheat and canola are a function of numerous factors of which some of the more significant are temperature, soil moisture and N-fertilization.
- Temperature is the main determinant of crop development rate. Higher temperature tends to accelerate phenological development with a net effect of reducing the amount and duration of green leaf area thus reducing yield potential. High temperature during the reproductive period can significantly reduce yield despite relatively high early season biomass.
- Excessive or inadequate soil moisture causes a progressive decline in the rates of cell and leaf expansion resulting in lower leaf area and green leaf duration and dry matter accumulation. Stress applied early in the growing season provides the greatest check on plant growth (although when removed early enough a plant may recover). Moisture stress applied late will affect mainly the salable portion of the biomass.
- The level of N-fertilization has profound impacts on all components of the vegetative canopy. It plays an important role in the rate of leaf expansion, final leaf size and longevity, branch formation and survival, and productivity.
- Whatever the source of stress within the growth cycle, the potential productivity of a canopy is expressed in the magnitude and duration of its green leaf area and biomass

and thus its ability to absorb photosynthetic radiation and convert it into salable biomass.

- The key, therefore, in the use of remote sensing is to be able to detect and quantify variations in biomass and LAI and green leaf duration, as they are indicators of potential yield.

2.3 The Optical Characterization of Crop Canopies

This section provides an outline of the factors affecting leaf and canopy reflectance in the optical portion (0.4 - 2.6 μm) of the electromagnetic spectrum (EMS). Factors affecting canopy reflectance external to crop condition are briefly reviewed, followed by a discussion of how variation in seasonal reflectance is indicative of crop condition and yield potential.

2.3.1 Optical Properties of Leaves

The optical portion of the EMS as defined here extends from 0.4 -2.6 μm. This portion of the spectrum has been used extensively to monitor vegetation. Green vegetation has a distinct spectrum, that is low reflectance in the visible portion of the spectrum and very high reflectance in the near infrared (NIR). The background soil reflectance exhibits a steady increase through the visible and NIR portions of the spectrum (Figure 2.11).

Electromagnetic energy entering the leaf is diffused and scattered. The degree to which light is scattered upward (reflected) and downward (transmitted) is a function of chlorophyll density, number of cell layers, size of cells, orientation of cell walls, heterogeneity of cell contents, and leaf water content (Guyot, 1990; Grant, 1987).

Within the visible (0.4-0.7 μm) portion of the EMS the 0.62-0.70 μm (red) range provides the greatest spectral contrast to soil background reflectance. Green leaves within this portion of the EMS typically reflect less than 15 % of the incident EM radiation because of strong absorption by pigments. The radiation is absorbed by chlorophyll a and b

(representing 60-75% of plant pigments), carotenoids (representing 25-35% of plant pigments), with the remainder being accounted for by anthocyanins and other minor pigments (Tucker and Sellers, 1986).

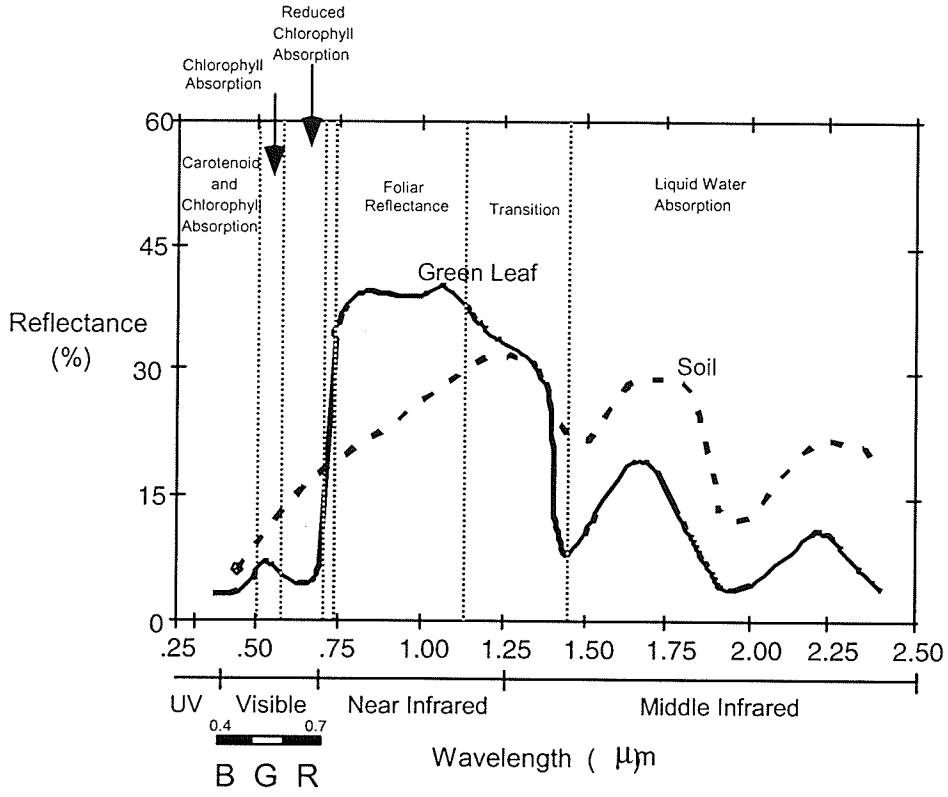

Figure 2.11 Spectral reflectance curves for green vegetation and soil (after Tucker and Sellers, 1986)

Within the near-infrared portion of the EMS (0.74-1.13 μm), the region of highest contrast to background reflectance is from 0.79-0.9 μm. Absorption of incident radiation by green vegetation at these wavelengths is minimal, while leaf reflectance and transmittance are high (85-90%). Since chlorophyll is transparent to infrared radiation, the degree to which light is scattered is then a function of the number of cell layers, the size of cells, and

their orientation. Approximately 50% of the radiation entering a leaf is reflected back through the surface of the leaf with the remainder being transmitted.

In the middle infrared portion of the EMS (1.3-2.5 μm), scattering and absorption of radiation is mainly a function of internal leaf structure and leaf water content. In the visible and near infrared (NIR), electromagnetic energy is transparent to liquid water in leaf tissues, while in the middle infrared (MIR) water is a strong absorber (Tucker and Sellers, 1986; Guyot, 1990). Within this spectral domain two wavelength ranges (1.55-1.75 μm and 2.1-2.3 μm) are used to monitor vegetation. Atmospheric water absorption bands centred at 1.45, 1.95 and 2.50 μm are typically avoided.

In general, the spectra for all mature green leaves are similar over the 0.5-2.5 μm range regardless of plant species (Sinclair et al., 1971; Gausman, 1973; Gausman and Allen, 1973) since the physical basis of the internal scattering mechanism of light within green vegetation is identical (Knipling, 1970).

The greatest changes in leaf reflectance are attributed to maturation and senescence. From early stages of growth until maturity, when leaves are rich in chlorophyll, leaf reflectance in the red portion of the spectrum remains consistently low in the visible portion of the EMS (Sinclair et al., 1971). In the NIR reflectance increases with maturation as a result of the increased number of cell wall-air interfaces that provides opportunity for increased multiple scattering of radiation. Leaf reflectance in a maturing plant is typically low in the MIR due to water absorption.

With the onset of senescence, the visible portion of the EMS shows the greatest relative change in reflectance, especially in the 0.65-0.67 μm range. During senescence chlorophyll content is reduced dramatically producing relatively large increases in the yellow-green and

red reflectance (Sinclair et al., 1971). Changes in the NIR result when leaves start to dry out and their internal structure changes. In the initial stages of senescence NIR reflectance actually increases despite dehydration and reduction of air spaces in the mesophyll. Initial increases in the NIR occur as cell walls are pulled apart and reoriented resulting in more cell wall/air interfaces (Sinclair et al., 1971). With advanced senescence, the NIR response eventually decreases as cells collapse and air spaces are reduced (Grant, 1987). The decrease in the NIR reflectance is not as dramatic as the increases in reflectance in the visible region. In the MIR, reflectance increases significantly due to reduced leaf water content in senescent leaves.

2.3.2 Soil Reflectance

A discussion of soil reflectance is warranted as it can have a very significant effect on plant canopy reflectance. The reflectance curve of soil shown in Figure 2.11 has considerably less variation over 0.4-2.6 μm than the vegetation curve. In general, soil reflectance increases progressively from the visible to middle infrared portion of the EMS. Water absorption bands appear in the MIR as they do for the vegetation curve.

Factors affecting soil reflectance include soil moisture, soil texture, surface roughness and organic content. Each of these factors is highly interrelated.

The soil spectra are significantly affected by soil moisture. As moisture increases, reflectance tends to decrease. Soils with high organic content are typically darker than mineral soils and have a higher water holding capacity. The extent to which organic matter is decayed also impacts reflectance; less decomposed material tends to have a higher

reflectance in the NIR due to enhanced reflectance attributable to the remnant cell structures of well-preserved fibres.

Soil reflectance due to texture is largely governed by soil particle size. Sand generally has the highest reflectance across the visible to MIR spectrum followed by silt then clay. Sand is typically well drained and has a low organic content. Finer textured soils are less well drained and have lower reflectance. In the absence of water, the reverse is true, i.e., fine-textured soils appear lighter than coarse-textured soils. Finer-textured soils form a smoother surface as there are fewer voids in which to trap incident radiation (Myers et al., 1983). Increasing surface roughness and irregularities through tillage tends to affect the distribution of illuminated and shadowed surfaces as seen by an optical device, hence increased soil roughness generally decreases reflectance.

2.3.3 Crop Canopy Reflectance

Canopy reflectance is primarily a function of the amount of vegetation present, as expressed by leaf area, biomass and percent cover (Ahlrichs and Bauer, 1983; Wiegand et al., 1979; Holben and Tucker, 1980; Asrar et al., 1985; Hinzman et al., 1986, and others). The effect of LAI, green biomass and percent cover on canopy reflectance (0.4-2.6 μm) for spring wheat is illustrated in Figure 2.12.

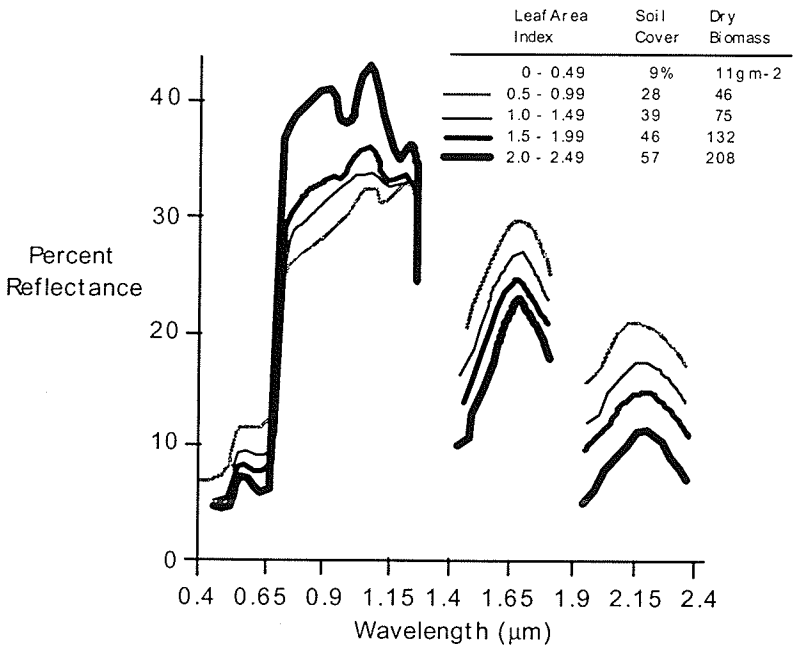

Figure 2.12 Canopy spectra as a function of LAI and green biomass for spring wheat, from seedling to anthesis (after Ahlrichs and Bauer, 1983)

As vegetation cover and LAI increase, reflectance in the visible domain decreases due to the progressive dominance of chlorophyll absorption over soil reflectance. Under ideal conditions the first layer of leaves absorb up to 90% of the incident radiation (Wiegand et al., 1979). This limits interaction of incident radiation (0.63-0.69 μm) to the upper portions of the canopy causing red reflectance to be a poor discriminator of LAI as red reflectance reaches its asymptotic limit at a LAI of 2.

The NIR reflectance (0.74-0.9 μm) changes proportionally more than in the visual domain due to an "enhancement effect." In the NIR, absorption of incident radiation is negligible (~10%) because close to 50% of incident radiation is transmitted through the canopy. Much of the transmitted light is reflected back to the upper portions of the canopy, thus enhancing upper canopy reflectance (Knipling, 1970). NIR reflectance measured at

the top of the canopy reaches an asymptotic limit at an LAI of 8 (Wiegand et al., 1979). The enhancement effect makes NIR reflectance an important spectral variable in discriminating crop canopy vigor and a dominant variable in red and NIR vegetation indices.

The MIR reflectances (1.3-2.5 μm) are generally thought to be a function of leaf water content; the higher the water content the lower the reflectance. From Kleman's and Fagerlund's study, this assumption was found valid for wavelengths near 1.4 μm and beyond the 1.8μm wavelengths (Kleman and Fagerlund, 1987). For the 1.65 μm region the relationship appeared to be more complex, as water absorption did not appear to be the most significant factor affecting reflectance since the plots with the highest water content had the highest reflectance. It appears that at the 1.65 μm wavelength the phenological stage and the structure of the canopy were as important as leaf water content.

2.3.4 Vegetation Indices

The fact that red radiance exhibits a non-linear inverse relationship between spectral radiance and green biomass, while the NIR component exhibits a non-linear direct relationship has been exploited to compute vegetation indices, that is, a single numerical vegetation-dominated index (VI). These are generally linear and ratio combinations of wavelengths spanning the 0.4-2.6 μm range. The most popular of these is the simple ratio (NIR/RED) first used by Jordon (1969), and subsequently by Pearson and Miller (1972) and Colwell (1974) and the normalized difference vegetation index (NDVI) first developed by Rouse et al., (1973, 1974).

$$NDVI = \frac{(NIR - RED)}{(NIR + RED)} \qquad [2.1]$$

These indices are designed to highlight variations in biomass while suppressing the effects of soil background. A high VI value is indicative of high (green) biomass, low values are indicative of low biomass. The simple ratio of NIR/Red (SR) tends to be more sensitive to variations in biomass where vegetation cover is greater than 50%. The NDVI index tends to be more sensitive to biomass variations in sparse canopies from 15 to 80% cover beyond which sensitivity is dramatically reduced.

Other indices have been developed specifically to minimize the effects of soil background reflectance, such as the perpendicular vegetation index (PVI) of Richardson and Wiegand (1977). This index utilizes the tendency for bare soil to fall in a straight line on a two dimensional plot (IR vs. Red), where the soil line is defined by:

$$NIR = a(RED) + b \qquad [2.2]$$

Where

a = slope

b = intercept

$$PVI = ((NIR - aRED - b) / (1+a^2)^{1/2} \qquad [2.3]$$

For the PVI any deviation of values from the soil plot is a function of vegetation density. PVI values typically range from 0 for bare soil to 35 for dense canopies. Although this index tends to minimize soil background reflectance it is also less sensitive to variations in biomass (Jackson et al., 1983).

The simple ratio and NDVI have also been modified to account for variation in soil background reflectance:

SAVI2 (Soil Adjusted VI) =

$$(NIR) / (RED+b/a) \quad [2.4]$$

TSAVI (Transformed Adjusted VI) =

$$a (NIR-aRED-b) / RED+aNIR - ab) \quad [2.5]$$

Although these indicies are promising, they do not necessarily outperform the original SR and NDVI transformations (Wiegand et al., 1993).

2.3.5 Factors External to Vegetation Affecting VIs

Vegetation reflectance, whether expressed by individual wavelengths or by VIs, is not only representative of biomass but is affected by factors external to the biomass. Among the most significant factors affecting the representation of a canopy within the optical region are soil background reflectance, atmospheric attenuation, and viewing and illumination geometry.

2.3.5.1 Soil background

Soil background reflectance can significantly affect the estimation of LAI and biomass using VIs (Heute et al., 1985; Heute 1988; Malthus et al., 1993).

As vegetation cover increases reflectance decreases due to absorption of radiant energy by chlorophyll in the red portion of the spectrum (0.63-0.69 μm). The decrease is most dramatic for the lighter soils. Darker soils on the other hand remain relatively invariant to

changes in vegetation cover. At 90% cover, canopy reflectance is independent of soil background (Figure 2.13).

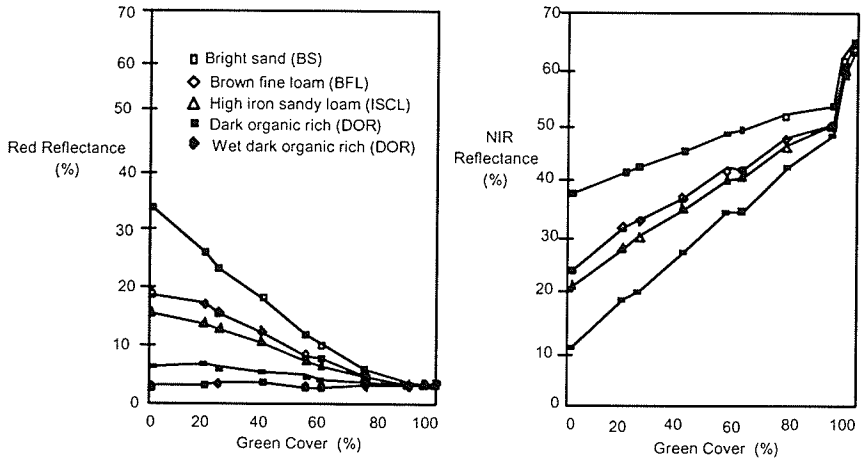

Figure 2.13 Reflectance as a function of percent cover and soil type for, a) RED reflectance and b) NIR reflectance (after Huete et al., 1985).

In the NIR (0.76-0.90 μm), reflectance increases linearly for all soil backgrounds as vegetation cover increases. Brighter soils consistently maintain higher reflectance in the NIR. Near 90% cover, reflectance for light and dark soils are similar. Recall that in the NIR portion of the EMS, transmission of radiant energy through the canopy is high, allowing it to interact with the soil even at a high percent cover thus enhancing canopy reflectance.

When VIs are computed the resultant effect is that darker soil tends to increase VIs. For example, a dark organic rich loam at 20% cover had the same SR index value as a 40% covered brown fine loam or a 55% green cover over a bright dry sandy soil (Huete et al., 1985). The PVI index tends to minimize the affects (Figure 2.14).

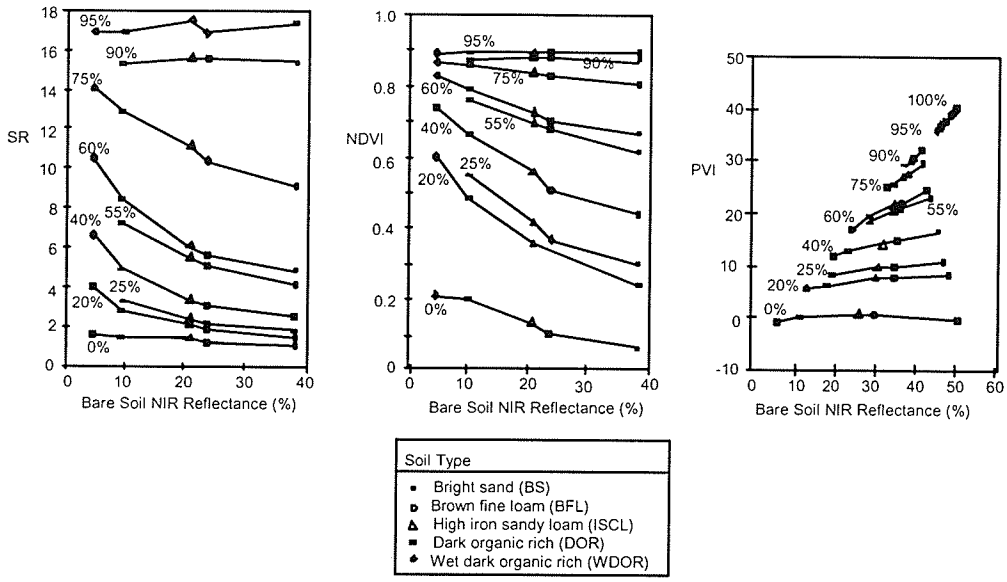

Figure 2.14 Vegetation indices affected by soil background reflectance as a function of percent cover (After Huete et al., 1985).

Vegetation indices such as SR, NDVI and PVI should help minimize the potential effects of soil background, but as evident in Figures 2.14 a-c, variations in canopy reflectance attributable to soil background are significant. For the SR vegetation cover between 20 and 75% shows increasing dependency on soil background with increasing vegetation cover. The NDVI index shows a greater sensitivity to variations $\leq$ 50% vegetation cover whereas at 75% cover NDVI is less affected by soil background. The PVI index is somewhat different despite the use of NIR and red channels. Bright soils increase vegetation index values and dark soils decrease values for the same percent cover. The PVI index suppresses variation due to soil background more so than the SR and ND index.

2.3.5.2 Directional Reflectance

Another factor that can potentially complicate the interpretation of EM scattering are the bi-directional reflectance properties of vegetation canopies. Variations in directional reflectance are related to illumination and view angles, or more precisely solar zenith angles, sensor azimuth angles and off-nadir view angles of optical sensors.

Most of the incident radiation intercepted by the canopy is scattered within the top layer; this is especially true in low sun angle situations. The proportion of canopy components viewed at any given layer or depth decreases as off-nadir view angles increase. Thus, for all homogenous, complete canopies and for all sun angles, the directional reflectance increases as the off-nadir view angle increases for any azimuth view direction. Kimes (1983) labelled this phenomena "Effect 1."

The higher reflectance in the backscatter direction is due to the sensor observing illuminated surfaces. In the forward scattering direction reflectance decreases due to an increase in shadowed surfaces (assuming vertical structure within the canopy). (Note: In the forward scattering direction the sensor looks towards the sun, in the backscatter direction the sensor observes the illuminated surface).

For sparse canopies, reflectance in the red portion of the spectrum decreases relative to the bare soil reflectance due to chlorophyll absorption. Nevertheless, directional reflectance is still strongly influenced by soil background. At very low sun angles when the soil may be completely covered by shadow, soils tend to have much less effect. At low sun angles a sparse canopy resembles the reflectance of a 100% vegetative surface. NIR

reflectance tends to mimic the soil reflectance as well. Slight increases in reflectance in the forward scattering direction are largely a function of "Effect 1."

For the full canopy chlorophyll absorption is strong, therefore the soil background has little effect. Reflectance off nadir increases in the backscattering and forward scattering direction due to Effect 1. NIR reflectance is azimuthally more symmetric due to increased transmission and scattering within the canopy. Reflectance increases strongly off nadir with backscatter reflectance slightly higher than in the forward direction. When NDVI are computed, variations due to illumination and viewing angle are more or less normalized with a slight bias in the forward scattering direction. To minimize the problem of bi-directional reflectance, near nadir angles should be used and bi-directional reflectance functions applied specific to the regional cover types (Chilar et al., 1992).

2.3.5.3 Atmospheric Attenuation

When using high altitude optical remote sensing platforms atmospheric scattering and absorption of reflected radiation from a crop canopy has to be considered. There are three major atmospheric influences that affect the interpretation of optical remotely sensed data, namely: 1) atmosphere-scattered wavelength dependent "path radiance" (or Rayleigh scattering) which represents an added component scattered onto the sensor detectors that is independent of surface reflectance; 2) optical thickness (or extinction) properties of the atmosphere which determines the amount a signal from the surface will be attenuated (scattered or absorbed); and 3) the influence of atmospheric scattering on the interpretation of neighbouring pixels that have high contrast, referred to the "adjacency effect" (Huete and Jackson, 1988).

Four atmospheric models simulating various atmospheric conditions were used to compute their effect on radiance as measured by AVHRR sensor (Holben et al., 1986). Model 1 assumes Rayleigh scattering in which only molecular scattering is taken into account thus representing added flux (no absorbing gases or aerosols). Model 2 incorporates gaseous absorption with Model 1 (i.e. O_2, O_3, CO_2 and H_2O). Models 3 and 4 (variations of Model 2) simulate the effect of increasing aerosol concentrations (optical thickness = 0.1 and 0.5) respectively (Holben and Fraser, 1984). The effects of these models were evaluated for their effect on vegetation canopies.

In the red portion of the spectrum red reflectance is typically low with reflectance increasing in the backscatter direction, when it is assumed there is no atmosphere. Vegetation reflectance increased for all of the above models. The largest increases in red reflectance were exhibited by Model 4, followed min order of Model 1(Rayleigh scattering), Model 3, and Model 2.

In the NIR, where vegetation canopies are typically highly reflective, Model 1 increased reflectance slightly, while models 2, 3, and 4 progressively decreased NIR reflectance. In the NIR water vapor absorption increases thus lowering path radiance contribution (Heute and Jackson, 1988).

When red and NIR reflectance are normalized using NDVI, index values are stratified such that surface reflectance (no atmosphere) consistently has the highest NDVI values. As atmospheric aerosol content increases (Models 1-4), NDVI decreases (Figure 2.15). This stratification is exploited in the generation of maximum value NDVI composite images used for regional and global monitoring of biomass.

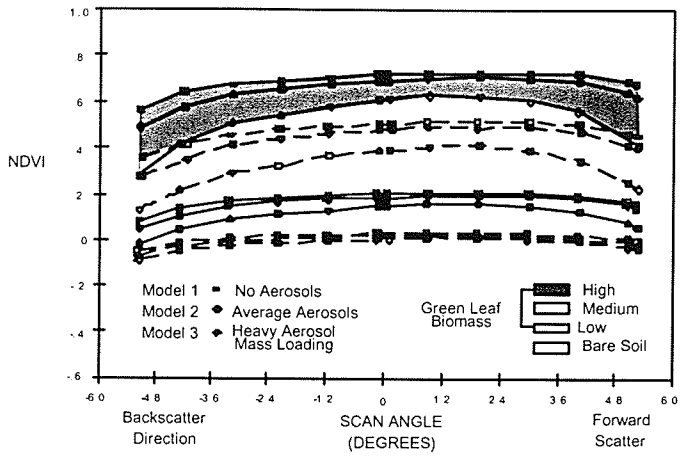

Figure 2.15 Stratification of cover types under various atmospheric conditions (after Holben and Fraser, 1984).

2.3.6 The Temporal Characterization of Canopies using VI's

Temporal plots of vegetation index values are indicative of crop growth and development (Aase and Siddoway, 1981; Wiegand et al., 1979; Hinzman et al., 1986; Rudorff and Batista, 1990a; Barnett and Thompson, 1982; Jackson et al., 1983). Figure 2.16 (a) and (b) illustrates the development of a wheat canopy and its relationship to leaf area index (LAI) and NDVI. From early emergence to tillering, soil reflectance dominates.

Early season soil moisture variations distinct in the red and NIR channels are minimized by the NDVI transformation. Early season NDVI values are characteristically low, indicating low vegetation densities.

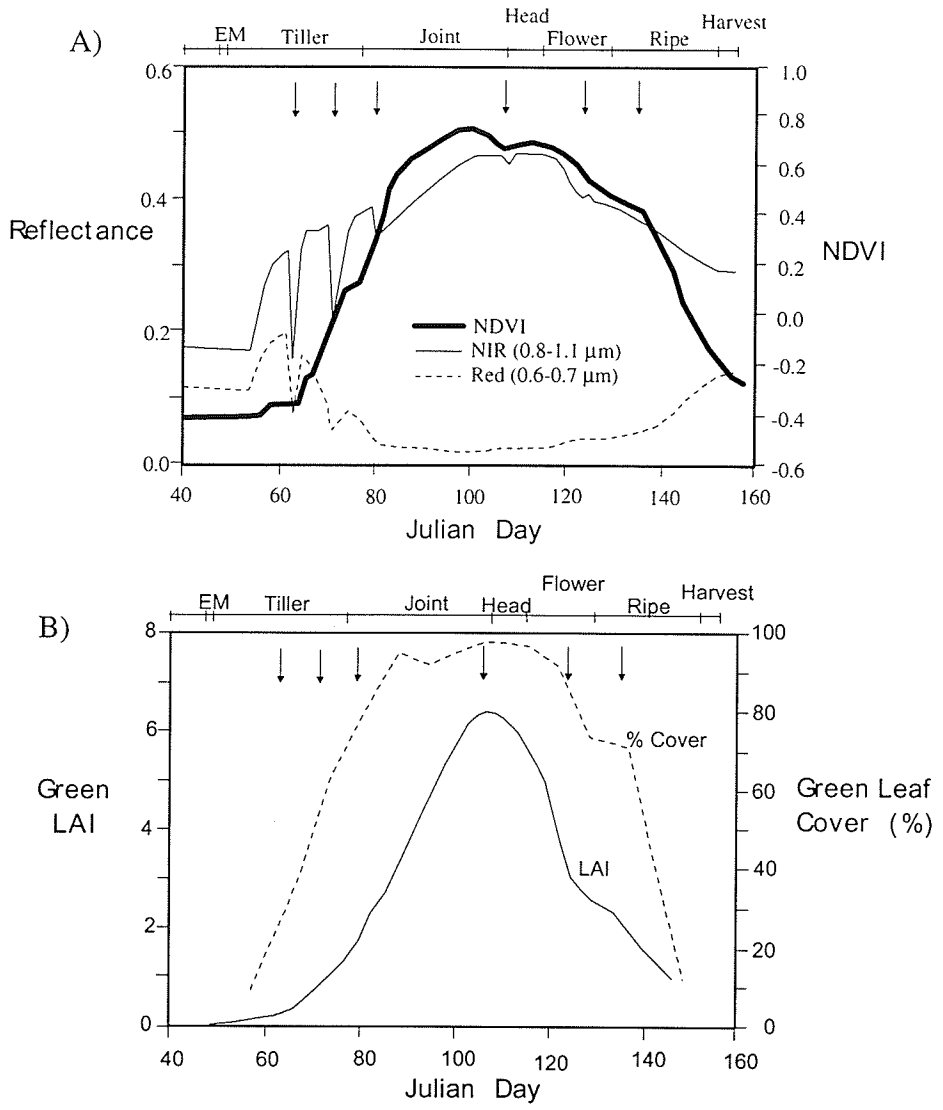

Figure 2.16 a) RED, NIR, and NDVI representations of the phenological development of spring wheat; b) Corresponding green leaf area index and percent cover for spring wheat (after Jackson et al., 1983).

As crop development accelerates the vegetation index values increase linearly. At the late jointing and early heading stage maximum LAI and percent cover is achieved (Jackson et al., 1983). Subsequent to peak LAI, wheat begins to ripen and senesce causing red reflectance to increase due to reduced leaf chlorophyll and increased soil background

reflectance. NIR reflectance decreases as leaf structure collapses and as percent cover and LAI decrease. Vegetation index (VI) values progressively decrease with crop senescence. Similar relationships between crop phenological stage and reflectance occur for other crops (Figure 2.17).

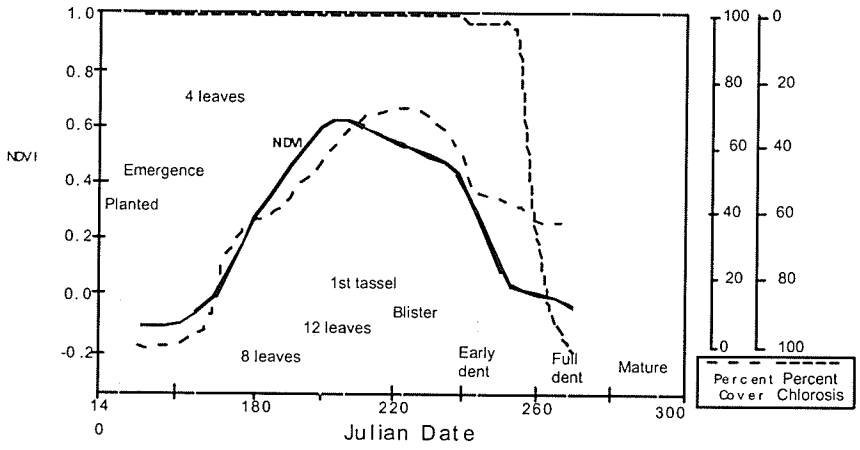

Figure 2.17 The phenological development of corn as represented by NDVI (after Tucker et al., 1979a).

Seasonal representation of canopy growth and development using VIs are highly correlated with green LAI and its persistence, canopy biomass, percent cover, and percent chlorosis. As such, VIs are a good measure of a canopy's "photosynthetic size" that is attributable to many factors, including vegetative stress, past and present management practices, spatial variation of soils, and climatic characteristics (Daughtry et al., 1980; Asrar et al., 1985; Aase and Siddoway, 1981; Wiegand and Richardson, 1990).

2.3.7 Crop Assessment

Since VIs are directly related to the physical properties of the canopy, they have been employed to assess crop condition and predict potential yield. VIs have been used to estimate crop yield for wheat (Asrar et al., 1985; Jackson et al., 1983; Daughtry et al., 1980; Rudorff and Batista, 1990; Aase and Siddoway 1981; Hinzman et al., 1986; Ahlrichs and Bauer, 1983; Tucker et al., 1980), barley (Kleman and Fagerlund, 1987) and soybean and corn canopies (Tucker et al., 1979; Tucker et al., 1979a; Crist 1984; Holben et al., 1980).

Whereas single date correlations of VIs versus yield are best near the booting stage (when green biomass and LAI are maximum), integrating VIs over the growing season provide the best correlations. Tucker et al. (1980) identifies the integration of the central portion of the VI curve as having the highest correlations (r = 0.81) (Figure 2.18).

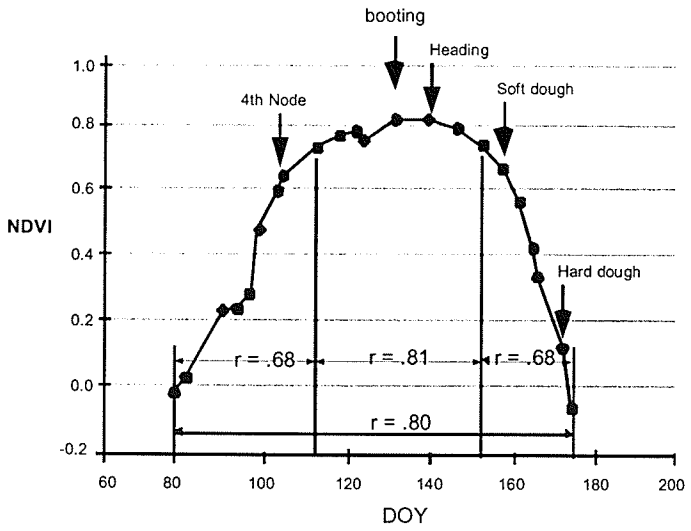

Figure 2.18 Correlation coefficients (Yield vs. NDVI) for single date observations and four integration periods in spring wheat (Adapted from Tucker et al., 1980).

Daughtry et al. (1980) found the best correlations with VIs from seeding to the flowering stage, and Rudorff and Batista (1990) found integrating NDVI data from the booting stage to when the crops were senesced highly correlated with yield (r = 0.81-0.96). The integration of VIs during the growth cycle provides a more robust estimation of yield potential as it accounts for both the magnitude and duration of photosynthetic biomass and leaf.

Where considerable variation exists in terms of biomass due to treatment effects (e.g., N fertilization and irrigation) single date correlations are as high as $r^2 = 0.97$ (Kleman and Fagerlund, 1987). Although lower correlations are generally expected, it is encouraging especially for those applications, such as precision farming, where single-date high-resolution satellite data, are required. For assessment of in-field variation, remote sensing acquisitions are preferred during peak LAI as it thus provides the best characterization of yield potential. The problem is often acquiring cloud free imagery during the booting or early heading period. If the primary interest is only mapping variability, then the acquisition window could be made somewhat broader because early season correlations are often quite high (Rudorff and Batista, 1990).

Whereas high resolution data, such as IRS SPOT and LANDSAT are ideal for mapping in-field variations of biomass, the operational monitoring of agricultural crops on regional and global scales utilizes NOAA AVHRR or MODIS data. The main advantage of this data, despite its relatively poor resolution (~1 km) is that it provides daily coverage of the Earth's surface.

By compositing daily NDVI images into weekly or biweekly composite images, relatively cloud-free images are generated thus providing the time series data necessary to

characterize the seasonal evolution of the crop and hence its potential yield (Hochheim and Barber, 1998; Benedetti and Rossini, 1993).

Cloud cover still remains a significant factor in using optical data. The availability of high resolution cloud free data is still problematic. For the regional and global monitoring applications much work remains in resolving problems associated with the maximum value NDVI data. These problems have been alluded to, and are cloud contamination, bi-directional reflectance, atmospheric attenuation and soil background effects.

2.3.8 Summary

Section 2.2 was intended to link crop growth and development to canopy reflectance. The following summary is provided with regard to the optical characterization of crop canopies.

- Red (0.62-0.70 μm), NIR (0.79-0.9 μm) and MIR (1.65 & 2.2 μm) reflectance is directly related to leaf area index (LAI), percent cover, dry and fresh biomass and chlorophyll content, all of which directly or indirectly estimate photosynthetically active phytomass (remote sensing detects variation, not the cause of it).
- Linear and ratio combinations of the RED, NIR (and MIR) wavelengths provide a vegetation dominated index that effectively characterizes LAI and green biomass etc., and is therefore an effective tool in assessing crop condition and yield potential.
- The highest single date correlations of VIs versus yield are obtained at the booting stage when LAI is maximum.

- If time series data is available, the integration of VIs is the most effective method for assessing crop condition and yield potential as it takes into account both the magnitude and duration of green LAI.
- VIs can be affected by factors external to crop condition, such as soil background, bi-directional reflectance, and atmospheric attenuation.
- Cloud cover/atmospheric attenuation remains the single most significant variable limiting the more effective use of optical data. This limitation in part provides the impetus to examine the potential of active microwave data by which to monitor crop growth and development for crop condition assessment.

2.4 Seasonal Microwave Backscatter from Canopies

2.4.1 Introduction

Whereas the use of optical data for crop monitoring is well understood, our understanding of microwave (MW) interaction with crop canopies continues to evolve. Optical sensors are passive instruments in that they rely on solar radiation to illuminate Earth surface features. Active microwave sensors provide their own source of illumination at frequencies ranging from 1-40 GHz (Table 2.2). The transmitted MW energy is intercepted by Earth surface features and subsequently backscattered to the sensor.

Table 2.2 Typical Microwave Frequencies.

Band	Wavelength (λ) (cm)	GHz
Ka	0.8-1.1	40-26.5
K	1.1-1.7	26.5-18
Ku	1.7-2.4	18-12.5
X	2.4-3.8	12.5-8.0
C	3.8-7.5	8.0-4.0
S	7.5-15.0	4.0-2.0
L	15.0-30.0	2.0-1.0
P	30.0-100.0	1.0-0.3

The amount of radiation received by a radar system from a target is expressed by the radar equation [2.6].

characterize the seasonal evolution of the crop and hence its potential yield (Hochheim and Barber, 1998; Benedetti and Rossini, 1993).

Cloud cover still remains a significant factor in using optical data. The availability of high resolution cloud free data is still problematic. For the regional and global monitoring applications much work remains in resolving problems associated with the maximum value NDVI data. These problems have been alluded to, and are cloud contamination, bi-directional reflectance, atmospheric attenuation and soil background effects.

2.3.8 Summary

Section 2.2 was intended to link crop growth and development to canopy reflectance. The following summary is provided with regard to the optical characterization of crop canopies.

- Red (0.62-0.70 μm), NIR (0.79-0.9 μm) and MIR (1.65 & 2.2 μm) reflectance is directly related to leaf area index (LAI), percent cover, dry and fresh biomass and chlorophyll content, all of which directly or indirectly estimate photosynthetically active phytomass (remote sensing detects variation, not the cause of it).
- Linear and ratio combinations of the RED, NIR (and MIR) wavelengths provide a vegetation dominated index that effectively characterizes LAI and green biomass etc., and is therefore an effective tool in assessing crop condition and yield potential.
- The highest single date correlations of VIs versus yield are obtained at the booting stage when LAI is maximum.

- If time series data is available, the integration of VIs is the most effective method for assessing crop condition and yield potential as it takes into account both the magnitude and duration of green LAI.
- VIs can be affected by factors external to crop condition, such as soil background, bi-directional reflectance, and atmospheric attenuation.
- Cloud cover/atmospheric attenuation remains the single most significant variable limiting the more effective use of optical data. This limitation in part provides the impetus to examine the potential of active microwave data by which to monitor crop growth and development for crop condition assessment.

2.4 Seasonal Microwave Backscatter from Canopies

2.4.1 Introduction

Whereas the use of optical data for crop monitoring is well understood, our understanding of microwave (MW) interaction with crop canopies continues to evolve. Optical sensors are passive instruments in that they rely on solar radiation to illuminate Earth surface features. Active microwave sensors provide their own source of illumination at frequencies ranging from 1-40 GHz (Table 2.2). The transmitted MW energy is intercepted by Earth surface features and subsequently backscattered to the sensor.

Table 2.2 Typical Microwave Frequencies.

Band	Wavelength (λ) (cm)	GHz
Ka	0.8-1.1	40-26.5
K	1.1-1.7	26.5-18
Ku	1.7-2.4	18-12.5
X	2.4-3.8	12.5-8.0
C	3.8-7.5	8.0-4.0
S	7.5-15.0	4.0-2.0
L	15.0-30.0	2.0-1.0
P	30.0-100.0	1.0-0.3

The amount of radiation received by a radar system from a target is expressed by the radar equation [2.6].

$$W_r = \int \frac{W_t G^2 \lambda^2}{(4\pi)^3 R^4} \quad \sigma^{\circ} \qquad [2.6]$$

where

W_r = the power received

W_t = the power transmitted

G^2 = gain of the transmitting antenna

λ^2 = wavelength

R^4 = slant range to target

σ° = backscatter cross section per unit ground area

All the factors on the right side of the equation are a function of instrument design including wavelength and polarization (polarization describes the send and receive orientation of the electrical vector of an EM wave, i.e., HH polarization is horizontally transmitted and received). The backscatter cross section (σ° (dB)) describes the target's scattering behaviour at a given incident angle, frequency and polarization. σ° is a ratio that describes the average backscattered power compared to the power of the incident field per m^2.

Backscatter from an agricultural surface is a function of numerous factors, including system parameters (microwave frequency, polarization and incident angle) and target parameters. The significance of system parameters will be alluded to throughout this discussion. The most significant target parameters affecting canopy backscatter include the dielectric and geometric properties of the vegetative surface (a function of crop phenology and crop type), and the dielectric and geometric characteristics of the underlying soil. The assessment of crop canopies using microwave data is further complicated by factors

external to crop condition, including row orientation and spacing, and environmental effects including dew and rain events as well as effects of wind on crop orientation.

The approach taken here will be to briefly introduce the dependence of vegetation and soil dielectrics on volumetric moisture and then discuss approaches used to model backscatter from agricultural canopies. Research examining the temporal backscatter from wheat (and other small grains), canola, corn and sorghum will be reviewed. Environmental factors affecting canopy backscatter are briefly discussed.

2.4.2 Vegetation and Soil Dielectrics

Interpretation of microwave backscatter as it relates to agricultural surfaces requires an understanding of how microwave energy interacts with the physical properties of agricultural canopies. The dielectric properties of a surface target are particularly important. The dielectric constant (ε) is used to express permittivity (ε') and loss (ε'') of a material [2.7].

$$\varepsilon = \varepsilon' + j\,\varepsilon'' \quad \text{where } j = \sqrt{-1} \qquad [2.7]$$

Permittivity (ε') measures how well MW energy is allowed to pass through a media; ε'' represents what happens to incident energy when it enters a media (transmission or absorption). A high permittivity value means that incident MW energy is reflected. The ε' of air for example is 1 (no reflectivity; high transmission), ε' for dry vegetation is ~ 1.5-2.0

and for dry soil ~ 3; in contrast ε' of water is ~80 (high reflectivity) (Dobson and Ulaby, 1986).

The dielectric properties of leaves and stalks are a direct function of volumetric moisture, Figure 2.19.

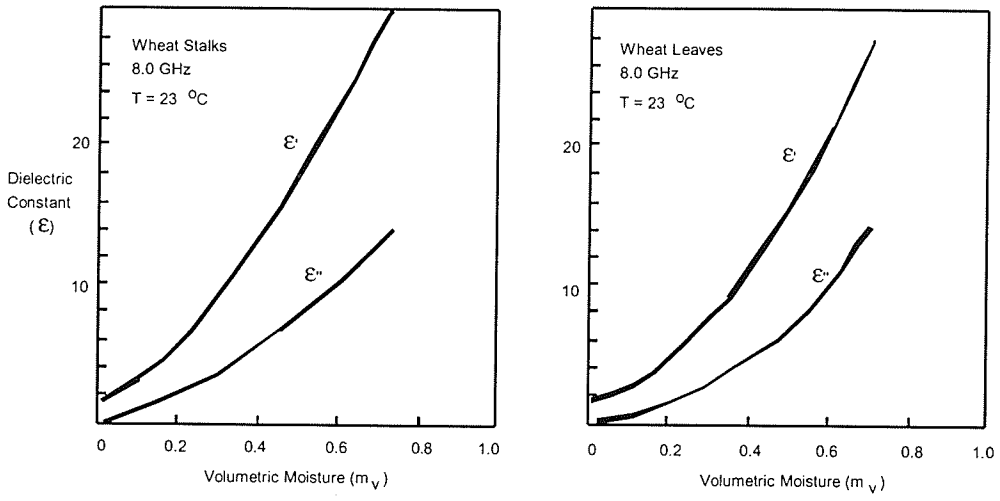

Figure 2.19 Measured moisture dependence of the dielectric constant for wheat stalks and wheat leaves at 8 GHz (Adapted from Ulaby et al., 1986).

Many empirical models still use volumetric moisture as input to backscatter models, although models such as MIMICS use Ulaby and El-Rayes (1987) dual dispersion model to estimate the dielectric properties of the component parts of the canopy. The dielectric constant of vegetation (ε_V) is computed as an additive mixture of three components: a) ε_r a non dispersive residual component; b) $v_{fw}\varepsilon_f$ a free water component where v_{fw} is the volume fraction of free water and ε_f is its dielectric constant; and c) $v_b\varepsilon_b$ a bulk vegetation bound component, where v_b is the volume fraction of the bulk vegetation bound water mixture and ε_b is its dielectric constant [2.8].

$$\varepsilon_v = \varepsilon_r + v_{fw}\varepsilon_f + v_b\varepsilon_b \qquad [2.8]$$

With ε_f and ε_b inserted:

$$\varepsilon_v = \varepsilon_r + v_{fw}\left[4.9 + \frac{75.0}{1+jf/18} - j\frac{18\sigma}{f}\right] + v_b\left[2.9 + \frac{55.0}{1+(jf/0.18)^{0.5}}\right] \qquad [2.9]$$

where

f = frequency in GHz.

$\sigma = 0.16S - 0.0013S^2$ = Ionic conductivity of the free water solution (siemens m^{-1})

S = salinity, total mass of solid salt in grams dissolved in 1 kg. of solution, (parts per 1000 (o/00))

The function forms of the remaining terms using volumetric moisture are:

$$\varepsilon_r = 1.7 + 3.2\,M_v + 6.5\,M_v^2 \qquad [2.10]$$

$$v_{fw} = M_v(0.82M_v + 0.166) \qquad [2.11]$$

$$v_b = 31.4\,M_v^2/(1+59.5\,M_v^2) \qquad [2.12]$$

As with vegetation, the dielectric properties of soil are a function of its volumetric water content. As soil moisture increases, ε' and ε'' increase in a curvilinear fashion, with ε' showing the greatest response, Figure 2.20.

For soil there is a small dependence of dielectrics on soil texture. At any given frequency, ε' is proportional to the amount of sand in the soil (and inversely proportional to clay) although the magnitude of the effect decreases with increasing frequency (Hallikainen et al., 1984). This relationship is largely explained by the fact that sandy soils tend to have less bound water, and bound water has a lower permittivity relative to free water. Dielectric models, as with the above model for vegetation, take into account the proportion of free and bound water by incorporating terms accounting for percent sand and clay (Hallikainen et al., 1985).

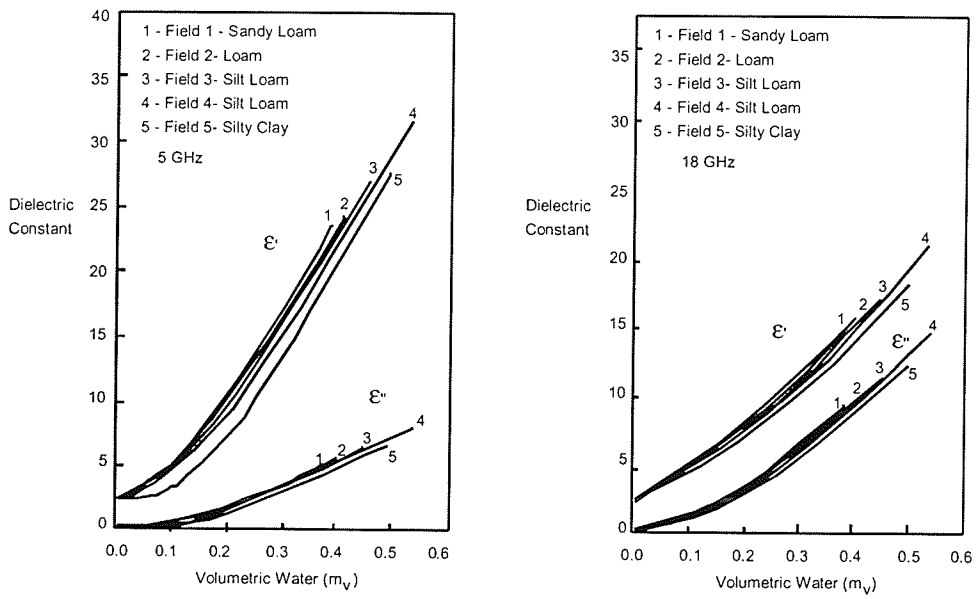

Figure 2.20. Measured dielectric constant for five soils at 5 and 18 GHz (Adapted from Ulaby et al., 1986).

For a given soil roughness and radar backscatter is linearly dependent on volumetric moisture in the upper 2-5 cm of soil with correlation r = 0.9 ($\sigma^o = A+Bm_v$), where, for a given frequency, polarization and incident angle, A is a function of roughness, and B is a function of M_v (Dobson and Ulaby, 1986).

Depending on the volumetric soil moisture, surface roughness can be a significant factor affecting backscatter of a canopy depending on frequency, incident angle, and above ground biomass. Surface roughness is a measure of variance of the surface height (σ) (root-mean-squared (rms) height); and the surface correlation length (l), a measure of horizontal roughness, and rms slope (m) (where $m = \sqrt{2}\sigma/l$). The σ is computed by digitizing a profile into discrete values at the mean height of the surface at some appropriate spacing (generally defined as $= 0.1\lambda$).

As a first order approximation, a smooth surface is defined by the Fraunhofer criteria whereby,

$$\sigma < \frac{1}{32\cos(\theta)} \qquad [2.13]$$

Electromagnetically σ is often expressed as $k\sigma$ (where $k = 2\pi/\lambda$). As a general rule a surface can be considered smooth if $k\sigma<0.2$ and rough if $k\sigma>1.0$ (Ulaby et al., 1986). Figure 2.21 shows the backscatter response of fives soils with a similar volumetric soil moisture, but varying rms heights.

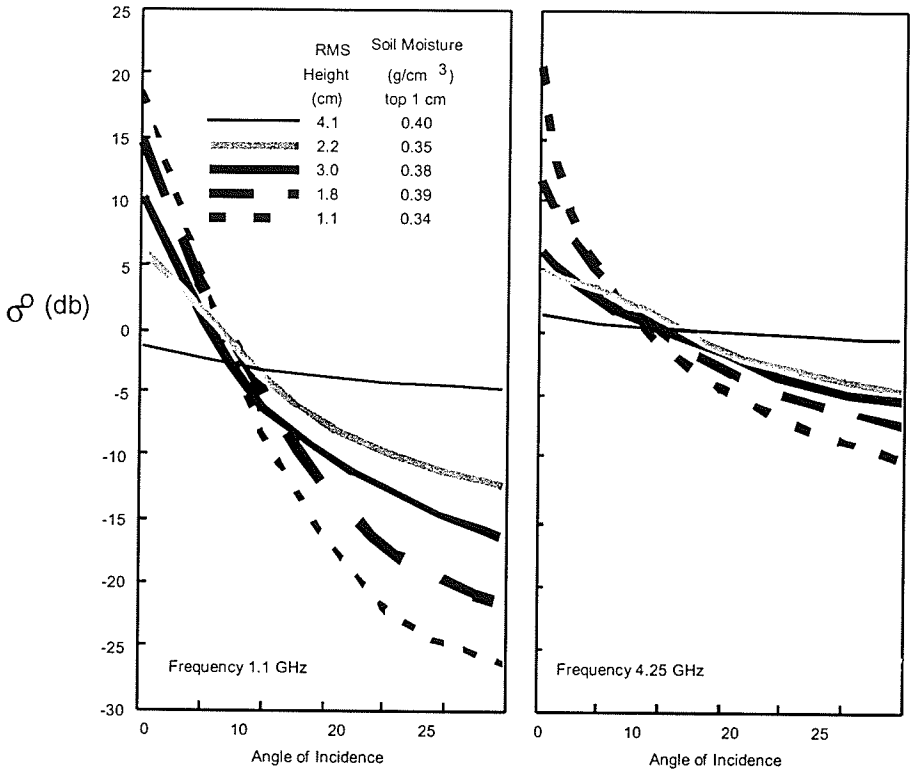

Figure 2.21 Backscatter response to rms height (Ulaby et al., 1986).

It demonstrates effectively that surface roughness can have profound influence on backscatter depending of course on the incident angle (θ), wavelength (λ) and M_v. (Note:

backscatter is independent of surface roughness at about $\theta = 10^{o}$. Depending on the amount and nature of above ground biomass, microwave backscatter from the soil surface can significantly affect the total backscatter from an agricultural surface (Ulaby et al., 1982).

2.4.3 Monitoring the Seasonal Evolution of Agricultural Crops

In the MW portion of the electromagnetic spectrum a vegetation canopy is typically described as a volume of scattering elements, bounded by air on top and by a scattering soil surface below (Ulaby et al, 1986). The relative contribution of the canopy and/or soil surface is a function of penetration depth, the height of a canopy, frequency and incidence angle. The penetration depth is a function the amount of moisture within the canopy, the geometry of the canopy (size and orientation of leaves, stalks and fruit), and the amount of biomass present as expressed by its volume fraction (which is largely air). The objective when monitoring a vegetative surface is to maximize the backscatter component of the canopy. The significance of all of the above parameters will be alluded to throughout the text as work relating to the seasonal evolution of crop canopies is reviewed.

Modeling efforts with respect to agricultural canopies are limited by the fact that canopies are in constant flux and mathematical parameterization of the component parts of the canopy in terms of geometry and moisture is complex. Due to the difficulty of modeling such a dynamic target, empirical models are often relied upon to describe a class of vegetation with similar physical characteristics (Ulaby et al., 1986).

One of the first empirical studies to successfully relate canopy backscatter to the physical properties of an agricultural canopy was conducted by Ulaby (1976). This study

examined the seasonal evolution of a corn canopy. Among the parameters recorded were volumetric soil moisture ($gm \cdot cm^{-3}$), plant height, and wet and dry weights per plant. Canopy backscatter was related to normalized plant water content and soil moisture at frequencies ranging from 8-18 GHz at incident angles (θ) from 0-70°. Results from this early work showed that soil background had a significant effect on canopy backscatter at incident angles from 0-25° throughout the growing season. Canopy heights ranged from 0.3-2.6 m. Canopy backscatter and normalized plant water (W_{pn} = plant H_20 / canopy height) were highly related at θ >30° (Figure 2.22 a and b). Correlation coefficients between observed backscatter (σ^o) and W_{pn} were highest at incident angles between 40-50° for both HH and VV polarizations. The best correlations occurred at the higher frequencies of 13-17 GHz ($r > 0.80$) and with VV polarization (Figure 2.22c), while the poorest correlations were observed at 8.6 GHz HH ($r = 0.60$). This study demonstrated the significant role of plant and soil volumetric moisture in determining the seasonal backscatter characteristics from an agricultural surface, and the need for larger incident angles, high frequencies and VV polarization to best characterize the vegetative canopy.

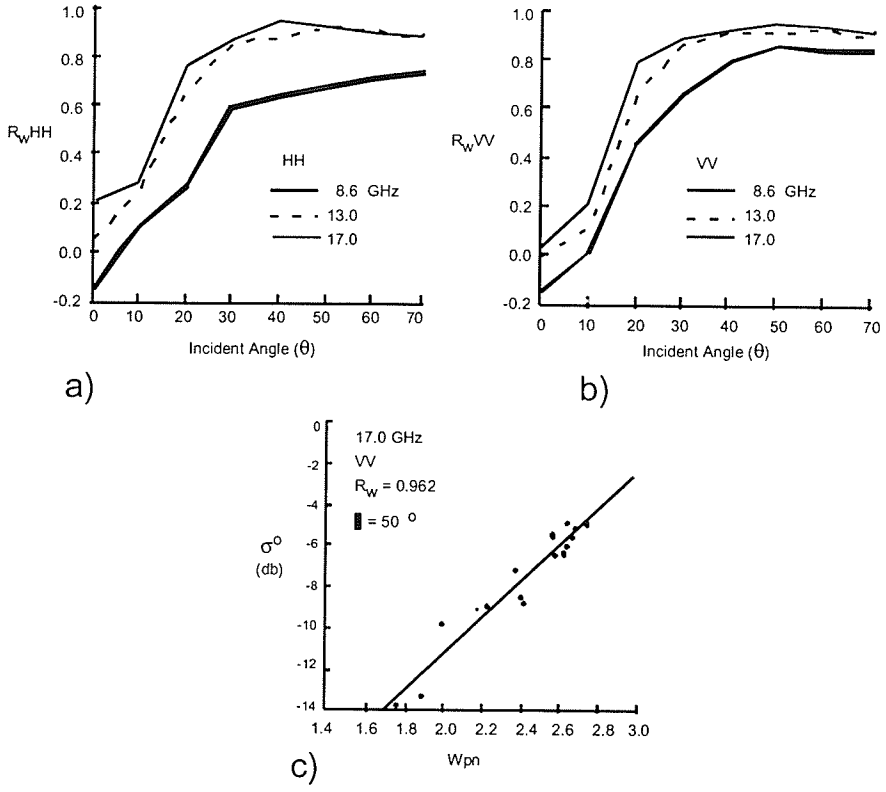

Figure 2.22 Plot of correlation coefficients (W_{pn} vs. σ^o) as a function of incident angle for a) HH polarization and b) VV polarization. c) W_{pn} vs. σ^o at 17 GHz, $\theta = 50^o$ (Adapted from Ulaby and Bush, 1976).

Based on this early work, Attema and Ulaby (1978) proposed a volumetric scattering model in which a vegetation canopy was modeled as a water cloud whose droplets are held in place by vegetation. The model assumed that the "cloud" represented by vegetation consisted of identical water particles uniformly distributed throughout space where cloud height and density were the most significant variables [2.14].

$$M_v = (m_w - m_d)n/h \qquad [2.14]$$

where:

M_v = volumetric moisture (kg/m^3)
n = number of plants per unit area
h = plant height
m_w = plant wet weight
m_d = plant dry weight

A volumetric soil moisture component was added to the model taking into account the additive nature of soil backscatter. A two way transmittance term (Ψ^2) included in the model took into account extinction due the canopy layer above it. Conceptually the canopy backscatter ($\sigma^o_{can}(\theta)$) is written:

$$\sigma^o_{can}(\theta) = \sigma^o_{cv}(\theta) + \Psi^2 \sigma^o_{ss}(\theta) \qquad [2.15]$$

where: backscatter from the vegetation canopy $\sigma^o_{cv}(\theta) =$

$$= f(N)\,[1-\psi^2(\theta)]\cos(\theta) \qquad [2.16]$$

where:

f(N) = is a constant replacing $(\sigma_v/2k_e)$ where $\sigma_v = (N\sigma_b)$ where
- σ_v = the radar cross section per unit volume, m^2/m^3; N = number of scattering particles per m^3, and σ_b = backscattering cross section of a single particle;
- $k_e = NQ_e$ where the total extinction cross section; Q_e = the extinction cross section per particle

$\Psi^2(\theta)$ = $\exp(-2A_1 m_v h/\cos(\theta))$ = two way transmittance of the canopy (m^2/m^2)
h = canopy height
A_1 = a constant for crop type
m_v = canopy volumetric moisture (kg/m^3)

and where:

backscatter from the soil surface $\sigma^o_{ss}(\theta) =$

$$= [C_s(\theta)m_s]\psi^2(\theta) \qquad [2.17]$$

where:

$C_s(\theta)$ = is a constant for a given wavelength and polarization
m_s = volumetric soil moisture content.

The constants for the various terms were computed using regression analysis. The modeled results agreed with the observed radar backscatter for wheat, corn, milo and alfalfa ($r = 0.74$-0.98).

Ulaby et al. (1984) and Le Toan et al., (1984) modified the original cloud model to take into account the backscatter contributions of the various component parts of the canopy, i.e., leaves, stalks, and fruit (in addition to the soil background). Ulaby et al., (1984) presented a model for wheat, and another for corn and sorghum.

The wheat model considered the backscatter contribution of leaves and heads while excluding stalks. Since LAI is highly correlated to wet and dry leaf biomass, LAI was substituted for normalized volumetric moisture (m_v/h) used in the cloud model.

$$\sigma^o_{can}(\theta) = \sigma^o_h(\theta) + \Psi^2_h \sigma^o_l(\theta) + \Psi^2_h \Psi^2_l \sigma^o_{ss}(\theta) \qquad [2.18]$$

subscripts h, l = heads and leaves

$\sigma^o_h(\theta)$ $= A_h(\theta)M_h$; A_h = constant (m^2/kg), M_h = head biomass(kg/m^2)

Ψ^2_h $= \exp(-2\alpha_h M_h \sec\theta)$; α_h = constant (m^2/kg).

Ψ^2_l $= \exp(-2\alpha_l L \sec\theta)$; α_l = constant; L = green leaf area index (LAI).

$\sigma^o_l(\theta)$ $= A_l[1-\exp(-b_l L/h)] \times [1-\Psi^2_l(\theta)]$; A_l & b_l are constants;
L/h = LAI divided by height of the leaf layer (number density of scatters).

$\sigma^o_{ss}(\theta)$ $= Cs(\theta)m_s$, C = constant; m_s = volumetric soil moisture.

Ulaby et al., (1984) presented results for 8.6, 13, 17, and 35.6 GHz, using VV polarization and $\theta = 50^\circ$. The coefficients of determination (r^2) of the observed vs. modeled backscatter using the above model were 0.57, 0.77, 0.86 and 0.80 respectively.

Ulaby et al.,(1984) concluded that seasonal backscatter profile for wheat was dominated by soil during early stages of growth (LAI <0.5). As LAI increased (>0.5), backscatter was dominated by leaf contributions, while later in the growing season backscatter was driven by wheat heads and soil volumetric moisture (Figure 2.23).

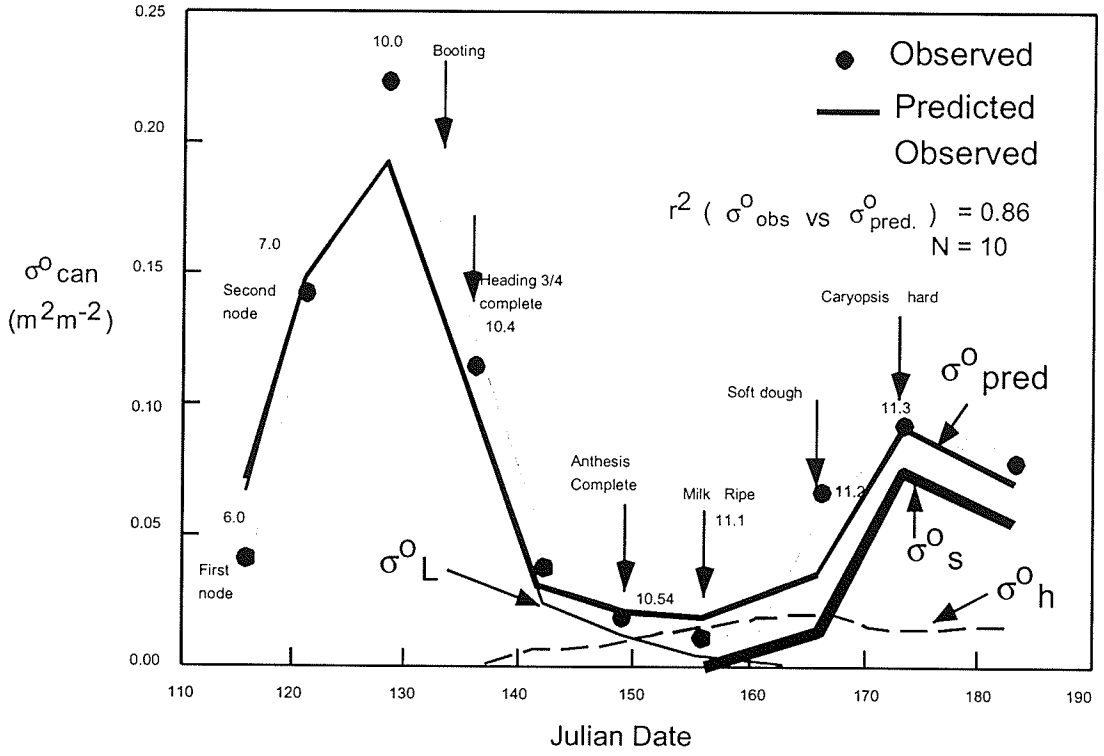

Figure 2.23 Observed and predicted seasonal backscatter of wheat, $\theta = 50^o$, 13 GHz, VV polarization. σ^o is expressed in power units ($m^2 \cdot m^{-2}$), (modified after Ulaby et al., 1984).

Ulaby et al. (1984) also tested a model using LAI as the only model parameter to estimate backscatter [2.19]. Modeled vs. observed backscatter were highly correlated ($r^2 = 0.90$), Figure 2.24.

$$\sigma^o_{can}(L) = A'_l L^n [1-\exp(-\alpha'_l L)] + C'_s \exp(-\alpha'_l L) \qquad [2.19]$$

Where : A'_l; α'_l; C'_s are constants and n=1 for wheat.

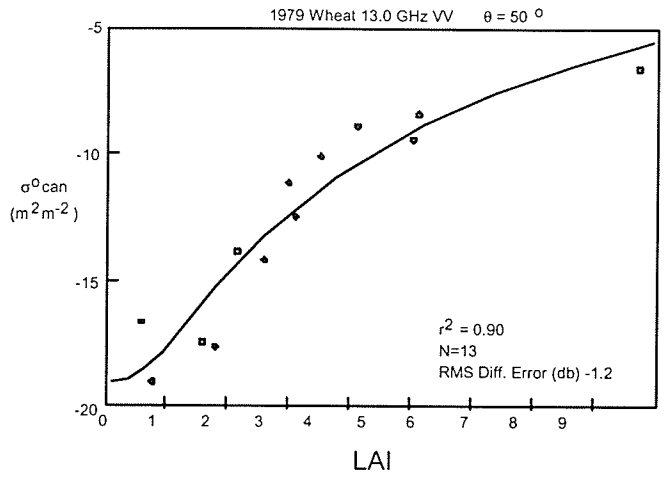

Figure 2.24 Leaf area index vs. σ^{o}_{can} (Adapted from Ulaby et al., 1984).

The modified cloud model was applied to corn and sorghum canopies by introducing a modification whereby the fruit was ignored and two layers were considered, an upper leafy canopy, and a lower canopy consisting of stalks. The observed backscatter versus predicted backscatter for corn was highly correlated (Figure 2.25).

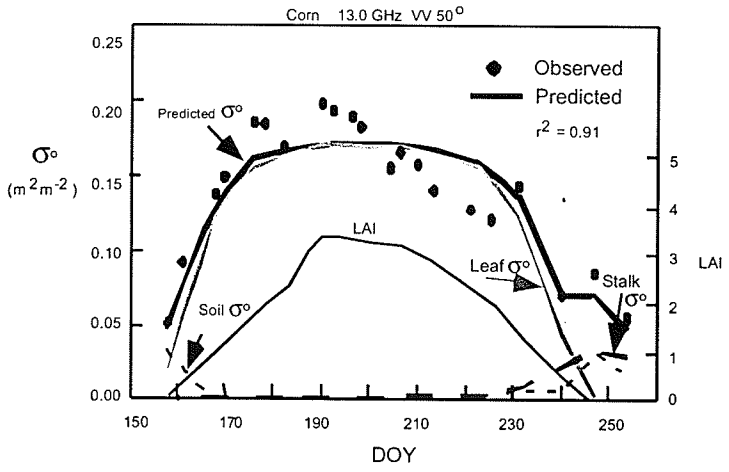

Figure 2.25 Measured vs. predicted corn backscatter (13 GHz VV).

The one parameter LAI model [4.14] for corn and sorghum showed that backscatter was closely related to LAI but reached its asymptotic limit at 2.0 LAI. In contrast, wheat backscatter and LAI were correlated beyond a LAI of 5.

Le Toan et al., (1984) examined the seasonal evolution of wheat using a number of frequencies ranging from 1.5 GHz (L-band), 3 GHz (S-Band), 4.5 GHz (C-Band), and 9 GHz (X-Band) at HH, VV, HV polarizations with incident angles from 0 to 60°. Based on the data collected the optimal imaging parameters for observing wheat were frequencies >8 GHz, VV polarization and $\theta > 40°$.

The results were presented for 9 GHz ($\theta = 40°$, HH, VV). Not unlike the previous results, Le Toan et al. (1984) showed a close relationship between seasonal backscatter, canopy volumetric moisture and LAI. It was shown that maximum backscatter occurs prior to heading and decreases quickly at heading with soil moisture being a significant factor affecting canopy backscatter as the crop senesced. It was also shown that a two layer cloud model was more effective in characterizing the seasonal evolution of the canopy.

The differences between HH and VV characterizations of the seasonal evolution were significant (Figure 2.26). The VV backscatter profile had a larger dynamic range than the HH profile. Early in the season VV backscatter is higher. As the crop headed both HH and VV backscatter decreased. It was suggested by Le Toan et al. (1984) that after heading the vertical heads absorb and scatter the incident wave, thus reducing direct backscatter from the leaves. Since the attenuation by the head layer was stronger at VV, the HH backscatter remained higher relative to the VV backscatter following heading and showed greater sensitivity to soil moisture.

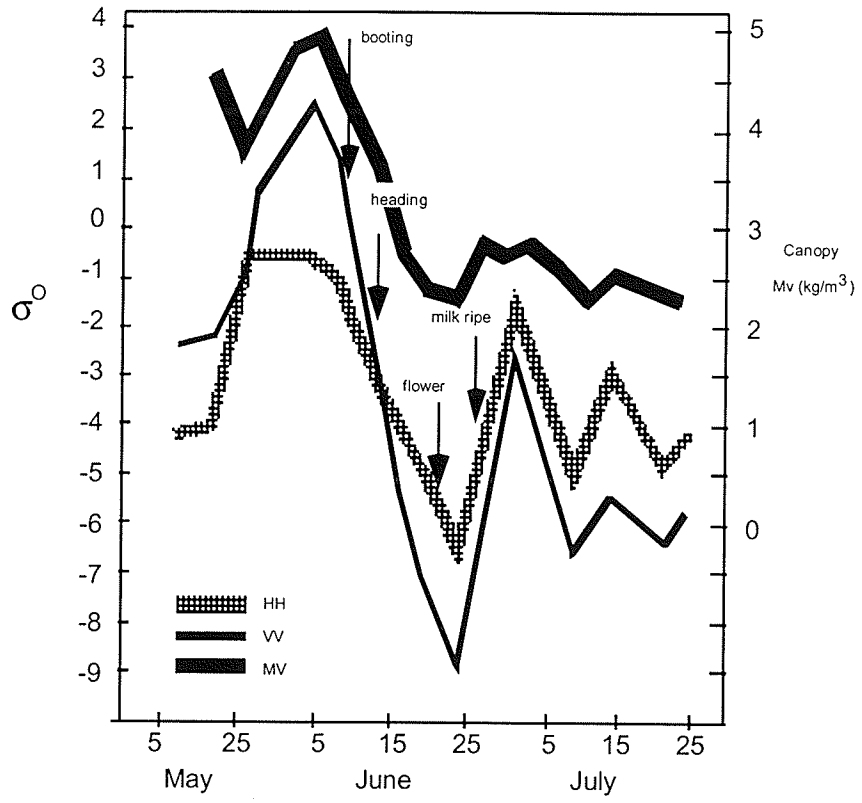

Figure 2.26 The seasonal σ^0 from wheat, 9 GHz, VV and HH polarizations (Adapted from Le Toan et al., 1984).

Bouman and van Kasteren (1990) show very similar trends in seasonal backscatter of wheat for HH and VV polarizations. Le Toan et al. (1984) also noted that the ratio of $\sigma^{o}_{vv}/\sigma^{o}_{hh}$ was more highly correlated ($r = 0.97$) with the volumetric moisture in the canopy (M_v), than either polarization response.

Le Toan et al. (1984) showed that canopy volumetric moisture and LAI were highly correlated and that the relationship varied depending on wheat variety (Figure 2.27a). Although canopy backscatter and LAI are highly correlated for both wheat varieties, the regression coefficients differed significantly due to the architecture of the canopy (Figure 2.27b).

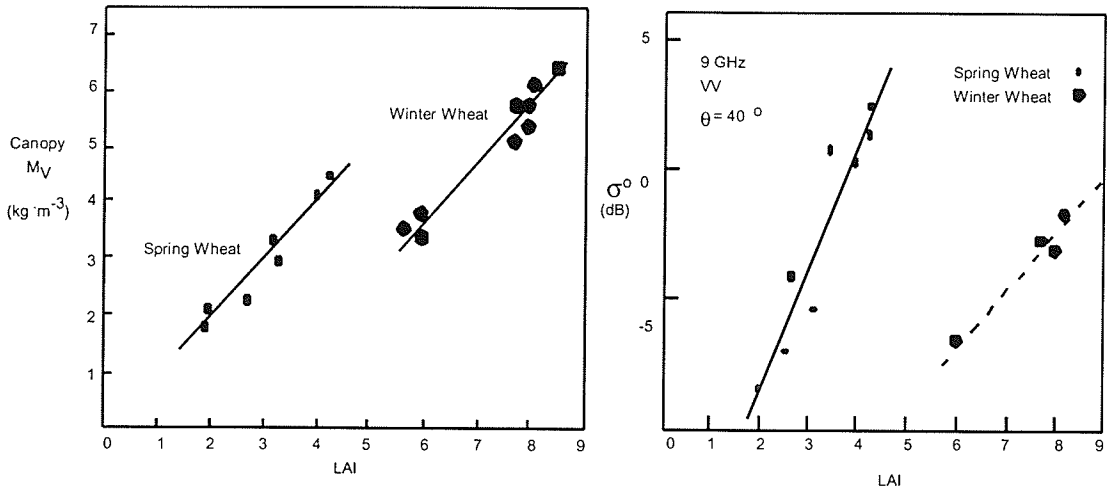

a) b)

Figure 2.27 a) LAI vs. M_v for spring wheat and winter wheat, b) LAI vs. σ^o for spring wheat and winter wheat (Adapted from Le Toan et al., 1984).

In this case, spring wheat leaves are oriented at 30-50° from the vertical, and the leaves for winter wheat variety are oriented 10° from the vertical. Despite the higher LAI and M_v (LAI 8; M_v 6kg·m^{-3}) for winter wheat, the spring wheat (LAI 4.5; M_v 5kg·m^{-3}) backscatter was at least 3 dB higher due to leaf geometry.

Paris (1986), proposed modifications to the cloud model to take into account the effects of size and water content for the individual scattering elements that constitute the "cloud" and the areal scattering element density [2.20].

$$\sigma^o = [C(A_l)^D \cos(\theta)/2E(m_w)](1 - \psi^2) + (F_1 + F_2 m_s)\,\psi^2 \qquad [2.20]$$

Where

$$\psi = \exp[-N_a E(m_w)/\cos(\theta)]$$

C, D, E, F, F are constants and the physical parameters are

A_l = leaf area m^2;

m_w = water mass kg;

m_s = volumetric soil moisture ,

N_a = aereal scattering element density

To obtain the mean leaf and stalk biophysical properties needed to relate to the microwave properties of the scattering elements, plant density (plants·m^{-2}) and the average number of leaves per plant are used. The average water mass per plant leaf and the average green leaf area of an average leaf were computed. The model results agree closely with observed backscatter (r^2=0.93) (Figure 2.28a). The relationship between the backscatter cross-section (cm^2) of the average green leaf and the area of the leaf (m^2) was r^2=0.98 (Figure 2.28b). When the water content of the leaf was used instead of the green leaf area the correlation between the predicted and observed backscattering coefficient dropped to r^2=0.70 (vs. 0.93) thus highlighting the significance of the size of leaves and their effect on the observed backscattering coefficient.

Variations in canopy backscatter due to soil moisture variations were noticeable late in the growing season when the crop was senesced and dry so nearly transparent to the incident MW energy. The rapid rise in backscatter early in the year showed a great sensitivity to changes in green leaf area. Of particular interest was the sudden drop in backscatter at the beginning of the reproductive stage (~day 190). Paris (1984) pointed out

that the MW data seemed sensitive to this phenological stage (tassling), something that an optical VI does not detect.

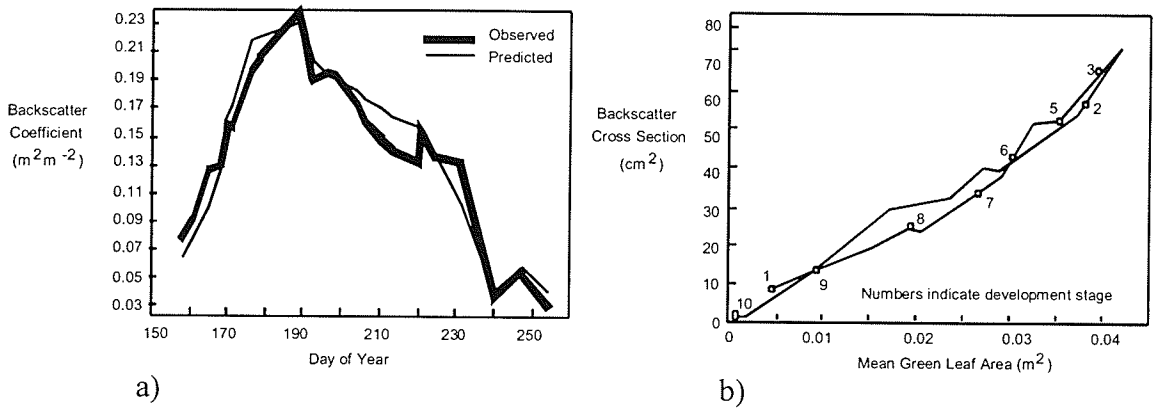

Figure 2.28 a) Observed vs. Modeled backscatter for corn plotted with derived seasonal values of the average green-leaf area of an average leaf and, b) the relationship between backscattering cross section and the average green-leaf area of an average leaf (17 GHz; $\theta=50^{o}$, VV).

Touré et al., (1994) adapted the MIMICS model (Ulaby et al., 1990) to examine the temporal evolution of wheat and canola using L and C bands. The MIMICS (Michigan Microwave Canopy Scattering) model was originally designed to model forest canopies. Geometrically, the original model divided the canopy into three components, the crown, trunk and soil surface. The model takes into account the sizes, shapes and orientation of the component parts of the canopy. Variables for the canopy included stem, petiole and leaf gravimetric moisture; stem length, diameter and density; leaf length (fixed), width (fixed), LAI, and leaf thickness. Canopy dielectrics were computed using Ulaby and El-Rayes (1987) dielectric model. Stems were assumed vertically oriented for both crops. Soil was characterized using correlation length, rms height, rms slope and volumetric moisture.

The MIMICS model was modified to the crop situation by eliminating the trunks, as well as the various scattering interactions related to the trucks, (e.g., trunk_ground, and ground_trunk). Interaction terms retained in the model are depicted in Figure 2.29.

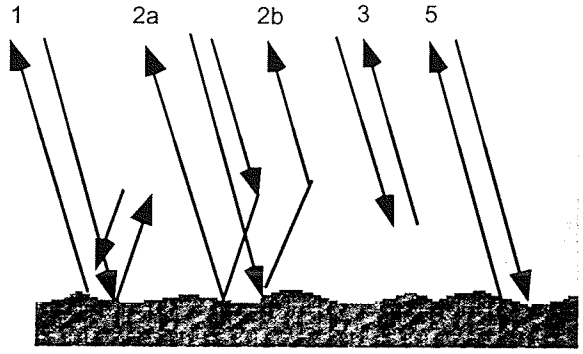

Figure 2.29 Interaction terms adapted for the agricultural context representing different scattering mechanisms: 1 ground_cover _ground; 2a covert_ground; 2b ground_cover; 3 direct cover; 5 direct ground (Adapted from Touré et al., 1994).

The assumption supporting the removal of trunks is that stem heights are on an order of a wavelength for both L-Band (15-30 cm) and C-band (3.8-7.5 cm), and do not occupy a distinct layer in the canopy. LAI was used indirectly to compute leaf density (N), [2.21].

$$LAI = hNVlf / th \qquad [2.21]$$

Where :

h = the cover height,

th = leaf thickness

Vlf = mean volume of the leaf

Stems were modeled as cylinders, wheat leaves as thin planar rectangles having a uniform distribution, and canola leaves were modeled as circular disks. It appears that heads and pods were not accounted for explicitly.

For C-band, soil was the largest component contributing to backscatter followed by the direct cover and ground_cover interactions which appeared to contribute equally (Figure 2.30).

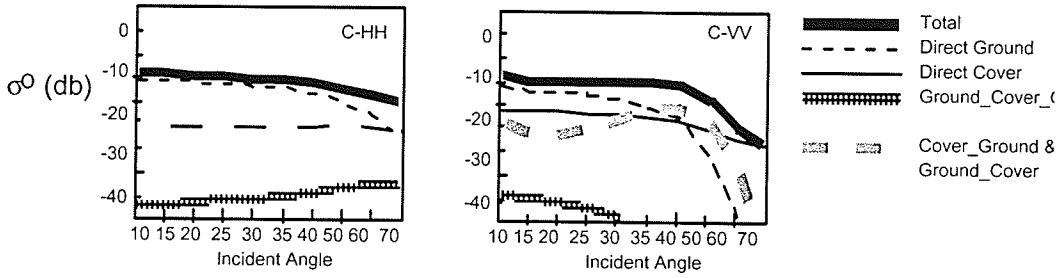

a) b)

Figure 2.30 Contributions of the various interaction mechanisms to total backscatter for wheat at a) C-HH and b) C-VV, July 18'88 (Adapted from Touré et al., 1994).

For the C-VV configuration, ground cover also dominated, although less at incident angles greater than 40°, this is to be expected since VV polarization is somewhat more sensitive to the vertical components of the canopy.

The seasonal plot of wheat (C-HH, VV) appears relatively invariant to LAI over the growing season. Based on the results of Ulaby et al. (1984) and Le Toan et al. (1984) a peak backscatter would have been expected to coincide with maximum LAI, followed by a decline due to heading which occurs approximately at maximum LAI. Figure 2.31 depicts a single peak closely associated with a peak in soil moisture. L-Band backscatter for the wheat canopy backscatter is almost exclusively dominated by the direct soil component, the temporal plot is much the same as that depicted in Figure 2.31.

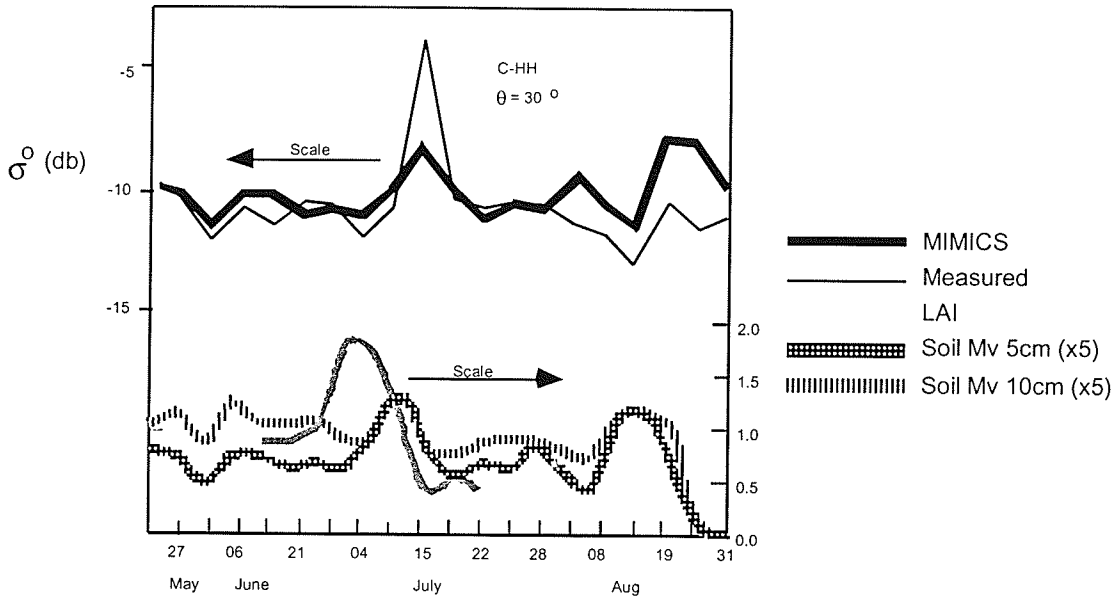

Figure 2.31 Seasonal backscatter of wheat, measured and modeled (MIMICS) results; $\theta=30^{o}$ (Adapted from Touré et al., 1994).

For the canola canopy (C-band, HH) the direct cover component of backscatter was the dominant mechanism followed by the ground_cover, cover_ground, and direct ground interaction terms. The direct cover component for the C-VV configuration was more significant compared to C-HH, Figure 2.32. For L-Band direct ground cover (soil) played a dominant role at 10-25° incident angles, the direct canopy contribution dominated at angles $\theta = 40^{o}$.

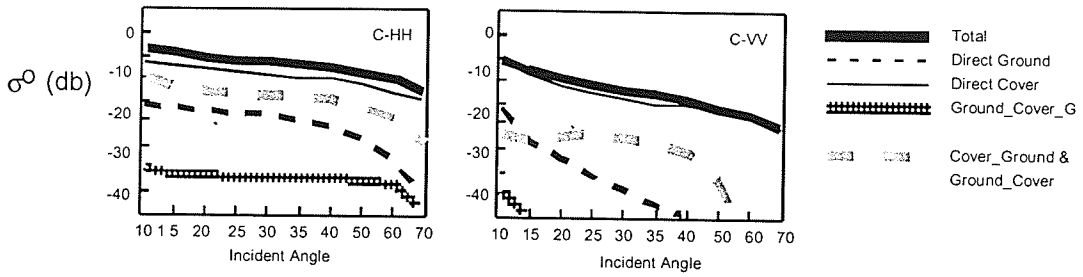

Figure 2.32 Contributions of the various interaction mechanisms to total backscatter for canola at a) C-HH and b) C-VV; July 19'88 (Adapted from Toure' et al., 1994).

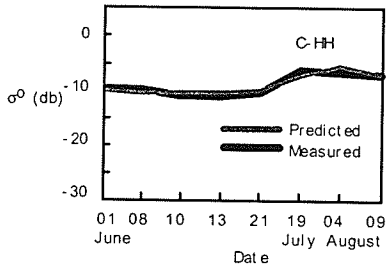

Figure 2.33 Seasonal backscatter of canola, measured and modeled results (MIMICS); $\theta=30^{o}$ (Adapted from Touré et al., 1994).

The seasonal backscatter profile shown in Figure 2.33 is not very meaningful as LAI was included only for the latter three dates during the acquisition period.

The MIMICS model used by Touré et al. (1994) assumed the canopy as a single layer. The empirical models presented earlier (Ulaby et al., 1984; Le Toan et al., 1984) clearly show that for wheat, heads have to be accounted for explicitly. The model results as presented here suggest that MIMICS is insensitive to LAI and heading. An evaluation of the seasonal evolution of the canola canopy is not possible, as model parameters were not applied consistently during the acquisition period. It is curious that no ground confirmation data was presented by Touré et al. (1994) regarding pods for canola, although mention was

made of a modeling attempt to incorporate pods without improving predicted results. Pods are a major canopy component towards the latter part of the growing season.

Brisco et al. (1992) examined the temporal backscatter of wheat and canola. Although these data were obtained to determine the optimal times during the growing season to differentiate crop types grown in western Canada, the plots suggest that wheat and canola do have unique temporal profiles (Figures 2.34-2.350. The pooled results from canola show a bell shaped profile both for K- and C-band (1.5 GHz & 5.17 GHz). The wheat backscatter profiles at 1.5 GHz resemble those of previous studies. The C-HH profile for wheat varies significantly on a weekly basis. No distinct seasonal profile is discernable (Figure2.35).

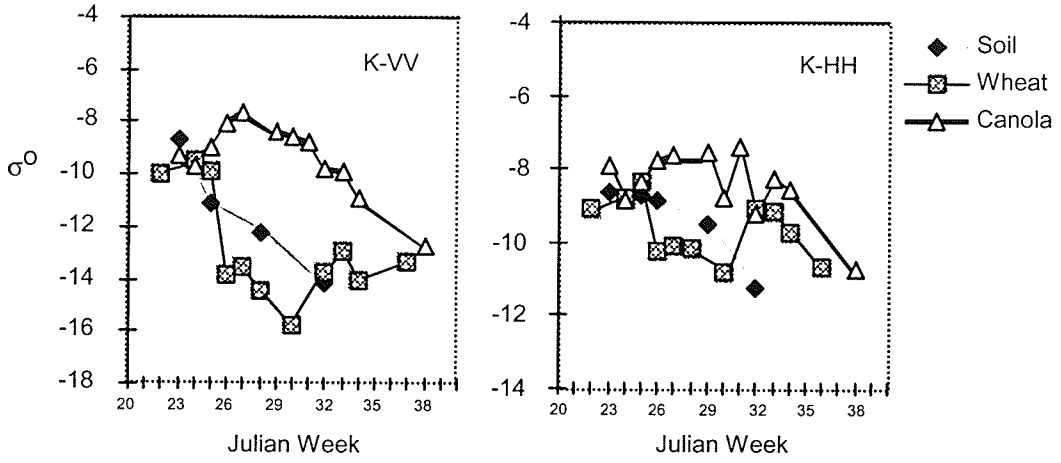

Figure 2.34 Temporal plots of canola, soil (summer fallow), and non-bearded wheat; 1.5 GHz (Adapted from Brisco et al., 1992).

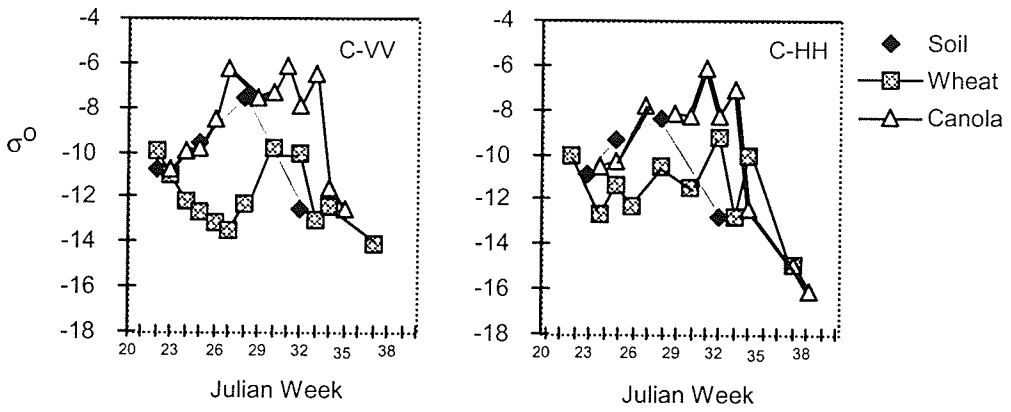

Figure 2.35 Temporal plots of canola, soil (summer fallow), and non-bearded wheat 5.17 GHz (Adapted from Brisco et al., 1992).

Skriver et al. (1999) examined the multi-temporal polarimetric C and L band signatures of a variety of crops including summer and winter rape (canola). Temporal data in this study was limited to four dates for winter rape. The winter rape data coincided with the rosette stage (10 cm height), the budding stage (60 cm height), the late bolting stage (73 cm height), and the ripening stage (fully podded, 150 cm height). Results showed that backscatter from winter rape was dominated by volume scattering from the canopy due to the large scatterers (leaves). The soil backscatter component at C-band (5.3 GHz) was absent whereas at L band some response from the soil surface was noted early in the season.

For winter wheat, observations coincided with early leaf development (10cm height), beginning of heading (60 cm height), end of flowering, and end of heading (>150 cm height). At L-band backscatter was dominated by surface scattering from early leaf development to the booting stage (Skriver et al., 1999). At C band, the early leaf stage was

dominated by surface scattering from the soil, whereas at the booting and to the end of head development, volume scattering dominated. The soil component therefore was negligible.

McNairn et al. (2002) examined RADARSAT-1 backscatter (C-HH) over wheat and canola, near Carman, Manitoba. RADARSAT backscatter over wheat was found to be highly correlated late in the season (July 29) to plant height ($r = -0.91$) , wet biomass ($r = -0.83$) and LAI ($r = -0.61$) and was positively correlated with plant water content ($r = 0.45$). When wet biomass, LAI and plant height were incorporated into a multiple regression model, the overall correlation was ($r = 0.91$) for July 29, the June 28 scene was also highly correlated ($r = 0.87$). Individual correlations with plant parameters on June 28 tended to be positive with the exception of plant water content which was negatively correlated. ($r = -0.51$). The negative correlations late in the season were attributed to change in wheat canopy structure due to heading, that is, there was greater attenuation within the higher biomass areas. It was suggested that change in geometry overrides the expected increases in backscatter with increased biomass, a typical response of higher frequency (X-band) microwave data (Ulaby et al. (1984); Le Toan et al. (1984); Bouman and van Kasteren, (1990)). Others have speculated that the inverse relationships are largely due to the underlying soil characteristics, that is, within low biomass areas backscatter response from a relatively wet soil is less attenuated and, therefore, higher (Cloutis et al., 1996; Taconet et al., 1994).

RADARSAT-1 backscatter from canola, on the other hand was not correlated to either leaf area index, wet biomass or plant water content from June 28 - July 29. The most significant correlations were with crop height ($r = 0.59 - 0.76$) on June 28 and July 5.

Results from a multivariate model incorporating one early and one late season, RADARSAT-1 scene, showed that crop height (r = 0.92), wet biomass (r = 0.89) and LAI (r = 0.86) were all highly correlated and were comparable to correlations derived from one late season multi-spectral SPOT scene. The canola data were poorly correlated. Plant height was the only significant variable for both the SPOT data (r = 0.69) and the RADARSAT-1 data (r = 0.59) (McNairn et al., 2002).

2.4.4 Factors Affecting Backscatter from Crop Canopies Independent of Crop Condition

Seasonal backscatter is not only a function of crop growth and development as expressed by canopy volumetric moisture and plant geometry, it is also a function of factors independent of crop condition.

Among the most profound effects are those induced by rainfall or dew events as they affect the dielectric properties of the canopy and the underlying soil. The presence of free water within the canopy can increase backscatter by 2-4 dB. Allen and Ulaby (1984) detected a 2-3 dB increase in backscatter over wheat, corn and soybean canopies after artificial spraying. Sofko et al. (1989) documented 2-4 dB increases in backscatter from wheat during a rainfall event. Like polarizations tended to be more sensitive than cross polarizations and longer wavelengths (L-band) had greater change than the shorter wavelength data (Ku-band). Dew events have a very similar effect on backscatter. Gillespie et al. (1990) reported a 2 to 4 (dB) increase in backscatter from wheat. The

increase in backscatter was most significant on the C-band HH data at $\theta = 20^{o}$. Wood et al., (2002) noted that RADARSAT-1 backscatter increased 1.7 to 2.5 dB as a result of dew.

Variations in soil background moisture from significant rain events days prior to a SAR acquisition can also increase canopy backscatter. The effects on backscatter are most significant at longer wavelengths (C, L-bands) and steeper incident angles. The effect is also dependent on crop type (canopy architecture) and biomass. For example, broad leaf crops and/or more dense canopies tend to exhibit a lower backscatter response to increased soil moisture (Brisco et al., 1993; Schullius and Furrer, 1992).

Management practices can affect backscatter independent of crop condition. Narrow row spacing (12.5 cm) increases percent cover. Backscatter from wheat with a narrow row spacing is higher early in the growing season and relatively lower at heading. Soil moisture effects on backscatter are small with a closed canopy and more pronounced with a larger row spacing (37.5 cm). Row spacing effects were on the order of 3 (dB) at $\theta = 20^{o}$, and 1.5 (dB) at $\theta = 50^{o}$. Row direction effects are significant (2-4 (dB)) when the radar look direction is perpendicular to row orientation. The increase in backscatter due to row direction varies depending on vegetative cover and incident angles (Batlivala and Ulaby, 1976; Ulaby and Bare, 1979)

Change in crop geometry can significantly affect backscatter. For instance, a strong wind can change the orientation of stems and ears. Bouman and van Kasteren (1990) noted that when stalks and ears for barley were oriented towards the radar backscatter decreased significantly (7 dB) at X-VV, and 2.5 dB at X-HH. What is surprising is that even the orientation of relatively dry standing stubble has an effect on microwave backscatter.

Stubble oriented toward the sensor has a lower backscatter response than stubble oriented away from the sensor (Bouman and Uenk, 1987).

2.4.5 Summary

Based on the work reviewed thus far, the following summary is provided regarding the characterization of the seasonal evolution of canopies using active microwave data.

- Canopy volumetric moisture (M_v) is highly related to seasonal backscatter as demonstrated by the cloud model (Ulaby and Bush, 1976; Attema and Ulaby 1978).
- Variants of the cloud model approach have been developed that incorporate multiple layers within the canopy, (heads vs. leaf layer), thus taking into account variations in the geometric characteristics of canopies (Hoekman, et al., 1982; Ulaby et al., 1984; Le Toan et al., 1984). These modifications to the model have helped in determining the nature of backscatter contributions as the crop evolves.
- Early and late season backscatter may have a significant backscatter component from the soil.
- The models have also shown that LAI can be substituted for volumetric moisture as the two parameters are highly correlated, but the correlations tend to be crop specific (Le Toan et al., 1984) with the added complication that leaf geometry can have a profound affect on backscatter for a given LAI.
- Paris (1986) showed that although water content of leaves was important in determining microwave backscatter, what was more significant was the

distribution of water as defined by the average green-leaf area of an average leaf and leaf density.

- Most of the early work has relied on microwave frequencies greater than 8 GHz, incident angles greater than 40° and VV polarizations to maximize canopy contribution to backscatter, especially as it relates to wheat canopies.
- Based on C-HH scatterometer data, Touré et al. (1994) suggest that the largest backscatter component over wheat is the direct ground component to canopy backscatter followed by the direct cover and ground_cover interactions which appeared to contribute equally. Based on a seasonal plot of the scatterometer data wheat LAI had no apparent effect on backscatter.
- Skriver et al. (1999) showed that C-band HH backscatter was dominated by surface scatter early in the season, with volume scattering dominating from booting to the end of heading.
- At L-band, the seasonal backscatter from the wheat canopy was dominated by a surface scattering component throughout the growing season.
- At C-HH canola backscatter has no discernable surface scattering component, volume scattering dominates throughout the season due to the large scatterers (leaves) (Skriver et al., 1999).
- The RADARSAT-1 (C-HH) results are promising in that LAI, wet biomass and crop height are correlated to backscatter from wheat, and highly correlated using two RADARSAT-1 acquisitions (early and late season). The correlations are comparable to that provided by a single late season SPOT scene (McNairn et al.,

2002). Correlations of backscatter vs. LAI, wet biomass and plant gravimetric moisture from canola were not significant.

- To-date no research has explicitly considered a detailed weekly physical representation of wheat or canola and how it relates to RADARSAT-1 backscatter.

2.5 Conclusions

This chapter has provided background with respect to the phenological development of wheat and canola including factors affecting crop growth and development. It was shown that soil moisture, soil fertility and air temperature have a profound effect on biomass accumulation and partitioning, and ultimately, on productivity. Whatever the source of stress within the growth cycle, the potential productivity of a canopy is expressed in the magnitude and duration of its green leaf area and biomass and its ability to absorb photosynthetic radiation and convert it into salable biomass.

With respect to optical remote sensing it was shown that red (0.62-0.70 μm), NIR (0.79-0.9 μm) and MIR (1.65 and 2.2 μm) reflectance is directly related to leaf area index (LAI), percent cover, dry and fresh biomass and chlorophyll content. It was shown that all of these parameters directly or indirectly estimate photosynthetically active phytomass . It was also shown that vegetation indicies (VIs) are effective in providing estimates of potential yield especially when they are integrated over time.

Microwave backscatter is closely linked to volumetric moisture within the canopy, canopy geometry and soil background characteristics, such as soil roughness and soil

volumetric moisture. Much of our understanding of microwave backscatter from agricultural crops has relied on scatterometer data using frequencies ≥ 8 GHz at VV polarization. Variants of the cloud model have shown that a multi-layer concept is important when modeling canopy backscatter. The multi-layer approach takes into account the changing geometry of a canopy (e.g., heads vs. leafy portion of the canopy). These studies have also shown that at a relatively low LAI (~0.5) soil background can be significantly attenuated, depending on frequency, incident angle and polarization. This result suggests a more detailed vertical characterization of canopies may be appropriate when modeling backscatter. One of the limitations of previous work has been the lack of appropriate coincident physical data (Ulaby et al., 1984; Toure' et al., 1994; Brisco et al., 1992), and / or an inadequate or unbalanced temporal sequence of EM data. (Skriver et al., 1999; Toure' et al., 1994).

These findings demonstrate that there is a need for a complete and detailed physical characterization of wheat and canola from emergence to harvest as it relates to the areal (m^2 m^{-2}) distribution of component parts of a canopy and the distribution of water ($gm \cdot cm^{-3}$) among the component parts of the canopy as a function of phenological stage. This type of parameterization is important as it relates to the microwave backscatter where size, location and density of component parts as well as their water content (diclectric properties) determine the nature of backscatter.

Previous work has also demonstrated a distinct lack of information regarding the seasonal backscatter characteristics of wheat and canola as observed by C-band HH, and RADARSAT-1 in particular.

Chapter 3: The Seasonal Active Microwave Backscatter of Wheat

3.1 Introduction

Most of what is known regarding the seasonal backscatter of microwave energy from wheat is based on scatterometer data. Generally, the imaging parameters in these studies were inconsistent with those of RADATSAT-1 (5.3GHz, HH) and the physical characterization of the canopy was either poor or incomplete. This chapter seeks to address both limitations by providing a detailed weekly physical characterization of wheat, and employing a new adaptive multi-layer volumetric model to examine the nature of RADARSAT-1 backscatter (Hochheim and Barber, 2003).

One of the most significant limitations with respect to the application of the cloud model to a wheat canopy is that the leaf portion of the canopy has typically been treated as a single layer throughout its phenological development. From Ulaby et al. (1984) and others it is known that the soil surface can be significantly attenuated by wheat early in the growing season (0.5 LAI) depending on wavelength, polarization and incident angle. Given the potential for attenuation of the soil surface with relatively small amounts of vegetation, it is reasonable to assume that as the canopy grows and develops, microwave energy may at certain phenological stages interact primarily with the upper portion of the canopy.

This chapter examines the use of weekly fine beam RADARSAT-1 data (5.3 GHz, HH pol) to monitor the seasonal growth and development of spring wheat (Glenlea variety) in southern Manitoba. A multi-layer characterization of the wheat is used to calculate the total

effective volumetric moisture (TMc) of the canopies which is correlated to the observed RADARSAT backscatter.

3.1.1 Objectives

The objectives of this chapter are two fold:

1) To provide a detailed temporal multi-layer characterization of three wheat canopies of varying biomass where component parts of the canopy (green leaves, stems and heads) per layer are measured for wet and dry biomass and leaf area (LA). Multiple layers within the leafy portion of the canopy (0-78 cm) are defined (in addition to the head layer) to examine attenuation within the canopy and of the underlying soil surface as a function of volumetric moisture.
2) To examine attenuation within the multi-layer canopy and correlate the total effective volumetric moisture (TMc) to RADARSAT-1 backscatter (σ^0 (dB)). A sensitivity analysis is conducted whereby extinction coefficients are manipulated to determine the nature of the observed backscatter, that is, which layers / components within the canopy contribute to the computed TMcs on any particular RADARSAT-1 pass.

3.2 Methods

3.2.1 Study Site

The study site is located in southern Manitoba in the Rural Municipality of Thompson (Township 5, Range 7). This site is at the foot of the Manitoba Escarpment which straddles two major physiographic subdivisions known as the Manitoba Plain (or Lowlands) and the Saskatchewan Plain (or the Western Uplands) (Michalyna et al. 1988). The soils within this area are typically very fine textured lacustrine deposits with localized glacio-fluvial (sandy) deposits. The terrain is generally flat and slopes gently towards the east (1-2°).

Using 1997 SPOT and yield monitor data, three intensive sample sites were selected (20x20m) within a spring wheat field (Glenlea variety) to represent low (Site 3 (S3)), medium (S2) and high biomass (S1) canopies (Figure 3.1).

3.2.2 Data Collection

3.2.2.1 RADARSAT-1 Data

RADARSAT-1 fine beam data were acquired at a 7-10 day intervals throughout the growing season (Table 3.1). RADARSAT-1 observations were limited to ascending

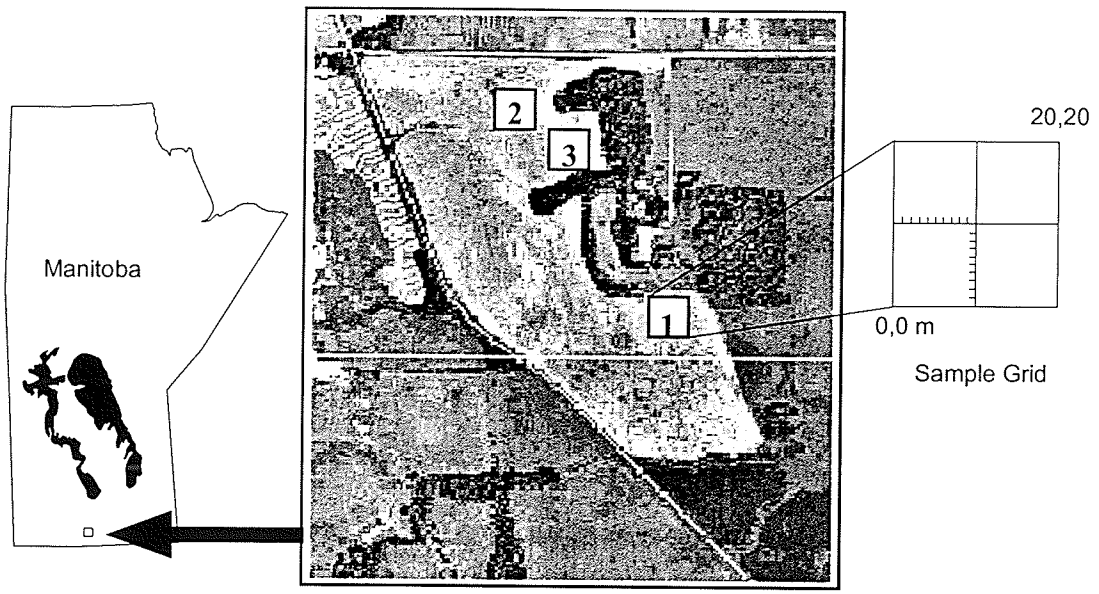

Figure 3. 1Sample locations (FLD_100-120).

passes so as to minimize environmental effects on backscatter, specifically those associated with early morning dew events.

The RADARSAT-1 data were calibrated to σ^{o} (dB) with an expected precision of the ± 0.5 dB. A 3x3 adaptive Lee Filter was used to reduce the coherent fading inherent with the single look fine beam data. Orthophotography, with site locations thematically embedded, were geometrically corrected to each RADARSAT-1 sub-scene. Mean σ^{o} statistics were extracted over sample locations using a 9x 9 window to ensure a statistically representative sample of the time series scattering.

Table 3.1 RADARSAT-1 Acquisitions, Miami MB. 1998.

Date	Year of Day	Beam	Incident Angle Range	Local Incident Angle
May-29	149	F5	45.39 - 47.82	46.12
Jun-5	156	F3	41.60 - 44.26	42.52
Jun-12	163	F1	36.93 - 40.13	38.27
Jun-23	173	F5	45.39 - 47.82	46.08
Jun-29	180	F3	41.60 - 44.26	42.64
Jul-4	187	F1	36.93 - 40.13	38.36
Jul-16	197	F5	45.39 - 47.82	46.18
Jul-23	204	F3	41.60 - 44.26	42.58
Jul-30	211	F1	36.93 - 40.13	38.25
Aug-9	221	F5	45.39 - 47.82	46.07

The weekly backscatter (σ^o) values were plotted for Sites 1-3. These curves were compared to the temporal biomass data collected at each site to detect the presence of "anomalous" backscatter observations resulting from environmental factors such as a precipitation. Rainfall events, not unlike dew events close to a RADARSAT-1 pass increase backscatter (due to a change in canopy/soil dielectrics) independent of crop condition, making correlations to physical canopy poor if not explicitly taken into account.

3.2.2.2 Ground Confirmation Data

The ground confirmation data consisted of biomass data, soils sample data and meteorological data obtained coincident with each RADARSAT-1 overpass.

Three biomass samples (replicates) were randomly selected per site. Plants samples were collected using a 0.5 m grid. Plants where removed intact so as to determine the

number of plants per sample and tillers per plant. Each replicate sample was bagged in the field and subsequently stored in a dark cold room (1.5^{o}C) until processing.

To assess the nature of observed backscatter from the canopy, biomass data were stratified at 26 cm intervals. The stratification interval was based on phenological development. At 0-26cm, height one (H1), the canopy was in the early vegetative (V) stage of development and biomass was dominated by leaves. At H2 (26-52 cm) the development of wheat is associated with stem elongation ending at the booting stage (B). H3and 4 (52-78; 78-104 cm) were associated with the various stages of heading (head emergence(H), anthesis (F), watery ripe (WR), soft dough (SD) and hard dough (HD)). Using this stratification scheme, component parts of the canopy (stems, brown leaves, green leaves and heads) were separated in the laboratory and processed to obtain wet and dry weights (gms), area (cm^2) and gravimetric moisture (gm), measurements per component part, per layer, per replicate, independent of their ultimate significance. The replicate data (three samples) were averaged on a per site basis.

Prior to the destructive processing of the biomass, nine plants per sample were measured for stem and tiller lengths, number of green and brown leaves per tiller, total plant height, height to head, head length, height to flag leaf, height to first green leaf (as measured from the base of the plant) and stem diameters at each height interval. These data were used to define the vertical space occupied by each component part of the canopy.

Three soil samples (two replicates per sample) were extracted per site at locations randomly selected for biomass extraction. Soil samples were extracted with a bulk density sampler at 1-4 and 4-7 cm depths. These data were used to calculate soil volumetric moisture (Ms) ($gm \cdot cm^{-3}$). The replicate data were averaged on a per site basis.

Meteorological data collected on site included air temperature, wind speed, wind direction and precipitation. Precipitation data were provided by a tipping bucket operated by the Prairie Farm Rehabilitation Agency (PFRA) at a site located 0.8 kms west of the wheat field. Leaf wetness sensors were also placed within the wheat canopy to collect data on the duration and magnitude of dew and rain events. All meteorological data were logged at 15 minute intervals throughout the growing season.

3.2.3 Data Analysis

Microwave backscatter is a function of volumetric moisture (Mv) within the vegetative canopy. Typically Mv is expressed as ($kg \cdot m^{-3}$ or $gm \cdot cm^{-3}$), where canopy volume is defined by $h/\cos(\theta)$ x area (m^2), (where h is canopy height) to take into account the viewing geometry (Figure 3.2).

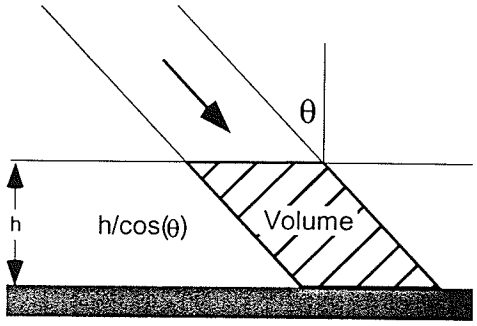

Figure 3.2 Viewing geometry.

Volumetric moistures within the canopy were calculated for each leaf layer and for the head layer. The maximum height of the green leaf (GL) layer per site was calculated using mean height (± 1SD). The layer occupied by heads was determined using equation [3.1].

$$H_{th} = (2(S.D.) + X_{hl}) / \cos(\theta) \quad [3.1]$$

Where:

H_{th} = head layer (cm)

S.D. = standard deviation of the measure height to head (cm).

X_{hl} = mean head length (cm)

An assumption is made that water within the canopy volume should be weighted by the normalized volume fraction of vegetation. This assumption recognizes that volumetric moisture is significant in terms of radar backscatter, but that its potential to interact with incident MW energy is also a function of its areal distribution or volume fraction.

The vegetative volume of green leaves (gl), heads (hd) and weeds (wd) were computed for each layer [3.2]

$$V_{gl,hd,wd} = A \times T_{gl,hd,wd} \quad [3.2]$$

Where:

V= vegetative volume

A = area (cm^2)

T = thickness (gl) = 0.02 cm

(hd) = 0.812 cm (S1-2); 0.75 cm (S3)

(wd) =0.02 cm

The volume fraction (VF) of each component was computed by dividing vegetative volume into the total volume per layer, taking into account variations in local incidence angle, per Day of Year (DOY) (Table 1). The volume fractions of leaves (VF_l), heads (VF_{hd}) and weeds (VF_{wd}) were normalized to the maximum seasonal value within the green leaf-weed component and head component per site ($NVF_{l, hd, wd}$).

The gravimetric moisture (gm) per component per layer was weighted by the normalized volume fraction ($NVF_{l,\ hd,\ wd}$) to yield the normalized volumetric moisture (nMv) for each canopy component.

The nMv's per layer including soil moisture (Ms) were integrated using equation [3.3] to compute the total effective volumetric moisture (TMc) for each day of RADARSAT-1 acquisitions.

$$TMc = nMv_m\ \psi^2_{i,j,k,l} + nMv_i\ \psi^2_{j,k,l} + nMv_j\ \psi^2_{k,l} + nMv_k\ \psi^2_l + nMv_l\ D\ \psi^2_{air} + Ms\ C\ \psi^2_{i,j,k,l} \quad [3.3]$$

where:

TMc = total effective volumetric moisture for canopy computed for a given Day of Year (DOY).
nMv = moisture per layer (gm) weighted by normalized volume fraction
where subscript :

i	= Green Leaves Height 1 (GLH1)
j	= GLH2
k	= GLH3
l	= Heads
m	= Weeds

Ms = Soil moisture ($gms \cdot cm^3$).
C = is a empirically derived constant to weight Ms; C=1000
ψ^2 = two way transmittance term = $\exp(-2*B*(nMv_l + nMv_j + nMv_k + nMv_lD))$
where:
B = is a empirically derived extinction coefficient e.g., (0.0038) (Figure 3.3)
D = is a empirically derived constant to weight Mv_l; D=0.45
$\psi^2_{air} = 1$

The S2 site was used to develop the model to compute daily TMc's. Weighting factors for heads (D) and soil (C) were empirically determined and then tested across all sites. The final weighting factors were universally applied (D = 0.45; C = 1000). A number of extinction coefficients (B) were used to provide a range of results for each site (Figure 3.3). A small extinction coefficient (B = 0.0001) simulated very high transmittance where all layers within the canopy (including soil) contributed significantly to the TMc.

These coefficients were progressively increased to simulate greater attenuation until some "optimum" was reached. In this context, 'optimum' was defined when the TMc profile matched the seasonal RADARSAT-1 backscatter profile.

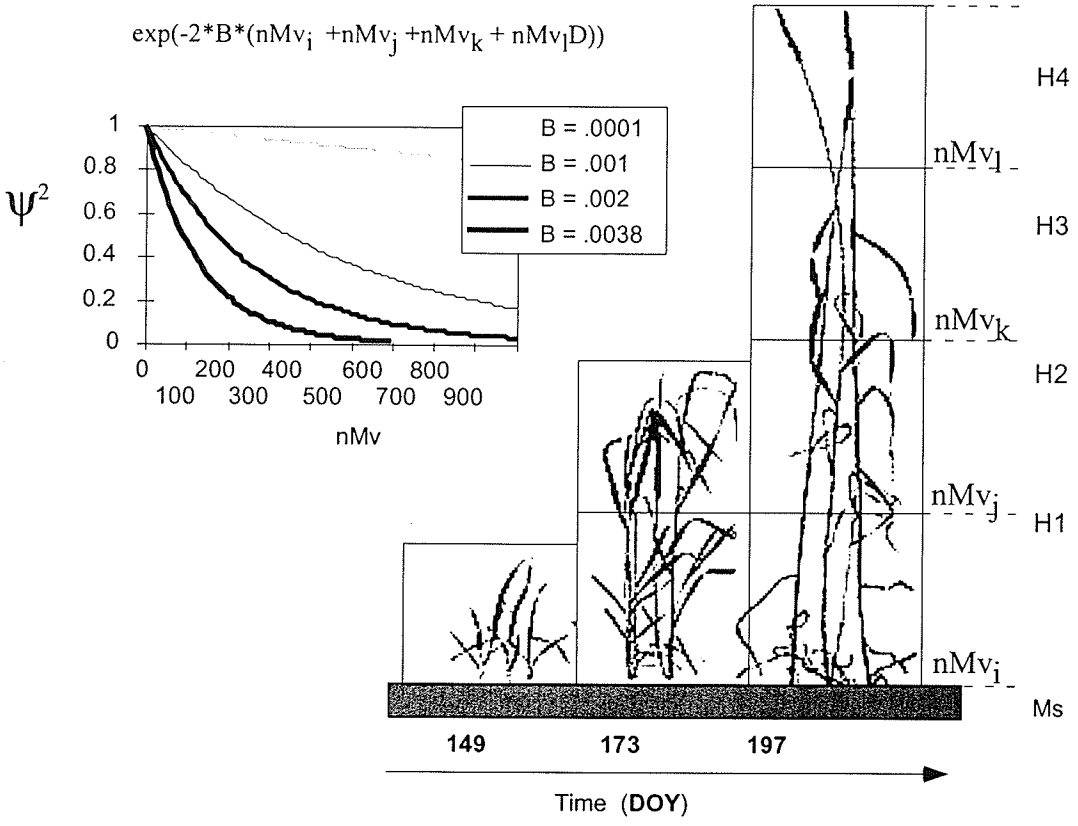

Figure 3.3 Crop canopy volumes and transmittance constants used to calculate TMc's.

To explore the relationship between the multi-layered physical/electrical data and the observed scattering a statistical sensitivity analysis was conducted in which various coefficients in the model were adjusted and the results observed through a series of regression analyses. For each extinction coefficient, RADARSAT-1 backscatter values were plotted with weekly TMc's per site. Plots showing the percent contribution of each layer to the TMc's are presented, and regression results of TMc's vs. σ^o(dB) per site are summarized in tables. This analysis framework allowed an exploration of the physical, electrical and scattering relationships as a function of spatial (layer) and temporal (date) characteristics of this system.

3.3 Results and Discussion

3.3.1 RADARSAT-1 Backscatter Profiles

Prior to examining the relationship between MW backscatter and physical properties of layered wheat canopies, the seasonal backscatter profiles of Sites 1-3 were reviewed to identify any obvious deviations in backscatter independent of crop condition.

The most notable deviations in backscatter occurred on Day of Year (DOY) 187. On this date a rainfall event occurred several hours before the RADARSAT-1 pass (Figure 3.4). The rainfall was significant enough to cause some minor temporary ponding of water on the soil surface, and a thorough wetting of the canopy. Based on previous work, precipitation or dew can increase canopy backscatter by 2-4 dB due to a significant change

in the canopy and/or soil surface dielectric properties (Sofko et al., 1989; Gillespie et al., 1990). Since the physical sampling of biomass and soil was completed before the rainfall event (for the wheat field), the physical data are representative of a "dry condition". Using regression relationships between observed backscatter and computed TMc's per site (excluding DOY 187), the predicted backscatter values for S1-3 on DOY 187 averaged 3.26 dB (S.D. 0.296) lower than the observed backscatter suggesting that the rainfall event increased backscatter by approximately 3 dB.

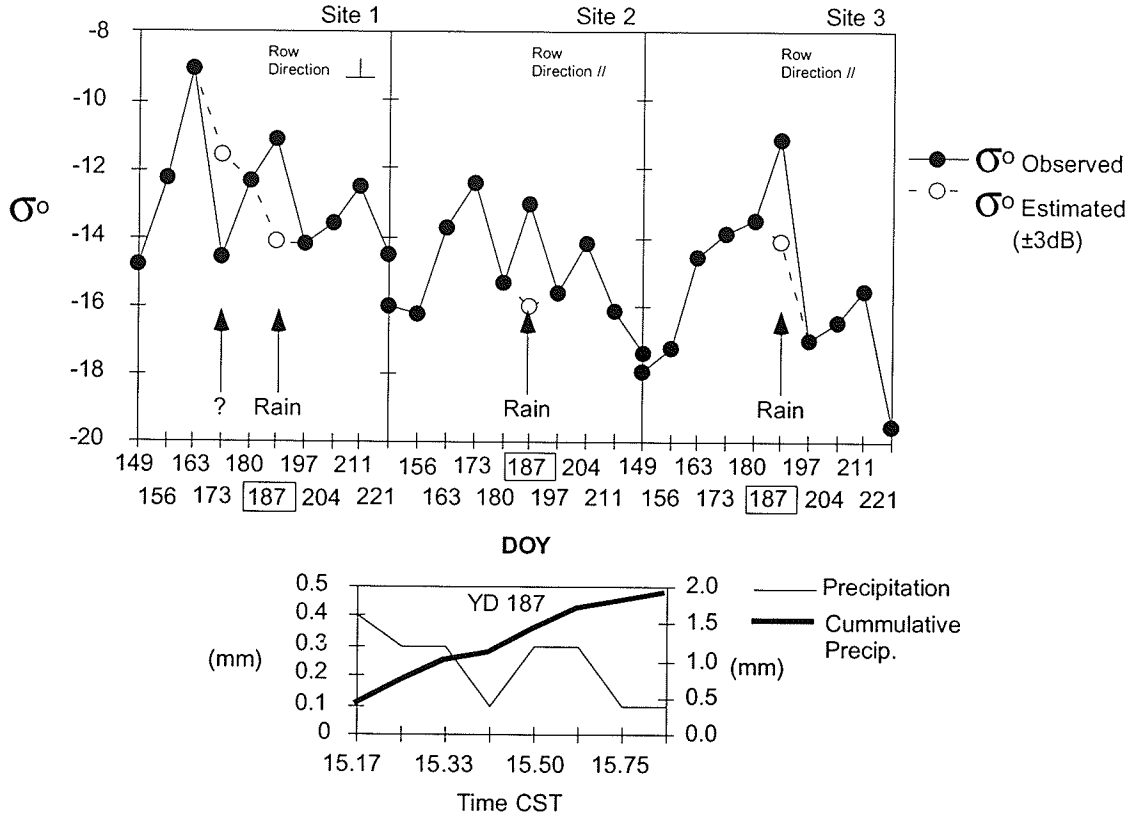

Figure 3.4 RADARSAT-1 backscatter vs. backscatter corrected for environmental effects, Sites 1-3.

A drop in backscatter occurred at Site 1 on DOY 173, one week before booting (row direction perpendicular (⊥)). Canopy height was 40 cm, tillering was at its maximum, and the canopy had not yet peaked in terms of green leaf area and biomass. This drop in backscatter was not observed at S2 and S3.

3.3.2 Physical Properties of Wheat

The seasonal evolution of the physical characteristics of the wheat canopy for Site 1-3 show the weekly mean area index ($m^2 \cdot m^{-2}$; vegetative area vs. soil area) and gravimetric moisture for each component part of the canopy (Figures 3.5 - 3.7). The RADARSAT-1 backscatter (σ^o) profile is included for illustrative purposes.

For S1-2 green leaves, heads and stems are major components of the canopy relative to senescent leaves and weeds (Figures 3.5 - 3.6). Both sites had a similar planting density (~200 plants m^2) and biomass. During the early part of the growing season green leaf area ($m^2 \cdot m^{-2}$) and green leaf moisture were related to canopy backscatter. For S2, green leaf area and moisture peaked at DOY 173, just as the canopy entered the booting stage (B) (Figure 3.5a). At S1 maximum green leaf area was attained at booting (DOY 180). Green leaf moisture remained relatively static through DOYs 163-180 but nevertheless peaked by DOY 180. The first brown leaves started to appear by DOY 163 at both sites. Senescent leaves dominated the leaf portion of the canopies by DOY 204. Both green leaf water and LAI decreased after booting at S1 and S2. By DOY 197, leaf gravimetric water content accounted for ~28% of canopy moisture (excluding stems), while heads accounted for 70% of canopy moisture. For both sites, head gravimetric moisture accounted for the secondary

peak in backscatter. Head moisture accounted for 92 percent of the canopy moisture (excluding stems) on DOY 221.

Maximum green leaf area for wheat at S3 (Figure 3.7a) was very low (<0.95 $m^2 \cdot m^{-2}$) compared to S1 and S2 (~3.0 $m^2 \cdot m^{-2}$). Weeds (green foxtail, (*Setaria viridis*)) covered

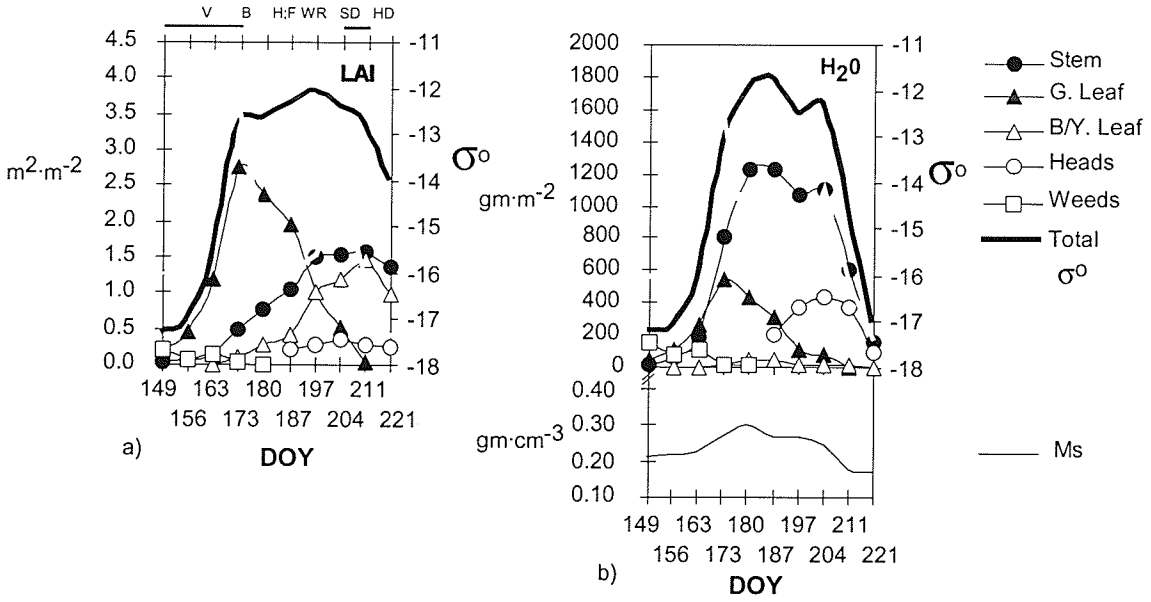

Figure 3.5 Site 2: a) Total mean area of each canopy component ($m^2 \cdot m^{-2}$); crop phenology along the upper x axis; b) Mean gravimetric moisture content ($gm \cdot m^{-2}$) per canopy component and soil moisture (Ms), ($gm \cdot cm^3$) for spring wheat.

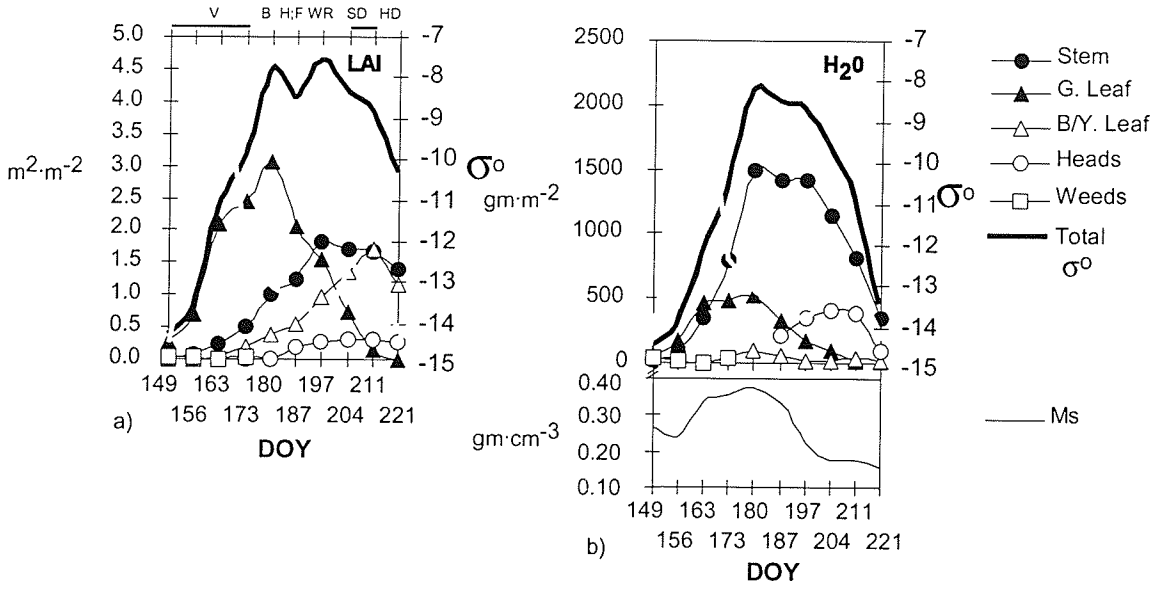

Figure 3.6 Site 1: a) Total mean area of each canopy component ($m^2 \cdot m^{-2}$); crop phenology along the upper x axis; b) Mean gravimetric moisture content ($gm \cdot m^{-2}$) per canopy component and soil moisture (Ms), ($gm \cdot cm^3$) for spring wheat.

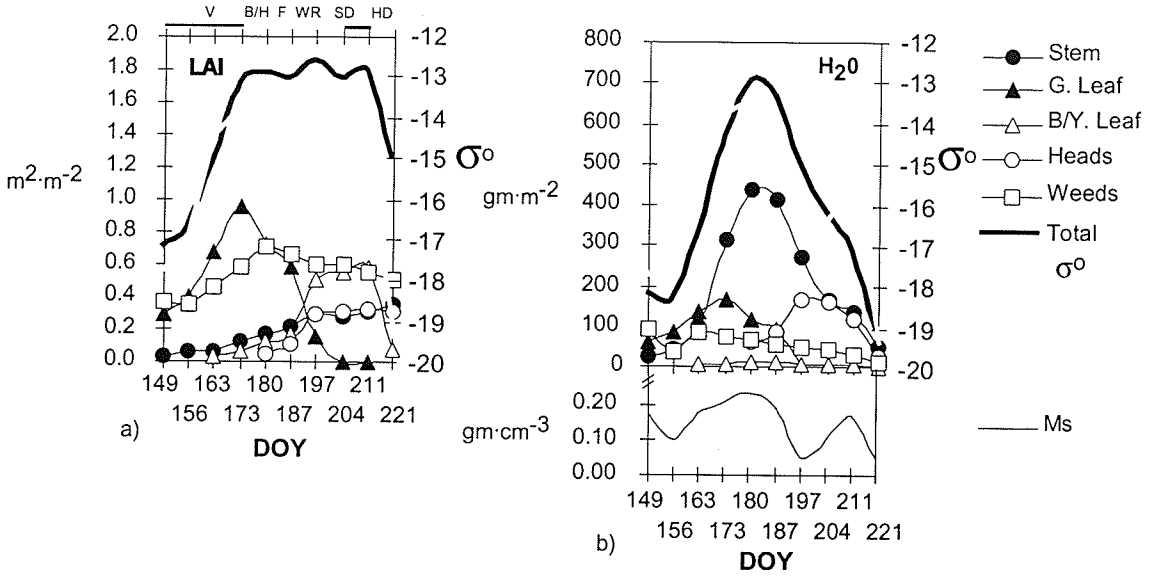

Figure 3.7 Site3 (Low Biomass): a) Total mean area of each canopy component ($m^2 \cdot m^{-2}$); crop phenology along the upper x axis; b) Mean gravimetric moisture content ($gm \cdot m^{-2}$) per canopy component and soil moisture (Ms), ($gm \cdot cm^3$) for spring wheat.

the site as a continuous mat (~5-15 cm high) throughout the growing season. This site typically had very low biomass due to its well drained, sandy soil.

In summary, the phenological development and scattering at these sites qualitatively show that: 1) early season green leaf area and moisture are significant in determining backscatter, and that peak (gravimetric) moisture and leaf area within the canopy do not necessarily coincide with peak backscatter (S1); 2) trends in soil moisture do not appear related to canopy backscatter for the bulk of the growing season, with the exception of the low biomass site (S3); and 3) stems dominate the canopy in terms of water content, yet have little or no bearing on the observed backscatter.

Based on the examination of the raw data, a number of decisions were made regarding the inclusion or exclusion of crop canopy parameters. Green leaves, heads and soil moisture would be used as inputs to calculate weekly TMc's for S1-3. Brown leaves were excluded due to their low moisture content and therefore low backscatter potential. Weeds were excluded at S1 and S2 as thistle density was very low and patchy, making a seasonal volumetric representation of this variable unreliable. Due to an early season application of herbicide, thistles were effectively eliminated by DOY 173. Weeds at S3 were included in the weekly computation of TMc's due to their dominance, and uniform distribution. Wheat stems were excluded from further analysis (S1-3) as they had little apparent effect on backscatter despite their high moisture content. The lack of MW interaction with stems is likely a function of: 1) stem geometry, i.e., stems are vertical and narrow (2-3.5 mm, very low LAI) and are likely therefore to have minimal interaction with incident MW energy given RADARSAT-1's imaging parameters (λ = 5.6 cm, HH); and 2)

stems are surrounded by leaves, therefore any direct interaction with incident MW energy is further minimized. The exclusion of stems at VV polarization would likely have been inappropriate given the greater potential for interaction.

3.3.2.1 Wheat as a Multi-layer Medium

A multi-layer representation of wheat is provided for each survey site (Figure 3.8). The canopy components used to characterize the wheat canopy include green leaves, heads and soil moisture. Parameters used to describe each component include area index ($m^2 \cdot m^{-2}$), gravimetric moisture, NVF, and volumetric moisture.

Though S1 and S2 are comparable, the seasonal evolution of each canopy differs. At S2 leaf area and water are more evenly distributed among the layers early in the season whereas S1 has a pronounced peak early in the season (DOY 163) when the canopy height was approximately 26 cm. S1-2 maximum green LAI per layer was 1.5 (m^2/m^2). In contrast, S3 had a maximum green LAI <0.68 for H1 and <0.28 for H2. Weed leaf area dominated S3 during most of the season. Senescence of leaves within each layer was quite evident (Figure 3.8a). Leaves were fully senesced two to three weeks following peak green LAI per layer.

Green leaf water content was highly related to green leaf area on a per layer basis. The results also show that relationships between these two parameters changed significantly over the vertical profile of the canopy. This was particularly evident for S1 and S2, which were high biomass sites (Figure 3.9 a and b, and Table 3.2).

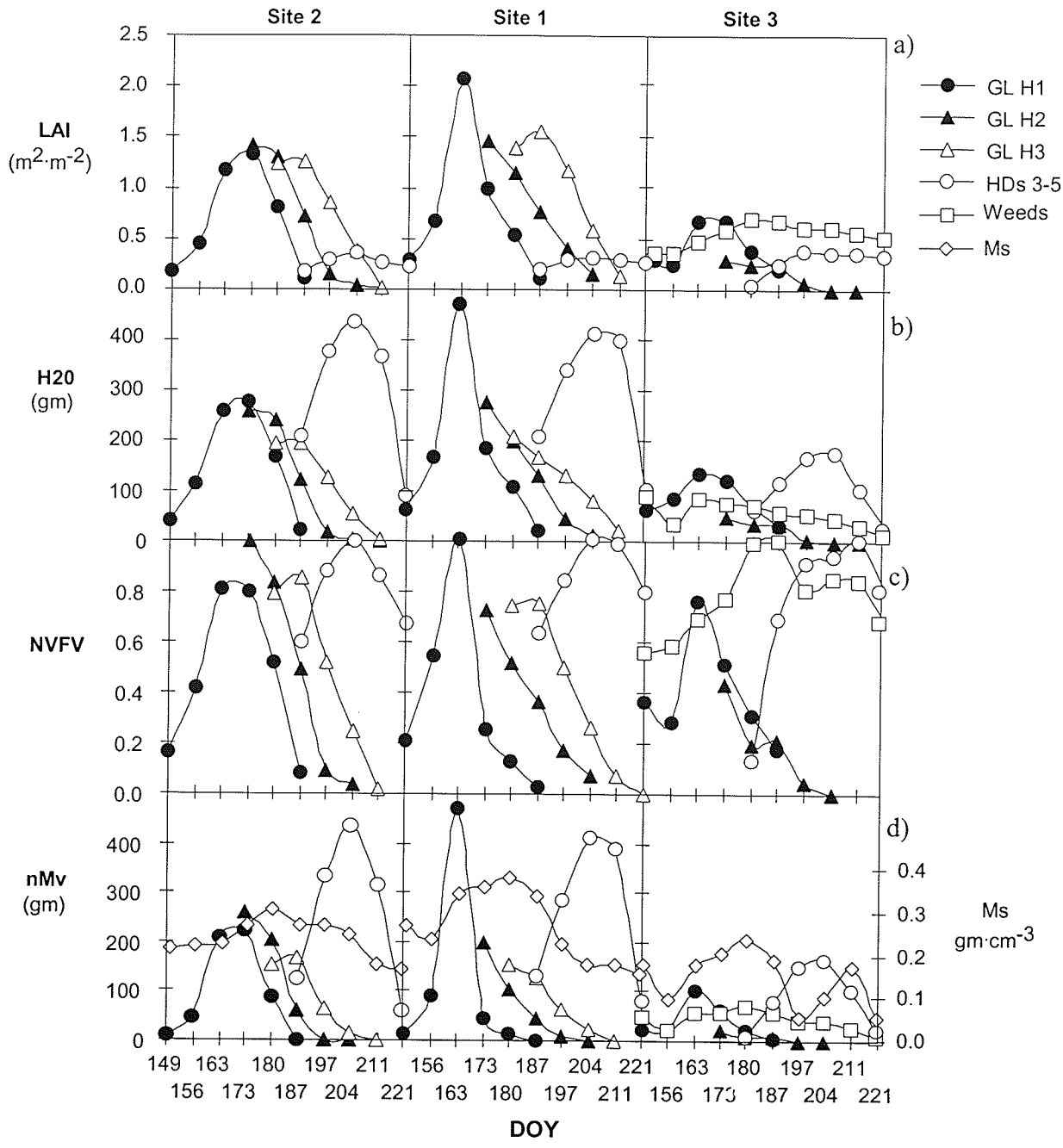

Figure 3.8 A multi-layer representation of wheat for Sites 1-3, a) area of green leaves and heads ($m^2 \cdot m^{-2}$) per layer, b) gravimetric water content of green leaves and heads per layer, c) normalized volume fraction (NVFV) of leaves and heads, d) water content weighted by NVFV per layer.

For example, at S2 for a given gravimetric moisture per leaf layer (e.g., 200 gm.), H3 (the upper layer) had 37% more green leaf area and H2 had 17% more green leaf area relative to H1. The fraction of water per leaf volume (cm^3) is therefore lower within the upper canopy (Figure 3.9b) suggesting that the upper leaves have a lower dielectric constant.

Leaf moisture generally peaked around DOY 163-180 and declined rapidly after heading (DOY 187). By DOY 211 leaves had fully senesced. Head gravimetric moisture was bell-shaped and peaked around the soft dough stage (DOY 204). Heads remained the most significant moisture component within the canopy to DOY 221 (Figure 3.8b).

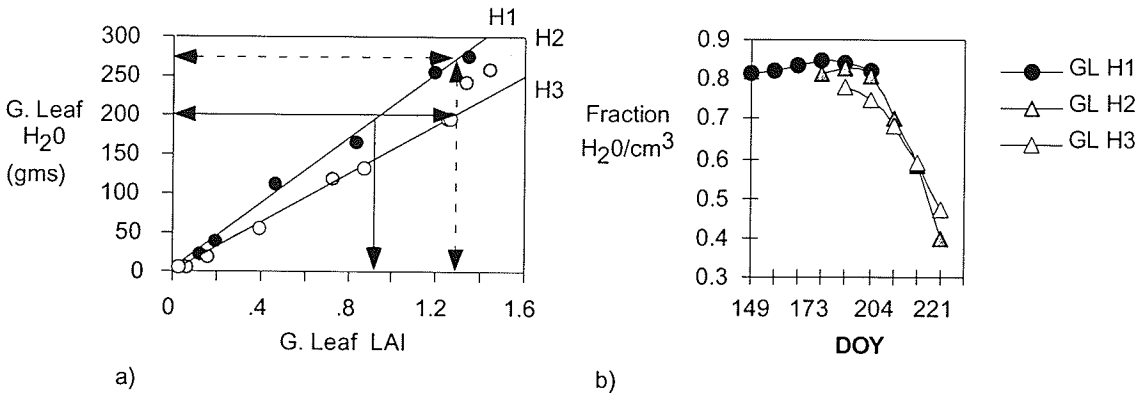

Figure 3.9 a) Green leaf area vs. moisture content per canopy layer (H3=upper layer), b) Fraction of water per cm^3 of wet green leaf biomass for spring wheat.

Table 3.2 Regression coefficients of green leaf area vs. green leaf moisture content for spring wheat, Sites 1-2.

Site	Canopy Layer	Regression Coefficients	Adj. r^2
2	H1	Y = 3.86 + 207.98 * X	0.99
2	H2	Y = -6.37 + 185.63 * X	0.99
2	H3	Y = -4.07 + 157.09 * X	0.97
1	H1	Y = -7.384 + 225.559 * X	0.99
1	H2	Y = -26.385 + 202.916 * X	0.99
1	H3	Y = -4.769 + 145.904 * X	0.96

The volumetric data used for input into the model, are presented in Figure 3.8d. The peak volumetric moisture in each leaf layer is followed by a rapid decrease, which generally occurred over a 2-week period. Volumetric moisture in green leaves was low late in the growing season (DOY 197-221) suggesting that backscatter from the canopy is largely related to the heads.

The volumetric soil moisture for all three sites peaked around DOY 180 (note, soil sampling DOY187 was completed before the rain event). The soils at S1 and S2 consisted of heavy clays. Site 1, located in a slightly lower portion of the field, tended to have the highest volumetric moisture, while Site 3, characterized by sandy soil, had the lowest volumetric moisture.

3.3.3 RADARSAT-1 Backscatter vs. TMc

The total effective volumetric moisture (TMc) was computed for each site using a range of extinction coefficients and correlated to the observed backscatter. A statistical

exploration of the layers versus scattering was conducted using a variety of conditions (Tables 3.3 - 3.5). Regression results are presented where: 1) backscatter data affected by factors external to crop condition (e.g., wind, rain) are excluded, designated (-ENV); 2) where the environmentally affected backscatter values are substituted with the predicted backscatter values (+/- 3dB) designated (^ENV) and 3) where all observed backscatter data are included (designated OBS). Discussion of results are restricted to the (-ENV) data unless otherwise stated.

For Site 2, at low extinction (B=0.0001), the total contributions from the various layers within the canopy are high and the overall correlations between σ^o and the computed TMc's are low (Figure 3.10 and Table 3.3; $r^2 = 0.46$, RMSE = 1.19 dB). In this scenario, the TMc of the canopy is grossly overestimated particularly for DOYs 173 - 197. As the extinction coefficient was increased to simulate higher attenuation, the TMc's become more strongly correlated to the observed backscatter (Table 3). The best correlation between TMc vs. σ^0 was achieved with B= 0.0038 (($r^2 = 0.97$; RMSE = 0.27 dB).

Based on the model result (B=0.0038), S2 early season (DOY 149-156) backscatter is largely due to the soil background (Ms), and thereafter largely attributed to the volumetric moisture within the upper layers of the wheat canopy. Green leaves dominated the TMc by DOY 163 (green leaf LAI = 1.19). Soil background contributions are almost totally attenuated in DOYs 173-180 (LAI 2.7; 2.3). At heading, the leaf portion of the canopy was still a significant factor although by the following week (DOY 197), the volumetric moisture within the head layer accounted for >70% of the TMc. On DOY 197, green leaf volumetric moisture was very low (Figure 3.8d). At hard dough (DOY 221) soil background dominated the TMc (>80%).

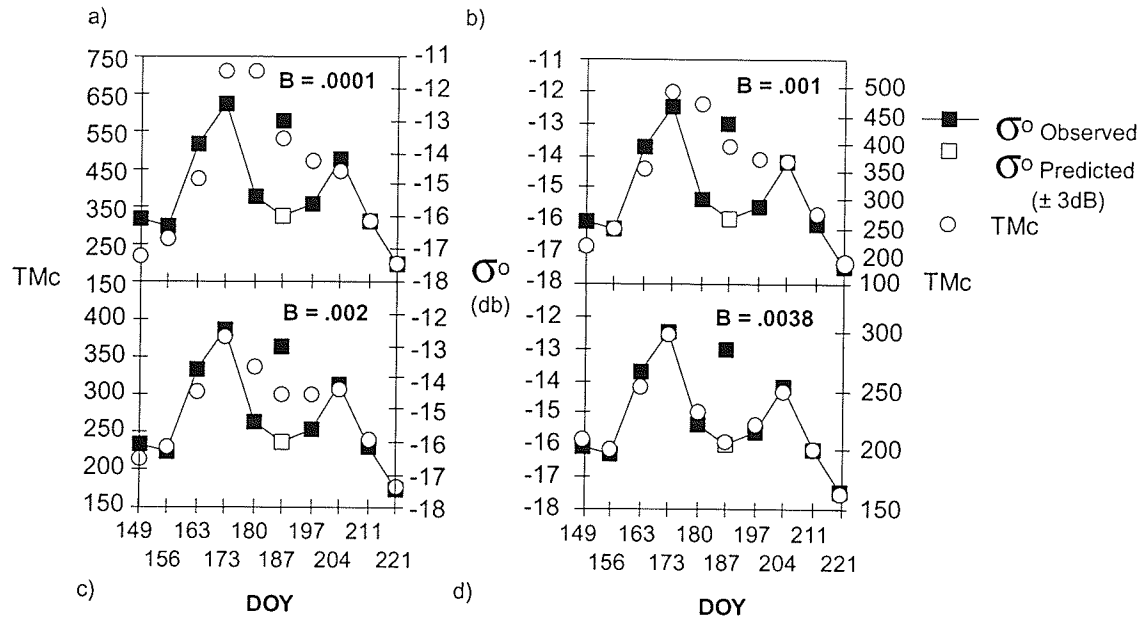

Figure 3.10 Site 2, RADARSAT-1 backscatter of spring wheat vs. the total effective volumetric canopy moisture (TMc) for spring wheat using attenuation constants, a) B = 0.0001 (high transmittance), b) B = 0.001, c) B = 0.002 and d) B = 0.0038 (low transmittance).

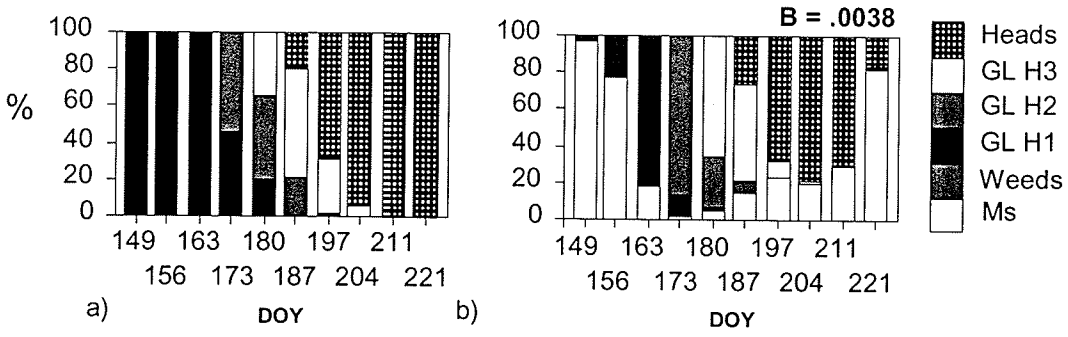

Figure 3.11 Site 2, a) Percent distribution of total volumetric moisture within the for spring wheat canopy excluding soil, b) Percent contribution of layers to the computed TMc's as a function of extinction coefficient (B = 0.0038) with the soil component.

Table 3.3 Correlations between TMc vs. σ^o (dB) for spring wheat, Site 2. Row direction parallel (//) to incident MW radiation.

Ψ Constant (B)		Regression Coefficients	Adj. r^2	RMSE (dB)	P-Value**
0.0001	*(-ENV)	Y = -17.671 + 0.006 • X	0.46	1.19	0.0194
0.001	(-ENV)	Y = -19.063 + 0.012 • X	0.55	1.10	0.0082
0.002	(-ENV)	Y = -20.877 + 0.020 • X	0.73	0.79	0.0020
0.0038	(-ENV)	Y = -23.988 + 0.039 • X	0.97	0.27	< 0.0001
	^ ENV	Y = -24.007 + 0.039 • X	0.97	0.26	< 0.0001
	OBS	Y = -22.800 + 0.035 • X	0.65	1.01	0.0050

*(-ENV) -DOY 187; ** P-Values > 0.05 indicate no significance

The seasonal correlation between σ^0 and Ms was not significant at the 95% probability level ($r^2 = 0.12$).

S1 results are summarized in Figures 3.12-3.13 and Table 3.4. Recall that S1 is a high biomass site with its row direction perpendicular to the incident MW radiation. The results are very similar to that of S2 with the correlations improving as the extinction coefficient was increased to B = 0.0038 (r^2 = 0.70). Early season TMc's (DOY 149 and 156) are poorly correlated with backscatter, the remaining observations are highly correlated (r^2 = 0.98, RMSE = 0.29 dB (^ENV)). The poor correlations may in part be due to row direction effects. When the row direction is perpendicular to the incident MW energy, the inter-row (soil) surface has a smaller cross section relative to the canopy. In contrast, if the row direction is parallel, the soil contribution should be more significant especially early in the season (Batlivala and Ulaby, 1976). When the soil weighting at S1 is reduced (C = 600), the correlation increases to r^2 = 0.76 (RMSE = 1.10; Table 3.4).

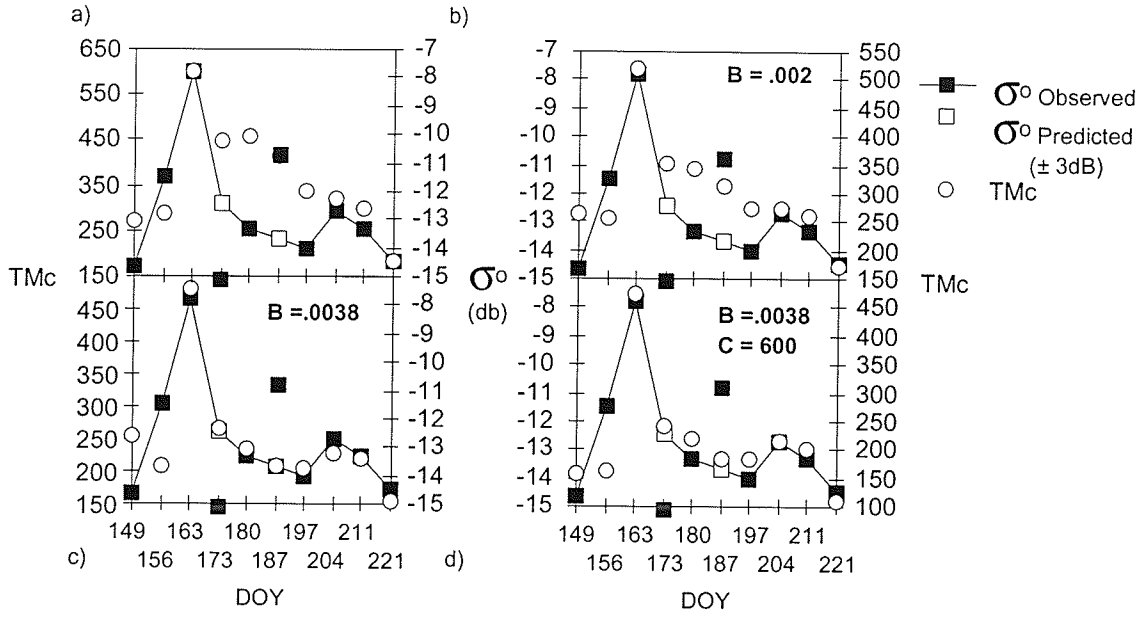

Figure 3.12. Site 1, RADARSAT-1 backscatter from spring wheat vs. (TMc) using attenuation constants a) B = 0.0001 (high transmittance), b) B = 0.001, c) B = 0.002 and d) B = 0.0038 (low transmittance).

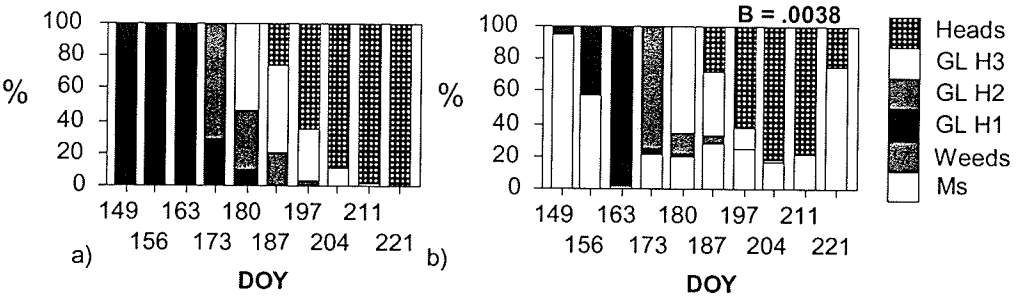

Figure 3.13. Site 1. a) Percent distribution of total volumetric moisture within the spring wheat canopy excluding soil, b) Percent contribution of layers to the computed TMc's as a function of extinction coefficient (B = 0.0038).

Note that DOY 156 backscatter remains low despite a relatively high TMc (Figure 3.12). If DOY 156 is omitted the correlation increases to $r^2 = 0.96$ (RMSE = 0.46, Table 3.4).

The model provided a good characterization of the seasonal backscatter for the remaining observations DOY (163-221) at S1. The volumetric moisture within the upper

canopy was the most significant component of the daily TMc's for DOYs 163 -211. Heads dominated the TMc for DOYs 197-211. The green leaf volumetric moisture that remained,

Table 3.4. Correlation's between TM_c vs. σ^0 (dB) for spring wheat, Site 1. Row direction perpendicular ($\perp$) to incident MW radiation.

Ψ Constant (B)	Soil Constant (C)	Regression Coefficients	Adj. r^2	RMSE (dB)	P-Value**
0.0001 (-ENV)*	1000	Y = -16.160 + .008 • X	0.45		0.0403
0.001 (-ENV)	1000	Y = -17.274 + .013 • X	0.61	1.50	0.0226
0.002 (-ENV)	1000	Y = -18.107 + .018 • X	0.67	1.28	0.0082
0.0038 (-ENV)	1000	Y = -17.564 + .020 • X	0.70	1.20	0.0059
0.0038 (-ENV)	600	Y = -16.505 + .018 • X	0.76	1.10	0.0031
^ ENV***		Y = -16.583 + .018 • X	0.76	1.03	0.0013
-ENV (-DOY 156)		Y = -17.227 + .020 • X	0.96	0.46	<0.0001
^ ENV (-DOY 156)		Y = -17.241 + .020 • X	0.96	0.42	<0.0001
OBS		Y = -16.084 + .017 • X	0.61	1.28	0.0045

*DOY 173 and 187 omitted.
** P-Values > 0.05 indicate no significance.
*** DOY 187 estimated (-3 dB)

was largely attenuated by the head layer (Figure 3.13). Early in the season (DOY 149-156), the soil portion of the TMc dominated. The same is true as heads begin to dry down. The seasonal correlation between σ^0 and Ms is not significant at the 95% probability level ($r^2 = 0.01$).

The wheat canopy at Site 3 had one third the green leaf area and biomass compared to S1 and S2. At S3, the model had problems with DOY 149 (Figures 3.14 - 3.15 and Table 3.5). The ground confirmation data and consequently the model, suggested relatively high volumetric moistures for both the soil and weeds. Including DOY 149, the correlations tended to decline as the extinction coefficient (B) was increased to simulate higher attenuation; the highest correlations were obtained using B=0.0001, (r^2 = 0.78; RMSE =

0.94). Excluding DOY 149 significantly improved all of the model results; r^2 = 0.95-0.97, (Table 3.5)

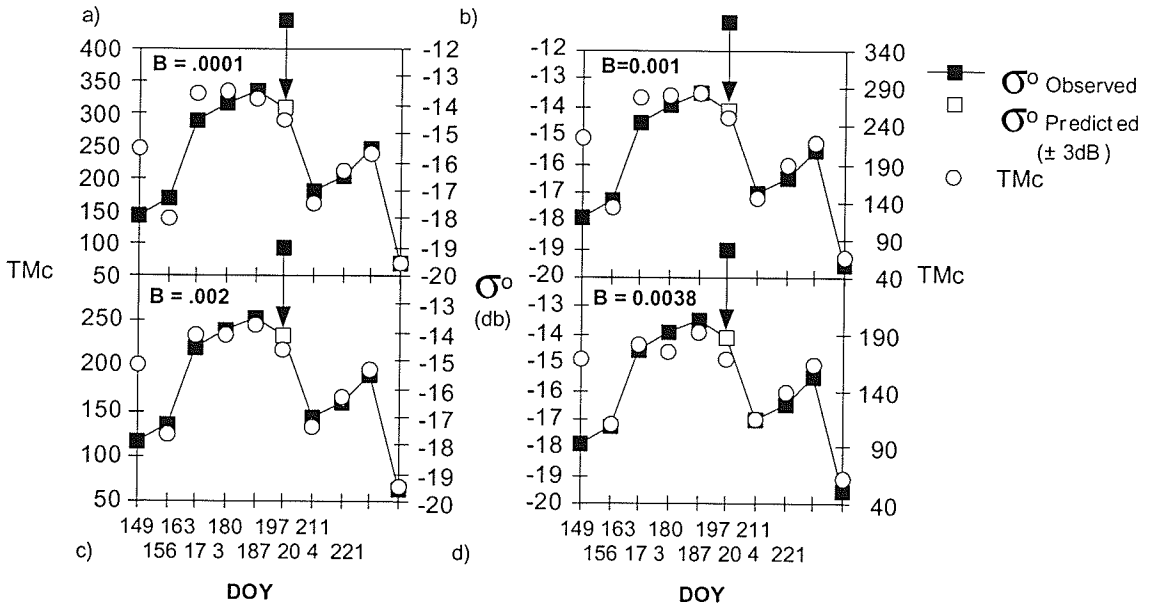

Figure 3.14 Site 3, RADARSAT-1 backscatter vs. (TMc) for spring wheat using attenuation constants a) B=0.0001 (high transmittance), b) B = 0.001, c) B = 0.002 and d) B = 0.0038 (low transmittance).

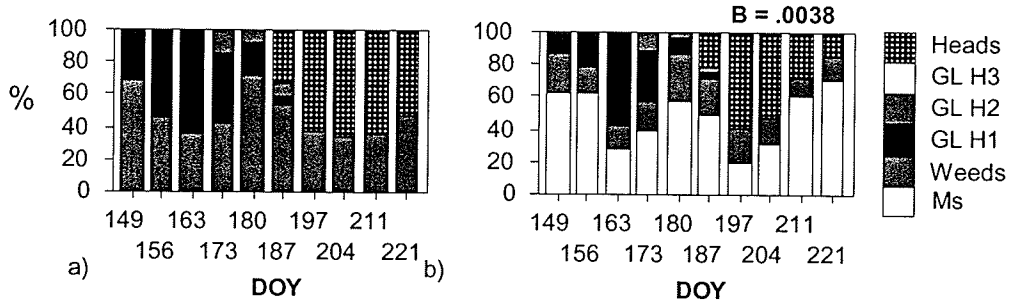

Figure 3.15. Site 3. a) Percent distribution of total volumetric moisture within the spring wheat canopy excluding soil, b) Percent contribution of layers to the computed TMc's as a function of extinction coefficient (B = 0.0038).

Table 3.5 Correlations between TMc vs. σ^o (dB), Site 3. Row direction parallel (//) to incident MW radiation.

Ψ Constant (B)	Regression Coefficients	Adj. r^2	RMSE (dB)	P-Value**
0.0001 (-ENV)	Y = -20.599 + .019 • X	0.78	0.94	0.001
(-ENV), -DOY 149	Y = -20.448 + .020 • X	0.95	0.46	<0.000
0.001 (-ENV)	Y = -20.915 + .023 • X	0.76	0.97	0.001
(-ENV), -DOY 149	Y = -20.889 + .025 • X	0.97	0.37	<0.000
0.002 (-ENV)	Y = -21.300 + .029 • X	0.73	1.02	0.002
(-ENV), -DOY 149	Y = -20.889 + .025 • X	0.97	0.32	<0.000
0.0038 (-ENV)	Y = -21.040 + .041 • X	0.67	1.15	0.004
-ENV (-DOY 149)	Y = -21.040 + .041 • X	0.96	0.41	<0.000
0.0038 ^ ENV	Y = -22.087 + .041 • X	0.67	1.13	0.002
^ ENV (-DOY 149)	Y = -22.433 + .046 • X	0.95	0.45	<0.000
OBS	Y = -22.424 + .046 • X	0.51	1.73	0.012

** P-Values > 0.05 indicate no significance

Due to the low vegetation cover, the results for S3 were relatively invariant with the extinction coefficients (-DOY 149). This was largely due to the predominance of the soil contribution to the TMc (Figure 3.15). When the model inputs were independently examined, it became evident that both soil and weed volumetric moisture were highly related to the observed backscatter (r^2 = 0.86 and r^2 = 0.80 respectively, excluding DOY 149 B=0.002). When these two parameters were included in the model, correlations improved, r^2 = 0.93 (RMSE = 0.51; B = 0.002). Changing the inputs to include only the wheat canopy (leaves and heads) resulted in a very poor correlation (r^2 = 0.07, RMSE = 1.9). When the soil component was combined with wheat components, the correlation once again improved (r^2 = 0.95, RMSE = 0.43). Integrating all of the model's inputs resulted in the highest observed correlation, r^2 = 0.97 (B = 0.002). The correlations for B=0.0038 were

marginally poorer, suggesting that a smaller extinction coefficient for a low biomass site was more appropriate.

The regression results for S1-3 (C =1000, B=0.0038, ^ENV) show row direction effects where the slope of the regression line for S1 (⊥) differs significantly compared to S2-3 where row direction is oriented parallel (//) to the incident radiation (Figure 3.16).

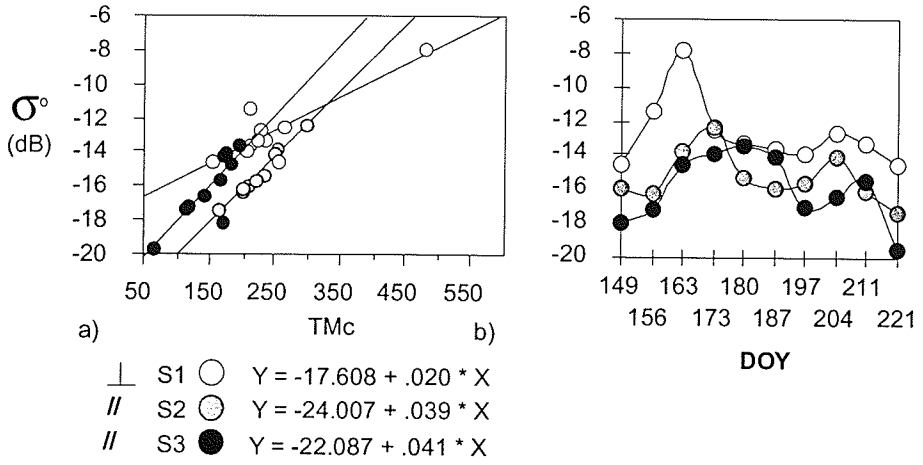

Figure 3.16 a) Regression plots for S1-3 using constants (C=1000, B=0.0038), b) RADARSAT-1 backscatter for S1-3.

Early season differences in backscatter due to row direction for S1 and S2 equalled ~3.5 dB (at TMc = 150). The difference is reduced to 0.64 dB at a TMc 300. S2 and S3 slopes are similar due to row direction, but offset due to variations in biomass, and TMc. The backscatter for sites S1 and S2 is similar for the bulk of the season (DOY 180-221) when the row effect is taken into account (Figure 16a-b). The backscatter from S3 (low biomass) is comparable to that of S1 and S2 and even exceeds it for DOY 180-187 when row direction is taken into account for S1. Early in the season (DOY 149) and late in the season (DOY 197-204, 221) S3 can be differentiated from S1-2. Early season differences appear to

be related to variations in soil moisture. Late season differences are largely attributed to head volumetric moisture and soil moisture.

3.4 Conclusions

Results show clear relationships between the physical characteristics of a wheat canopy and the time series RADARSAT-1 (fine beam) backscatter. The detailed physical representation of the canopy provided a unique opportunity to explore the nature of temporal backscatter from RADARSAT-1.

The physical time series data showed there was a clear bimodal distribution of water within the canopy associated with green leaves early in the season and heads late in the season. The data also show that the peak seasonal gravimetric and volumetric moisture within the canopy did not necessarily coincide with peak backscatter. Examination of the physical data supported the premise that successful characterization of a wheat canopy using the cloud model assumptions necessitates a multi-layer representation of the canopy. This multi-layer system should include stratification of the leaf layer especially during periods of peak green LAI and canopy volumetric moisture.

Through manipulation of the extinction coefficient (B), it was demonstrated that a high extinction coefficient within a multi-layer scheme mimicked the observed backscatter and was internally consistent for both low and high biomass sites. Backscatter appeared to respond to the volumetric moisture within the upper layers of the canopy, with the exception of low biomass sites where soil volumetric moisture played a dominant role.

Since backscatter is not necessarily indicative of total volumetric moisture within the canopy (due to attenuation), it may point to a potential limitation of using MW data to detect variations in biomass within a field. It is also evident that row direction plays a significant role in the seasonal representation of backscatter. Both of these issues require further work to clarify the conditions which may confuse geophysical inversion algorithms.

The results demonstrate that the multi-layer volumetric model effectively mimics the observed RADARSAT-1 backscatter, and it is useful for determining the nature of backscatter. In the next Chapter, the same volumetric model will be adapted to examine the nature of canola backscatter.

Chapter 4: The Seasonal Backscatter of Canola as Observed by Radarsat-1

4.1 Introduction

Whereas Chapter 3 examined the weekly backscatter (σ^o (dB)) of Radarsat-1 from spring wheat, Chapter 4 examines the weekly backscatter from canola (*Brassica napus*). A modified version of the multi-layer volumetric moisture model is used to calculate the weekly total effective volumetric moisture (TMc) of canola; the computed TMc's are correlated to the observed backscatter (Hochheim and Barber, 2003).

4.1.1 Objectives

The objectives of this chapter are twofold:

1) To provide a detailed physical representation of canola canopies of varying biomass at 7-10 day intervals throughout the growing season (from seedling to maturity) coincident with RADARSAT-1 data (5.3 GHz, HH pol.). The physical representation of the canopy is examined in terms of gravimetric moisture, area ($m^2 \cdot m^{-2}$) and normalized volumetric moisture (nMv) of each component part of the canopy, vertically stratified at 30 cm intervals.
2) To develop an appropriate volumetric moisture model in order to compute total effective volumetric moisture (TMc) and correlate it to the observed

RADARSAT-1 backscatter (σ^0 (dB)). The model results were used to assess the nature of the observed backscatter and which layers/components within the canopy contribute to the computed TMc on a given RADARSAT-1 pass.

4.2 Methods

4.2.1 Study Site

The study site was located about 1.6kms north of the spring wheat field (Chapter 3) located in the Rural Municipality of Thompson (Township 5, Range 7), (Figure 4.1).

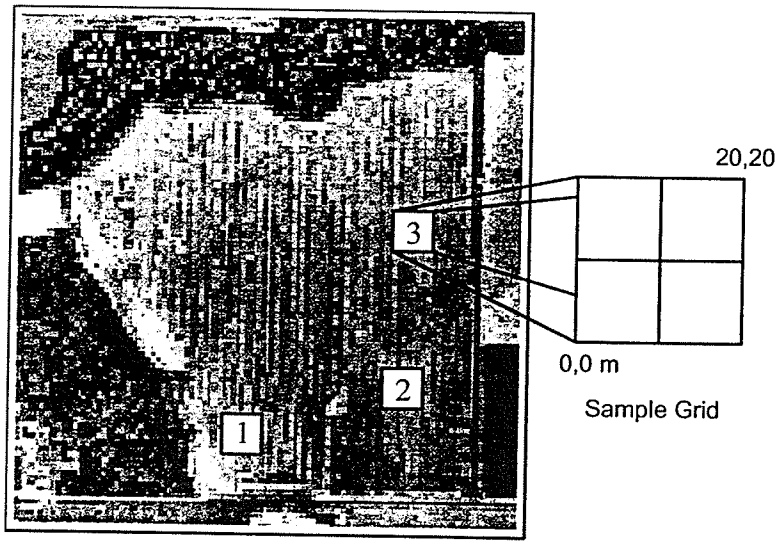

Figure 4. 1 Sample site map, canola field , 1998 (FLD_1).

Using August 1997 SPOT data and yield monitor data, three intensive sample sites were selected (20x20m) within a canola field (*Brassica napus*, Liberty Link) to represent low Site 1 (S1), medium (S2) and high biomass (S3) canopies.

4.2.2 Data Collection

4.2.2.1 Ground Confirmation Data

The ground confirmation data consisted of biomass and soil moisture data obtained coincident with each RADARSAT-1 overpass. Three biomass samples (replicates) were randomly selected per site. Plant samples were collected using a 0.5m grid. Each replicate sample was bagged in the field and subsequently stored in a dark, cold room (1.5^{o}C) until processing.

To assess the nature of the observed backscatter from the canopy, the biomass data were stratified at 30 cm intervals. The stratification interval was loosely based on phenological development. The first 30 cm interval (H1) coincided with the seedling (S) to rosette (R) stages. The second height interval (30-60 cm, H2) was associated with the budding (B) and stem elongation. Flowering (F) and ripening (Rp) were associated with heights H3-4 (60-120 cm).

Using the above stratification scheme, each biomass sample was processed to obtain wet and dry weights (gm), gravimetric moisture (gm) and leaf area index (LAI, $m^2 \cdot m^{-2}$) for each component part of the canopy, per layer, per replicate independent of their ultimate significance in scattering. Component parts of the canopy included, green leaves, brown leaves, stems, petioles, pods, and buds / flowers. The replicate data were averaged on a per site basis.

Prior to the destructive sampling, plants were measured for stem length, height to secondary stems, length of each secondary stem, height to buds, flowers and pods per stem,

number of green and brown leaves per height interval, height to first green leaf, total height of green leaf layer per plant, and stem diameters per height interval. These data were used to define the vertical space occupied by each component part of the canopy.

Three soil samples (two replicates per sample) were extracted per site at locations randomly selected for biomass extraction. These data were used to calculate soil volumetric moisture (Ms) ($gm \cdot cm^{-3}$). The replicate data were averaged on a per site basis.

4.2.3 Data Analysis

Volumetric moistures within the canopy were calculated for leaves, stems, pods and buds/flowers. The maximum height of the green leaf (GL) layer per site was calculated using mean height (cm) of the upper GL layer (+1) standard deviation (S.D.), height to first green leaf was calculated using mean height (-1) S.D., height to first pod was computed using the mean (-1) S.D.

An assumption adopted here, as in the case of wheat, is that water within the canopy volume should be weighted by the normalized volume fraction of vegetation. This assumption recognizes that moisture within the canopy is significant in terms of radar backscatter, but that its potential to interact with incident MW energy is also a function of its aerial distribution or volume fraction.

The vegetative volume of green leaves (l), flowers/buds (fl), pods (p) and stems (st) were computed for each layer [4.1].

$$V_{l,pd,st} = A \times T_{l,pd,st} \qquad [4.1]$$

Where:

V= vegetative volume

A = area (cm^2)
T = thickness l = 0.02 cm
fl = 0.02 cm
p = 0.35 cm
st = various depending on layer and phenological stage (0.1 - 0.45cm).

The volume fraction (VF) of each component was computed by dividing vegetative volume into the total volume per layer taking into account variations in local incidence. The volume fraction of leaves (VF_l) and flowers (VF_{fl}) were normalized to the maximum seasonal value (VF_l), pods (VF_p) and stems (VF_{st}) were normalized to the maximum seasonal (VF_p).

The gravimetric moisture per component per layer was weighted by the normalized volume fraction for each component ($NVF_{l,\ fl,\ p,\ st}$) to yield the normalized volumetric moisture for each canopy component ($nMv_{l,\ fl,\ p,\ st}$).

The nMv's per layer including soil moisture (Ms) were integrated using equation [4.2] to compute the total volumetric moisture (TMc) for each day of RADARSAT-1 acquisitions.

$$TMc = nMv_{gl1}\psi^2_{St2\text{-}4,l2\text{-}3,p2\text{-}4,fl} + nMv_{st1}\psi^2_{st2\text{-}4,l\text{-}3,p2\text{-}4,fl} + nMv_{gl2}\psi^2_{st3\text{-}4,l3,p2\text{-}4,fl} + nMv_{st2}\psi^2_{st3,l3,p2\text{-}4,fl} + nMv_{p2}\psi^2_{st3\text{-}4,l3,p3\text{-}4,fl} + nMv_{l3}\psi^2_{st4,p4,fl} + nMv_{st3}\psi^2_{st4,l3,p3,4,fl} + nMv_{p3}D\psi^2_{st4,\ p4,fl} + nMv_{st4}\psi^2_{p4,fl} + nMv_{p4}D\psi^2_{fl} + nMv_{fl}\psi^2_{air} + MsC\psi^2_{\ st1\text{-}4,l1\text{-}3,p2\text{-}4,fl} \quad [4.2]$$

TMc = Total volumetric moisture for canopy computed for a given DOY
nMv = moisture per layer (gm) weighted by normalized volume fraction
where subscript :
l1-3 = Green leaves , number identifies canopy layer
p2-4 = Pods, number identifies canopy layer(s) (2 to 4).
st1-4 = stems, number identifies canopy layer(s).
fl = flowers
Ms = Soil moisture ($gms{\cdot}cm^3$)
C = is a empirically derived constant to weight Ms; C=100

ψ^2 = two way transmittance term e.g., $\exp(-2*B*(nMv_{st2\text{-}4}+nMv_{l2\text{-}3}+nMv_{p2\text{-}4}+nMv_f))$
where:
B = is a empirically derived extinction coefficient e.g., (0.0038) (Figure 4.2).
D = is a empirically derived constant to weight Mv_p; D=1 (Site 1, (S1)); D=0.55 (S2); D=0.3 (S3)
$\psi^2_{air} = 1$

The assumptions implicit in this formulation are:1) backscatter is a function of volumetric moisture within the canopy; 2) volumetric moisture contribution of a given layer to the TMc is modified by the layer above it as expressed by some extinction coefficient (B); and 3) leaves, pods and flowers directly attenuate the nMv contribution of stems in any given layer.

Weighting factors for soil (C) were empirically determined and then tested across all sites. The final weighting factors for soil were universally applied (C = 100). For the upper pod layer within the canopy, the weighting factor (D) varied depending on volumetric moisture of the upper pod layer relative to the peak TMc of the canopy prior to pod development. Based on the results of work in Chapter 3 dealing with the seasonal evolution of wheat, a high extinction coefficient (B=0.0038) was found to be most appropriate. Assuming volumetric moisture to be significant factor in determining backscatter, it is logical to assume a high extinction within the canola canopy as well. Significant deviations in the ability of the volumetric model to mimic the seasonal backscatter of canola are assumed to be indicative of the nature of scattering within the canopy, e.g., surface scattering versus volume scattering, which is a function of phenological stage geometry of the component parts of the canopy.

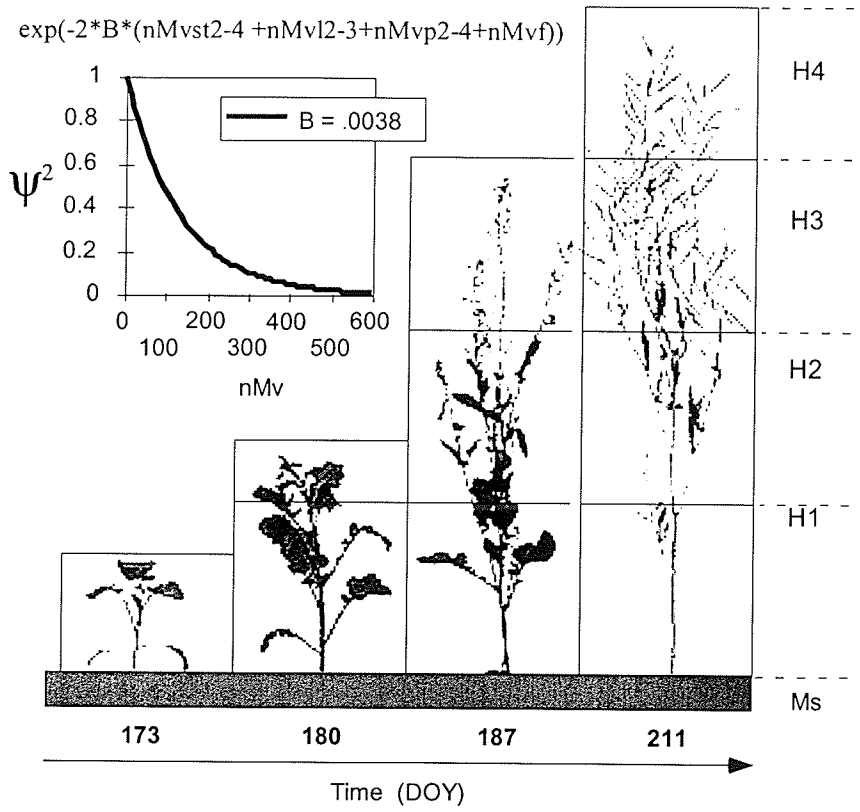

Figure 4.2 Canopy layers and transmissivity term with extinction coefficient (B=0.0038).

4.3 Results

4.3.1 RADARSAT-1 Backscatter Profiles

Prior to examining the relationship between MW backscatter and physical properties of canola canopies, the seasonal backscatter profiles of Sites 1-3 were reviewed to identify any obvious deviations in backscatter independent of crop condition (Figure 4.3).

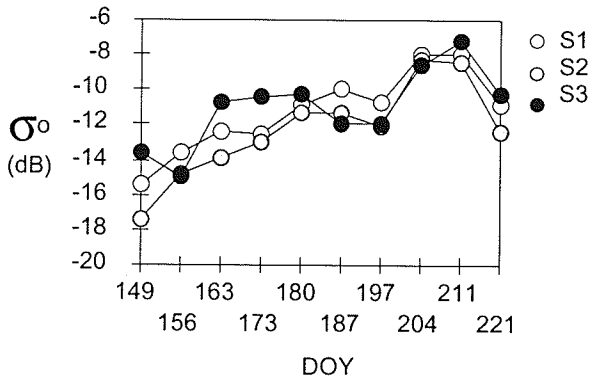

Figure 4.3 Seasonal RADARSAT-1 backscatter profiles for canola, Sites 1 to 3.

The seasonal backscatter plots for canola show that backscatter increases linearly early in the growing season for S1 and S2 to Year of Day (DOY) 187, followed by a small decrease in backscatter DOY 197 with seasonal maximums centred around DOYs 204-211. The backscatter for S3 (high biomass) was significantly higher early in the season (DOYs 163 to 173), although the reason for this is not immediately apparent it is likely due to a combination of factors including a higher soil moisture content and potential differences in leaf geometry (size and orientation) that enhance early season backscatter relative to S1 and S2. The seasonal ranges in backscatter for Sites 1-3 were 7.5, 7.9 and 9.1 (dB) respectively. The backscatter for S1 and S2 are highly correlated related (r^2 = 0.97),

although, the backscatter for S1 (low biomass) was consistently higher than S2. The higher backscatter at S1 is in part due to soil roughness and row orientation owing to there being a secondary "tillage" pattern overlaid on the north-south pattern typical of the field. The secondary pattern (caused by packer wheels of the air seeder as it was removed from the field) was oriented in a NW-SE direction.

A rainfall event on DOY 187 ending approximately 3 hours prior to the RADARSAT-1 pass had little or no apparent affect on canopy backscatter within the canola field. During the rainfall event short-term ponding of water was observed on the soil surface within the low biomass site (S1). In contrast, the wheat field located approximately 1 km south of the canola field showed a consistent 3 dB increase in backscatter across all sample sites.

The difference in response between wheat and canola due to the rainfall event can likely be attributed to differences in plant geometry/structure and the potential of each canopy to retain moisture at a given phenological stage. The dramatic response of wheat to the rain event at heading suggests that heads may provide a trap for moisture and hence cause a significant increase in the surface dielectric of the canopy. Another potential factor is that senescent leaves are retained within the wheat canopy and tend to absorb moisture during a rainfall event, thus increasing the canopy dielectric. The ability of the soil to contribute to backscatter must also be considered, especially within lower biomass canopies. In contrast, canola does not appear have comparable structures within the upper canopy to act as a trap for moisture, nor does it retain dry senescent leaves that have the potential to retain moisture. Leaf geometry (size and planophile orientation) in the canola

canopy may also preclude significant backscatter contributions from the soil surface given that green leaf area for canola reached its maximum on DOY 187.

4.3.2 Physical Properties of Canola

The time series evolution of canola for S1-S3 are examined in terms of weekly phenological development, mean gravimetric moisture, area index ($m^2 \cdot m^{-2}$; vegetative area vs. soil area) and normalized volumetric moisture (nMv) for each component part of the canopy. RADARSAT-1 backscatter profiles are included for illustrative purposes.

4.3.2.1 Crop Phenology

On DOY 149, canola plants throughout the field were at the seedling stage (S), plants consisted of a short stem (1.5 - 2 cm) and 2 cotyledons (Figure 4.4a). From DOY 156-173 true leaves emerged (Rosette stage (R)), and the 6-7 leaf stage was achieved by DOY 173. This date also coincided with budding (Stage 3.1), Table 4.1 and Figure 4.4. Canola was bolting by DOY 180, and by DOY 187 numerous secondary stems (branches) had developed within the second layer of the canopy (H2, 30-60cm). By DOY 187 many flowers had opened, and lower pods were starting to elongate (Stage 4.2). Maximum bud-flower biomass was achieved by DOY 187, flowering generally ended DOY 204. From DOY 204 to 221 pods developed and ripened. Shortly following DOY 221, the crop was swathed.

4.3.2.2 Gravimetric Moisture

Early in the season (DOY 149-180), 65-87% of the average total gravimetric moisture within the canopy across Sites 1 to 3 was located in the leaves (Figure 4.4 b).

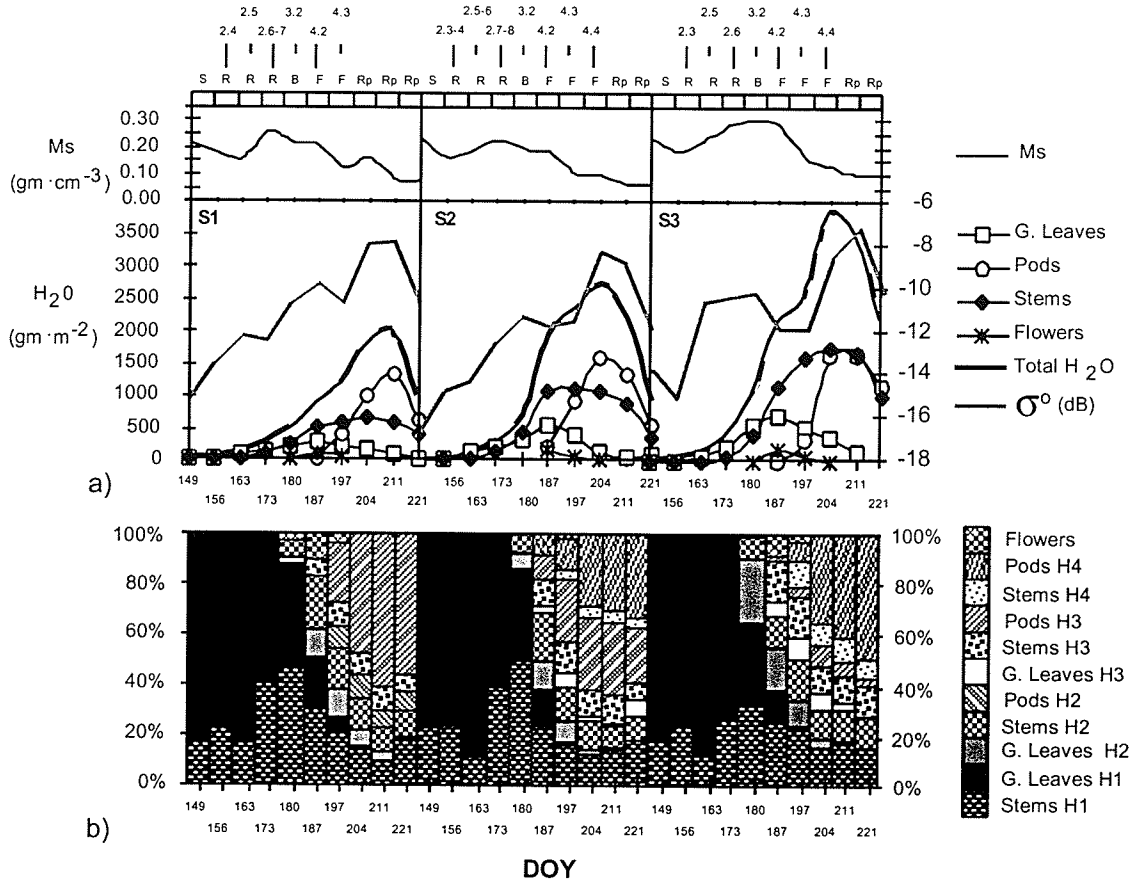

Figure 4.4 a) Total gravimetric moisture per canopy component per site for canola, including soil moisture ($gm \cdot cm^{-3}$), b) Percent distribution of moisture within the canopy per component and layer.

By DOY 180 water distribution within the canopy was more evenly distributed between leaves and stems. DOY 187 was the point of maximum flowering and maximum total average green leaf moisture. S1 green leaf moisture peaked at 270 $gm \cdot m^2$, S2 and S3 peaked at 640 and 705 $gm \cdot m^2$, respectively (Figure 4.4a). On DOY 187 flowers /buds, green leaves and stems comprised 10%, 32% and 60% of the canopy moisture respectively.

Table 4.1 Phenological stages of canola.

Stage	Description	Stage	Description
1	Seedling	4	Flower
2	Rosette	4.1	First flower open
2.1	1st true leaf	4.2	Many flowers open
2.2,... etc.	2nd true leaf, ...etc.	4.3	Lower pods starting to fill
3	Bud	4.4	Flowering complete
3.1	Flower cluster (Centre)	5	Ripening
3.2	Flower cluster raised above leaves		

Adapted from Thomas (1984)

DOY 197 was marked by a significant decrease in green leaf moisture (18%) and for the first time pods became a significant moisture component within the upper canopy. From DOY 187-197 the stem component accounted for the largest single gravimetric moisture

component within the canopy (45-55%). From DOY 204 to 221 pods dominated the canopy in terms of gravimetric moisture to a maximum of 59% on DOY 211. Stems on average comprised 34-37% of canopy moisture with the remaining portion (3-7%) attributed to green leaves (Figure 4.4b). Considerable variation in seasonal gravimetric moisture existed between the three sites. Differences in pod moisture were also apparent. It is evident that moisture within the pods was retained longer at the high biomass site (S3), thereby indicating more favorable growing conditions (Figure 4.4a).

4.3.2.3 Areal Distribution of Biomass

Although the amount of water within the canopy is important with respect to radar backscatter, its areal distribution as expressed in $m^2 \cdot m^{-2}$, is equally important as it identifies those elements that are more likely to interact with the incident MW energy.

In terms of areal distribution of biomass, green leaf area accounted for 90-98% of the early season areal biomass (DOY 149-180), Figure 4.5. Maximum LAI and flowering were generally achieved by DOY 187. The areal component of green leaves remained quite significant to DOY 197 (~ 55%) after which it rapidly decreased in a linear fashion to 16% by DOY 211. Pods had the single largest areal component of the canola canopy as of DOY 204. Average total stem area across all sites relative to other components within the canopy was relatively small (6%) early in the season (DOY 149-180), later in the season (DOY 187-211) it increased to 20% and as high as 34% by DOY 221. S1 had the lowest green leaf area index ~1.0. S2 had an LAI of (1.8), and S3 had a maximum LAI of 2.6. Pod area ($m^2 \cdot m^{-2}$) was comparable between S2 (1.34) and S3 (1.4), and lowest at S1 (1.08)

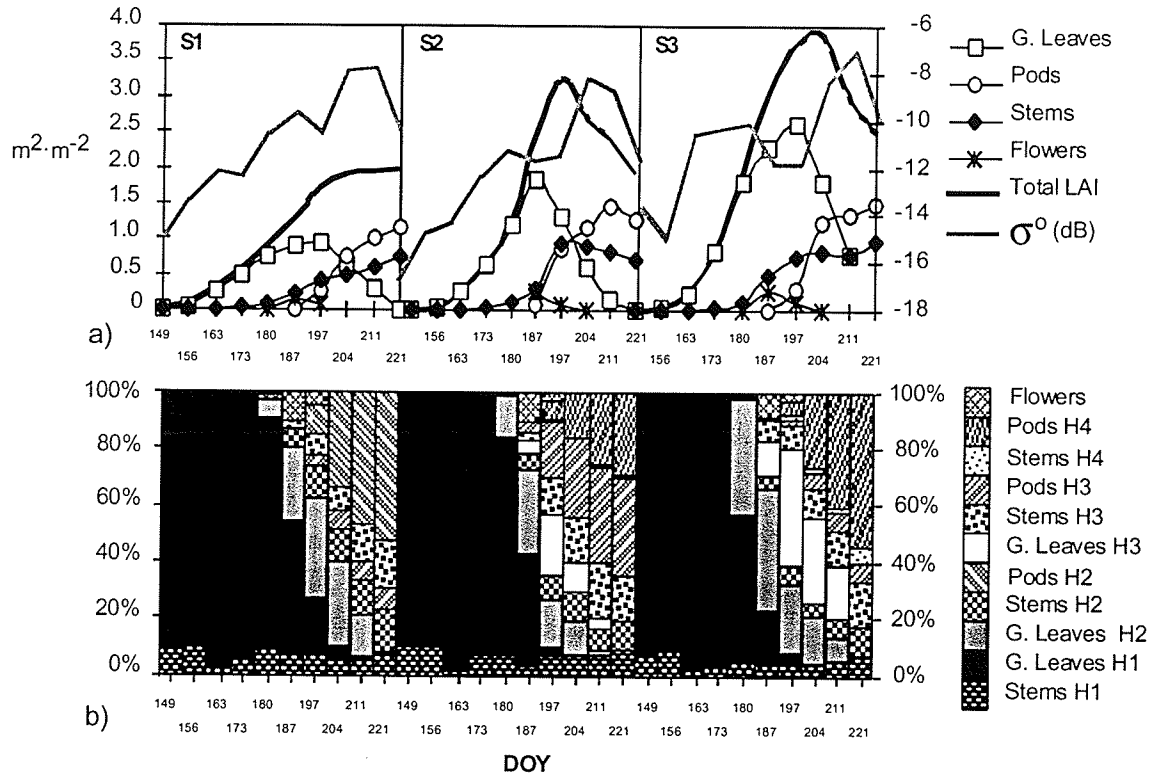

Figure 4.5 a) Total mean area ($m^2 \cdot m^{-2}$) per canopy component per site for canola; b) Percent areal distribution of canopy components per layer.

4.3.2.4 Normalized Volumetric Moisture (nMv)

The assessment of canopy backscatter is based on the nMv of the component parts of the canopy (Figure 4.6). The data show that early season (DOY 149-180) volumetric moisture is dominated by green leaves (87-98%) and stems (2-13%). Green leaf nMv peaks on DOY 187 across all sites with average total portion of green leaf volumetric moisture at (71%) followed by stems at (20%) and flowers at (8%). Green leaf volumetric moisture

decreases linearly from 71% to ~1% from DOY 187-211 with stem volumetric moisture reaching its maximum from DOY 197-204 (Figure 4.6a). From DOY 204 to 221 the canopy was dominated by pod Mv (72-85%). The total average portion of the nMv within the canopy attributed to pods for this period ranged from 84% for S1 (low biomass), 82% for S2 and 74% for S3 (high biomass).

From the above data some general observations can be made. It is evident that the relative portions of canopy components (stems, leaves, pods) are similar across all sites despite absolute differences in biomass as expressed by gravimetric moisture, ($m^2 \cdot m^{-2}$) and

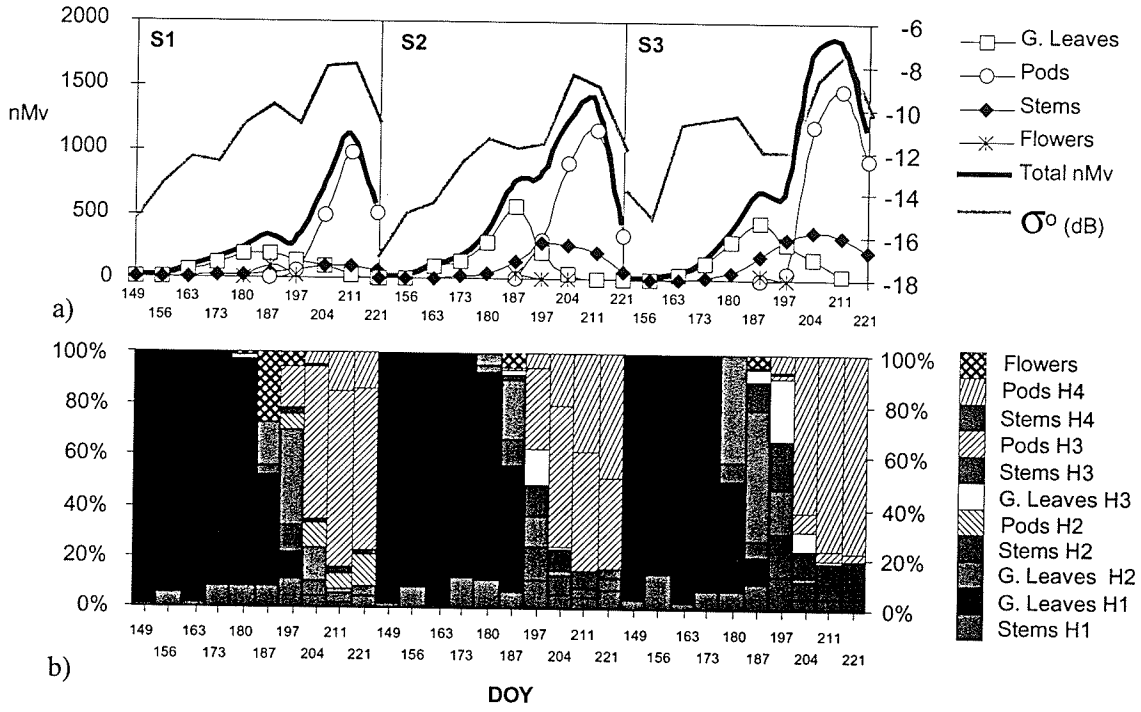

Figure 4.6. a) Total normalized volumetric moisture (nMv) per canopy component per site for canola; b) Percent distribution of nMv within the canopy per component and layer.

volumetric moisture (nMv). Green leaf gravimetric and volumetric moisture peaked by DOY 187 across all sites. This period also coincided with the development of secondary branches within the canopy. DOY 197 appears to be a transitional point between DOY 187 (peak green leaf moisture) and DOY 204 where pods become the single most dominant canopy feature. This transition period appears to coincide with a minima in backscatter. Pod volumetric moisture dominated the canopy over DOY 204-221, a period which is delineated in the temporal RADARSAT-1 backscatter plots as a significant increase in backscatter followed by a decline as pods began to dry down (DOY 221).

4.3.3 RADARSAT-1 Backscatter vs. TMc

Early in the growing season backscatter from an agricultural surface is often a function of soil surface conditions, that is, soil volumetric moisture, soil roughness and row direction. Variations in Ms ($gms \cdot cm^{-3}$) were evident throughout the growing season. Site 3 tended to have the highest moisture content and S2 soil moisture was generally lower than S1 (Figure 4.4). Row direction was north-south throughout the field, although S1 had a secondary "tillage" pattern that was oriented NW -SE and evident early in the season.

It is interesting to note that as soil moisture declined at Sites 1-2 from DOY149 to 156, backscatter increased significantly, suggesting that very small amounts of canola have a disproportionate effect on early season backscatter. Early season correlation (DOY 149 to 180) between backscatter and Ms at S1 and S2 were not significant at the 95 percent probability level (r^2 =0, P-Value = 0.83, N=10). S3 showed a positive trend between early season Ms and backscatter (r^2 = 0.57) but the relationship was deemed not significant (P-

Value =0.09, N=5). No correlation between backscatter and Ms (r^2 =0.02) was observed across Sites 1 to 3 late in the season (DOY 187-221). Due to the relatively low impact of soil moisture on backscatter, soil weighting applied to Ms in (2) was minimized (C= 100).

The overall seasonal time series of backscatter versus TMc for S1 was highly correlated (r^2 = 0.79; RMSE = 1.07 dB), (Figure 4.7a, Table 2.2). The backscatter for S1 increased linearly to DOY 187, even though the computed TMc peaked by DOY 180.

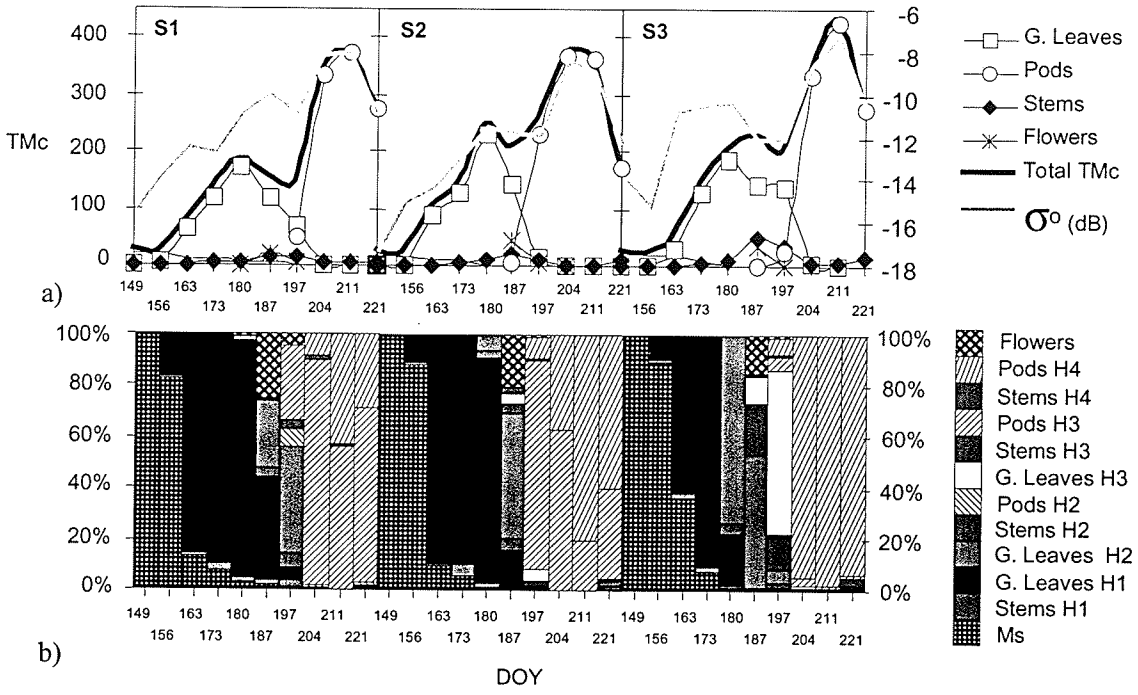

Figure 4.7. a) TMc per component part of the canopy per site. b) The percent contribution of component parts of the canopy to the computed TMc per layer

This may suggest that the rain event on DOY 187 may have increased backscatter over this site independent of the computed TMc which was decreasing at the time. Omitting DOY 187 from the regression improved the correlation marginally (r^2 = 0.85, RMSE = 0.94). The decrease in backscatter on DOY 197 is coincident with a marked decrease in green leaf

nMv. The sharp increase in backscatter on DOY 204 and 211 is attributed to pod volumetric moisture (nMv_p). As pods started to dry down, backscatter decreased significantly (DOY 221). Based on the model's assumptions, the stem component of the TMc was negligible largely due to the dominance of leaf volumetric moisture early in the season versus pods late in the season.

Table 4.2. Regression relationships, TMc's vs. σ^o (dB), Sites 1 to 3.

Site	Regression Coef.	Adj. r^2	RMSE (dB)	P-Value *
S1	Y = -14.194 +0.017 * X	0.79	1.07	0.000
S2	Y = -16.401 +0.021 * X	0.90	0.85	<0.000
S3	Y = -13.685 +0.014 * X	0.67	1.33	0.002
S3**	Y = -14.857 +0.017 * X	0.90	0.82	0.000
S1-3	Y = -14.673 +0.017 * X	0.73	1.27	<0.000
S1-3**	Y = -15.089 +0.018 * X	0.82	0.82	<0.000
S1-3 (DOY 149-197)	Y = -14.533 +0.016 * X;	0.46	1.50	0.000
S1-3** " "	Y = -14.982 +0.018 * X	0.57	1.30	0.000
S1-3 (DOY 204-221)	Y = -16.606 +0.023 * X	0.94	0.42	<0.000

* P-Values > 0.05 indicate no significance
** S3 DOY 163 & 173 omitted.

The computed TMc for S2 was highly correlated with the observed backscatter (r^2 = 0.90, RMSE = 0.85 dB) (Figure 4.7 and Table 4.2). As in S1, early season backscatter was dominated by the soil component to DOY 156. Green leaves accounted for the bulk of the TMc to DOY 187, with the peak green leaf TMc occurring on DOY 180. Pod volumetric moisture was the most significant component within the canopy from DOY 197 to 221. Stem volumetric moisture was not a significant factor throughout the growing season. Not unlike S1, the dip in backscatter on DOY 197 appears to be associated with the observed decrease in leaf volumetric moisture and the early development of pods.

The RADARSAT-1 backscatter profile for S3 differed significantly from S1 and 2 (DOYs 156-173). Site 3 had the highest biomass and Ms. The decrease in backscatter DOY on 156 may be related to a dip in soil moisture. This was not the case for S1 and S2 where

backscatter continued to increase despite decreases in Ms. DOY 163 is characterized by a rapid increase in backscatter (4.3 dB), after which it remained relatively invariant to DOY 180 at (-10.2 to -10.7 dB) Figure 4.7a. The volumetric model could not explain this rapid increase in backscatter, and is likely evidence of enhanced surface scattering due to a combination of leaf geometry (size and orientation) and soil background moisture. Backscatter late in the season (DOY 197-221) was closely associated with the decline in leaf volumetric moisture and with pod development as in S1 and S2. Overall correlation between TMc and backscatter was relatively low at S3 ($r^2 = 0.67$, RMSE = 1.33 dB). When observations for DOY 163 and 173 were omitted from the model the correlations improved ($r^2 = 0.90$, RMSE = 0.82 dB), Table 2.

Integrating the TMC data over Sites 1 to 3 the correlation to the observed backscatter is $r^2 = 0.73$; RMSE = 1.27, (Figure 4.88 and Table 2.2). The correlation is improved considerably to $r^2 = 0.82$ when the two early season observations (DOY 163 and 173) from Site 3 are omitted.

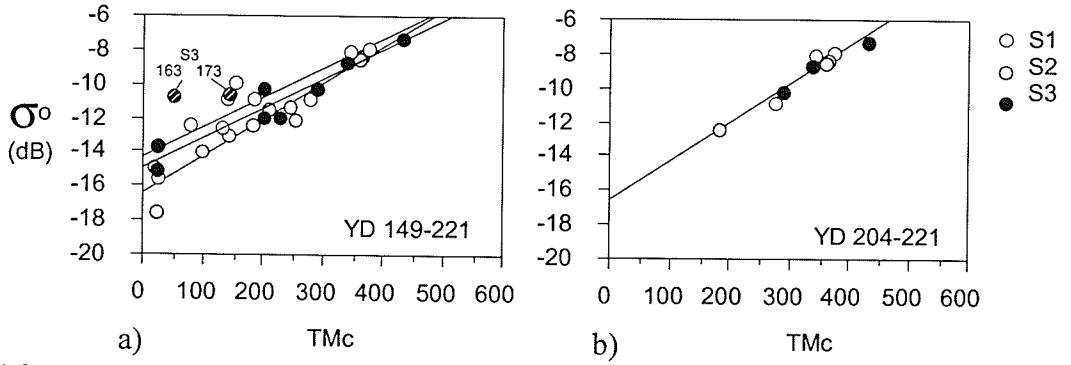

Figure 4.8 a) RADARSAT-1 backscatter vs. TMc, Site 1 to 3, DOYs 149-221,

b) RADARSAT-1 backscatter vs. TMc, Site 1 to 3, DOYs 204-221.

It is apparent from the data shown in Figures 4.7 and 4.8 that backscatter varies somewhat across Sites 1-3 independent of the computed TMc. Correlating the early season (DOY 149-197) TMc data to backscatter yields a low correlation (r^2 = 0.46), suggesting that 54% of the backscatter is explained by factors such as variations in crop geometry. Late in the growing season (DOY 204-221) when leaves are no longer a significant backscatter element, and pods are the dominant canopy component, correlations between the computed TMc and backscatter are high (r^2 = 0.94, RMSE = 0.42 dB). This result suggests that as the canopy enters the later stages of its phenological development, that volume scattering dominates thus meeting the assumptions of the volumetric model.

4.4 Conclusions

The physical data showed that the two most significant components within the canopy were green leaves (DOYs 149-197) and pods (DOYs 204-221). Although stems appeared to be significant in terms of gravimetric moisture (DOYs 187-221), they were relatively minor components in terms of areal distribution ($m^2 \cdot m^{-2}$) and normalized volumetric moisture (nMv). The canopy as represented by nMv showed a clear bimodal distribution of moisture associated with green leaves early in the season and pods late in the season.

The multi-layer volumetric model used to assess RADARSAT-1 backscatter for wheat (Chapter 3) was adapted for canola. The model used a high extinction coefficient (B = 0.0038) and a significantly reduced weighting for soil volumetric moisture (C = 100). The computed TMc correlated well with RADARSAT-1 backscatter for S1 and S2, while for S3 the early season backscatter was disproportionately high compared to the canopy TMc.

When the results over Sites 1 to 3 were integrated, it became apparent that a volumetric characterization of the canola canopy early in the growing season (DOY 149-197) did not adequately represent the canola surface ($r^2 = 0.46$). This result was expected given that the model is based on volumetric moisture and does not consider canopy structure. Since the leaf size was comparable to the wavelength (5.6 cm), leaf geometry (size and orientation) plays a significant role as it relates to variations in backscatter over time and between sites. Later in the season (DOY 204-221) when pods dominated the canopy, the volumetric model worked much better ($r^2 = 0.94$).

The multi-layer volumetric model proved to be a useful tool in understanding the nature of SAR scattering over canola. The data showed that the nature of scattering changed as a result of crop phenology and illustrated the need to integrate a scattering model based on leaf geometry early in the growing season to better model the observed backscatter. The seasonal backscatter plots revealed a clear relationship with crop phenology coinciding with the decline of green leaf area and the emergence of pods as a dominant feature within the canopy.

Chapters 3 and 4 have examined the nature of backscatter as a function of phenology. Chapters 5 and 6 will examine the extent to which RADARSAT-1 data can be used to differentiate biomass at the field scale for wheat and canola respectively. Differentiation of biomass/LAI is critical if RADARSAT-1 data are to be used for crop condition assessment.

Chapter 5: Detection of In-field Variability Using Radarsat-1 Backscatter, Wheat

5.1 Introduction

The previous two chapters sought to model the seasonal evolution of wheat and canola using a multi-layer volumetric moisture model. The model demonstrated that the backscatter from RADARSAT-1 is directly linked to the phenological development of wheat and canola, but is not necessarily indicative of the total volumetric moisture within the canopy. It also revealed that low biomass areas within a field may have backscatter comparable to higher biomass areas. The question then arises, to what extent can RADARSAT-1 backscatter be used to assess in-field variability?

This chapter will examine the ability of RADARSAT-1 data to detect and map in-field variability as it relates to wheat biomass. The approach used in this chapter will be to illustrate the nature and degree of variability in the wheat field (hence designated FLD_100-120) based on physical data, such as soil texture, soil organic matter (OM) and yield. It will be shown that seasonal and inter-annual NDVI are closely related to the soil parameters as expressed by variations in biomass (green leaf area and duration, plant water content, etc.). Based on the known variation, an evaluation of RADARSAT-1's potential to identify variation per DOY will be made. The investigation will initially centre on FLD_100-120, and then broaden to include all wheat fields within the study area.

5.1.2Objectives

The objectives of this chapter are:

1) To examine the nature of in-field variation in FLD_100-120 as a function of soil texture, organic matter (OM), and yield as well as seasonal and inter-annual NDVI as derived from CASI and SPOT data (1997-1998). In support of this objective additional physical data will be examined to demonstrate that NDVI are indicative of significant variations in green leaf area and duration, crop water content, and density. The results are used to support the use of NDVI as a stratification variable for assessing the seasonal backscatter characteristics of RADARSAT.
2) To examine the seasonal backscatter (σ^{o} (dB)) from wheat vis-à-vis relative productivity zones as defined by mid- and late-season NDVI and to determine if backscatter trends are evident over productivity zones, and whether the backscatter trends change as a function of phenological stage.
3) To determine if per DOY trends can be exploited to for crop condition assessment of present.

5.2 Methods

5.2.1 Study Site

The study site includes the wheat field from Chapter 3 (designated FLD_100-120, Figure 5.1) where detailed ground confirmation data exist, and twelve additional fields within the South Tobacco Creek Conservation Area. FLDs_100-180 are situated at the foot of the Manitoba Escarpment, on the Manitoba Plain (or Lowlands), whereas FLDs_190-240 are situated above the escarpment on the Saskatchewan plain (or the western Uplands).

Little is known about the other wheat fields, other than the planting date, harvest date and average yield in bushels per acre (BPA) (Table 5.5). What is known of in-field variability per field is derived from the SPOT data (Section 5.3.1.3.2)

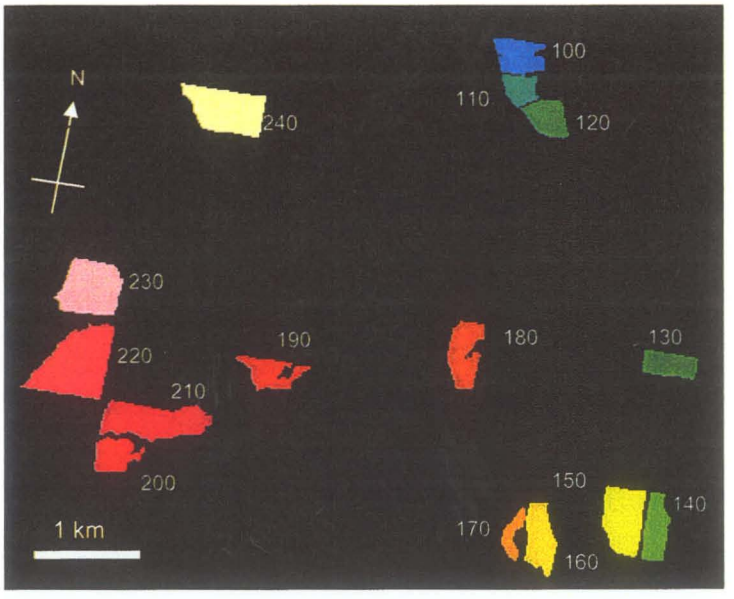

Figure 5.1 Field (FLD) identifiers for wheat fields in the Miami study site (FLDs_100-240).

5.2.1 In-Field Variability Maps

To assess RADARSAT-1's ability to discern in-field variability, the nature of variation within a field must first be understood. Variation was defined as a function of soil texture, organic matter (FLD_100), yield (FLD_100-120), and seasonal and inter-annual NDVI (FLD_100-240). The following sections outline the methods used to generate the various representations of in-field variation. Statistical methods used to correlate the various parameters are outlined and methods used to evaluate the capability of RADARSAT-1 to identify "known" variability.

5.2.1.1 Soil Parameters

During the 1998 field season, Westco conducted an intensive soil sampling campaign within FLD_100 in support of the precision farming component of this project (conducted by Wendy Kulzer, a Masters student at the Centre for Earth Observation Science, Department of Geography). The sampling scheme consisted of nine sample sites per acre, where 12 soil samples were extracted within a 10 m radius of each sample site location. The 12 samples were bulked to determine a per site average for each of the soil and fertility parameters measured. A total of 47 acres were sampled (403 sample sites), Figure 5.2.

Soil samples were measured by Enviro-Test Laboratories in Winnipeg to determine soil texture, soil organic matter (OM), pH, conductivity and soil fertility including macro- and micro-nutrients.

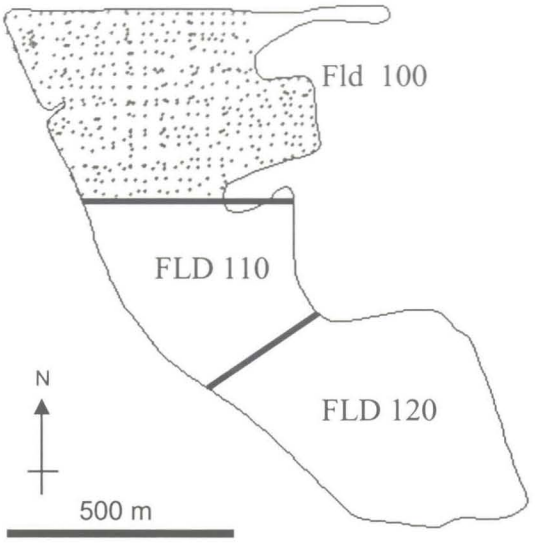

Figure 5.2 Soil sample locations within FLD_100 (47 acres).

Soil texture and soil organic matter were used in this work to help explain the observed in-field variations of biomass and yield. Soil texture was of particular interest as significant sand lenses occur within FLD_100-120. These areas are typically poor yielding due to significant water deficits throughout the year. The soil texture data were collected at two depths: 1) the surface layer 0-15 cm (designated Texture_1); and 2) the subsurface layer 15-30 cm (Texture_2). The soil texture was classified into the following classes: sand, sandy loam, loamy sand, loam, loamy clay, clay loam, or clay. Soil organic matter was expressed as percent.

The point observations for Texture_1, Texture_2, and organic matter (OM) were interpolated using the Inverse Distance Weighted (IDW) method using Spatial Analyst®. This interpolation method assumes that each input point has a local influence that diminishes with distance. It weights the points closer to the processing cell greater than

those farther away. A neighbourhood of six points was used to determine the output value for each location using a weighting factor (Power) of 0.3. The inverse distance function and weighting parameters were deemed appropriate in this case due tothe high density of observations relative to the local variation within the field, and the relatively systematic distribution of sample points.

5.2.1.2 Yield Data

Yield monitor data were obtained in 1997 and 1998. These data provided another measure of in-field variability and served as a ground confirmation source to assess the effect of soil texture and OM on productivity and the effectiveness of NDVI to assess yield potential.

In 1997, a Case International combine with differentially corrected GPS was used to obtain a yield map for FLD_100-120 (Figure 5.3). The field was planted in canola. The crop was swathed by mid August and combined 2.5 weeks latter. In 1998, more yield monitor data were to be acquired for this field. The service provider supplied a combine equipped with a yield-monitoring, but no way of logging the data. Due to delays already incurred in waiting for yield monitoring equipment and the need to harvest the wheat without further delay, attempts were made to manually log the yield data. This effort was terminated after several rounds of the field. The 1997 data therefore represents the only spatial representation of yield potential for this field. The yield data were classified in ArcView® into ± 0.5 SD. intervals around the mean.

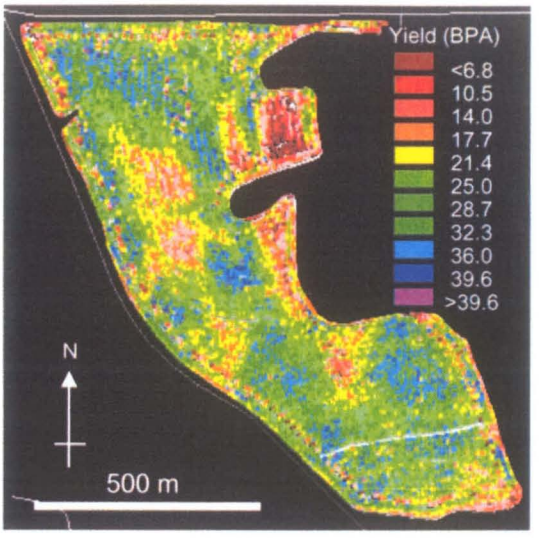

Figure 5.3 Yield monitor data for FLD_100-120, 1997.

Yield monitor data contains variability independent of actual yield due to a combination of factors. These include: 1) zero or near zero recordings at the start of each run; 2) periods during which the harvester is operating but not taking in crop (where the combine is reversing or is recovering from some unexpected interruption in grain flow; and 3) variations due to fluctuations in forward speed. Grain flow is a function of forward speed and cutting width to calculate a spot yield per unit area. Very high yield readings are attributed to situations where rapid deceleration occurs while grain already cut is still being processed (e.g., at the end of a row); and 5) grain flow and recorded grain yield is reduced if the cutting width set on the monitor is not used (Murphy et al., 1995).

To eliminate some of the problems inherent with yield data, anomalous low values associated with the beginning of each run and anomalous high values at the end of each run were removed from the database. Following classification of the yield data, a 7x7

post classification mode filter was applied to the raster yield data to eliminate micro-scale variations.

5.2.1.3 Optical Remote Sensing Data

The optical remote sensing data in 1997 consisted of a CASI (Compact Airborne Spectrographic Imager) scene acquired July 15, 1997 (DOY 195) and a SPOT MSS scene acquired August 6, 1997 (DOY 218). CASI data was acquired in spatial mode (3m resolution); 19 channels (0.5913- 0.9482 μm). In 1998, two SPOT scenes were acquired, the first on July 12 (DOY 193) and second on July 27, (DOY 208). The mid-July scenes coincided with heading for wheat, and flowering for canola, the scenes acquired for early August (1997) and late July (1998) coincided with the soft dough stage for cereal grains, and the ripening stage for canola (Stage $\geq$ 5.0, Table A-2, Appendix A).

The optical data were used to generate normalized difference vegetation index (NDVI) images [5.1].

$$NDVI = \frac{(NIR - RED)}{(NIR + RED)} \qquad [5.1]$$

The intent of using NDVI was to a provide relative index of variation within and between fields for wheat and canola during the 1997 and 1998 growing seasons.

5.2.1.3.1 Calibration of Remote Sensing Data

The SPOT digital counts were calibrated to spectral radiances as follows:

$$L = (X/A) + B \qquad [5.2]$$

Where:

L = the equivalent irradiance at the input of the instrument ($W\ m^{-2} * sr^{-1} * \mu m^{-1}$)

X = the count (0 to 255),

A = absolute calibration gain, for the considered spectral band

B = absolute calibration offset, for the considered spectral band.

The gains and offset for the red (0.61 to 0.68 μm) and near infrared (0.78 to 0.89 μm) bands where referenced within the header file of each band and are listed in Table 5.1. The CASI data was calibrated to radiances by ITRES. Band 11 (0.7255 μm) and band 13 (0.8043 μm)) were used to calculate NDVI.

Table 5.1 Gains and offsets used to calculate SPOT radiances for bands 2 and 3.

Sensor	Acquisition Date	Band 2 Gain (A)	Offset (B)	Band 3 Gain (A)	Offset (B)
Spot 1 MSS	Aug. 06 '97	2.89019	0.0000	1.69080	0.0000
Spot 1 MSS	July 12 '98	2.87509	0.0000	1.69120	0.0000
Spot 1 MSS	July 27 '98	2.87720	0.0000	1.69790	0.0000

To ensure that the various NDVI data sets were comparable, additional relative radiometric corrections to the data were undertaken. Since ground based spectrometer data were unavailable, absolute calibrations were not possible. Instead the radiances were corrected relative to July 12, 1998 radiances using a series of "standard targets" within 5 km radius of the study site. The targets included gravel pits, large asphalt surfaces (in

Miami, MB.), summer fallow (dry), and selected forested areas. Radiances were extracted for the bands 2 and 3 (SPOT data) and regressed against those of July 12, 1998, SPOT image. The gains and offset computed from the standard targets are in Table 5.2.

The CASI data was treated somewhat differently. Given that the Red and NIR wavelengths were slightly different and the bandwidths much narrower, the application of a series of gains and offset to mimic the SPOT radiances was considered inappropriate. Instead, the NDVI product was generated from the CASI radiances. A linear gain and offset was then applied to the CASI NDVI data to match the upper and lower limits of the August 06, 1997, calibrated SPOT NDVI (Table 5.2).

Upon review of NDVI histograms for 1997 and 1998, it was found that the resultant NDVI for 1997 required an additional linear adjustment to match the maximum NDVI of 1998 (Table 5.3).

Table 5.2 Offsets and gains applied to data for relative calibration to July 12, 1998 radiances.

Date	Sensor	Band	Offset	Gain
07/27/98	SPOT	2	-0.891	1.237
		3	-0.495	1.138
08/06/97	SPOT	2	2.243	0.9799
		3	5.445	0.7039
07/15/97	CASI	NDVI	0.338	0.474

Table 5.3 Linear gain and offsets applied to the 1997 NDVI data.

Date	Sensor	Band	Offset	Gain
08/06/97	SPOT	NDVI	-0.0129	1.1290
07/15/97	CASI	NDVI	-0.0102	1.1024

5.2.1.3.2 Classification of NDVI

The calibrated NDVI were classified relative to the mean NDVI of all wheat fields within the study area as represented by the July 12, 1998, SPOT image. The NDVI categories were based on equal intervals with each NDVI category representing a change in NDVI of 2.5 % (Table 5.4).

Table 5.4 Categorization of NDVI for SPOT and CASI data, 1997-98.

NDVI Class	NDVI Lower Limit	Upper Limit	Relative NDVI (%) Lower Limit	Upper Limit
1	<	0.3623		<0.5375
2	0.3623	0.3791	0.5375	0.5625
3	0.3791	0.3960	0.5625	0.5875
4	0.3960	0.4128	0.5875	0.6125
5	0.4128	0.4297	0.6125	0.6375
6	0.4297	0.4465	0.6375	0.6625
7	0.4465	0.4634	0.6625	0.6875
8	0.4634	0.4803	0.6875	0.7125
9	0.4803	0.4971	0.7125	0.7375
10	0.4971	0.5140	0.7375	0.7625
11	0.5140	0.5308	0.7625	0.7875
12	0.5308	0.5477	0.7875	0.8125
13	0.5477	0.5645	0.8125	0.8375
14	0.5645	0.5814	0.8375	0.8625
15	0.5814	0.5982	0.8625	0.8875
16	0.5982	0.6151	0.8875	0.9125
17	0.6151	0.6319	0.9125	0.9375
18	0.6319	0.6488	0.9375	0.9625
19	0.6488	0.6656	0.9625	0.9875
20	**0.6656**	**0.6825**	**0.9875**	**1.0125**
21	0.6825	0.6993	1.0125	1.0375
22	0.6993	0.7162	1.0375	1.0625
23	0.7162	0.7330	1.0625	1.0875
24	0.7330	0.7499	1.0875	1.1125
25	0.7499	0.7667	1.1125	1.1375
26	0.7667	0.7836	1.1375	1.1625
27	0.7836	0.8004	1.1625	1.1875
28	0.8004	>	>1.1875	2

This categorization was not only effective in depicting variation within a given field but it also captured the seasonal change in NDVI as related to crop development within and between fields for both wheat and canola.

5.2.2 Statistical Relationships Between Soil Characteristics, Yield and NDVI, FLD_100-120

FLD_100 was examined in detail so as to provide some rudimentary insight into the nature of the variability within FLD_100-120. Soil texture and soil organic matter were used as indicators of variability, as well as yield monitor data acquired in 1997.

The soil texture, OM, yield and NDVI statistics were extracted using the grid shown in Figure 5.4. This same grid was used to extract RADARSAT-1 mean backscatter (σ^{o}(dB)) values per field. The grid represents an area equivalent to an 11 x11 pixel sample area for RADARSAT-1 fine beam data (9m pixel spacing). Scatterplots showing the correlations between the NDVI, soil parameters and yield were generated for Fld_100 accompanied by tables summarizing the regression coefficients. Statistical results relating yield to seasonal NDVI were also summarized for the whole field (FLD_100-120) .

Additional ground confirmation data from 1998 are presented to show that NDVI were indicative of significant variations related to green leaf area and duration, plant density, and plant water content. These data illustrated that NDVI could be used as a relative indicator of biomass and, hence, a stratification variable to assess the potential of RADARSAT-1 backscatter to discriminate in-field variation.

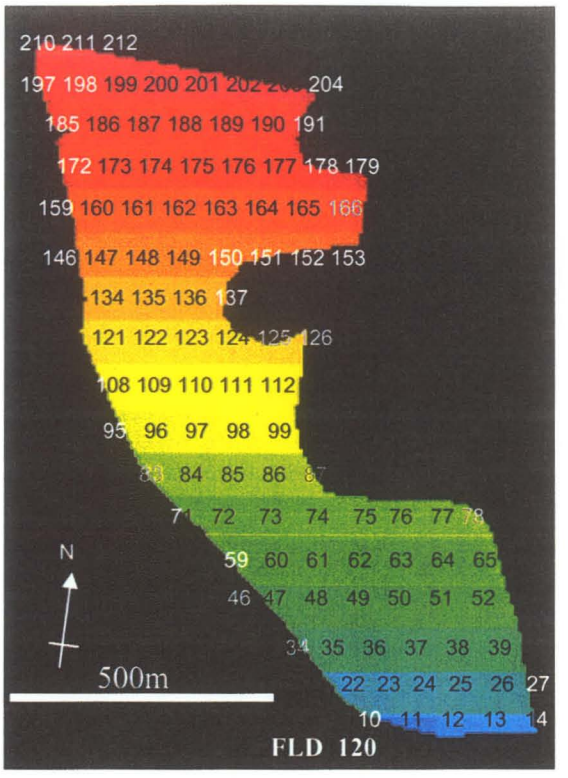

Figure 5.4 Grid used to extract soil, yield and NDVI averages, FLD_100-120.

5.2.3 RADARSAT-1 Backscatter vs. In-field Variability

Several methods were used to assess the ability of RADARSAT-1 to map in-field variability.

1) Method 1: Using the grid in Figure 5.4, mean statistics for soil texture (Texture_1 and _2), OM, and mid (SP98_ND_12) and late season (SP98_ND_27) NDVI for FLD_100 were extracted and correlated against the weekly RADARSAT-1 data (σ^o (dB)). Scatterplots per DOY and associated tables summarizing the regression

coefficients are presented. Based on the initial results from this field, Method 2 was then employed.

2) Method 2 used "productivity zones" within FLD_100 as defined by soil texture, OM and mid-(SP98_ND_12) and late-season (SP98_ND_27) NDVI to extract seasonal backscatter. Using productivity zones to extract RADARSAT-1 backscatter data had the advantage of reducing the variability of SAR data to better discern weekly backscatter trends relative to productivity zones. Scatterplots per DOY were presented for each of the stratification variables with associated tables summarizing the regression coefficients

   Method 2 was extended to FLD_100-120 and subsequently to other wheat fields within the study area (Figure 5.1) where no ground confirmation data are available. Mid (SP98_ND_12) and late-season (SP98_ND_27) NDVI were thus relied upon to define relative "productivity zones" to assess the seasonal nature of RADARSAT-1 backscatter trends per DOY.

3) Method 3 is a slight modification of Method 2 whereby RADARSAT-1 backscatter was extracted per NDVI zone averaged over all the wheat fields within the study area. The assumption being that if RADARSAT-1 was to be effectively used at more regional scales, then the relationships between productivity zones and observed backscatter must be consistent over multiple fields.

5.3 Results

5.3.1 In-field Variability

5.3.1.1 Soil Parameters Maps

The interpolated soil texture and OM surfaces for FLD_100 are presented in Figure 5.5. Soil texture within the field varied from sand to clay. The central portion of the field tended to be more clayey. Distinct sand lenes were evident towards the south end of the field and to the east at intensive sampling Site 3. The lowest OM was associated with the sandy areas; there was also some evidence of lower OM matter associated with a drainage feature on the west central portion of the field.

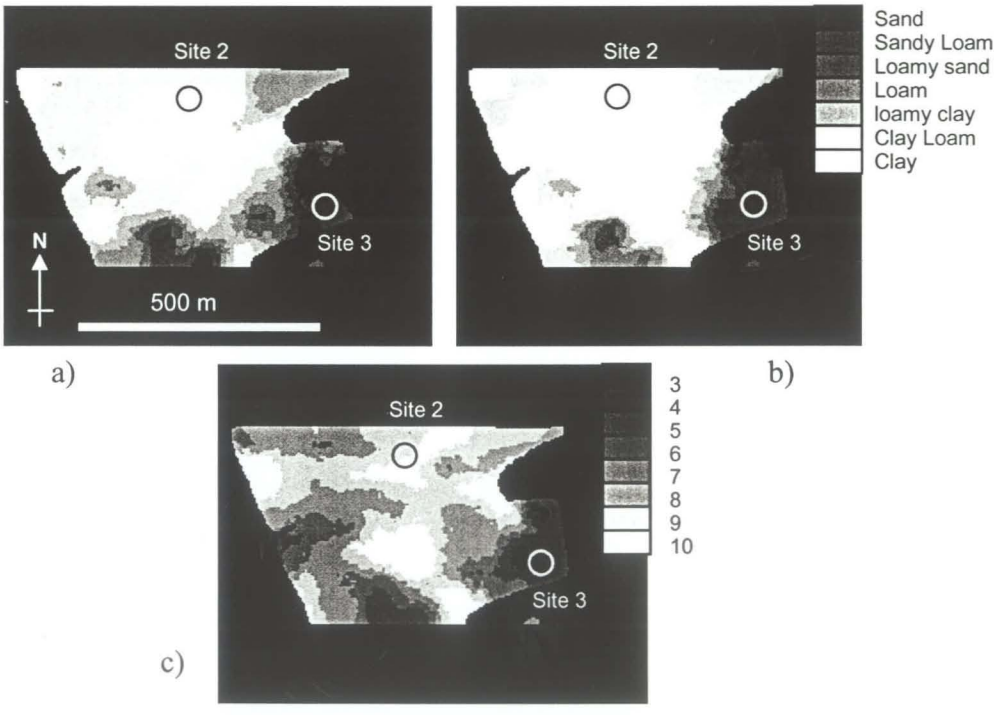

Figure 5.5 Fld_100 soil parameters, a) soil texture, 0 - 15 cm (Texture_1); b) soil texture, 15 - 30 cm (Texture_2); c) soil organic matter (OM) in percent.

5.3.1.2 Yield Maps

The yield information obtained for FLD_100-120 represents canola yield in 1997. The histogram of the edited yield data reveals that the yield distribution within the field is slightly skewed to the left (Figure 5.6). The mean yield was ~ 25 bushels per acre (BPA), with a standard deviation (S.D.) of 7.3 BPA. The data are classified using a 0.5 SD interval.

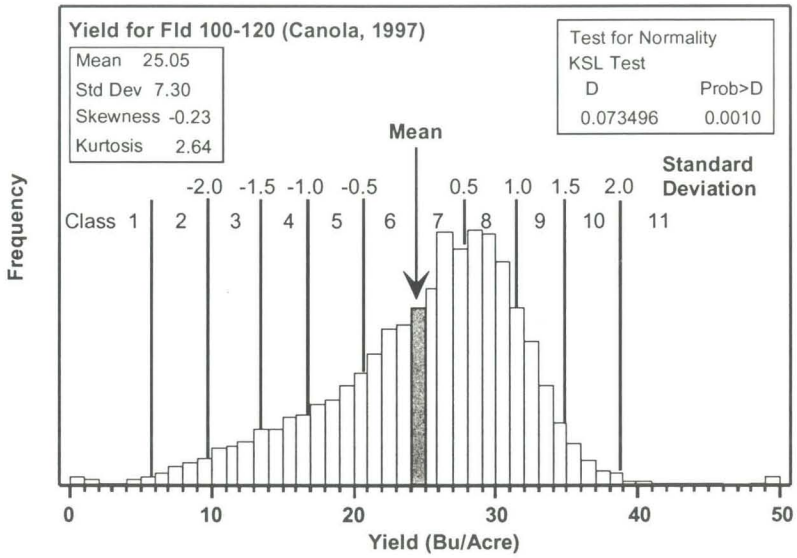

Figure 5.6 Frequency histogram of edited yield monitor data for FLD_100-120.

Yields within the field varied significantly, from 7 bushels to approximately 36 bushels in the filtered data. The low yield areas were associated with the more sandy locations with the exception of location (A) (Figure 5.7) where yield reduction was due to a large thistle patch.

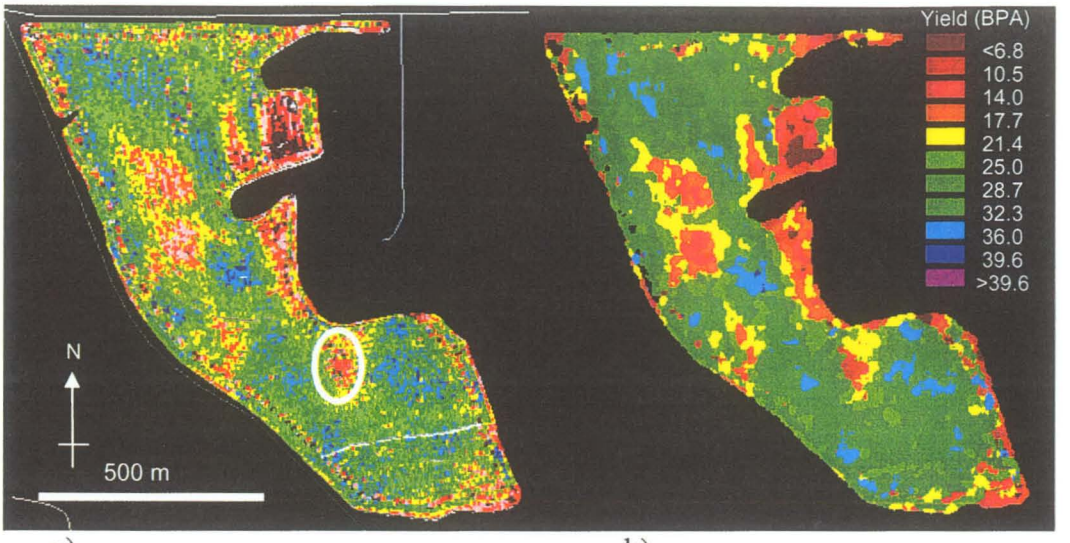

a) b)

Figure 5.7 a) Classified yield monitor data, b) post classification filter applied to yield monitor data.

5.3.1.3 Optical Remote Sensing Data

5.3.1.3.1 Classification Results: FLD_100-120

This section presents the classified CASI and SPOT NDVI data including some qualitative observations. Sections 5.3.2.1 and 5.3.2.2 will discuss in detail the relationships between seasonal and inter-annual NDVI, soil parameters and yield. Section 5.3.2.3 will introduce some additional ground confirmation data that show NDVI are highly related to variations in biomass and crop condition.

The NDVI generated from the CASI and SPOT data were classified according to the methods outlined in Section 5.2.1.3.2, such that variations in (relative) NDVI due to crop type, condition and phenological development could be revealed.

The NDVI data from 1997 are shown for FLD_100-120 (Figure 5.8). The CASI NDVI data (CASI97_ND) are representative of canola in full bloom, hence the suppression of NDVI values. The late season SPOT scene (SP97_ND) is more representative of green biomass within the field, with the canopy fully podded, hence the relative increase in NDVI. Shortly after August 18th (DOY 230), the crop was swathed. Approximately 2.5 weeks later the crop was combined.

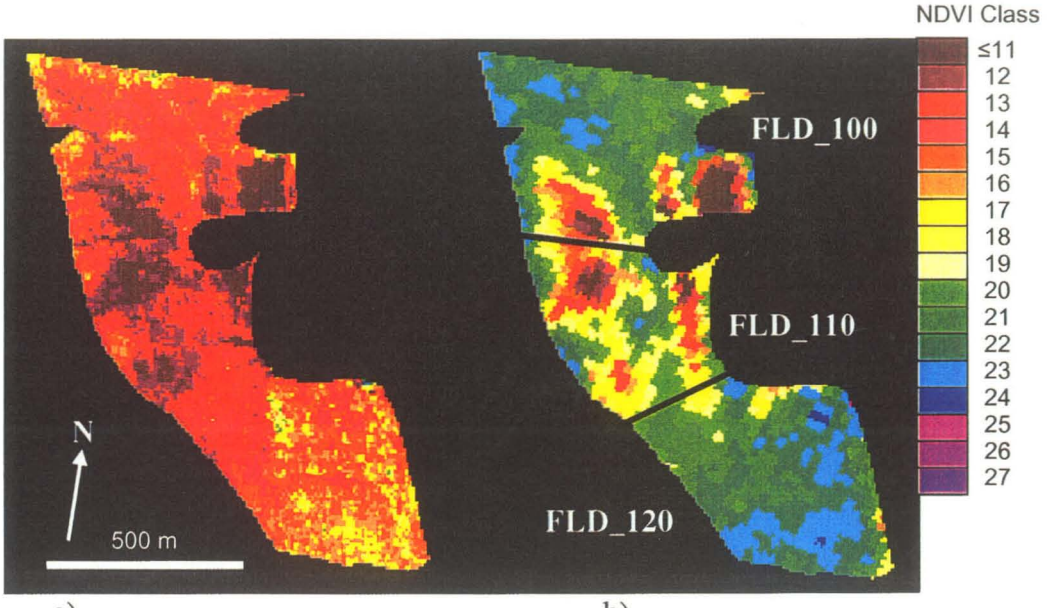

Figure 5.8 FLD_100-120 a) CASI NDVI (CASI97_ND), July 15, DOY 195; b) SPOT NDVI data (SP97_ND), August 6, DOY 218.

Similar in-field patterns are evident in the 1998 SPOT data, Figure 5.9. The mid season NDVI image (SP98_ND_12) clearly shows areas of low biomass associated with the sandy soils within the field, similar to that of SP97_ND. The second SPOT scene (SP98_ND_27) shows that the wheat is senescing, and highlights the differential

senescence within the field. NDVI category "<11", clearly outlines the coarser textured soils within the field. The higher NDVI tend to be associated with the more clayey soils to the north and south where growing conditions are more favorable, hence a longer green leaf duration and higher NDVI.

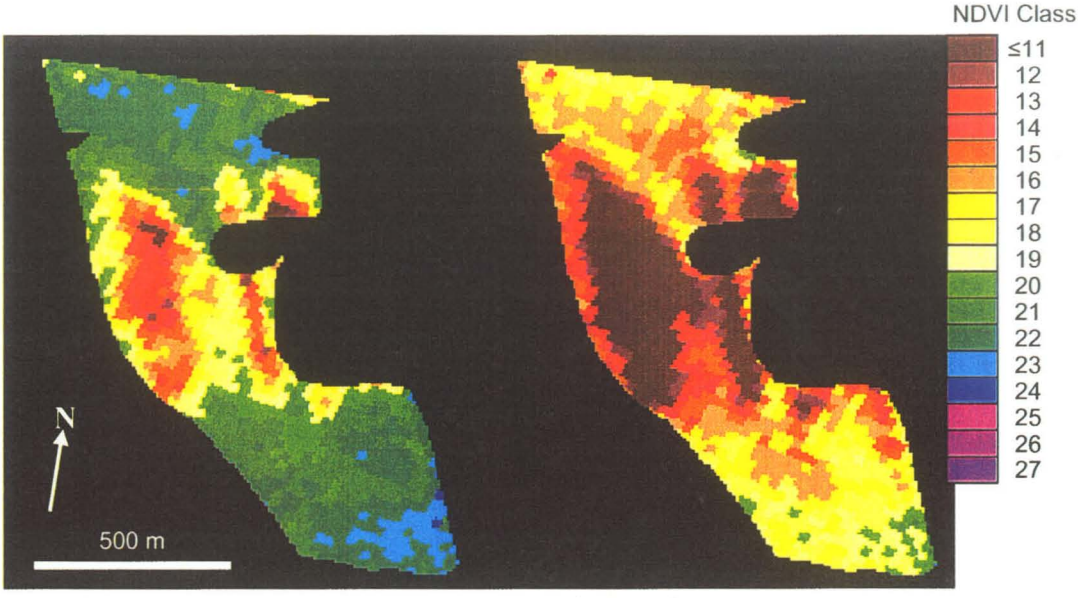

a) b)

Figure 5.9 SPOT NDVI data for FLD_100-120, 1998, a) July 12, DOY 193 (SP98_ND_12), b), July 27, DOY 208 (SP98_ND_27).

5.3.1.3.2 Classification Results: FLD_130-240

In addition to FLD_100-120, twelve other wheat fields are included in the study (Figures 5.10 and 5.11). SP98_ND_12 shows that there are distinct variations within and between fields with respect to green biomass. The fields to the east, which lie at the base of the Manitoba Escarpment (in the Manioba Plain) generally tend to have lower NDVI than those fields situated at a higher elevation to the west of the escarpment.

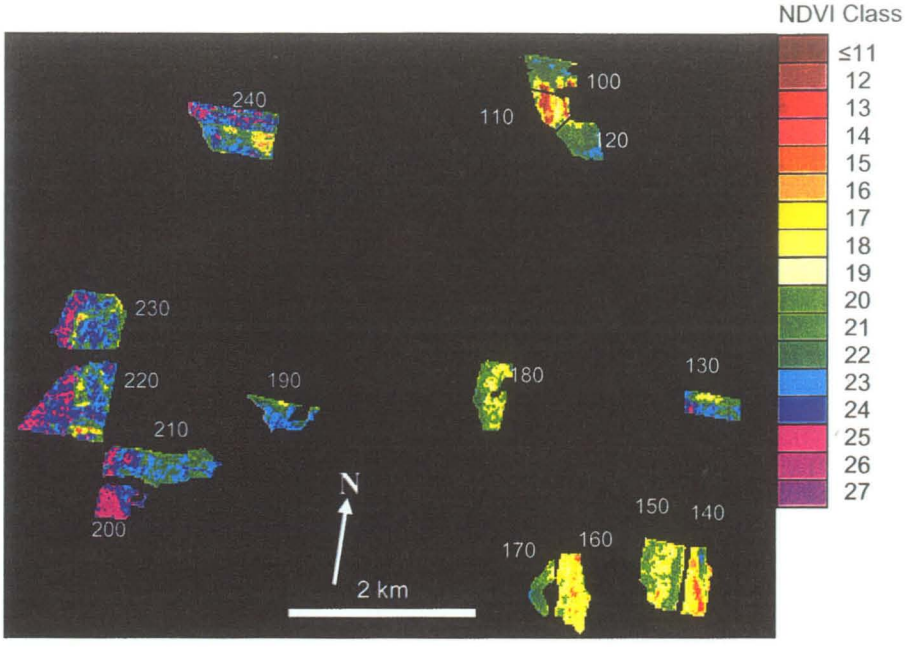

Figure 5.10 NDVI for FLD_100-240, July 12, 1998 (SP98_ND_12).

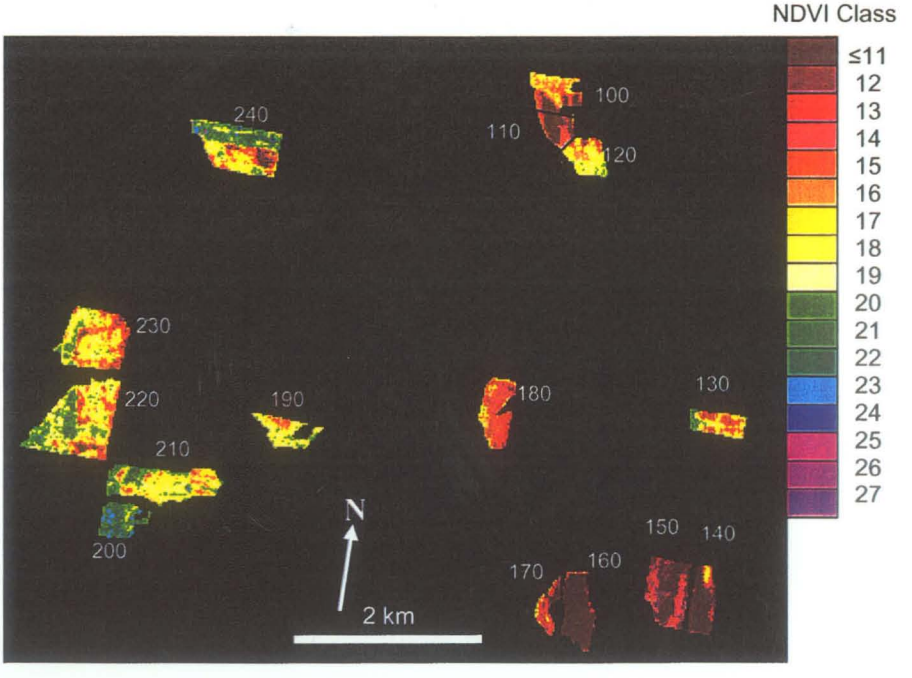

Figure 5.11 NDVI for FLD_100-240, July 27, 1998 (SP98_ND_27).

These differences are not necessarily indicative of productivity differences between fields (e.g., FLD_220 and 230 and FLD_160 and 170 each have an average yield of 45 BPA; Table 5.5), but rather of differences associated with crop phenology. The NDVI suggest that the crops to the east are more advanced and are therefore senecing earlier as evidenced in SP98_ND_27. This situation highlights the problems of using single date imagery for regional crop yield estimation, that is, inter-field NDVI at any given time may not nessessarily be indicative of yield potential. In this work, NDVI are simply used as a relative indicator of green biomass

Table 5.5 Supporting field data for FLD_130-240, 1998.

Field ID	Seed Date		Harvest Date		Yield
	Week	Month	Week	Month	(BPA)*
130	2	5	1	9	42
140	2	5	2	9	35
150	2	5	2	9	35
160	2	5	2	9	45
170	2	5	2	9	45
180	2	5	3	8	40
190	2	5	4	8	50
200	2	5	4	8	50
210	2	5	4	8	50
220	1	5	2	9	45
230	1	5	2	9	45
240	3	5	2	9	35

* Bushels per acre

5.3.2 Observed In-Field Variability vs. NDVI

Prior to assessing the ability of RADARSAT-1 to discriminate in-field variation, the relationship between NDVI and other physical measures of in-field variability, including soil texture, OM, yield and biomass are examined in FLD_100.

The relationships between the various indicators of variability were examined to help understand the nature of variation within FLD_100, and by extension to the whole field (FLD_100-120). These data will show that NDVI are indicative of significant variations in crop biomass, as a function of soil texture and OM as expressed by variations in green leaf area and duration, crop height, tiller survivability (density) and yield. Many of these factors should have a direct bearing on crop volumetric moisture over time and space.

The results presented in this Section will provide the rationale for using NDVI as a stratification variable to assess RADARSAT-1s sensitivity to "known variation," (Objective 1).

5.3.2.1 In-Field Variability vs. NDVI: FLD_100

As shown in Section 5.3.1.1, significant variations in soil texture and organic matter are present in FLD_100. Soil texture and organic matter have direct bearing on a number of factors related to crop growth, not the least of which is the ability of the soil to retain and make available the moisture needed for crop growth. The correlations of soil texture and OM to seasonal and inter-annual NDVI as well as to crop yield in 1997 are presented in a scatterplot matrix (Figure 5.12).

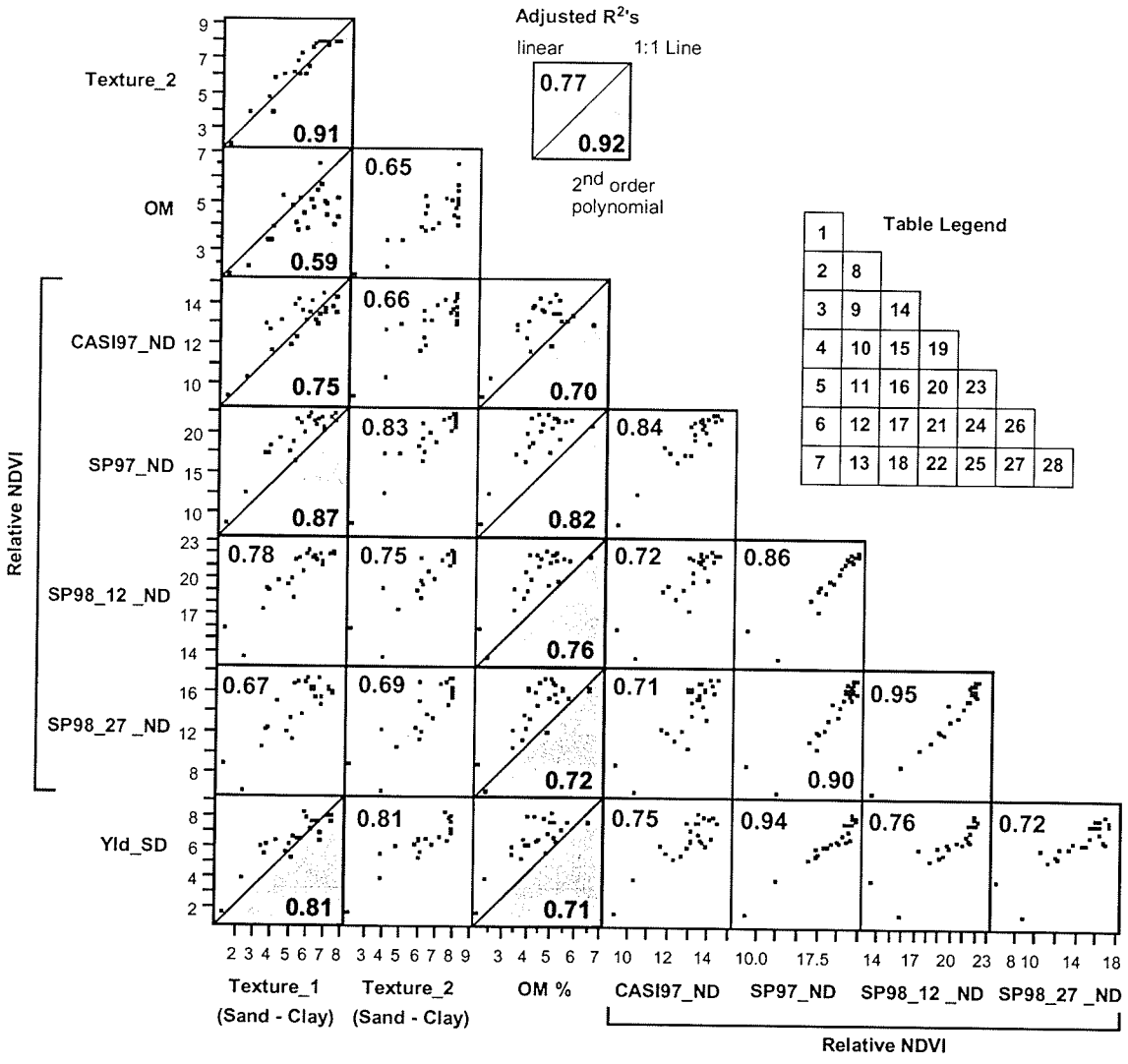

Figure 5.12 Scatterplot showing relationships between soil parameters, yield and seasonal and inter-annual NDVI for FLD_100. The table legend identifies the variables regressed (see Table 5.6).

The scatterplots show the coefficients of determination (adjusted r^2s) and indicate whether the relationships are linear or polynomial. Table 5.6 summarizes the regression coefficients and levels of significance. The highlighted areas within the table indicating

the regression coefficients that are significant at the 95% probability level and appropriate for each set of variables within the scatterplot (either linear or polynomial).

Surface and subsurface soil textures (Texture_1 and Texture_2) were highly correlated to each other (r^2 =0.91) and to soil organic matter (r^2 = 0.59 and 0.65). Both soil texture parameters were highly correlated to the 1997 yield for canola (r^2 = 0.81). Soil organic matter is also correlated to yield, but not as strongly (r^2 = 0.71).

Table 5.6 Regression coefficients, FLD_100 (see Figure 5.12 for variable IDs)

	Linear			Reg. Coef.		Polynomial	(2nd)	order			Reg. Coef.		
ID	R2	RMSE	P_Value	Intercept	B1	R2	RMSE	P_Value	P_Val B1	P_Val B2	Intercept	B1	B2
1	0.89	0.54	<.0001	1.53	0.94	**0.91**	0.50	<.0001	**<.0001**	**0.0470**	0.13	1.63	-0.07
2	0.51	0.72	<.0001	1.99	0.45	**0.59**	0.66	<.0001	**0.0034**	**0.0304**	-0.03	1.45	-0.11
3	0.66	0.71	<.0001	9.71	0.61	**0.75**	0.61	<.0001	**0.0003**	**0.0088**	7.36	1.77	-0.12
4	0.77	1.59	<.0001	9.72	1.79	**0.87**	1.22	<.0001	**<.0001**	**0.0008**	3.36	4.92	-0.33
5	**0.78**	1.05	**<.0001**	13.75	1.20	0.80	1.01	<.0001	0.0027	0.1133	11.53	2.29	-0.12
6	**0.67**	1.69	**<.0001**	6.28	1.47	0.68	1.66	<.0001	0.0148	0.1900	3.31	2.94	-0.16
7	0.76	0.74	<.0001	2.21	0.80	**0.81**	0.66	<.0001	**0.0003**	**0.0198**	0.00	1.88	-0.11
8	**0.65**	0.61	**<.0001**	1.04	0.51	0.64	0.62	<.0001	0.1594	0.6508	0.47	0.74	-0.02
9	**0.66**	0.72	**<.0001**	8.95	0.62	0.67	0.70	<.0001	0.0282	0.2026	7.08	1.37	-0.07
10	**0.83**	1.40	**<.0001**	7.11	1.86	0.84	1.32	<.0001	0.0021	0.0798	2.18	3.84	-0.18
11	**0.75**	1.12	**<.0001**	12.37	1.19	0.74	1.13	<.0001	0.5109	0.5463	13.78	0.62	0.05
12	**0.69**	1.63	**<.0001**	4.26	1.51	0.69	1.64	<.0001	0.7247	0.4518	6.81	0.48	0.09
13	**0.81**	0.65	**<.0001**	1.04	0.83	0.82	0.64	<.0001	0.0108	0.2214	-0.61	1.49	-0.06
14	0.40	0.95	0.0007	9.56	0.78	**0.70**	0.67	<.0001	**<.0001**	**0.0001**	2.10	4.57	-0.45
15	0.62	2.05	<.0001	7.90	2.59	**0.82**	1.41	<.0001	**<.0001**	**<.0001**	-8.50	10.92	-0.99
16	0.63	1.36	<.0001	12.50	1.74	**0.76**	1.11	<.0001	**0.0001**	**0.0026**	3.52	6.30	-0.54
17	0.64	1.75	<.0001	3.95	2.32	**0.72**	1.56	<.0001	**0.0012**	**0.0182**	-5.53	7.13	-0.57
18	0.58	0.97	<.0001	1.52	1.13	**0.71**	0.80	<.0001	**0.0003**	**0.0035**	-4.76	4.31	-0.38
19	**0.84**	1.32	**<.0001**	-13.20	2.50	0.86	1.24	<.0001	0.0156	0.0697	-52.20	9.05	-0.27
20	**0.72**	1.18	**<.0001**	-0.03	1.56	0.71	1.21	<.0001	0.6215	0.9723	-0.73	1.67	0.00
21	**0.71**	1.59	**<.0001**	-12.20	2.03	0.70	1.61	<.0001	0.8369	0.5126	5.41	-0.93	0.12
22	**0.75**	0.75	**<.0001**	-7.34	1.06	0.77	0.71	<.0001	0.0278	0.0815	-28.75	4.66	-0.15
23	**0.86**	0.84	**<.0001**	8.17	0.62	0.90	0.72	<.0001	0.2658	0.0081	16.02	-0.40	0.03
24	0.83	1.22	<.0001	-1.38	0.81	**0.90**	0.92	<.0001	**0.0329**	**0.0005**	12.64	-1.03	0.06
25	**0.94**	0.37	**<.0001**	-1.95	0.44	0.94	0.38	<.0001	0.0368	0.8948	-1.76	0.41	0.00
26	**0.95**	0.66	**<.0001**	-11.74	1.28	0.95	0.63	<.0001	0.792	0.0863	1.95	-0.22	0.04
27	**0.76**	0.73	**<.0001**	-5.42	0.59	0.77	0.72	<.0001	0.4558	0.1832	6.56	-0.73	0.04
28	**0.72**	0.79	**<.0001**	0.29	0.44	0.71	0.81	<.0001	0.3146	0.9599	0.15	0.46	0.00

Indicates significance at 95%

In general the NDVI for 1997 are strongly correlated to yield. The CASI image acquired while the crop was in bloom had the lowest coefficient of determination (r^2 =0.75), the late season NDVI from the SPOT satellite had the highest (r^2 = 0.94). At the blooming stage, the sensitivity of the NDVI to variations in green biomass is reduced significantly as indicated by the range of NDVI for that date. It is interesting to note that the NDVI for 1998 (SP98_ND_12 and 27) were also highly correlated to the 1997 yield (r^2 = 0.75 and 0.72) in FLD_100. The coefficients of determination do not tell the whole story in this case, since one observation within the field largely accounts for the relatively lower correlations. In general, all the seasonal and inter-annual NDVI for this field were highly correlated to each other (r^2 = 0.71 - 0.94) as in-field variability was largely a function of soil texture and OM.

5.3.2.2 In-Field Variability versus NDVI: FLD_100-120

Extending the relationships of NDVI and yield to the whole field (FLD_100-120), shows that 1997 yields remain strongly correlated with end of year NDVI (SP97_ND), (r^2 = 0.80). Mid season NDVI (CASI97_ND) remain poorly correlated (r^2 = 0.39), Figure 5.13 (Table 5.7). This is primarily due to variations in bloom within the field that generates a wide range of NDVI values that are independent of green biomass and yield potential.

NDVI in 1998 are poorly correlated to the previous years canola yield. This is expected to some extent as wheat reflectances are indicative of a crop starting to senesce. Therefore, NDVI are offset and are not representative of yield potential.

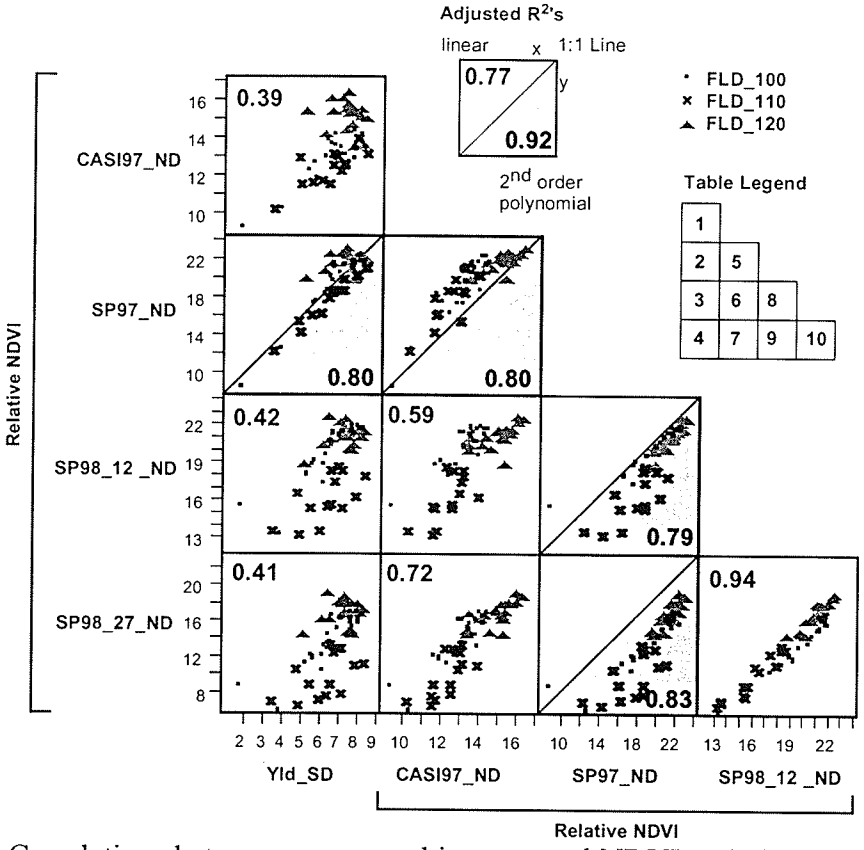

Figure 5.13 Correlations between season and inter-annual NDVI and yield for FLD_100-120; see Table 5.7.

Table 5.7 Regression parameters for NDVI and yield for FLD_100-120 (see Figure 5.13 for variable IDs).

	Linear			Reg. Coef.		2nd order Polynomial					Reg. Coef.		
ID	R2	RMSE	P_Value	Intercept	B1	R2	RMSE	P_Value	P_Val B1	P_Val B2	Intercept	B1	B2
1	**0.39**	1.19	**<.0001**	8.534	0.752	0.40	1.18	<.0001	0.0164	0.1714	6.077	1.673	-0.080
2	0.78	1.37	<.0001	6.323	1.996	0.80	1.32	<.0001	**<.0001**	**0.0225**	1.664	3.741	-0.151
3	**0.42**	2.01	**<.0001**	10.554	1.350	0.42	2.02	<.0001	0.5192	0.6027	12.149	0.752	0.052
4	**0.41**	2.76	**<.0001**	2.041	1.796	0.40	2.78	<.0001	0.6061	0.5385	4.631	0.826	0.084
5	0.74	1.48	<.0001	-2.635	1.647	**0.84**	1.16	<.0001	**<.0001**	**<.0001**	-54.543	9.573	-0.298
6	**0.59**	1.69	**<.0001**	1.389	1.342	0.60	1.66	<.0001	0.0223	0.1037	-19.249	4.493	-0.119
7	**0.72**	1.90	**<.0001**	-13.087	2.002	0.72	1.91	<.0001	0.1380	0.5542	-21.616	3.304	-0.049
8	0.72	1.40	<.0001	4.338	0.774	**0.79**	1.22	<.0001	**0.0156**	**<.0001**	20.337	-1.149	0.055
9	0.73	1.85	<.0001	-6.786	1.059	**0.83**	1.49	<.0001	**0.0006**	**<.0001**	19.010	-2.043	0.089
10	**0.94**	0.88	**<.0001**	-11.709	1.316	0.94	0.86	<.0001	0.7662	0.0969	-1.711	0.198	0.030

Indicates significance at 95%

Seasonal NDVI within a given year are highly related to each other (in 1997, $r^2 = 0.80$) and (in 1998; $r^2 = 0.94$) as were inter-anual NDVI ($r^2 = 0.59 - 0.83$).

5.3.2.3 NDVI vs. Crop Canopy Characteristics: FLD_100-120

In Section 5.3.2.1 it was shown that NDVI in a given year are highly related to variations in soil texture, organic matter and yield. This section will briefly highlight that NDVI within FLD_100-120 are directly and indirectly indicative of crop canopy characteristics such as green leaf duration and plant water content (in leaves, stems, heads), crop height and tiller survivability.

The sample data presented in Chapter 2 are presented here but in the context of NDVI, Figure 5.14. Having only three intensive sample locations, the discussion remains largely qualitative.

Figures 5.15 and 5.16 are presented to provide the seasonal representation of the LAI and water content of the component parts of the canopy (note the different scales along the y-axis). It is evident that there is significant variation in LAI and water content between the low- and high-biomass sites. The SPOT data acquired on DOY 193 (SP98_ND_12) coincides with the end of the watery ripe stage. Green leaf area is on a linear decline, whereas head area and water content are increasing.

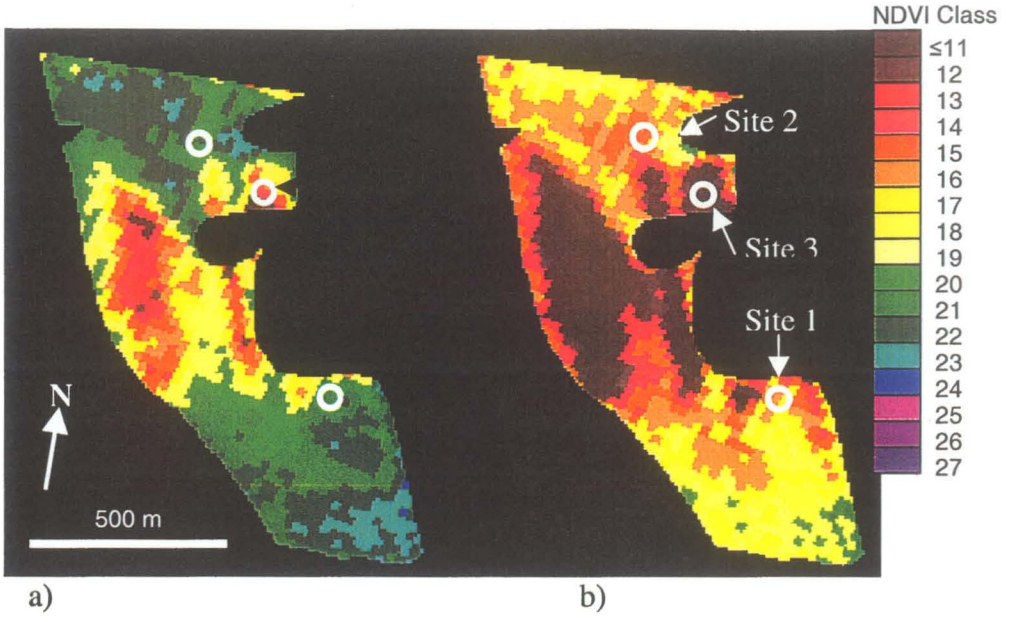

Figure 5.14 Sample site locations, FLD_100-120, a) SP98_ND_12, b) SP98_ND_27.

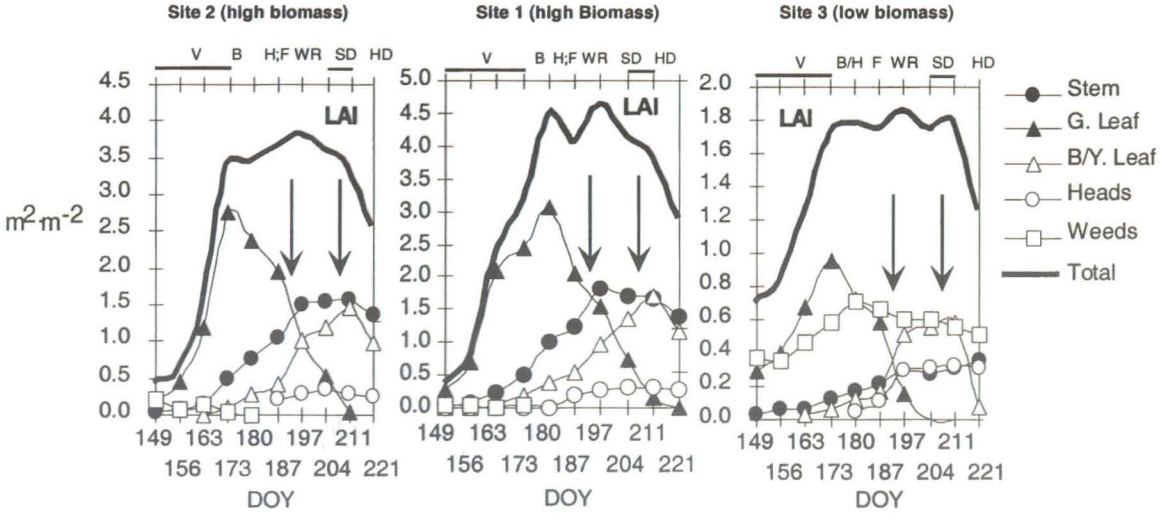

Figure 5.15 Variation in areal extent ($m^2 \cdot m^{-2}$) for the component parts of the canopy, vs. DOY. Arrows indicate acquisition dates for the SPOT imagery, DOY 193 (SP98_ND_12) and DOY 208 (SP98_ND_27)

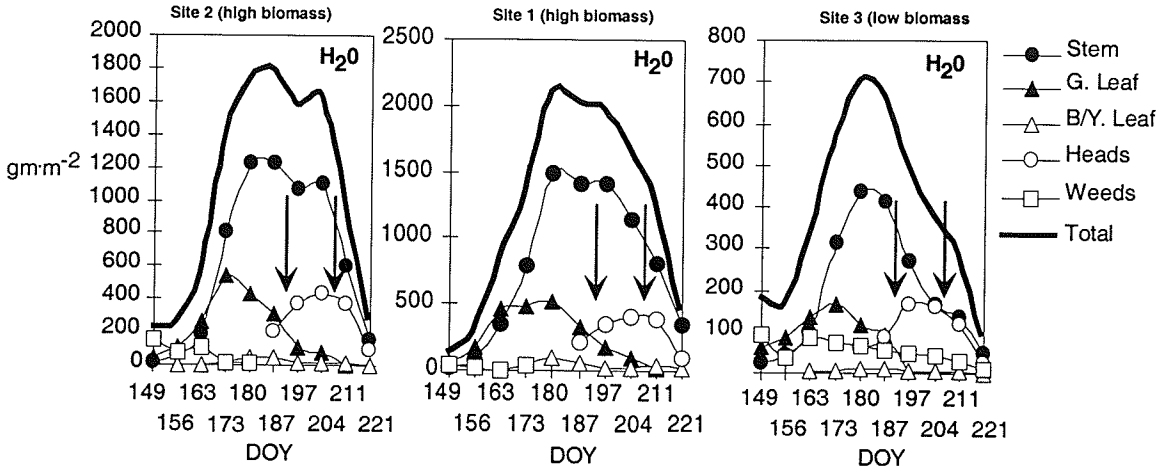

Figure 5.16 Variation in water content ($gm \cdot m^{-2}$) for the component parts of the canopy, vs. DOY. Arrows indicate acquisition dates for the SPOT imagery, DOY 193 (SP98_ND_12) and DOY 208 (SP98_ND_27).

The SPOT scene acquired DOY 208 (SP98_ND_27) coincided with the soft dough stage. Green leaf area at this point was very low and different rates of senesce between the sites are evident, for example, Site 3 (low biomass) has no green leaf biomass DOY 208.

Figure 5.17 summarizes the differences in LAI and water content specific to the SPOT acquisition dates. On DOY 193 green leaf water content was similar at Sites 1 and 2 (~250 $gm \cdot m^{-2}$) and significantly less at Site 3 (~50 $gm \cdot m^{-2}$). Site 1 had the highest green leaf duration (Figure 5.16b) followed by Site 2; and Site 3.

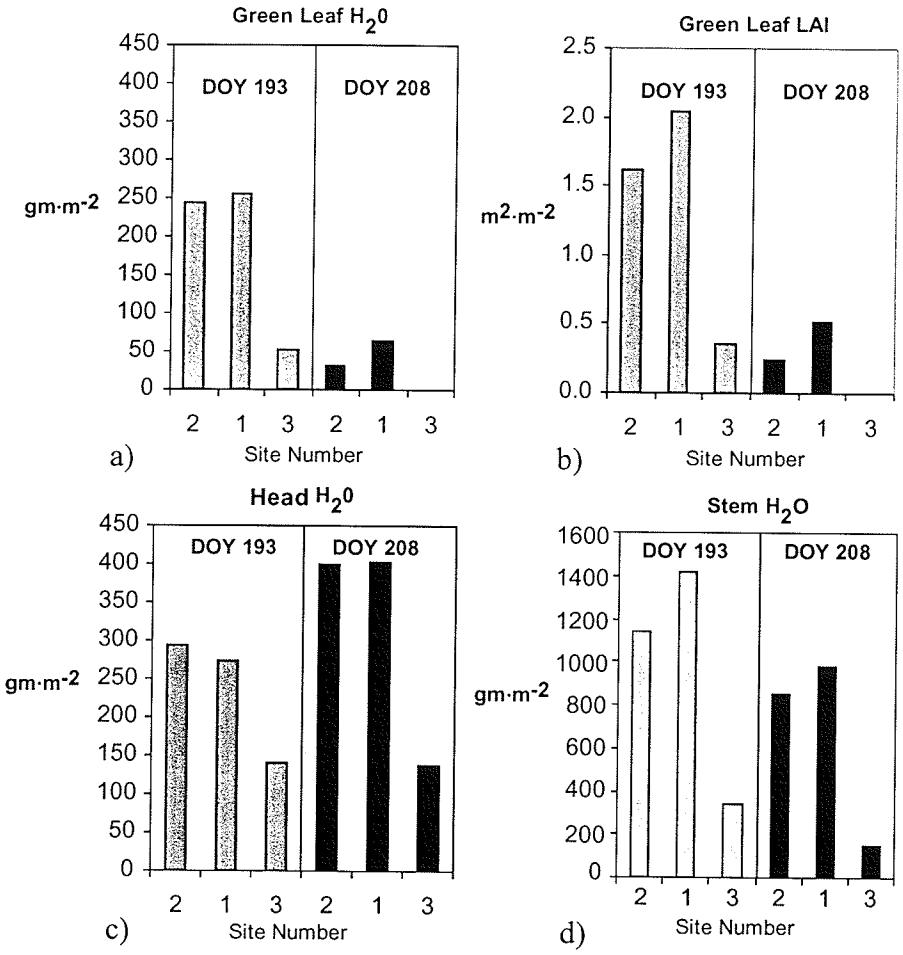

Figure 5.17 a) Estimated gravimetric moisture content of green leaves, b) green leaf area (LAI), c) head gravimetric moisture and d) stem gravimetric moisture for SPOT acquisition dates, DOY 193 and 208, FLD_100-120.

The gravimetric moisture of heads on DOY 193 was slightly higher than the total green leaf moisture content in the canopy. On DOY 208 the gravimetric moisture content of heads was much higher than leaves (400 versus ~45 $gm \cdot m^{-2}$ for S1 - 2; 100 vs. 0 $gm \cdot m^{-2}$ for S3). Head gravimetric moisture continued to increase over both dates for S1 and S2, whereas head moisture at S3 remained static. Stem moisture also showed a definite

stratification across all sites with Site 1 having the greatest moisture content, followed by Site 2 and Site 3.

Soil parameters within the field also have specific impacts on crop height and plant density expressed as the average number of tillers per plant. Figure 5.18 shows that early in the season crop height was comparable but differentiates around DOY173, (note, biomass changes are already significant independent of crop height). Sites 1 and 2 had comparable canopy heights (~110 cm) DOY 197-221; Site 3 canopy height was much lower (<80 cm).

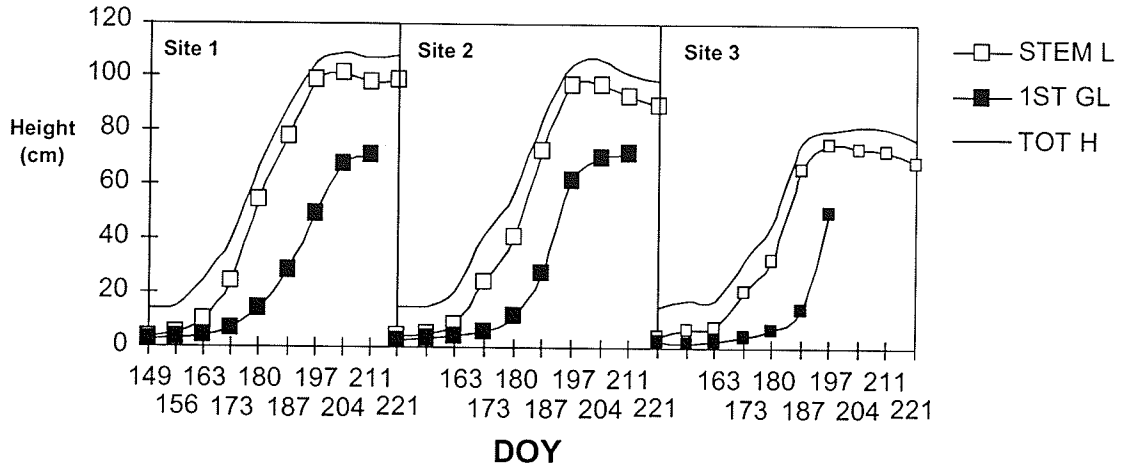

Figure 5.18 Wheat canopy height characteristics; total crop height (TOT H), stem length (STEM L) and height to first green leaf (1^{ST} GL), Sites 1-3, FLD_100-120.

The number of plant tillers and tiller survivability are an indicator of growing conditions within the field. From Figure 5.19 it is evident that early in the growing season (DOY 149) canopies were relatively comparable, but changed quickly starting

DOY 156. The maximum number of tillers per plant occurred between DOY 173 to 187 (booting to anthesis) within the high biomass areas (DOY 180 for Site 3). By DOY 197 the final number of tillers per plant remained more or less static for the remainder of the growing season across all sites. Tiller development was poorest at Site 3, where close to 60-70% of the plants were comprised of a single stem. Site 1 had the highest number of tillers per plant followed closely by Site 2.

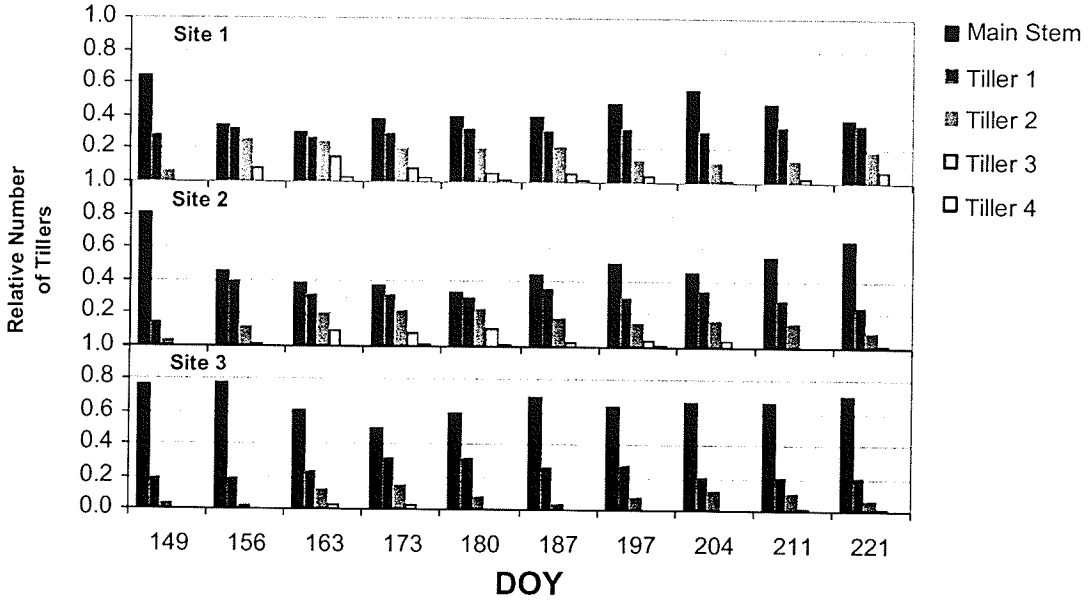

Figure 5.19 The seasonal distribution of tillers per plant, Sites 1-3, FLD_100-120.

5.3.2.4 Summary: In-field Variability versus NDVI

Section 5.3.2 examined the nature of in-field variability and its relationship to NDVI. The data provide the rationale for using NDVI as a stratification variable to assess the ability of RADARSAT-1 to detect biomass variation, especially in fields where ground confirmation data are poor or absent.

- Section 5.3.2.2 showed that there were high correlations between the seasonal NDVI and soil texture (r^2 = 0.66-0.87), organic matter (r^2 = 0.70 - 0.82) and yield in FLD_100 (r^2 = 0.74 - 0.94).
- Seasonal NDVI were highly correlated to each other (in 1997, r^2 = 0.84 and in 1998, r^2 = 0.95), as were the inter-annual NDVI for FLD_100. (r^2 = 0.71 - 0.90)
- When extended to the whole field (FLD_100-120), Section 5.3.2.3, similar results were obtained, i.e., seasonal NDVI were highly correlated to each other (r^2 = 0.80, 1997 and r^2 = 0.94, 1998). In 1997 the end of year yield for canola was highly related to end of season NDVI (r^2 = 0.80), and poorly correlated to mid-season 1997 NDVI (r^2 = 0.39).
- Sample sites within FLD_100-120 showed that NDVI were associated with large variations in green leaf LAI and plant water content.
- NDVI were indicative of differential rates of senescence as a function of green leaf area duration and hence potential productivity.
- Low versus high productivity areas identified by NDVI can also be indicative of crop canopy characteristics including crop height and number of tillers per plant.

- The results suggest that many of the canopy characteristics related to NDVI may also have some direct and indirect significance to radar backscatter (re: plant density, and moisture content)

5.3.3 RADARSAT-1 Backscatter vs. In-field Variability

The overall intent in examining the seasonal (per DOY) backscatter over wheat is to determine if and when RADARSAT-1 backscatter is indicative of biomass variability (Objective 2) and to determine whether seasonal backscatter trends can be exploited to map in-field variability (Objective 3). The approaches used to examine backscatter trends within the study site are outlined in Section 5.2.3.

5.3.3.1 RADARSAT-1 Backscatter vs. In-field Variability: FLD_100 (11x11 Grid)

Using the 11x11 grid (Figure 5.4) mean RADARSAT-1 backscatter, soil texture (Texture_1 & 2), OM and NDVI (SP98_ND_12 and 27) were extracted for FLD_100 (Method 1, Section 5.2.3). The assumption made in using the various measures of variability is that during the growing season, variations in either soil moisture or crop characteristics such as crop density, canopy volumetric moisture (re: green leafs, heads), and/or crop geometry (re: phenological stage), may be indirectly correlated with one or more of these measures of variability.

Scatterplots showing the correlations per DOY of backscatter versus measures of in-field variation based on soil parameters and NDVI are presented in Figure 5.20. Tables B1-B5 (Appendix B) summarize the regression coefficients for each variable.

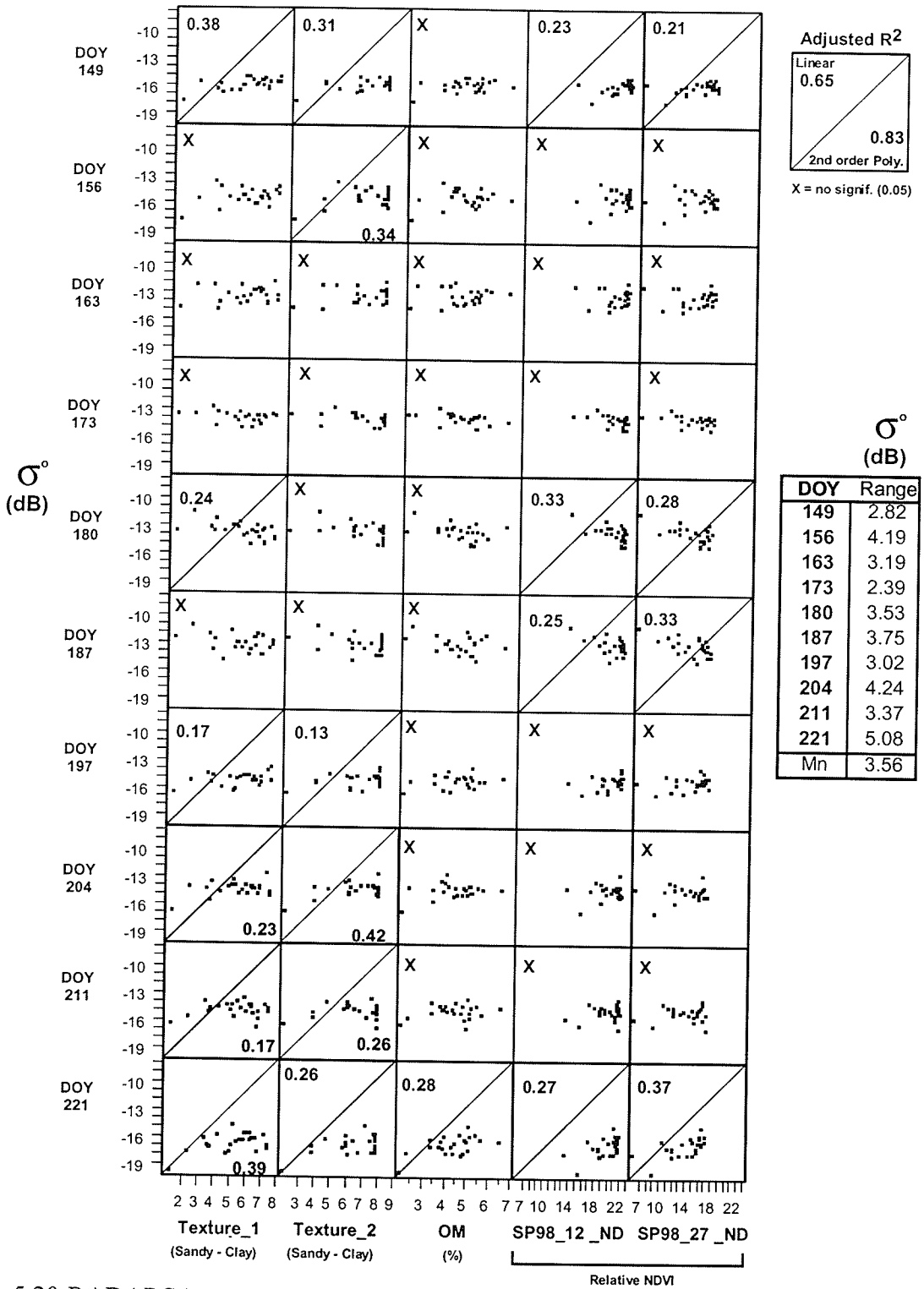

DOY	Range
149	2.82
156	4.19
163	3.19
173	2.39
180	3.53
187	3.75
197	3.02
204	4.24
211	3.37
221	5.08
Mn	3.56

Figure 5.20 RADARSAT-1 backscatter vs. measures of in-field variability (11x11 grid), FLD_100.

The results revealed that the overall correlations between RADARSAT-1 backscatter and the various measures of in-field variability were poor. Variability as expressed by soil texture zones (Texture_1 and _2), were the two most frequently correlated variables with the highest coefficients of determination occurring early in the year (Texture_1, r^2 = 0.38; Texture_2, r^2 = 0.31) and again latter in the season to backscatter. No significant correlations for Texture_1 were observed on DOY 156-173 and DOY 187 as was the case for Texture_2 on DOY 163-187. From DOY 197-221 coefficients of determination ranged anywhere from 0.13 to 0.42, a period associated with heading and progressive crop senescence. OM essentially had no significant correlations until DOY 221 (r^2 = 0.28).

The NDVI representation of variation was correlated to backscatter on DOY 149 (r^2 = 0.21-0.23), on DOY 180-187, booting to heading (r^2 = 0.25 - 0.33) and DOY 221 (r^2 = 0.27- 37) (hard dough stage). NDVI correlations were on DOY 149 and 221 (high backscatter associated with high NDVI). Correlations were negative on DOY 180-187 (high backscatter associated with low NDVI).

It is interesting to note that no correlations between NDVI zones and backscatter were observed between DOY 197 and 211 (watery ripe - soft dough), although for the same period, zones defined by soil texture showed correlations. Toward the end of the year (DOY 221) backscatter was positively correlated to all the indicators of in-field variability, the strongest relationships were with Texture_1 (r^2 = 0.39) and SP98_ND_27 (r^2 = 0.37). The daily range in backscatter per DOY was on average 3.56 dB for FLD_100 using the 11x11 cell means. The maximum range (5.08 dB) was observed on DOY 221.

5.3.3.2 RADARSAT-1 Backscatter vs. In-field Variability: FLD_100 (Area Means)

In this Section "productivity zones" within FLD_100 as defined by soil texture, OM and mid (SP98_ND_12) and late season (SP98_ND_27) NDVI are used to extract seasonal backscatter, Method 2 (Section 5.2.3). The intent is to reduce the inherent variability of SAR data to better discern weekly backscatter trends relative to productivity zones.

5.3.3.2.1 Backscatter vs. Soil Zones, FLD_100

The scatterplots of backscatter (σ^o (dB)) versus soil texture and OM zones and NDVI per DOY are presented in Figures Figure 5.21 and 5.22. Regression coefficients for backscatter versus soil parameters and NDVI can be referenced in Appendix B, Tables B6-B9, and Tables B9-B-11 respectively.

Backscatter trends as defined by OM showed the lowest correlations. Backscatter trends over OM zones are insignificant for most days with the exception of DOY 173 (r^2 =0.67, σ^o range 1.09 dB) and DOY 187 (r^2 =0.95, σ^o range 1.62 dB). Both trends are negative, that is, zones of high backscatter represent soils with low organic matter (and low biomass).

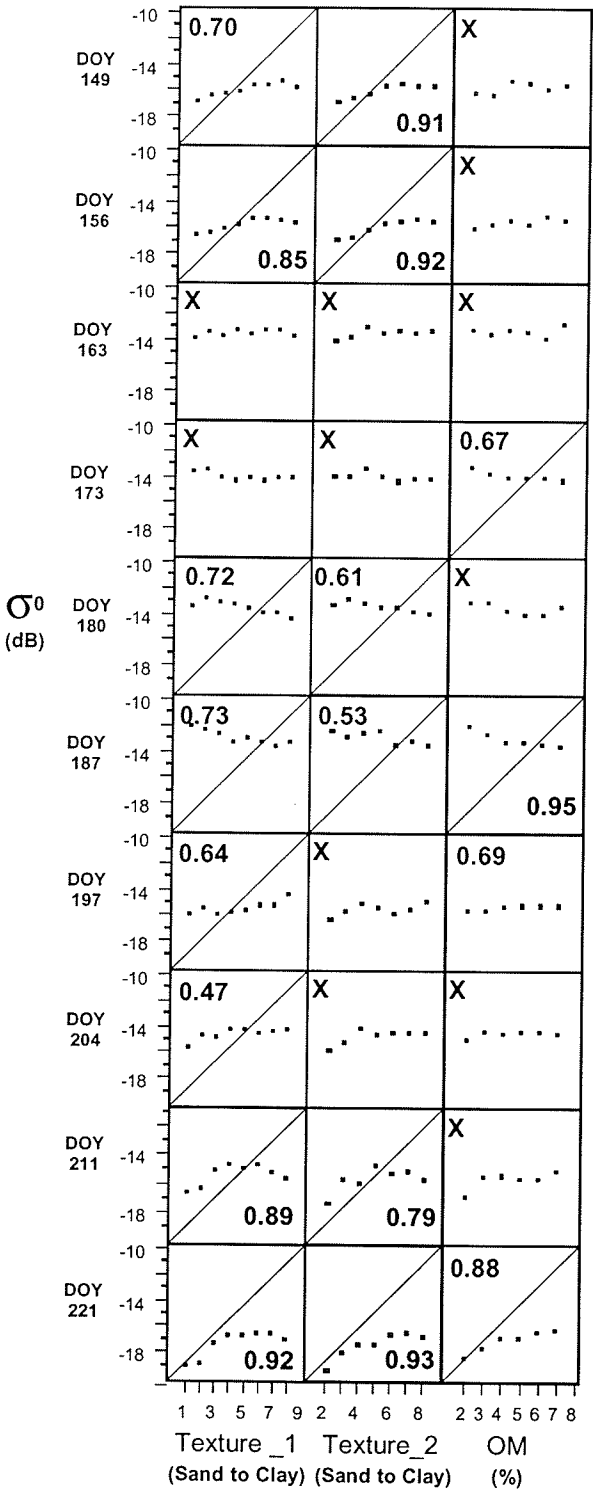

Adjusted R^2

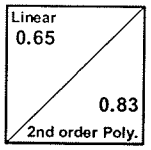

X = no signif. (0.05)

Backscatter Range per DOY per Variable

DOY	Texture_1	Texture_2	OM
149	1.53	1.43	1.24
156	1.36	1.72	1.07
163	0.73	1.15	1.20
173	0.96	1.03	1.09
180	1.64	1.28	1.11
187	1.71	1.17	1.62
197	1.76	1.45	0.57
204	1.50	1.91	0.77
211	2.10	3.02	2.10
221	2.68	3.01	2.31
Mn	**1.60**	**1.72**	**1.31**

Figure 5.21 RADARSAT-1 backscatter averaged over zones of variability for Texture_1, Texture_2 and OM, FLD_100.

On DOY 197 a slight positive trend in backscatter is observed in relation to OM (r^2 = 0.69, σ^o range 0.57dB) and a strong positive trend DOY 221 (r^2 = 0.88, σ^o range 2.31 dB).

In-field variation as expressed by soil texture is more highly correlated to the mean backscatter per zone. Early in the season (DOY 149, 156) the trends appear to be positive and generally curvilinear (r^2 = 0.70 and 0.92), i.e., soil Texture_1 and 2 zones tend to have lower backscatter over sandier soils, and are likely to be associated with soil moisture early in the season.

There are no significant backscatter trends apparent over the soil texture zones for DOY 163 and 173. The dynamic range of σ^o over the soil texture zones are at a seasonal low during this period. Starting DOY on 180 (booting stage) backscatter trends tend to be negative, that is, sandy areas (i.e., low biomass areas) have higher backscatter relative to the clay soils (high biomass areas), (r^2 = 0.72, Texture_1; r^2=0.61, Texture_2). During this period in the growing season, trends in backscatter are related more to scattering from the vegetative surface. DOY 180 is associated with the booting stage, a period of maximum green leaf LAI. The same trend continues for DOY 187 (heading). The in-field variation as defined by Texture_1 shows weak positive correlations (high biomass = high backscatter) on DOY 197 and DOY 204 (r^2 = 0.64 and 0.47 respectively), while Texture_2 shows no significant correlations over this period.

On DOY 211 and 221, Texture_1 and _2 zones are highly correlated to backscatter. The relationships are positive and curvilinear, with coarser textured soils showing the lowest backscatter. Soil moisture differences are negligible across FLD_100-120 on DOY 211 (0.176, 0.174,and 0.169 $gm \cdot cm^{-3}$ for Site 1-3 respectively) therefore, backscatter variations seem to be indicative of differences in the vegetative canopy. This

observation is supported by the ground confirmation data that shows significant differences in head and stem moisture between high and low biomass sites (and to a lesser extent leaf moisture), (Figure 5.16).

5.3.3.2.2 Backscatter vs. NDVI Zones, FLD_100

Backscatter variations as defined by the NDVI zones provide an interesting contrast to those defined by soil texture for FLD_100, Figure 5.22. Regression coefficients are referenced in Tables B9-B10, Appendix B.

Whereas soil texture zones were highly correlated to backscatter on DOY 149-156, backscatter as defined by NDVI zones showed relatively poor correlations DOY 149 (r^2 = 0.56-0.70) and almost no correlation on DOY 156 therefore suggesting that the primary target is the soil surface. Backscatter was not significantly correlated to either soil texture or NDVI zones on DOY 163-173. On DOY 180 and 187 strong negative correlations were observed for SP98_ND_12 vs. backscatter, (r^2 = 0.94 and 0.88, respectively) and for SP98_ND_27 vs. backscatter, (r^2 = 0.85 and 0.77, respectively). The coefficients of determination are at least 20% higher for the NDVI zones versus the soil texture zones, therefore suggesting that backscatter is largely due to variations in biomass. The high correlations with NDVI coincide with booting and heading. It is also noteworthy that the dynamic range in backscatter (σ^o) over NDVI zones is 0.65 - 1.0 dB higher relative to those defined by soil texture.

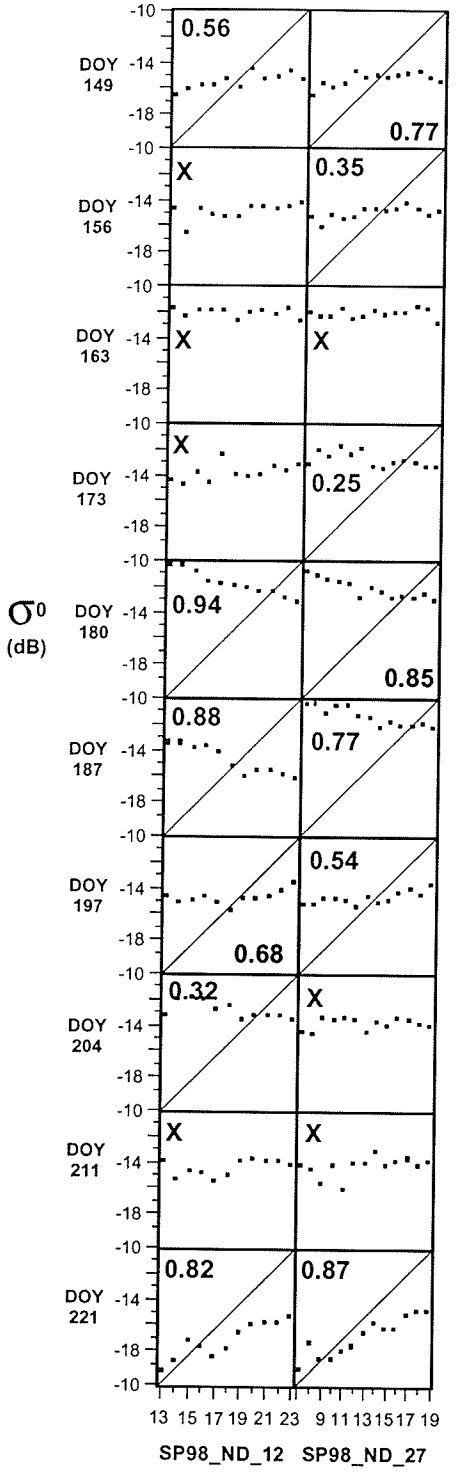

Backscatter Range per DOY per Variable

DOY	SP98_ND_12	SP98_ND_27
149	1.67	1.65
156	1.93	1.56
163	0.86	1.11
173	1.86	1.49
180	2.32	1.93
187	2.36	2.26
197	1.91	1.40
204	1.39	1.11
211	1.42	2.35
221	3.33	3.68
Mn	1.90	1.85

Figure 5.22 RADARSAT-1 backscatter averaged over zones of variability as defined by SP98_ND_12 (DOY 193) and SP98_ND_27 (DOY 208), FLD_100.

The relationships between backscatter and NDVI are poor or absent from DOY 197-211 (watery ripe to soft dough). DOY 221 strong linear positive correlations occurred between backscatter vs. NDVI zones (r^2 = 0.82 - 0.87), in contrast to the curvilinear trends apparent over soil texture zones. The dynamic range in backscatter is on average 0.66 dB higher on DOY 221 using NDVI as a stratification variable.

The physical data suggest that soil moisture is at a seasonal low across FLD_100-120, although clayey soil still has relatively higher soil moisture (Ms = 0.16 (clayey) vs. 0.05 $gm \cdot cm^{-3}$ (sandy soil)). The biomass data show a similar trend in terms of normalized volumetric moisture (nMv) of heads. Stem moisture, not considered in the volumetric model (Chapter 3), shows a similar stratification (Figure 5.23a). Although the soil and canopy moisture regimes coincide, the greatest moisture component resides within the canopy, resulting in backscatter being strongly correlated to in-field zones as defined by the NDVI.

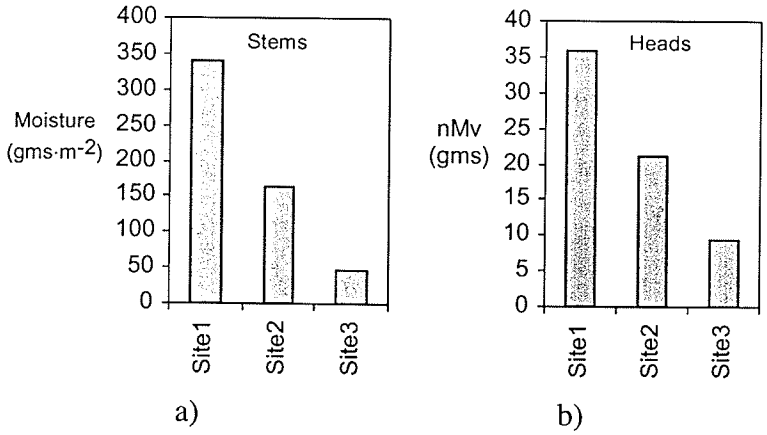

Figure 5.23 a) Gravimetric stem moisture per m^2; b) Normalized volumetric moisture of heads, DOY 221, FLD_100-120.

5.3.3.3 RADARSAT-1 Backscatter vs. In-field Variability: FLD_100-120 (Area Means)

Extending the observations beyond FLD_100, backscatter trends over the whole field (FLD_100-120) are examined using the NDVI zones as the stratification variable. Each field is examined independently and then as an aggregate.

The mid-season NDVI data (SP98_ND_12) shows FLD_120 has the highest NDVI (Avg. 21.2), followed by FLD_100 (Avg. 20.8) and FLD_110 (Avg. 16.3), (Figure 5.24).

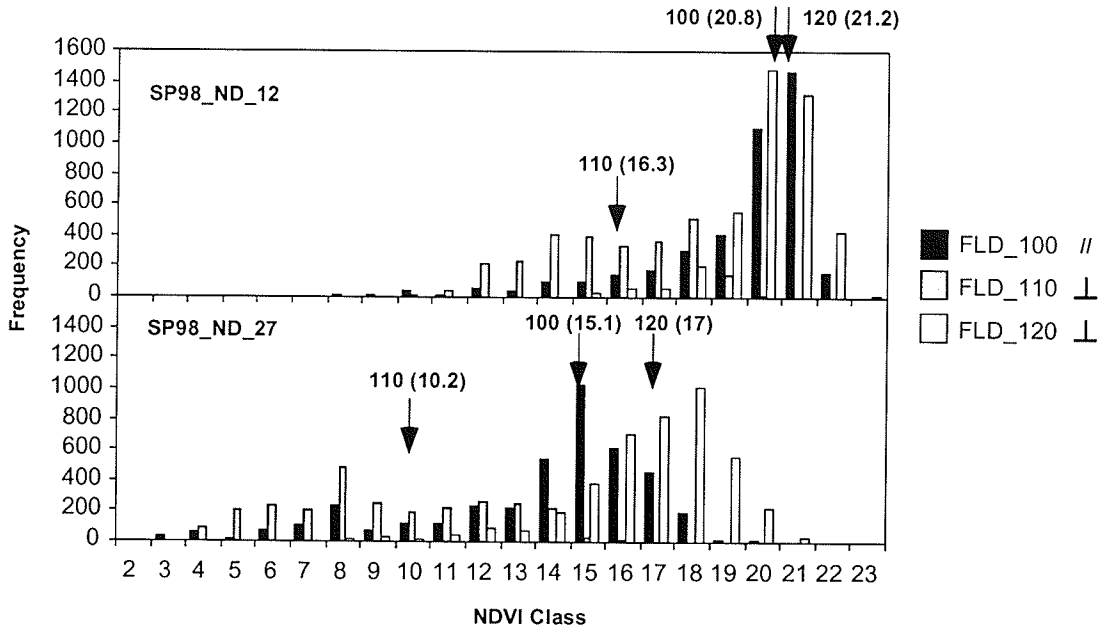

Figure 5.24 Frequency of NDVI classes July 12 (SP98_ND_12) and 27, 1998 (SP98_ND_27) for FLDs_100 to 120.

The range of NDVI is broader for FLD_100 and _110 as they contain a wider range of soil textures. Later in the season (SP98_ND_27) NDVI classes shifted considerably. FLD_120 NDVI are still quite high indicating longer green leaf duration (more favorable

growing conditions). The same is true for FLD_100 although at this time of year differences between FLD_100 and 120 are more evident.

The seasonal backscatter per DOY for FLD_100 to 120 as a function of SP98_ND_12 zones is presented, including the aggregated backscatter for FLD_100-120, in Figure 5.25. Regression coefficients are referenced in Tables B11-B14, Appendix B.

From the scatterplots, it is evident that the backscatter per field per DOY is quite different. FLD_100 backscatter is generally lower per NDVI zone than FLD_110 and 120. This is primarily a function of row direction. Recall that row orientation in FLD_100 is parallel (//) to the incident microwave beam, whereas FLD_110 and 120 rows are oriented perpendicular ($\perp$) to the incident beam. Using the mean backscatter extracted over NDVI classes 19-20 (common to FLDs_100 to 120), differences in backscatter per DOY as a function of row direction are most evident from DOY 149 to 173 (2-3 dB) and later in the season from DOY 211 to 221, as the crop starts to senesce (~2dB), Figure 5.26.

For FLD_110, the strongest trends in backscatter as a function of NDVI zones occurred on DOY 180 and 187 (r^2 = 0.71 and 0.83 respectively), the trends were linear and negative (i.e., low NDVI = high backscatter). On DOY 221 the trends were positive (r^2 = 0.87). The trends in backscatter vs. NDVI for FLD 120 were generally linear and negative (high NDVI = low backscatter) over the growing season with the exception of DOY 221 where FLD_120 started to show a positive trend. For all three fields, DOY 180 and 187 showed strong negative linear trends in backscatter (r^2 = 0.83-0.88) (booting-heading) and positive linear trends on DOY 221.

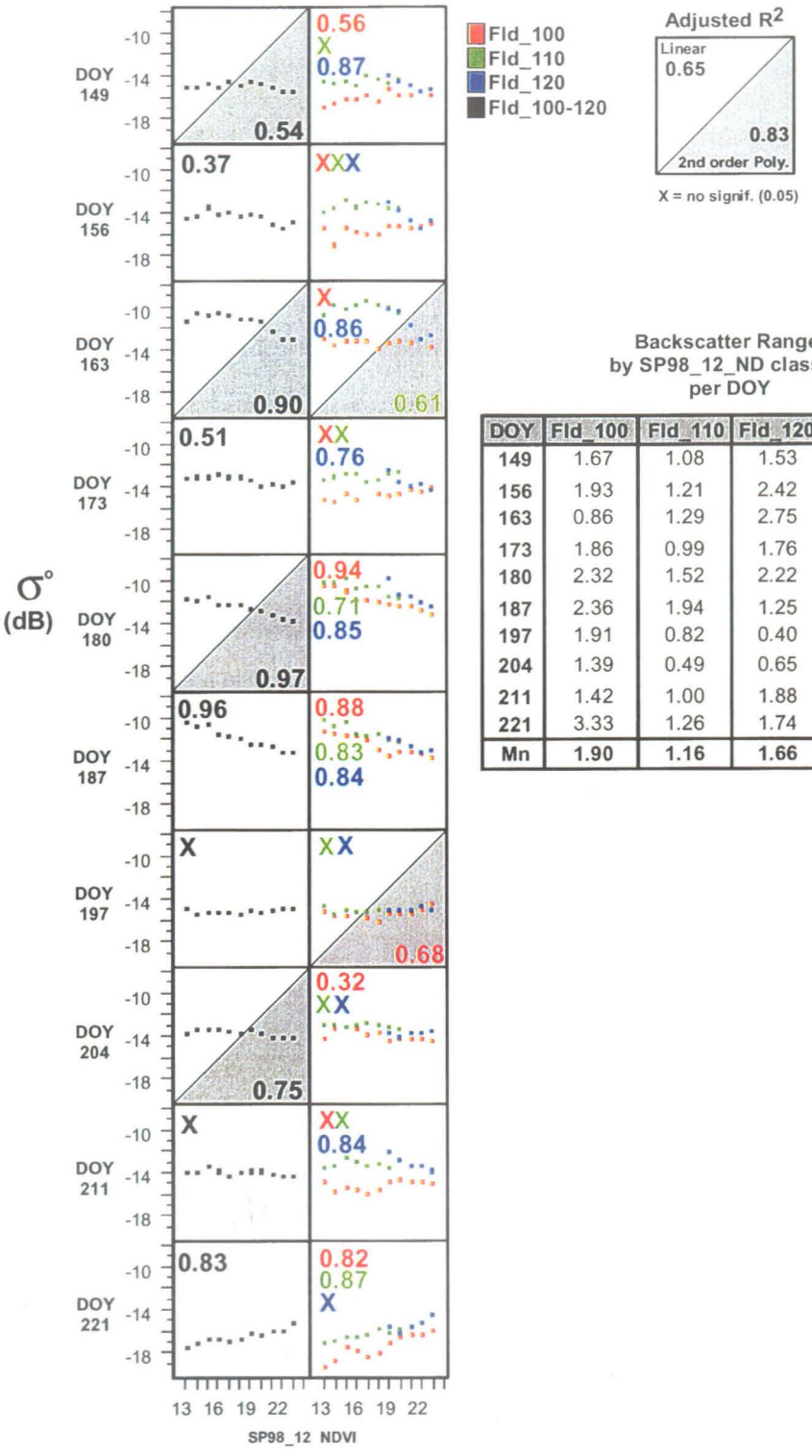

Backscatter Range
by SP98_12_ND classes
per DOY

DOY	Fld_100	Fld_110	Fld_120	Fld_100-120
149	1.67	1.08	1.53	1.05
156	1.93	1.21	2.42	2.10
163	0.86	1.29	2.75	2.67
173	1.86	0.99	1.76	1.28
180	2.32	1.52	2.22	2.32
187	2.36	1.94	1.25	2.82
197	1.91	0.82	0.40	0.77
204	1.39	0.49	0.65	0.95
211	1.42	1.00	1.88	1.15
221	3.33	1.26	1.74	2.35
Mn	**1.90**	**1.16**	**1.66**	**1.75**

Figure 5.25. RADARSAT-1 backscatter trends per DOY for FLDs_100-120 as defined by SP98_ND_12 zones.

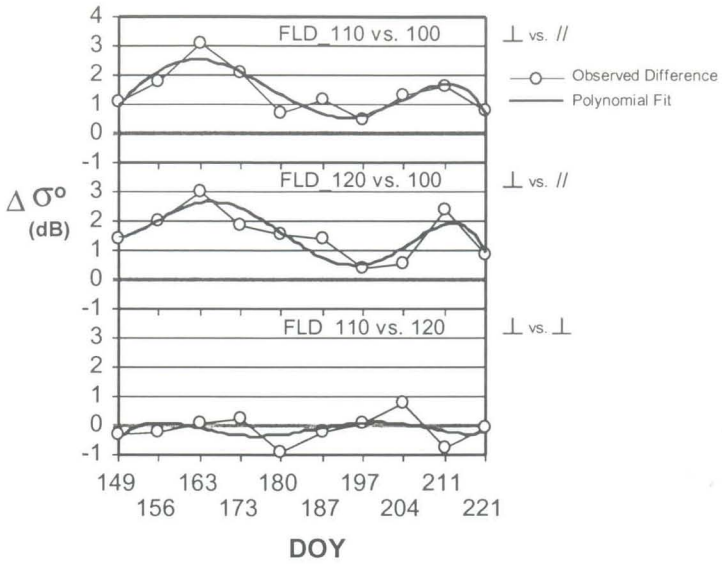

Figure 5.26 Differences in mean backscatter ($\Delta\sigma^o$) over NDVI classes 19-20 (SP98_ND_12) as a function of row orientation, in FLD_100-120.

On DOY 197 and 204 (watery ripe to soft dough) the dynamic range in σ^o (dB) across NDVI zones for each field was at its seasonal low (0.4 - 0.95 dB).

The backscatter trends integrated over all three fields (independent of row direction) show that the strongest trends for FLD_100-120 occurred on DOY 180 and 187 ($r^2 = 0.97$ and 0.96 respectively) and on DOY 221 ($r^2 = 0.83$). Despite the rain event on DOY 187, trends in backscatter at mid-season were consistently negative suggesting that crop canopy parameters were driving the backscatter. The backscatter trends using SP98_ND_27 zones showed similar trends in backscatter per DOY for FLD_100-120, see Figure B1 and Table B.15-B18 (Appendix B). This result is expected as the NDVI scenes are highly correlated.

5.3.3.4 RADARSAT-1 Backscatter vs. In-field Variability: FLD_130-170 (Area Means)

Additional wheat fields within the study area are included in the assessment of RADARSAT-1 to map in-field variability (FLDs_130-240). No physical data exist for these fields, other than SPOT data, which provides some information regarding the distribution of green biomass within each field (Figures 5.11 and 5.12).

Since the results are comparable for FLDs_130-240, trends for FLDs_130-170 are presented using SP98_ND_27 zones as the stratification variable, Figure 5.27, (Tables B19-B23, Appendix B). It is evident from the plots that considerable variation in backscatter between the fields occurs early in the season (DOY 149-163) and later in the season (DOY 204 - 221). On DOY 180 and 187, the backscatter trends for FLDs_130-170 tend to be more consistent across FLDs_130-170. NDVI are inversely correlated to the observed backscatter DOY 180-187 and positively correlated DOY 221. These results are consistent with those of FLD_100-120.

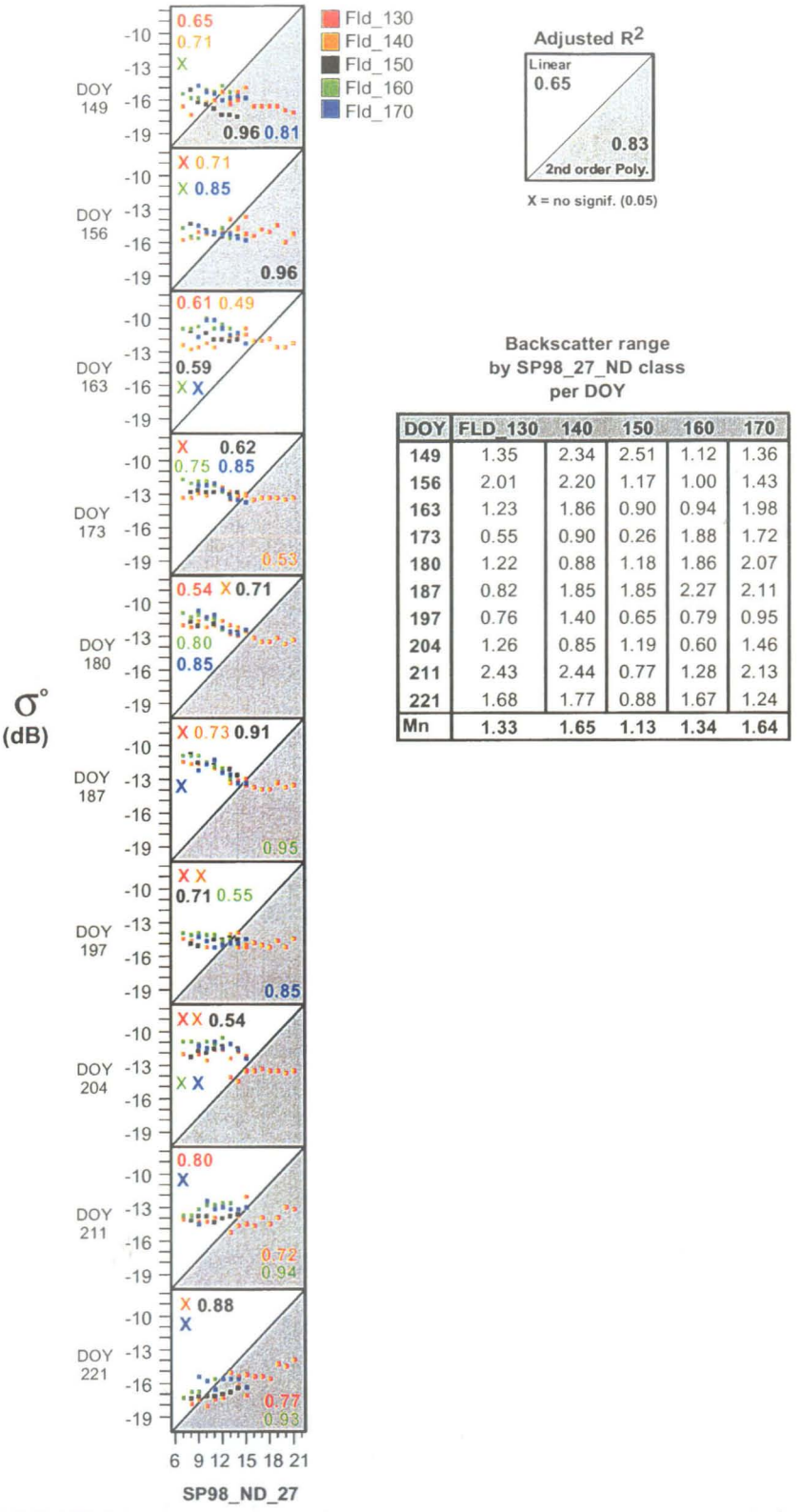

Backscatter range
by SP98_27_ND class
per DOY

DOY	FLD_130	140	150	160	170
149	1.35	2.34	2.51	1.12	1.36
156	2.01	2.20	1.17	1.00	1.43
163	1.23	1.86	0.90	0.94	1.98
173	0.55	0.90	0.26	1.88	1.72
180	1.22	0.88	1.18	1.86	2.07
187	0.82	1.85	1.85	2.27	2.11
197	0.76	1.40	0.65	0.79	0.95
204	1.26	0.85	1.19	0.60	1.46
211	2.43	2.44	0.77	1.28	2.13
221	1.68	1.77	0.88	1.67	1.24
Mn	1.33	1.65	1.13	1.34	1.64

Figure 5.27 RADARSAT-1 backscatter trends per DOY for FLD_130-170 as defined by SP98_ND_27 zones.

5.3.3.5 RADARSAT-1 Backscatter vs. In-field Variability Integrated over FLD_100-240.

If RADARSAT-1 is to be effectively used at regional scales, the relationships between productivity zones and observed backscatter need to be consistent over multiple fields. Backscatter statistics were therefore extracted per NDVI zone over all the wheat fields in the study area (FLD_100-240), Method 3 (Section 5.2.3). The trends revealed by these data were quite remarkable (Figure 5.28). The associated regression coefficients are referenced in Tables B24-B25 (Appendix B).

The highest correlations occurred from DOY 180 to 187 (r^2 = 0.92 - 0.95) and DOY 221 (r^2 = 0.98 - 0.99). The dynamic range in σ^o (dB) on DOY 180 is 1.96 to 2.06. On DOY 187 the dynamic range improved marginally to 2.31 - 2.48 dB. The dynamic range of σ^o (dB) on DOY 221 was 3.99 - 4.77 dB. In general, it appears that backscatter trends early in the season are negatively correlated to NDVI, whereas at the end of the season backscatter and NDVI are positively correlated.

Figure 5.29 shows the temporal backscatter profiles averaged over all the wheat fields in the study area by NDVI zone (SP98_ND_27). The plot shows quite effectively that RADARSAT-1 backscatter is indicative of green biomass over much of the year, especially around the booting-heading period (DOY 180-187) and as the crop is senescing DOY 221. The peak at DOY 163 is likely associated with a rain event 2 days (~ 30mm) prior to the RADARSAT acquisition. It is important to note that despite

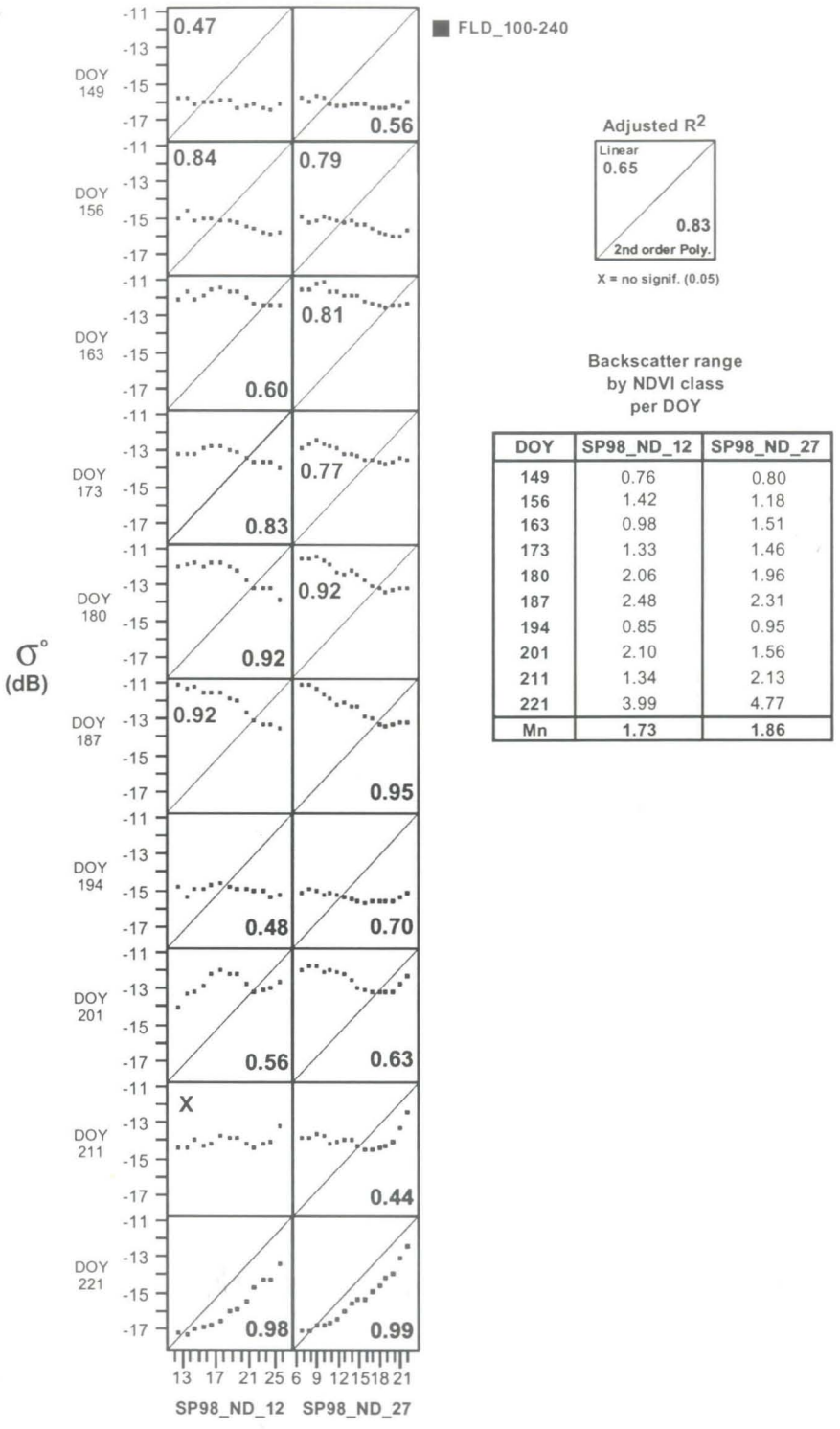

Figure 5.28 RADARSAT-1 backscatter per DOY as a function of NDVI zones (FLDs_100-240).

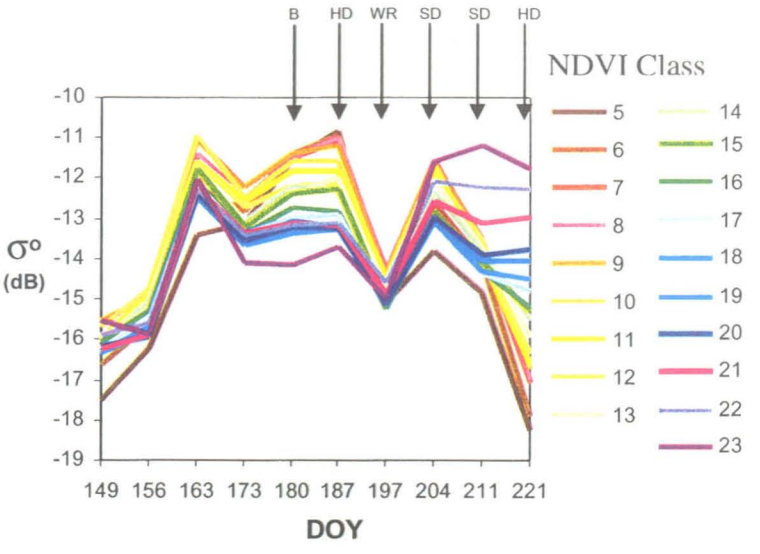

Figure 5.29 Wheat backscatter profiles per NDVI class (SP98_ND_27) averaged over 14 wheat fields (B-booting, HD-heading, WR-watery ripe, SD-soft dough, HD-hard dough).

backscatter being modulated by increases soil moisture, relative backscatter is still indicative of biomass variation over much of the growing season. The largest backscatter trends occurring late in the season are likely due to differential senescence.

Although these data are good at discerning general backscatter trends per DOY, the correlations in Figure 5.28 are somewhat misleading since the backscatter was averaged over large areas representative of NDVI classes, thus significantly reducing the variation inherent in SAR data. When the 11x11 grid cells per field were used to extract mean backscatter and NDVI, coefficients of determination naturally decreased (Figures 5.30-5.32, Table 5.8).

On DOY 180, the coefficient of determination for backscatter versus SP98_ND_12 dropped to 0.38 and 0.39 for SP98_ND_27 using the 11x11 grid data (Figure 5.30). The coefficients of determination improved on DOY 187, to 0.51 and 0.49 respectively (Figure 5.31). On DOY 221, the coefficient of determination between backscatter and SP98_ND_12 was 0.46 and 0.60 for SP98_ND_27 (Figure 5.32). The single date correlations are significant, especially given that row direction effects are not taken into account.

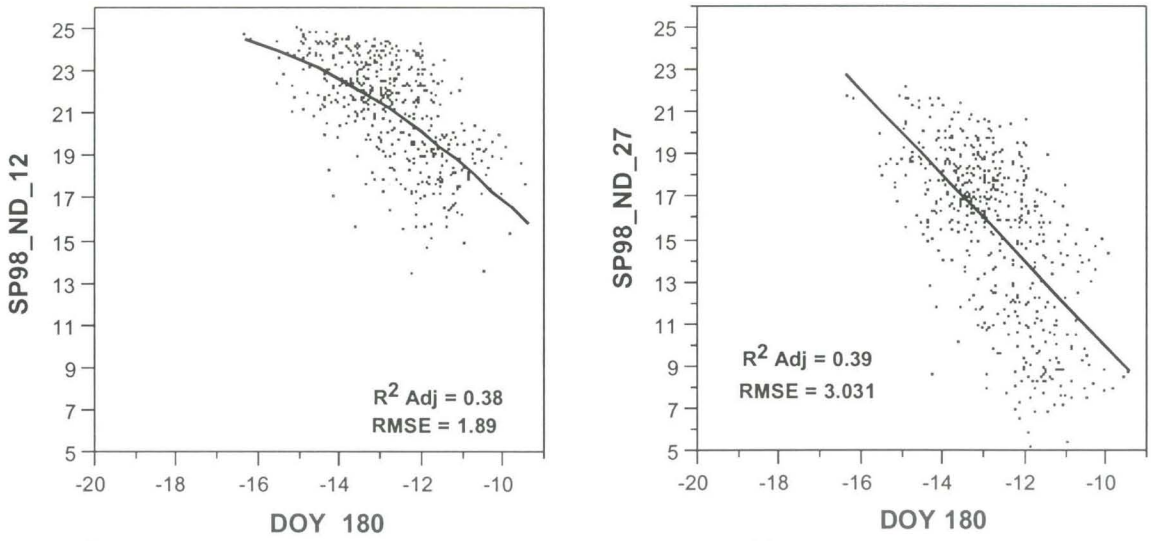

Figure 5.30 RADARSAT-1 backscatter vs. NDVI, a) DOY 180 (σ^o) vs. SP98_ND_12; b) DOY 180 (σ^o) vs. SP98_ND_27.

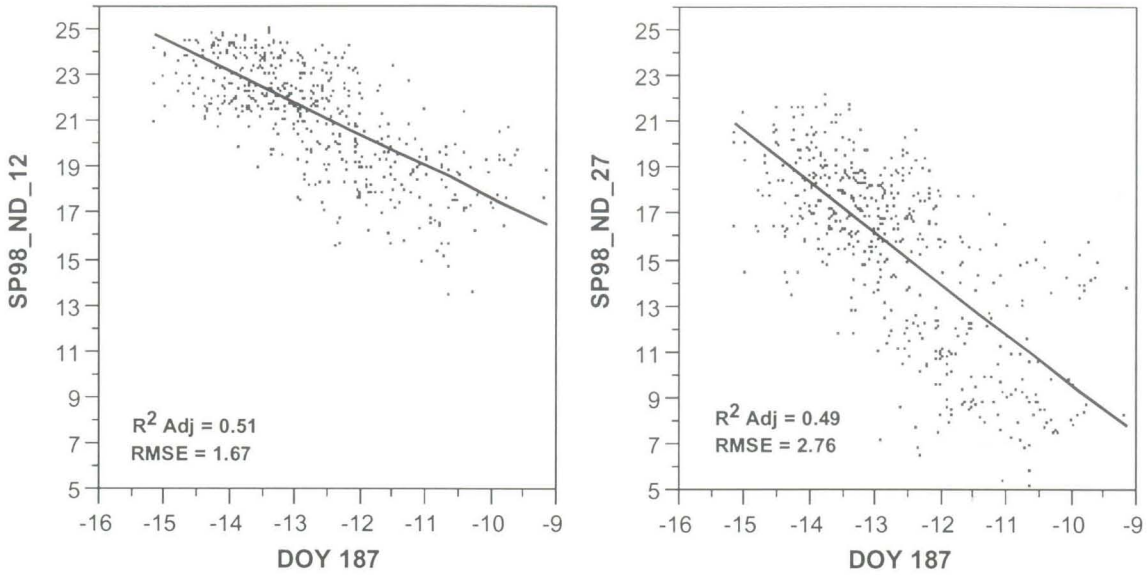

Figure 5.31 RADARSAT-1 backscatter vs. NDVI, a) DOY 187 (σ^o) vs. SP98_ND_12; b) DOY 187 (σ^o) vs. SP98_ND_27.

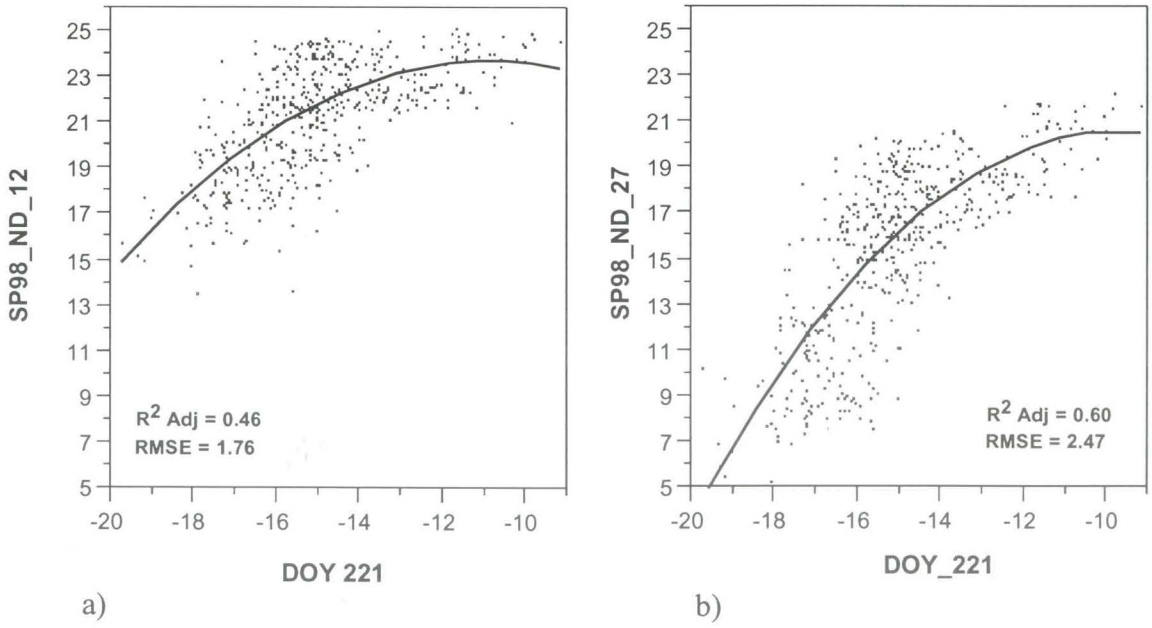

Figure 5.32 RADARSAT-1 backscatter vs. NDVI a) DOY 221 (σ^o) vs. SP98_ND_12, b) DOY 221 (σ^o) vs. SP98_ND_27.

The strong negative correlations between backscatter and NDVI on DOY 187 and the strong positive correlations on DOY 221 pointed to the potential of using these trends to map variations in biomass. The ratio of DOY 187 and DOY 221 backscatter generated significantly higher correlations with NDVI when compared the single date regressions (r^2 = 0.64 (DOY 187/221 versus SP98_ND_12) and r^2 = 0.72 (DOY 187/221 versus SP98_ND_27), Figure 5.33 (Table 5.8)).

Using the regression parameters in Table 5.8, two maps were produced using the ratio data (Figure 5.34 and 5.35). The same colour lookup table was applied to the SPOT and the RADARSAT-1 data. Many of the in-field patterns evident in the SPOT data are evident in the RADARSAT data particularly in the late season SPOT scene (Figure 5.35).

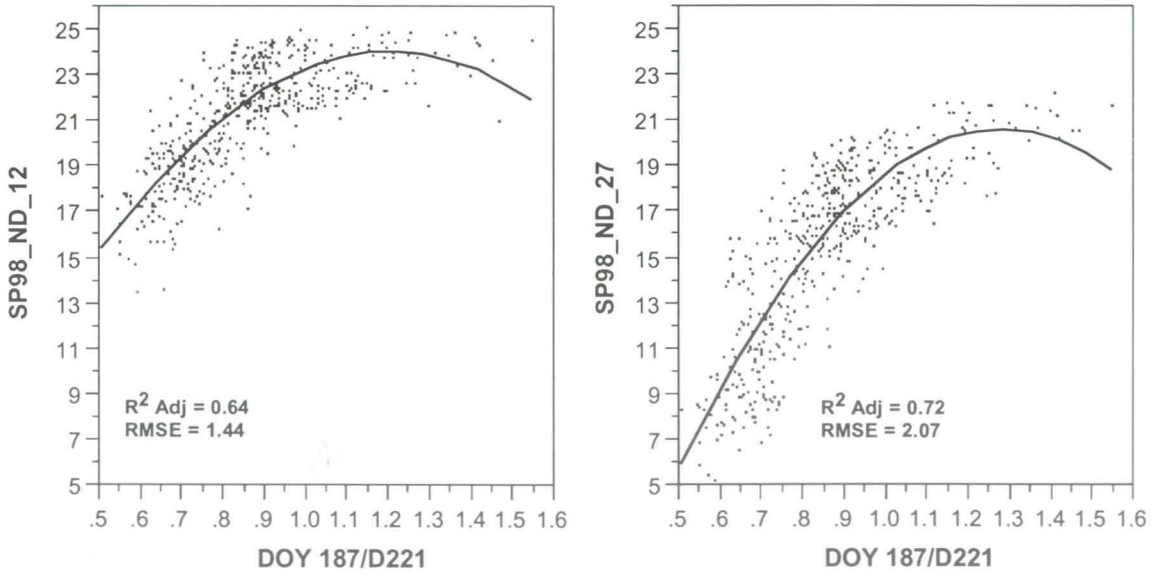

Figure 5.33 DOY 187/221 ratio vs. a) SP98_ND_12 and b) SP98_ND_27.

Table 5.8 Regression coefficients for RADARSAT-1 backscatter vs. NDVI.

	Linear			Reg. Coef.		2nd	order	Polynomial			Reg. Coef.		
DOY	R2	RMSE	P_Value	Intercept	B1	R2	RMSE	P_Value	P_Val B1	P_Val B2	Intercept	B1	B2
180_12 *	0.38	1.89	<.0001	5.838	-1.224	0.38	1.89	<.0001	0.0017	0.0378	-8.975	-3.577	-0.093
180_27 *	0.39	3.03	<.0001	-10.242	-2.025	0.39	3.02	<.0001	0.0025	0.0542	-32.237	-5.520	-0.138
187_12	0.51	1.68	<.0001	4.081	-1.367	0.51	1.68	<.0001	0.0960	0.7738	2.346	-1.652	-0.012
187_27	0.49	2.76	<.0001	-12.127	-2.182	0.49	2.76	<.0001	0.6377	0.3853	-3.495	-0.768	0.057
221_12	0.41	1.84	<.0001	33.682	0.817	0.46	1.76	<.0001	<.0001	<.0001	10.222	-2.471	-0.113
221_27	0.56	2.59	<.0001	38.758	1.546	0.60	2.47	<.0001	<.0001	<.0001	4.887	-3.201	-0.163
187/221_12	0.52	1.66	<.0001	13.117	9.597	0.64	1.44	<.0001	<.0001	<.0001	-1.688	42.690	-17.697
187/221_27	0.63	2.37	<.0001	0.766	17.089	0.72	2.07	<.0001	<.0001	<.0001	-19.863	63.199	-24.658

Indicates significance at 95%

*_12 (SP98_ND_12); _27 (SP98_ND_12)

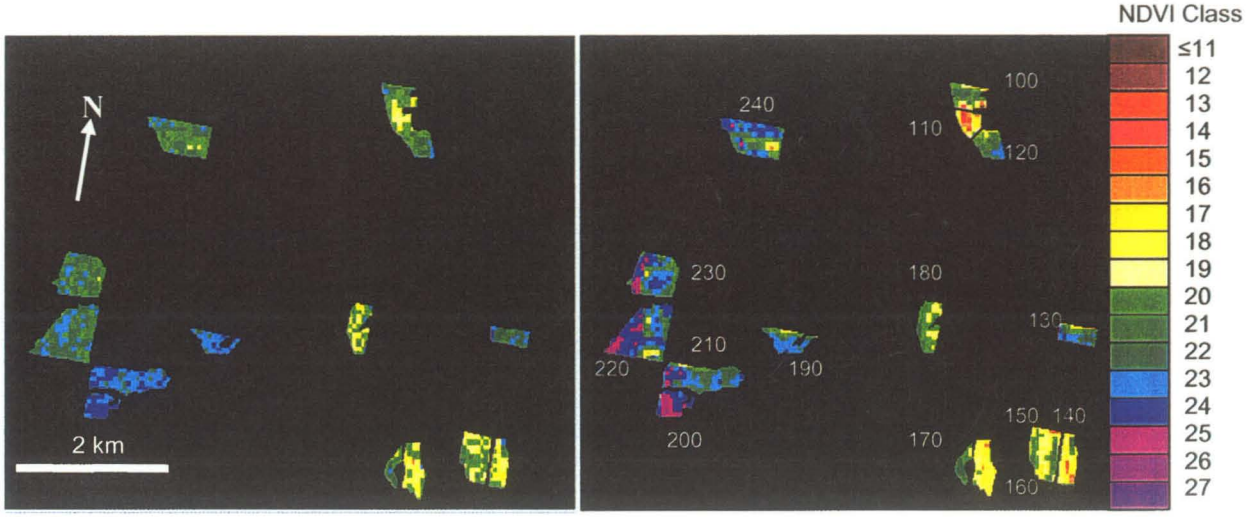

a) b)

Figure 5.34 a) DOY187/221 ratio vs. SP98_ND_12, b) July 12, 1998 SPOT NDVI (SP98_ND_12).

It should be noted that the RADARSAT-1 data show in-field variation relative to DOY 221 (advanced senescence). Recall that the mid-season SPOT data represent variation on DOY 193, and the late season SPOT data represent variation on DOY 208.

This may account for some of the variation evident in SPOT and RADARSAT data. The similarity of the maps is remarkable given that microwave and optical data sense very different (yet related) crop canopy parameters, with the former being sensitive to variations in crop canopy moisture, geometry and soil moisture, while the later being sensitive to green biomass and LAI.

Correlations of RADARSAT-1 backscatter vs. NDVI data on a per field basis (11x11 grid data) show that many of the relationships are poor (Table 5.9 and 5.10). This is likely due to a combination of factors including, the difference in acquisition dates, low in-field variation per field, variation due to fading and, simply the fact, that NDVI and microwave data provide complementary data.

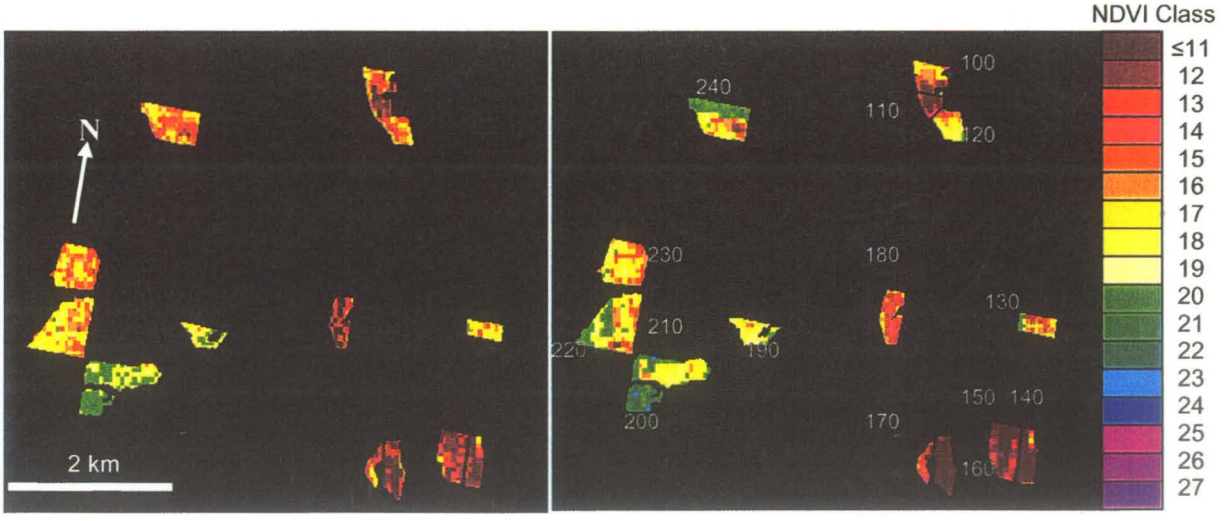

a) b)

Figure 5.35 a) DOY187/221 ratio vs. SP98_ND_27, b) July 27, 1998 SPOT NDVI (SP98_ND_27).

Table 5.9 Correlations between DOY 187/221 σ^o vs. SP98_ND_12 per field.

	Linear			Reg. Coef.		2nd	order	Polynomial			Reg. Coef.		
FLD	R2	RMSE	P_Value	Intercept	B1	R2	RMSE	P_Value	P_Val B1	P_Val B2	Intercept	B1	B2
100-120	0.6	1.52	<.0001	3.265	21.47	0.62	1.47	<.0001	**0.0037**	**0.0223**	-24.363	95.336	-48.71
130	-0.03	1.2	0.5659	19.414	2.744	-0.1	1.23	0.7479	0.5991	0.6149	-7.062	62.291	-33.35
140	0.63	1.13	**<.0001**	7.609	15.44	0.62	1.14	<.0001	0.9318	0.5798	12.281	2.069	9.35
150	0.16	0.85	**0.0019**	14.623	6.914	0.16	0.85	0.0043	0.1826	0.2539	0.353	46.917	-27.86
160	0.11	0.77	**0.0349**	14.838	4.716	0.1	0.77	0.0842	0.5206	0.4513	25.132	-27.337	24.716
170	0.95	0.23	**0.003**	12.299	10.14	0.96	0.2	0.0184	0.2059	0.2922	-1.331	43.332	-19.97
180	-0.02	0.74	0.517	20.755	-1.319	-0.1	0.75	0.6745	0.5184	0.5437	27.545	-21.18	14.375
190	0.38	0.73	**0.0038**	15.425	6.558	0.36	0.74	0.0141	0.3945	0.5198	5.152	26.251	-9.37
200	-0.03	0.52	0.4944	23.76	0.607	0.03	0.51	0.297	0.1562	0.1658	8.767	24.103	-9.107
210	0.13	0.82	**0.0024**	20.021	2.529	0.16	0.8	0.0017	0.0341	0.057	8.219	23.518	-9.201
220	0.22	1.42	**<.0001**	14.342	9.718	0.22	1.42	<.0001	0.3525	0.5541	6.767	26.551	-9.281
230	0.14	1.16	**0.001**	17.003	6.905	0.13	1.17	0.0044	0.5268	0.6634	10.551	21.989	-8.757
240	0.37	1.53	<.0001	9.831	15.1	0.43	1.45	<.0001	**0.0017**	**0.005**	-38.429	133.06	-71.43

Indicates significance at 95%

Table 5.10 Correlations between DOY 187/221 σ^o vs. SP98_ND_27 per field.

	Linear			Reg. Coef.		2nd	order	Polynomial			Reg. Coef.		
FLD	R2	RMSE	P_Value	Intercept	B1	R2	RMSE	P_Value	P_Val B1	P_Val B2	Intercept	B1	B2
100-120	**0.63**	1.91	**<.0001**	-7.863	29.040	0.64	1.90	<.0001	0.0444	0.1839	-28.308	83.704	-36.049
130	-0.04	1.48	0.7467	14.902	1.892	-0.10	1.52	0.9452	0.9068	0.9170	8.137	17.108	-8.522
140	**0.58**	1.69	**<.0001**	-4.941	20.980	0.62	1.59	<.0001	0.1604	0.0472	19.246	-48.228	48.406
150	**0.21**	1.00	**0.0003**	4.619	9.601	0.20	1.01	0.0014	0.5021	0.6591	-1.893	27.855	-12.713
160	**0.15**	0.47	**0.0150**	6.411	3.385	0.12	0.48	0.0545	0.9072	0.9904	6.513	3.068	0.245
170	**0.70**	0.59	**0.0496**	5.092	9.545	0.79	0.49	0.1033	0.2292	0.2615	-32.052	100.012	-54.424
180	-0.04	0.93	0.7857	15.078	-0.690	-0.04	0.93	0.613	0.3384	0.3459	28.200	-39.073	27.780
190	**0.20**	1.01	**0.0346**	11.537	6.187	0.15	1.04	0.1154	0.9246	0.9598	12.657	4.042	1.021
200	-0.04	0.66	0.6624	20.746	0.488	-0.05	0.66	0.5853	0.3427	0.3533	7.869	20.670	-7.822
210	**0.47**	0.94	**<.0001**	10.926	6.933	0.47	0.94	<.0001	0.7230	0.3700	17.373	-4.533	5.026
220	**0.24**	1.73	**<.0001**	6.951	12.284	0.23	1.74	<.0001	0.7241	0.9999	6.948	12.290	-0.003
230	**0.22**	1.48	**<.0001**	6.853	11.616	0.22	1.48	0.0001	0.2970	0.4333	-7.954	46.229	-20.095
240	**0.37**	2.35	**<.0001**	-1.030	23.343	0.39	2.32	<.0001	0.0493	0.1042	-44.854	130.458	-64.869

Indicates significance at 95%

5.4 Conclusions

The results presented in this chapter have shown that seasonal and inter-annual NDVI were highly correlated in FLD_100-120 (r^2 = 0.70-0.95), and that in-field variation as expressed by the NDVI was largely a function of soil texture (r^2 = 0.66 - 0.87) and OM (r^2 = 0.70-0.87) and predictive of yield (r^2 = 0.74 - 0.94). NDVI were shown to be representative of biomass variations as related to green leaf area and duration, and indirectly to gravimetric moisture content of component parts of the canopy (leaves, stems and heads), canopy height and plant density (# of tillers per plant). It was shown that as the crop matured, variations in green leaf duration (re: phenological stage), were indicative of the degree of residual moisture within the canopy and an indicator of its distribution within the canopy. This is of particular significance as it shows that NDVI are directly and indirectly sensitive to parameters that affect microwave backscatter (i.e., crop density, crop height, and the dielectric properties of component parts of the canopy). Based on the data presented, it was concluded that NDVI are a good indicator of relative in-field variation and a suitable stratification variable by which to assess the sensitivity of RADARSAT-1 data to in-field variation.

Using the 11x11 grid data, RADARSAT-1 backscatter from FLD_100 showed considerable variation in relation to within field zones defined by soil texture, OM and NDVI. Variability as defined by soil texture showed early season correlations (r^2 = 0.31 - 0.38) and late season correlations (r^2 = 0.17-0.42) with backscatter whereas NDVI showed significant mid season correlations (r^2=0.25-0.33) and late season correlations (r^2=0.27-0.37) with backscatter.

Using soil texture zones as a stratification variable to extract mean backscatter revealed that soil texture was the most frequently correlated variable per DOY (FLD_100) suggesting variously that soil moisture variations (early in the season) and/or resulting crop canopy parameters (later in the season) have a strong association with soil texture zones. NDVI zones were best correlated to backscatter from booting to heading (r^2 = 0.77-0.94) and at hard dough (r^2 = 0.82-0.87) when canopy moisture per component part of the canopy showed significant stratification in stems and heads across NDVI (biomass) zones. RADARSAT-1 backscatter was inversely related to NDVI (low NDVI = high backscatter) at booting and heading and directly related to NDVI late in the season.

When backscatter was extracted per NDVI zone across all wheat fields within the study area, the relationships between NDVI and backscatter became much stronger. The seasonal NDVI vs. backscatter trends appeared consistent across most wheat fields within the study site.

Exploiting the inverse seasonal trends in microwave backscatter, the 11x11 grid data were used to generate DOY 187/221 backscatter ratios. The ratio data were highly related to seasonal NDVI and hence to biomass variations (r^2 = 0.64, SP98_ND_12; r^2 = 0.72 SP98_ND_27).

The results suggest that RADARSAT-1 data may be useful in discriminating general variations in biomass at the in-field scale and/or regionally. Additional data and research are required to provide a more quantitative assessment of the potential of RADARSAT data to provide yield potential information.

Chapter 6: Detection of In-field Variability Vs. Radarsat-1 Backscatter, Canola

6.1 Introduction

In Chapter 5 the nature of in-field variation was examined for wheat fields. It was shown that soil texture, OM, and crop yield were strongly correlated with NDVI. The NDVI were directly linked to variations in biomass as expressed by LAI and green leaf duration, and indirectly to variations in crop canopy moisture and density (tillering and canopy height). Using NDVI as a surrogate for biomass, RADARSAT-1 backscatter was shown to be indicative of biomass variations from booting to heading (DOY 180-187) and as the crop senesced (DOY 221).

This chapter examines the ability of RADARSAT-1 to detect biomass variations within canola fields per DOY. The approach used in Chapter 5 will be adopted in this chapter. A link between the physical properties of canola and NDVI will be established, followed by the assessment of RADARSAT-1 backscatter to detect relative variations in biomass as defined by NDVI.

6.1.1 Objectives

The objectives of this chapter are:

1) To examine in-field variation of canola biomass in FLD_1 as defined by seasonal and inter-annual NDVI derived from CASI and SPOT data tosupport the use of

NDVI's as a stratification variable for assessing seasonal RADARSAT-1 backscatter.

2) To examine the seasonal RADARSAT-1 backscatter (σ^o (dB)) from canola vis-à-vis relative productivity zones as defined by mid and late season NDVI and to determine if significant backscatter trends are evident per DOY that can be exploited to derive crop condition information.

6.2 Methods

6.2.1 Study Site

The canola fields within the Miami study site include FLD_1 (from Chapter 4) and 14 additional canola fields, Figure 6.1. Fields 1-4 (FLDs_1-4) are located at the foot of the Manitoba Escarpment, on the Manitoba Plain. FLDS_5-15 are situated above the escarpment on the Saskatchewan Plain.

The only information available for these fields include planting date, harvest date, and average yield expressed as bushels per acre (BPA). Relative in-field variability is derived from the SPOT and CASI data.

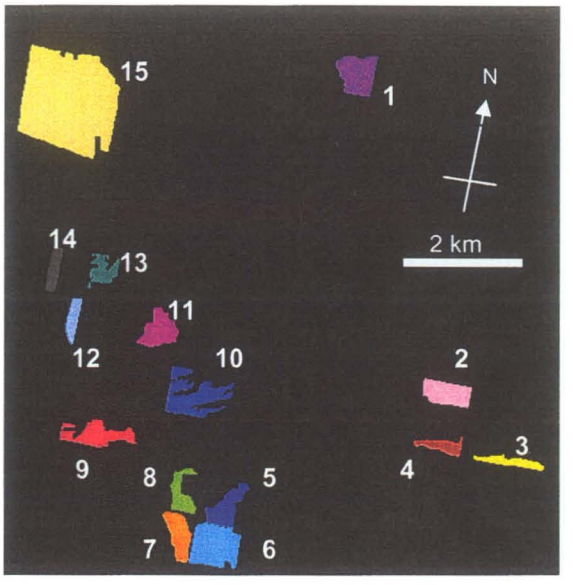

Figure 6.1 Field (FLD) identifiers for canola fields in the Miami study Site (FLDs_1-15).

6.2.2. In-field Variability Data

6.2.2.1 Yield and Optical Remote Sensing Data

The in-field variability data for FLD_1 are much less extensive than FLD_100-120, in Chapter 5. The soil texture and OM data are absent, although yield data were obtained in 1997.

In 1997 FLD_1 was seeded to oats. The yield database was edited to remove anomalous low values associated with the beginning of each run and anomalously high values at the end of each run. The data were classified in ArcView into ± 0.5 SD intervals around the mean.

The inter-annual optical data (CASI and SPOT) used to characterize relative variation within the canola fields are described in Section 5.2.1.3 and include its calibration (Section 5.2.1.3.1) and classification (Section 5.2.1.3.2). Relationships between the inter-annual and seasonal NDVI are examined using regression analysis to establish the consistency of the NDVI / productivity zones.

6.2.3 RADARSAT-1 Backscatter vs. In-field Variability

Several methods are used to assess the ability of RADARSAT-1 vis-à-vis in-field variability, as outlined in Section 5.2.3 with some modifications.

1) Method 1. Using the 11x11 cell grid in Figure 6.2, statistics were extracted for mid (SP98_ND_12) and late season (SP98_ND_27) NDVI for FLD_1 and correlated against the weekly RADARSAT-1 data (σ^o (dB)). Scatterplots per DOY and associated tables summarizing the regression coefficients are presented.
2) Method 2. Using productivity zones as defined by NDVI (SP98_ND12, and SP98_ND_27) mean RADARSAT-1 backscatter statistics for FLD_1 are extracted and regressed against NDVI. Scatterplots showing per DOY trends are presented as well as associated tables summarizing regression coefficients.

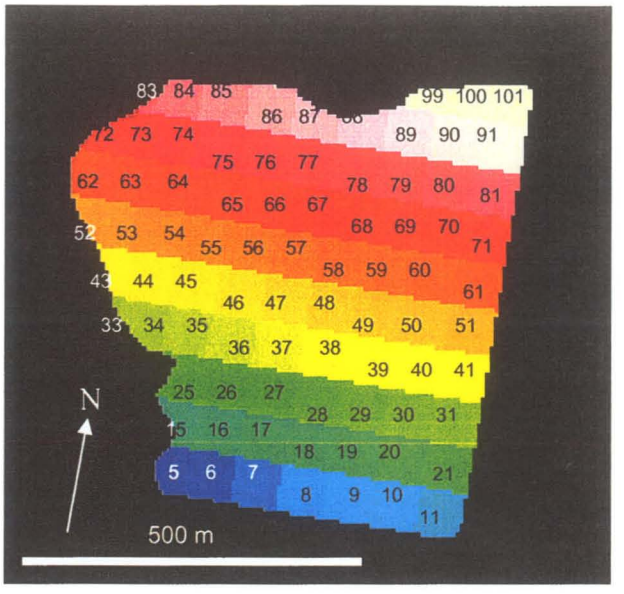

Figure 6.2 The 11x11 grid used to extract NDVI and RADARSAT-1backscatter averages, FLD_1. Numbers in field represent grid identifiers.

3) Method 3. To streamline the analysis of backscatter trends for the remaining canola fields, seasonal backscatter profiles were extracted for each field using multiple NDVI zones (Section 6.3.3.3). Fields were grouped into one of two classes based on their seasonal profile characteristics (designated Group_1 and Group_2 FLDs). Backscatter trends were subsequently extracted using NDVI zones over Group 1 and 2 FLDs and finally over all fields (FLDs_1-15) to assess the potential of RADARSAT to identify within and between field variations per DOY.

6.3 Results

6.3.1 In-field Variability

6.3.1.1 Yield Mapping

Yield monitor data for FLD_1 were obtained in 1997, when the field was sown to oats. The mean yield for FLD_1 was 74 bushels per acre. The yield distribution is relatively narrow when compared to FLD_100-120 in the previous chapter. Yields within FLD_1 generally ranged from 50 to 85 bushels (Figure 6.3).

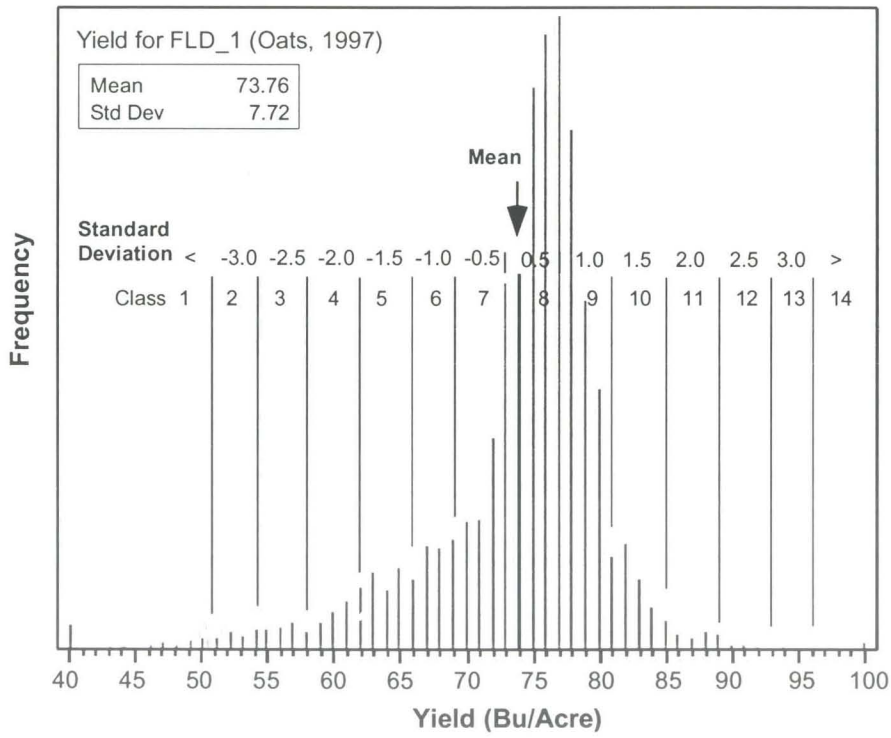

Figure 6.3 Frequency histogram yield monitor data for FLD_1, 1997.

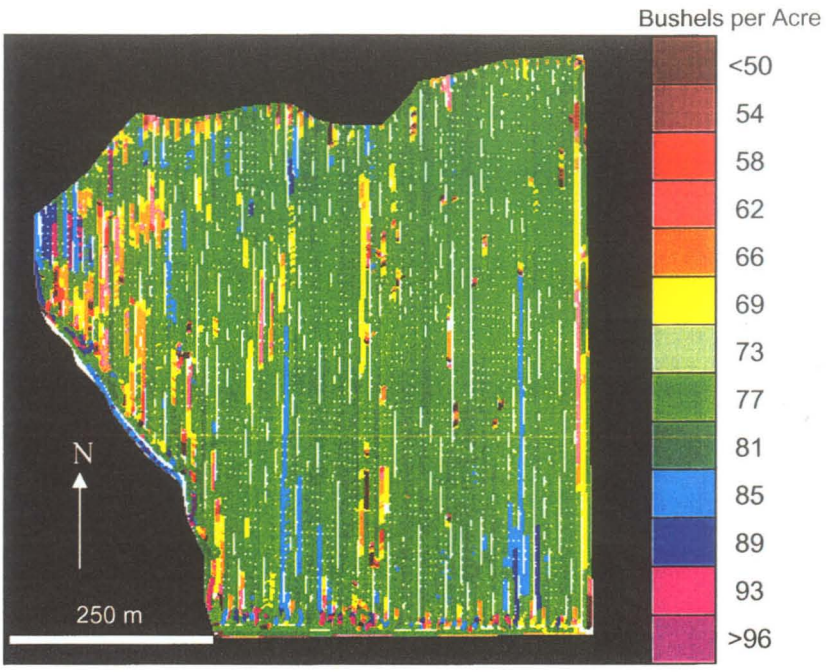

Figure 6.4 Classification of yield monitor data, FLD_1, 1997.

The yield map for FLD_1 was found to be highly problematic due to considerable banding evident in the data (Figure 6.4). The banding suggested operator-induced variation as opposed to in-field variation, especially when viewed in association with the inter-annual NDVI data (Figures 6.5 and 6.6). The banding problem was not evident in FLD_100-120 (different operator) where late season NDVI (SP97_ND) were highly correlated to canola yield ($r^2 = 0.94$). The yield data obtained for FLD_1 were deemed unusable.

6.3.1.2 Optical Remote Sensing Data

6.3.1.2.1 Classification Results: FLD_1

This Section presents the classified CASI and SPOT NDVI data for 1997-1998 for FLD_1. Section 6.3.2.1 examines the seasonal and inter-annual relationships between the NDVI in FLD_1. Section 6.3.2.2 examines physical data to demonstrate that NDVI are related to significant variations in biomass as expressed by leaf area and duration, plant water content and crop height.

As mentioned previously, FLD_1 had been planted to oats in 1997. The mid-season NDVI data (CASI97_ND) were obtained at heading (Figure 6.5a). FLD_1 NDVI were relatively uniform over a large portion of the field with pockets of lower biomass in the southeast and southwest corners of the field and along the western and north-western portions of the field. Towards the latter part of the season, the crop started to senesce, and more subtle variations in biomass appeared as a function of green leaf duration (Figure 6.5b).

Similar in-field patterns were apparent in the 1998 SPOT data. On July 12 (SP98_ND_12) the canola in FLD_1 was in full bloom (Figure 6.6a). The NDVI, which are sensitive to green biomass, were therefore suppressed due to the dominance of yellow flowers in the upper canopy. The suppression of NDVI was also noted in the CASI data over FLD_100-120 (CASI97_ND). On July 27, (SP98_ND_27) the canola had podded and was ripening. The central portion of the field had the highest NDVI (high biomass) with pockets of low NDVI (low biomass) to the north and south.

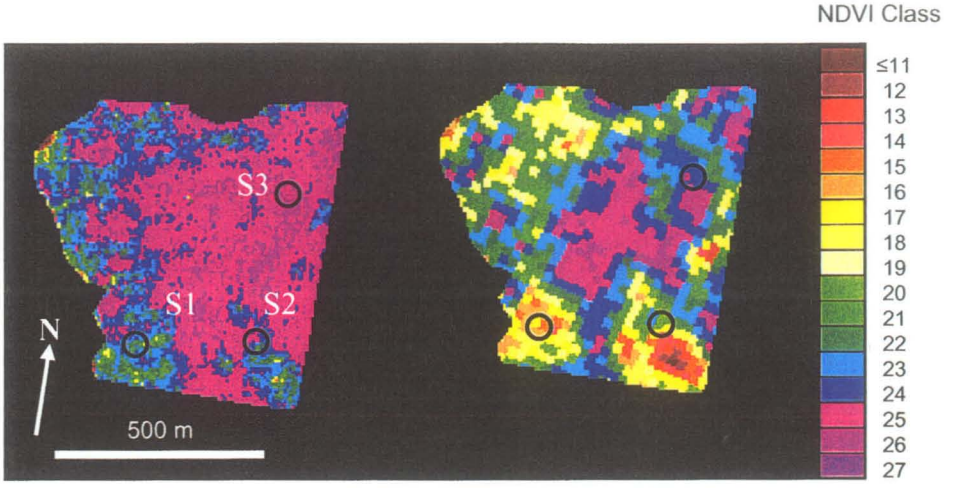

a) b)

Figure 6.5 FLD_1 a) CASI NDVI, July 15, 1997, DOY 196 (CASI97_ND); b) SPOT NDVI data, Aug. 6, 1997; DOY 218 (SP97_ND). Intensive sample site location identified, S1-S3 (low to high biomass).

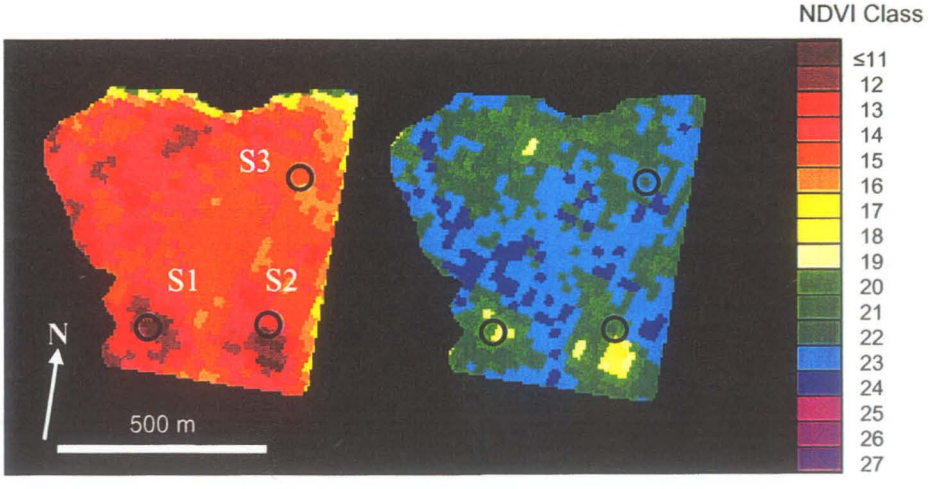

a) b)

Figure 6.6 SPOT NDVI data, FLD_1 a) July 12, '98, DOY 193 (SP98_ND_12), b), July 27, DOY 208 (SP98_ND_27).

6.3.2 In-Field Variability vs. NDVI

Prior to assessing the ability of RADARSAT-1 to discriminate variations in biomass within FLD_1 the relationships between seasonal and inter-annual NDVI are examined together with supporting physical data. The results presented provide support for using NDVI as a stratification variable to assess RADARSAT-1 sensitivity to "known variation" within and between wheat fields within the study area where little or no ground verification data exist.

6.3.2.1 In-Field Variability vs. NDVI: FLD_1

The relationships between the seasonal and inter-annual NDVI for FLD_1 are presented in Figure 6.7 and Table 6.1. In 1997, early season NDVI derived from the CASI data (CASI97_ND) were poorly correlated ($r^2 = 0.48$) with the end of season SPOT data (SP97_ND), and the 1998 SPOT data ($r^2 = 0.48$, SP98_ND_12; $r^2 = 0.17$, SP98_ND_27), Figure 6.7. The poor correlations between the CASI and SPOT NDVI are attributed to a combination differences in crop type and crop phenology at the time of data acquisition.

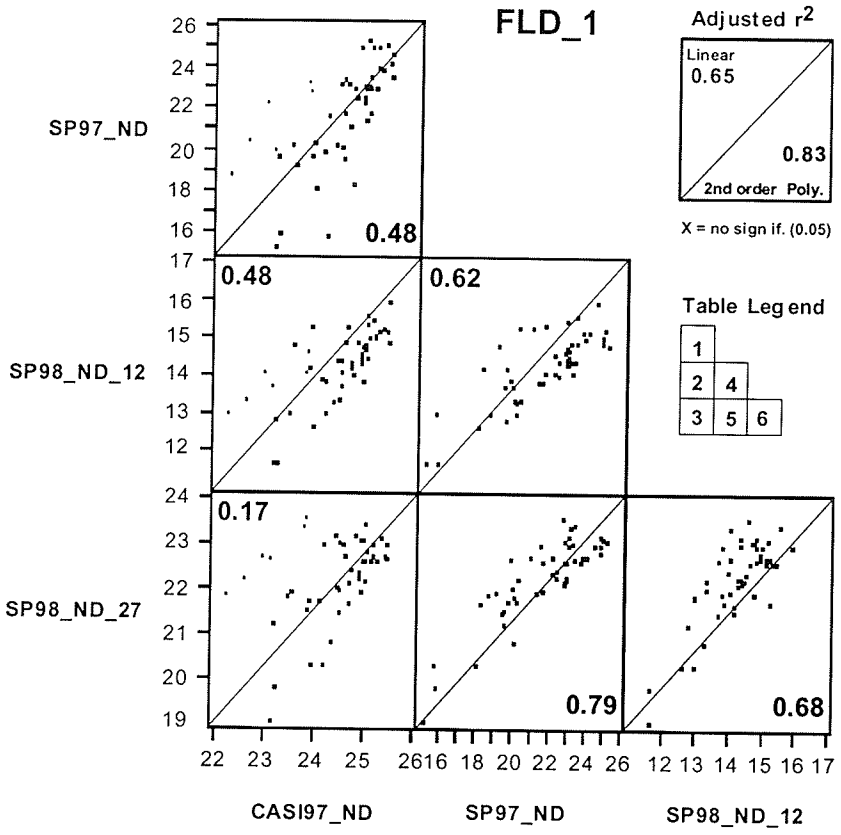

Figure 6.7 Correlations between season and inter-annual NDVI for FLD_1. NDVI in 1997 are representative of oats, in 1998 they are representative of canola.

Table 6.1 Regression parameters for NDVI and yield for FLD_100-120 (see Figure 5.13 for variable IDs)

	Linear			Reg. Coef		2nd order Polynomial					Reg. Coef		
ID*	R2	RMSE	P_Value	Intercept	B1	R2	RMSE	P_Value	P_Val B1	P_Val B2	Intercept	B1	B2
1	0.43	1.86	<.0001	-28.045	2.036	**0.48**	1.78	<.0001	**0.0337**	**0.0257**	459.21	-38.427	0.839
2	**0.48**	0.68	**<.0001**	-5.706	0.817	0.49	0.67	<.0001	0.1601	0.1277	118.27	-9.478	0.213
3	**0.17**	0.85	**0.0016**	9.726	0.512	0.19	0.85	0.0028	0.1838	0.1650	151.46	-11.258	0.244
4	**0.62**	0.58	**<.0001**	7.691	0.303	0.62	0.58	<.0001	0.0948	0.2915	2.54	0.806	-0.012
5	0.75	0.47	<.0001	15.036	0.331	**0.79**	0.43	<.0001	**0.0002**	**0.0028**	3.68	1.441	-0.027
6	0.61	0.59	<.0001	11.074	0.782	**0.68**	0.53	<.0001	**0.0002**	**0.0009**	-32.92	7.138	-0.228

Indicates significance at 95%

*see Table Legend Figure 6.7 for variable IDs

The inter-annual and seasonal SPOT data were more highly related (r^2 = 0.62 - 0.79). The late season inter-annual SPOT data (SP97_ND vs. SP98_ND_27) had the highest coefficient of determination (r^2=0.79), the seasonal 1998 data were also highly correlated despite the suppression of NDVI during flowering stage (r^2 = 0.68).

6.3.2.2 NDVI vs. Crop Canopy Characteristics: FLD_1

The data show that within field variations as expressed by NDVI are relatively consistent seasonally and inter-annually. This section will briefly illustrate that NDVI are indicative of growing conditions and variations in plant biomass, green leaf area and duration, plant water content, and crop height (factors that directly and indirectly affect microwave backscatter).

The physical data were obtained at the intensive sample sites identified in Chapter 4 but discussed here in context of NDVI. Site 1 represents low biomass, Site 2 moderate biomass, and Site 3 high biomass.

The surface (0-7cm) soil sample data used to determine soil moisture in Chapter 4 were analyzed for soil texture by the Manitoba Soil Surveys Branch, Table 6.2. Based on these very limited data, the soils at all three sites were classified as fine sandy loams. The low biomass site within the field tended to have a higher sand content, the high biomass site had the lowest portion of sand and highest portion of silt. Although these data cannot be considered conclusive due to the limited sample size and depth, the results were consistent with those of FLD_100-120 that showed soil texture was a determining factor as related to in-field variations of biomass and productivity.

Table 6.2 Surface soil texture (0-7 cm) for sites 1-3, FLD_1.

Field	Site	Lab #	Depth	Sand					TOT Sand	TOT Silt	TOT Clay	Texture Class
				VCS	CS	MS	FS	VFS				
FLD_1	S1	8001	1 to 7	3	7	35	30	3	78	8	14	FINE SANDY LOAM
FLD_1	S2	8003	1 to 7	5	3	14	34	13	69	11	20	FINE SANDY LOAM
FLD_1	S3	8006	1 to 7	1	2	5	26	25	59	30	11	FINE SANDY LOAM

Seasonal variations in the areal extent ($m^2 \cdot m^{-2}$) and water content of the component parts of the canopy are presented in Figure 6.8 and 6.9. These data show significant temporal and spatial differences in green leaf area and duration as well as gravimetric moisture.

Figures 6.10 - 6.11 summarize the area ($m^2 \cdot m^{-2}$) and water content ($gm \cdot m^{-2}$) per component part of the canopy associated with the SPOT data (SP98_ND_12 & 27). DOY 193 green leaf area is the dominant aerial component across all sites, but that changes quickly as the canopy matures so that by DOY 208 stems and pods are the most significant components. Water content within the component parts of the canopy shows a particularly strong stratification across the low to high biomass sites which is very significant as it has direct bearing on the dielectric properties of the canopy and, hence on microwave backscatter. The stratification is particularly well defined on DOY 208.

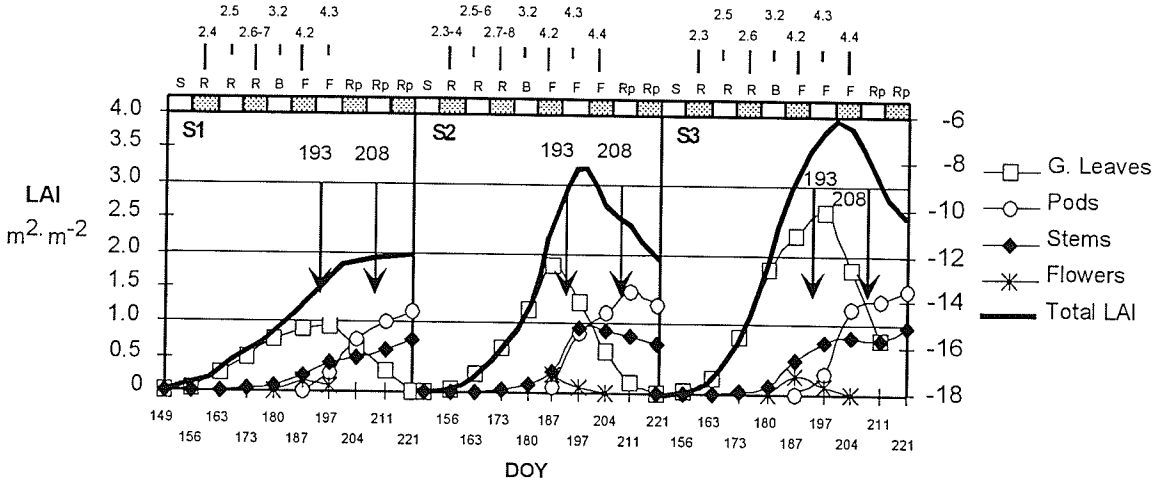

Figure 6.8 LAI ($m^2 \cdot m^{-2}$) of the component parts of the canopy, vs. DOY. Arrows indicate acquisition dates for the SPOT imagery, DOY 193 (SP98_ND_12) and DOY 208 (SP98_ND_27). See Appendix A, Table A-2 for crop phenology.

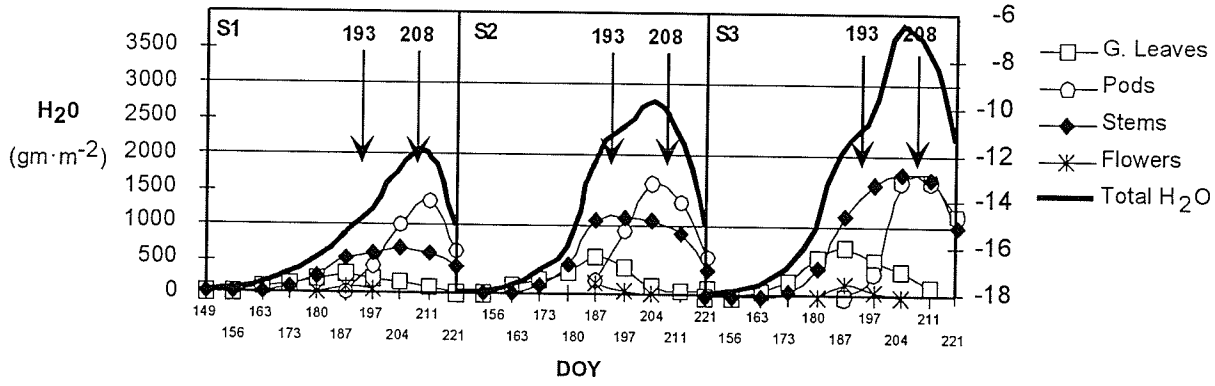

Figure 6.9 Water content ($gm \cdot m^{-2}$) of the component parts of the canopy, vs. DOY. Arrows indicate acquisition dates for the SPOT imagery, DOY 193 (SP98_ND_12) and DOY 208 (SP98_ND_27).

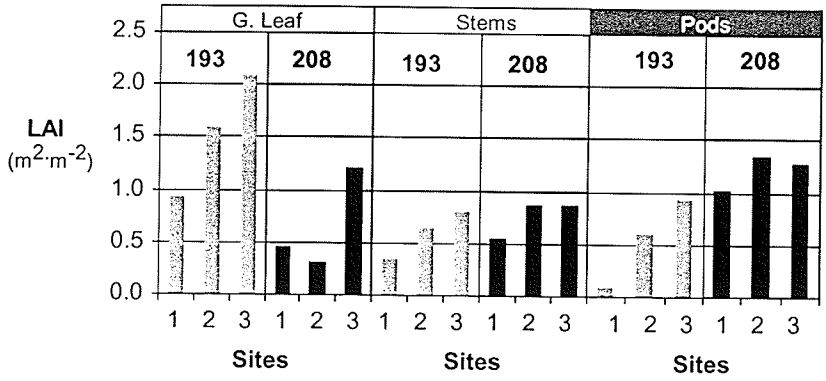

Figure 6. 10 Aerial distribution of component parts of the canopy coincident with SPOT acquisitions DOY 193 and 208.

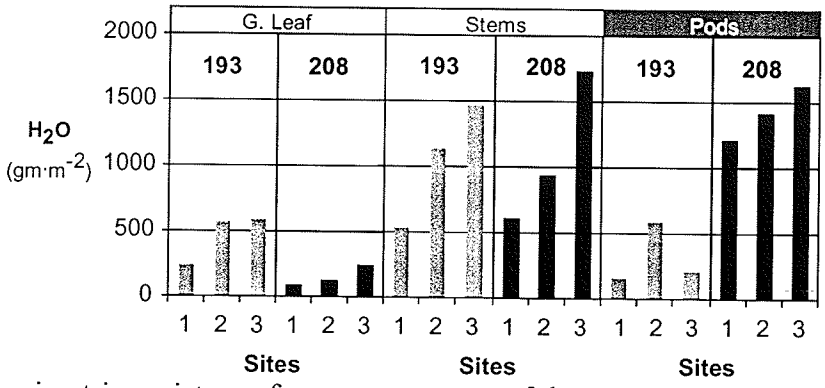

Figure 6.11 Gravimetric moisture of component parts of the canopy coincident with SPOT acquisitions DOY 193 and 208.

Unlike cereal grains, the component parts of the canola canopy remain relatively green until the canopy is swathed, therefore NDVI stay highly related to crop canopy parameters late into the season. The NDVI extracted over the sample sites showed stratification consistent with the observed biomass (Figure 6.12), suggesting that NDVI are therefore useful in delineating relative variations within a field.

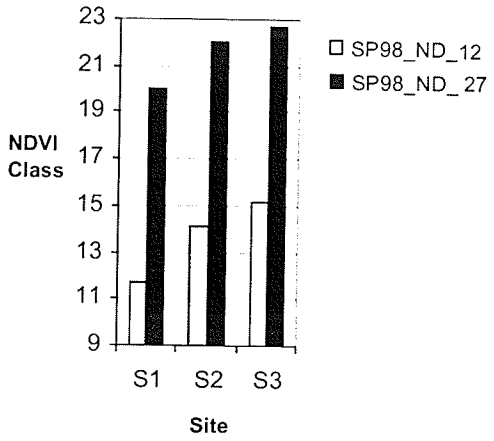

Figure 6.12 Average NDVI per sample site, DOY 193 and 208, 1998.

Variations in crop biomass are also associated with differences in crop height (Figure 6.13). The figure shows total height (Tot H) plus 1 standard deviation (+1 S.D.), maximum height of the leaf layer (U leaf), lower limit of the pods (Pods L), lower limit of the green leaf layer (L. Leaf) and the height at which secondary stems (2nd Stem) start.

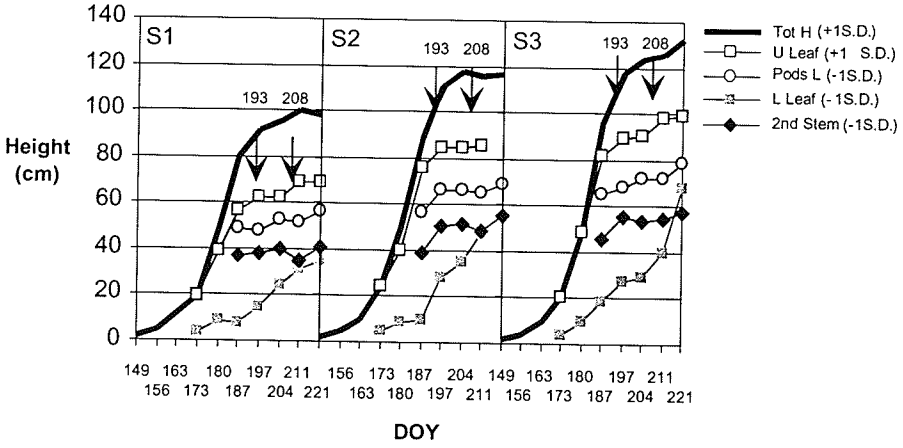

Figure 6.13 Height of component parts of the canola canopy per sample site.

6.3.3 RADA RSAT-1 Backscatter vs. In-field Variability

The overall intent in examining the seasonal (per DOY) backscatter over canola is to determine if and when RADARSAT-1 backscatter is indicative of variations in biomass and to determine whether seasonal backscatter trends can be exploited to map in-field variability. The approaches used to examine backscatter trends within the study site are outlined in Section 6.2.3.

6.3.3.1 RADARSAT-1 Backscatter vs. In-field Variability: FLD_1 (11x11 Grid)

Using the 11x11 grid (Figure 6.2), mean RADARSAT-1 backscatter and NDVI (SP98_ND_12 & 27) were extracted for FLD_1. Scatterplots showing the correlations between RADARSAT-1 and observed within field variability as defined by NDVI are presented in Figure 6.14. Tables C1 and C2 in Appendix C summarize the regression coefficients per variable per DOY.

The results show considerable variation in backscatter independent of NDVI zones. Overall, the correlations are very poor. On DOY 163 and 173 mid-season NDVI (SP98_ND_12) are correlated to backscatter (r^2 = 0.25 and 0.35 respectively), coinciding with phenological stage 2.5-2.6, (Appendix A, Table A-2). A weak correlation is also evident on DOY 187 during the flowering stage, r^2 = 0.25.

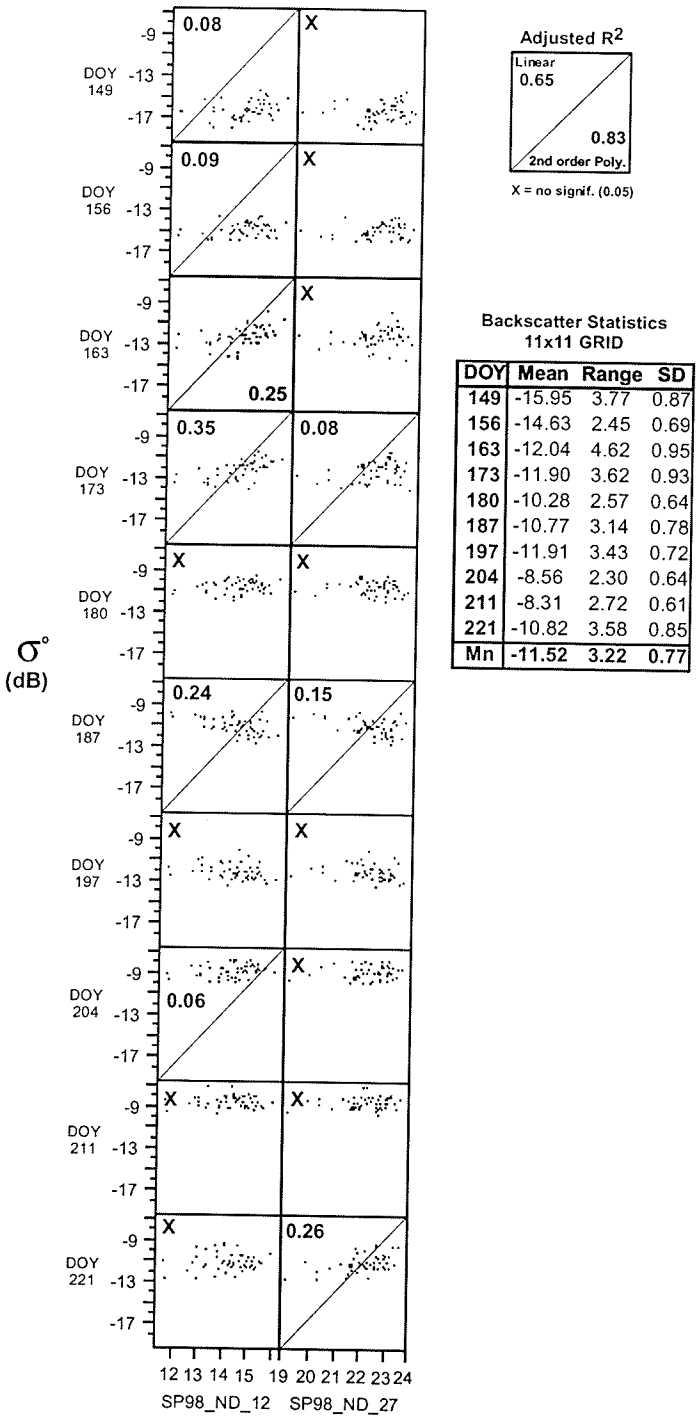

Figure 6.14 RADARSAT-1 backscatter vs. measures of within field variability (11x11 grid), FLD_1.

Whereas the backscatter trends are positive on DOY 163 to 173, (high NDVI, high backscatter) the trend is negative DOY 187.

Backscatter trends over canola relative to SP98_ND_27 are very poor as well. The best correlations are on DOY 187 ($r^2 = 0.15$) and DOY 221 ($r^2 = 0.26$). The backscatter trends are negative on DOY 187 and positive on DOY 221. The seasonal range of backscatter (σ^o (dB)) from DOY 149 to 221 is 7.53 dB and the average per DOY range in backscatter for FLD_1 is 3.22 dB.

6.3.3.2 RADARSAT-1 Backscatter vs. NDVI Zones: FLD_1 (Area Means)

In this section NDVI zones are used to extract mean backscatter values for FLD_1 (Method 2, Section 6.23). As with wheat, the intent is to reduce the inherent variability of SAR data to better discern weekly backscatter trends relative to productivity zones.

The scatterplots for FLD_1 are presented in Figure 6.15, while the regression coefficients are presented in Tables C3-C4 in Appendix C. Using SP98_ND_12 as the stratification variable, it is apparent that all the backscatter trends are positive with the exception of DOY 187. The highest correlations occur more consistently towards the end of the year, DOY 204 - 221 ($r^2 = 0.72$ - 0.84). During this time the crop was ripening, so it is a period associated with peak biomass where pods dominate the canopy in terms of area ($m^2 \cdot m^{-2}$) and gravimetric water content ($gm \cdot m^{-2}$). DOY 163 also is highly correlated ($r^2 = 0.87$) and is associated with the rosette stage (stage 2.5, five true leaves emerged).

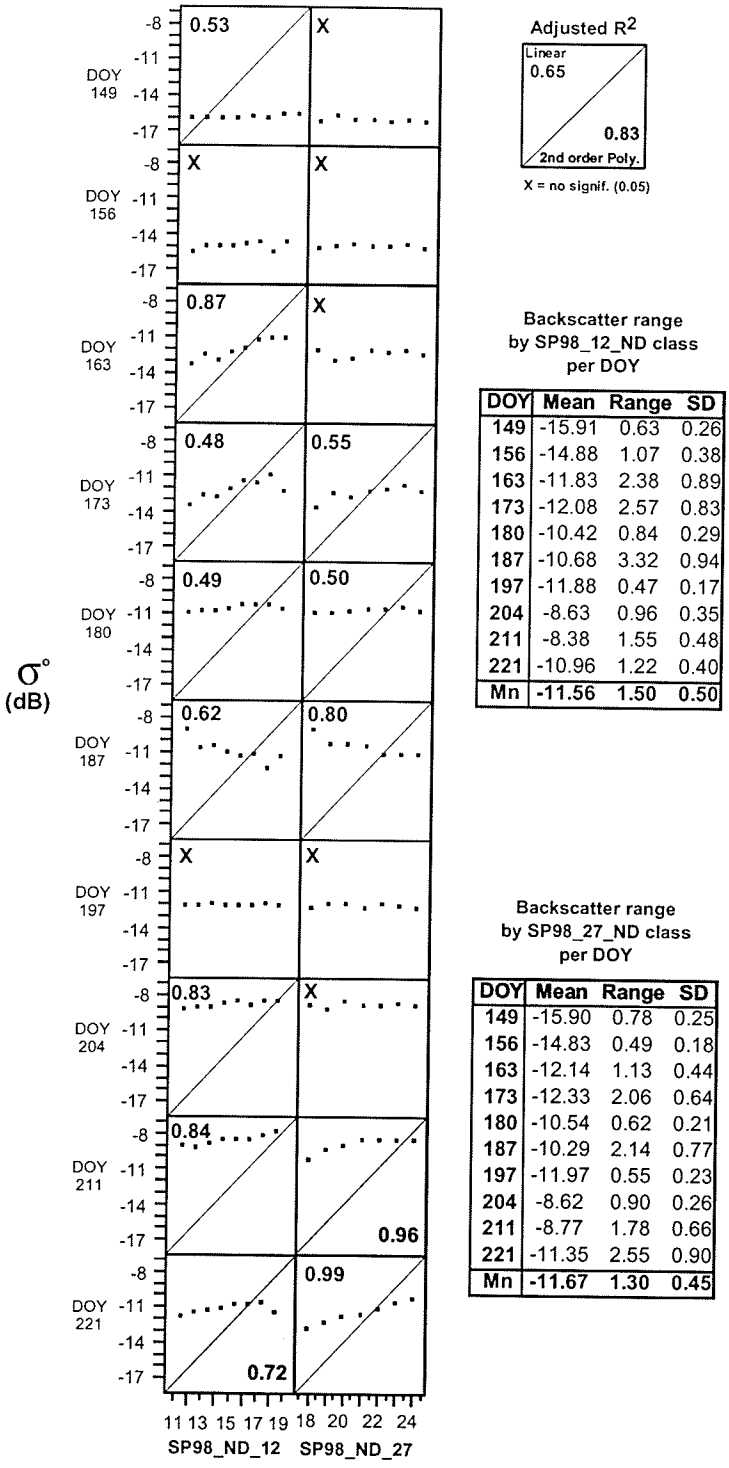

Backscatter range by SP98_12_ND class per DOY

DOY	Mean	Range	SD
149	-15.91	0.63	0.26
156	-14.88	1.07	0.38
163	-11.83	2.38	0.89
173	-12.08	2.57	0.83
180	-10.42	0.84	0.29
187	-10.68	3.32	0.94
197	-11.88	0.47	0.17
204	-8.63	0.96	0.35
211	-8.38	1.55	0.48
221	-10.96	1.22	0.40
Mn	-11.56	1.50	0.50

Backscatter range by SP98_27_ND class per DOY

DOY	Mean	Range	SD
149	-15.90	0.78	0.25
156	-14.83	0.49	0.18
163	-12.14	1.13	0.44
173	-12.33	2.06	0.64
180	-10.54	0.62	0.21
187	-10.29	2.14	0.77
197	-11.97	0.55	0.23
204	-8.62	0.90	0.26
211	-8.77	1.78	0.66
221	-11.35	2.55	0.90
Mn	-11.67	1.30	0.45

Figure 6.15. RADARSAT-1 backscatter vs. measures of within field variability, FLD_1.

Positive backscatter trends are also apparent on DOY 173 to 180 (r^2 = 0.48-0.49). The range in backscatter values on DOY 163-173 is approximately 2.5 dB. Later in the season backscatter ranges across FLD_1 are lower, ranging from 0.96 dB (DOY 204) to 1.55 dB (DOY 211).

Using late season NDVI zones (SP98_ND_27) to define within field variation in FLD_1, the strongest backscatter trends were evident on DOY 187 (r^2 = 0.80), and DOY 211 to 221 (r^2 = 0.96, 0.99 respectively). On DOY 187 the backscatter trend was negative (low biomass, high backscatter) whereas the other trends were positive. The negative trends associated with the rain event may indicate increased backscatter due to the soil contribution within the low biomass areas. Within field backscatter ranges averaged over SP98_ND_27 zones for DOY 187, 211 and 221 were 2.14 dB, 1.78 and 2.55 dB respectively. The seasonal range of RADARSAT-1 backscatter over SP98_ND_27 zones was 6.28 dB (σ^o), with a seasonal average backscatter range of 1.3 dB per DOY across FLD_1.

Figure 6.16b is a mapped representation of SP98_ND_ 27 versus backscatter DOY 221 (r^2 = 0.99). Based on the regression relationship (Figure 6.17b), backscatter averaged per NDVI zone increased by ~0.42 dB per NDVI class.

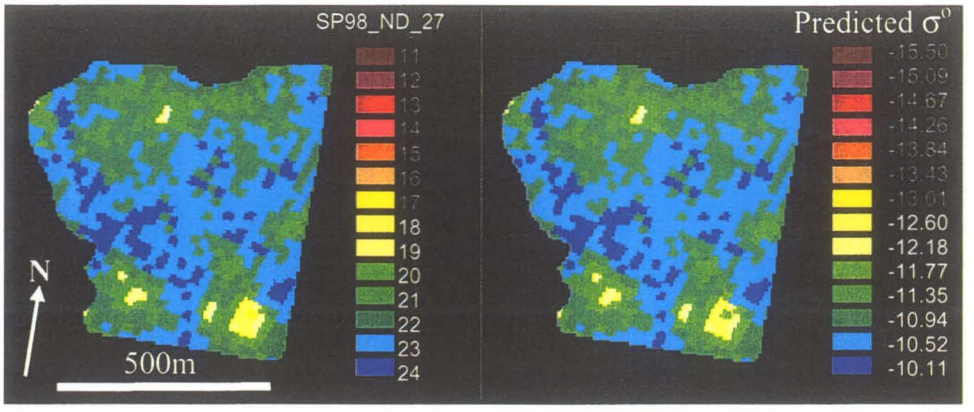

a) b)

Figure 6.16 FLD_1 a) Observed NDVI classes for SP98_ND_27 (DOY 208); b) estimated RADARSAT backscatter (σ^o dB) per NDVI class (out of range classes shaded).

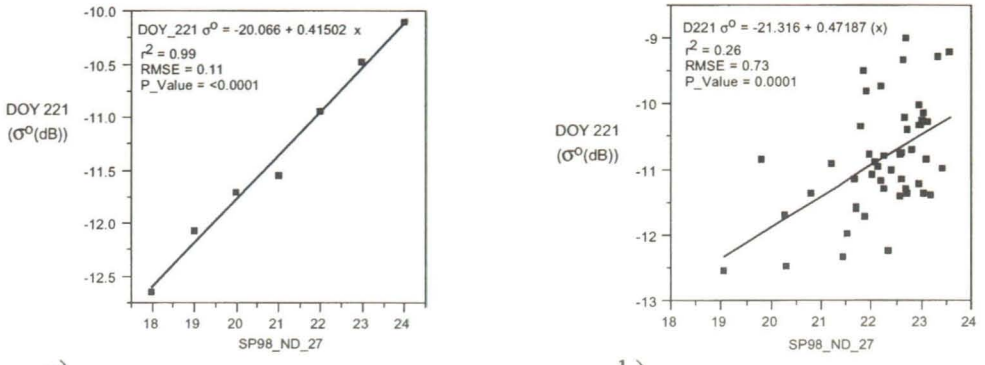

a) b)

Figure 6.17 FLD_1 a) SP98_ND_27 vs. DOY 221 backscatter averaged over NDVI zones; b) SP98_ND_27 vs. DOY 221 backscatter averaged over 11x11 grid cells).

The regression in Figure 6.17b is a representation of NDVI versus RADARSAT-1 backscatter using the 11x11 grid data for FLD_1 (r^2 = 0.26, RMSE 0.73). The inherent variation of the RADARSAT-1 data, combined with a low dynamic range of backscatter

ithin FLD_1 (mean range per DOY, 3.22 (dB)) results in a representation of in-field variation as depicted in Figure 6.18b. It bares little resemblance ($r^2 = 0.24$, RMSE = 0.82) to that estimated by the optical data, which, in turn, are highly correlated to biomass and yield potential.

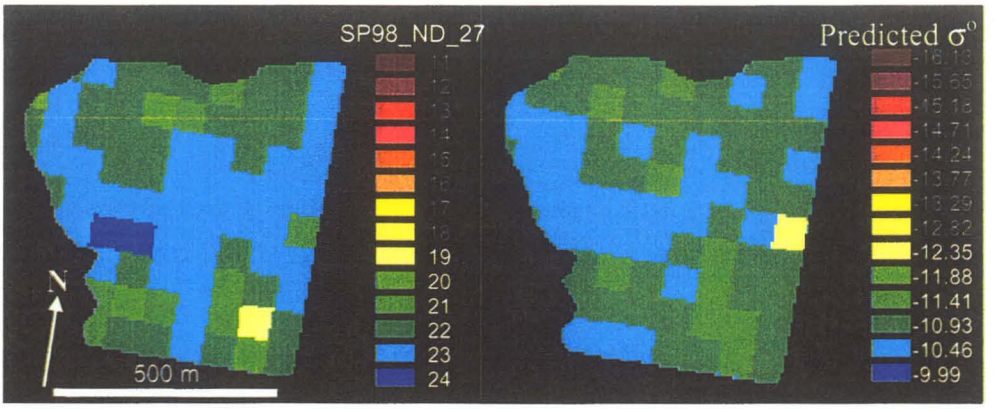

a) b)

Figure 6.18 a) FLD_1 within variation based on SP98_ND_27 classes (11x11 grid data); b) predicted (^) variation based inversion of the regression relationship in Figure 6.17b (out of range classes shaded).

6.3.3.3 Canola Backscatter Profiles, FLDs_1-15

Prior to examining RADARSAT-1 backscatter trends across the remaining canola fields, seasonal backscatter profiles for each field were plotted. This was done to establish the consistency of canola backscatter profiles, relative to FLD_1, and to determine if individual or groups of fields varied in their seasonal representation. The seasonal profiles represent backscatter averaged over NDVI zones per field.

Examination of the plots resulted in two major groups of profiles being identified. The first group of profiles (Figure 6.19) included FLDs_1-3, 5 and 10 (hereafter referred to as Group-1 FLDs). They are characterized by early season linear or curvilinear profiles (DOY149-187) and a pronounced backscatter minima on DOY 197, followed by an increase in backscatter on DOY 204. DOY 204 to 211 represents a period of peak backscatter (associated with pod filling), followed by a decrease in backscatter DOY 221 as the crop matures (starts to senesce).

The Group 2 profiles (FLDs 4,6-9, 11-15) are characterized by an early season peak (DOY 163) that may be due to a rain event 2 days prior to the RADARSAT-1 acquisition and /or unique canopy architecture (Figure 6.20). The minimum observed on DOY 197 in Group_1 FLDs is not evident, and the majority of fields (FLDs 6-8, 11-14) have very low backscatter on DOY 221, which is indicative of senescence towards the end of the year. These factors potentially indicate that the profiles are related to canola variety, as expressed by canopy architecture and a shorter growing season, or it may simply be a function of variations related to differences in phenological development. Note that FLDs 4, 9,and 15 tend to have a higher end of year backscatter (DOY 221) indicative of

higher volumetric moisture within the canopy. The exact nature of the profiles cannot be determined due to insufficient ground confirmation data.

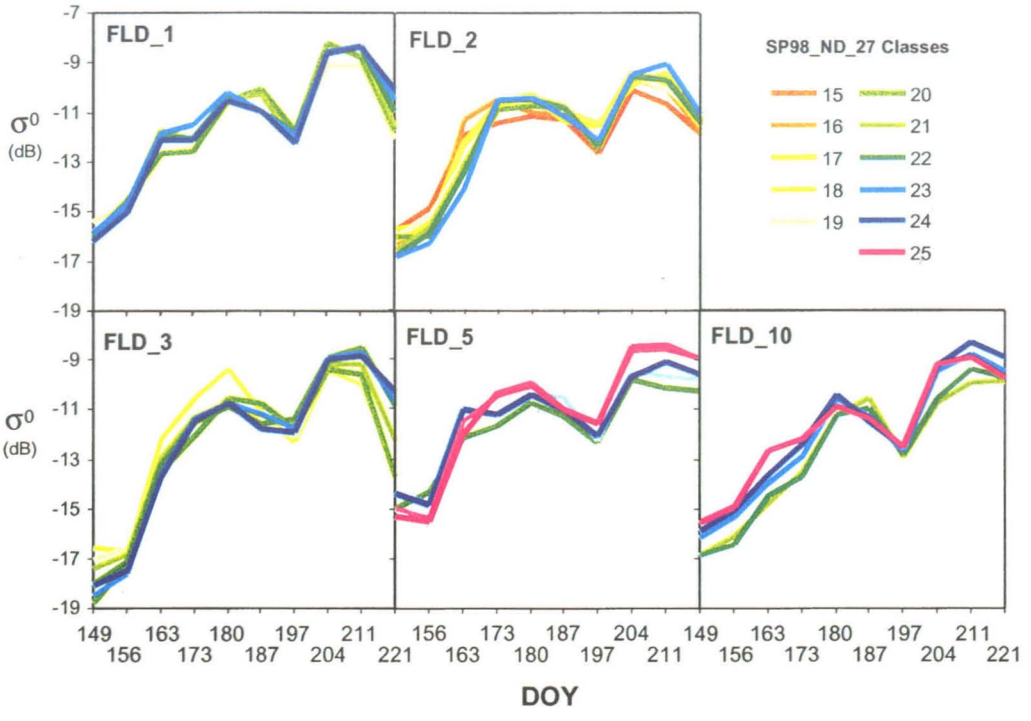

Figure 6.19 Seasonal backscatter profiles for Group-1 FLDs (canola). Backscatter data are averaged over SP98_ND_27 classes.

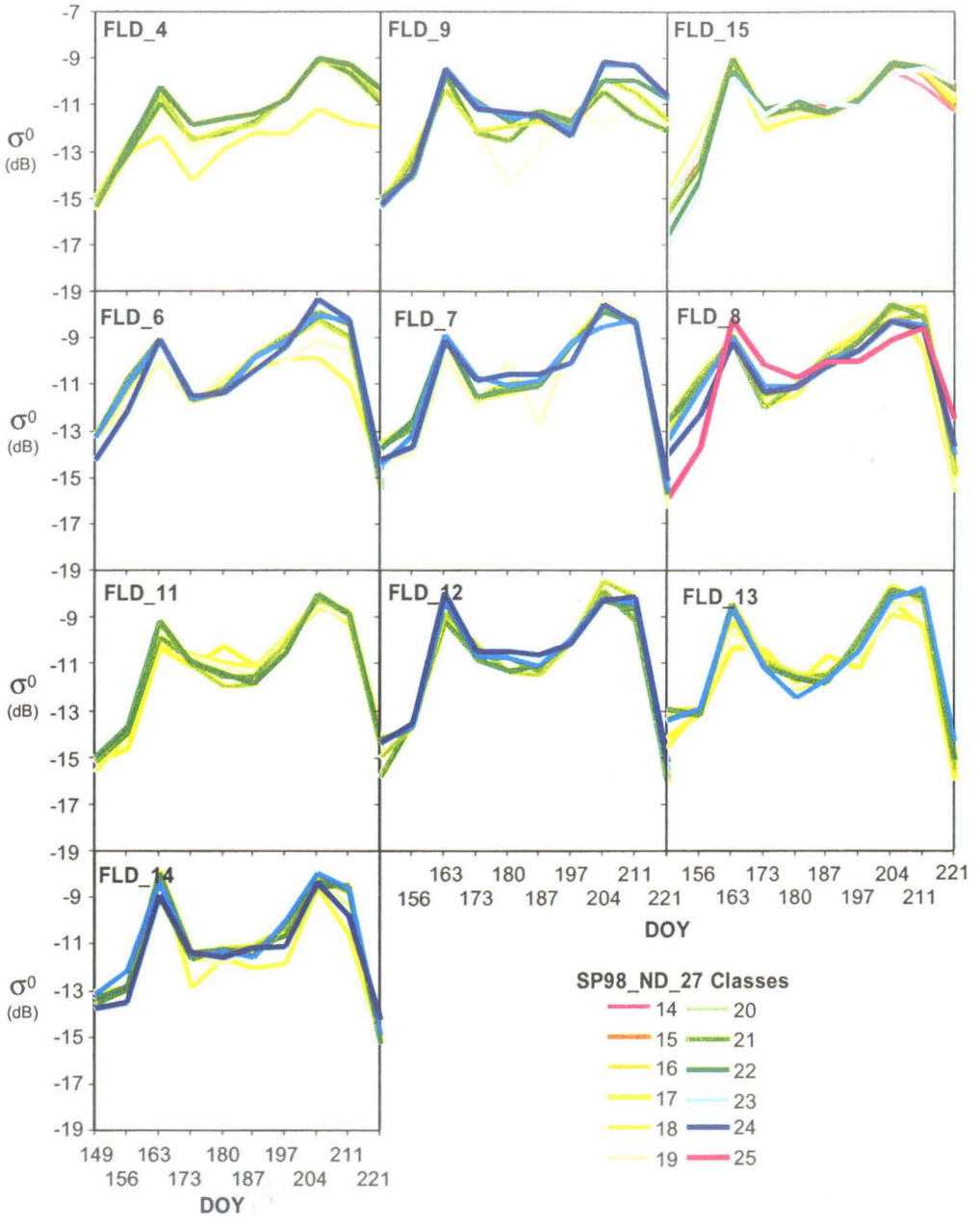

Figure 6.20. Seasonal backscatter profiles for Group-2 FLDs (canola). Backscatter data are averaged over SP98_ND_27 classes.

6.3.3.4 RADARSAT-1 Backscatter vs. NDVI Zones (Large Area Means)

Rather than examining RADARSAT-1 backscatter over individual fields, Group-1 FLDs are examined followed by Group-2 FLDs and FLDs_1-15 (all fields).

6.3.3.4.1 Group 1 Fields

RADARSAT-1 backscatter over Group-1 FLDs was extracted using both mid- and late-season NDVI (SP98_ND_12 & 27), Figure 6.21. Associated regression coefficients can be referenced in Tables C5-C6, (Appendix C). Results show that backscatter trends are relatively invariant over NDVI zones (SP98_ND_12). On DOY 187 a negative trend was observed (r^2 = 0.93, RMSE = 0.07), and a similar trend was observed on DOY 197 (r^2 = 0.77, RMSE =0.11). The trends represented a dynamic range of only 0.89 and 0.82 dB respectively. The largest dynamic range in backscatter was observed DOY 221 at 2.22 dB, (r^2 = 0.91, RMSE = 0.25).

The backscatter trends over late season NDVI (SP98_ND_27) were not much better. The trends are very weak, with DOY 211 and DOY 221 showing the best correlations (r^2 = 0.95 and 0.94). The backscatter range over the NDVI zones for DOY 211 and 221 were 1.50 and 2.77 dB respectively.

Figure 6.22b shows the predicted (^) NDVI class based on the inversion of the regression relationship between SP98_ND_27 and DOY 221 backscatter (Figure 6.23a). The two maps are highly correlated (r^2 = 0.87), although some minor variations are evident. The difference in backscatter between NDVI zones is ~ 0.46 dB.

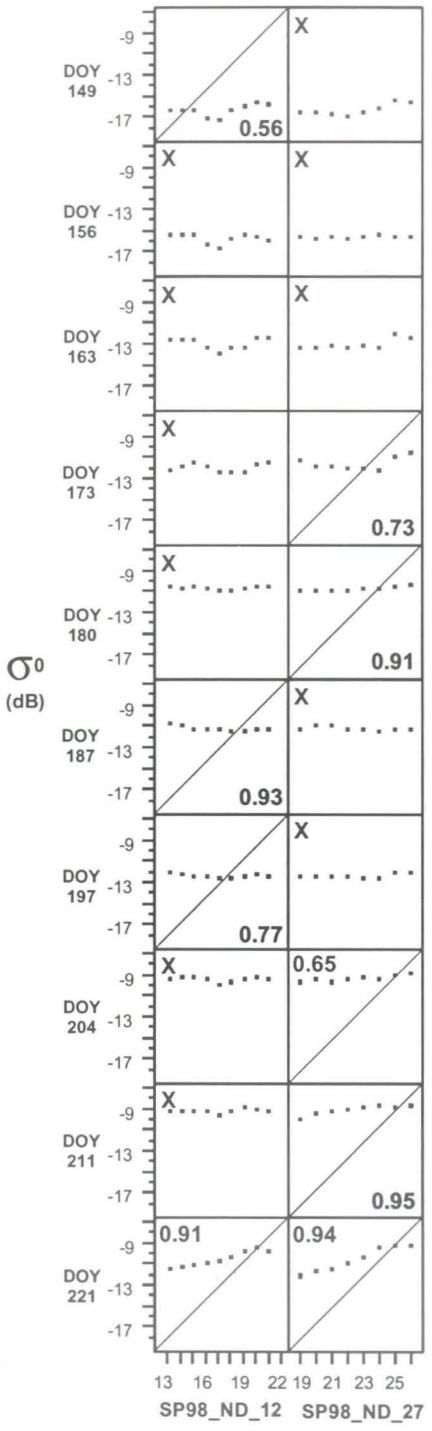

Adjusted R^2

Linear	
0.65	0.83
	2nd order Poly.

X = no signif. (0.05)

Backscatter Statistics over SP98_ND_12

DOY	Mean	Range
149	-16.17	1.71
156	-15.59	1.47
163	-12.84	1.68
173	-11.67	1.16
180	-10.51	0.62
187	-11.06	0.89
197	-12.15	0.82
204	-9.26	1.03
211	-8.94	0.92
221	-10.33	2.22
Mn	**-11.85**	**1.25**

Backscatter Statistics over SP98_ND_27

DOY	Mean	Range
149	-16.03	1.61
156	-15.49	0.59
163	-12.72	1.50
173	-11.44	1.80
180	-10.47	0.75
187	-11.00	0.79
197	-12.08	0.79
204	-9.12	0.96
211	-8.97	1.50
221	-10.38	2.77
Mn	**-11.77**	**1.30**

Figure 6.21. RADARSAT-1 backscatter per DOY over Group-1 fields as a function of NDVI zones

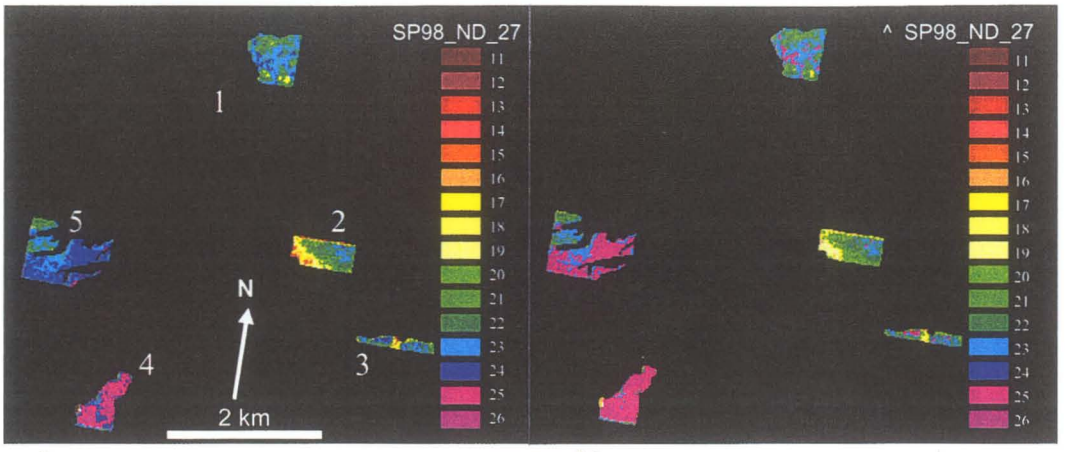

a) b)

Figure 6.22. Group-1 fields (area means) a) Observed NDVI classes for SP98_ND_27 (DOY 208); b) predicted (^) variation based inversion of the regression relationship in Figure 6.23a.

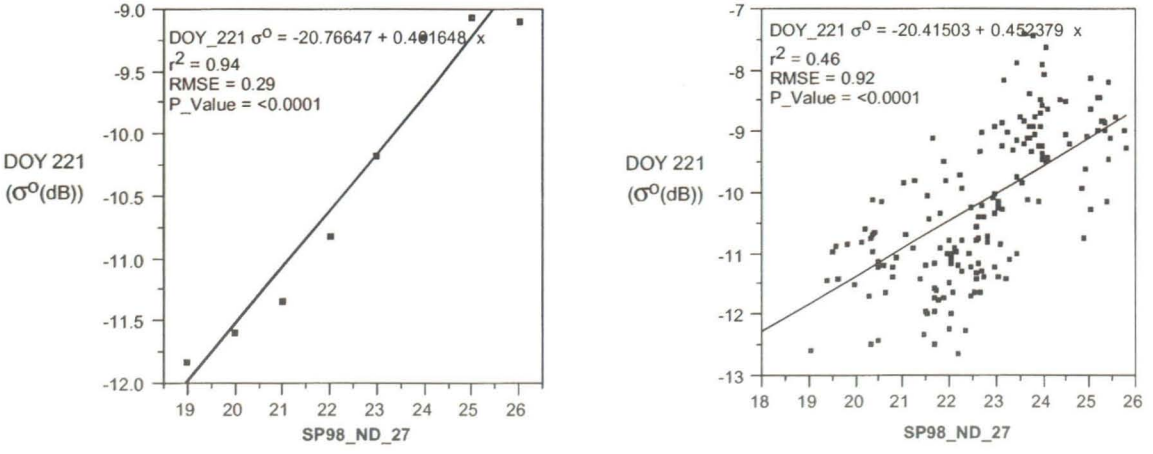

a) b)

Figure 6.23. Group-1 fields a) SP98_ND_27 vs. DOY 221 backscatter averaged over NDVI zones; b) SP98_ND_27 vs. DOY 221 backscatter averaged over 11x11 grid cells.

A more realistic representation of backscatter versus variation based on SP98_ND_27 is presented in Figure 6.23b using the 11x11 grid means. The regression shows considerable variation in backscatter across NDVI zones for the Group-1 FLDs (r^2 = 0.46, RMSE = 0.92).

Figure 6.24b shows the predicted variation based on the inversion of the regression presented in Figure 6.23b. A per pixel correlation between these two representations of within field variation is r^2 = 0.41, RMSE = 1.72.

a) b)

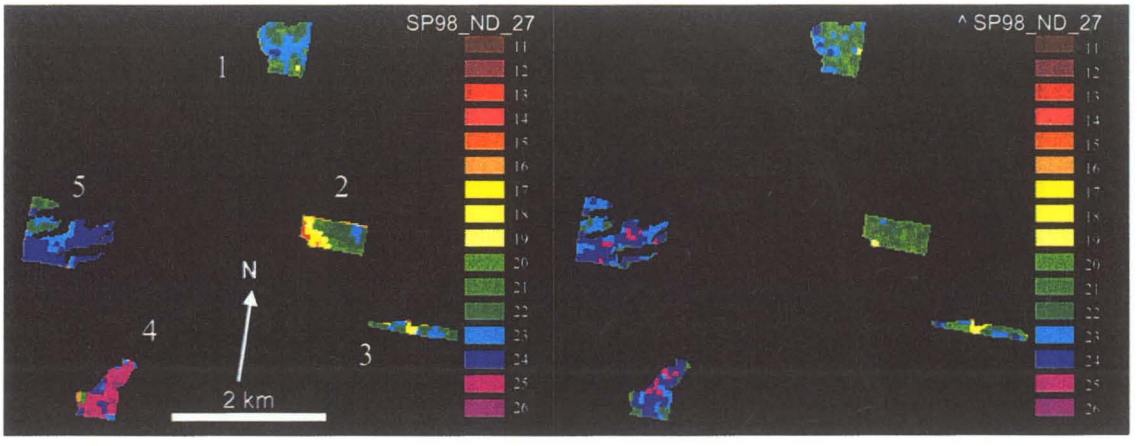

Figure 6.24 Group-1 FLDs, (11x11 means), a) observed variation based on SP98_ND_27, b) predicted variation based inversion of the regression relationship in Figure 6.23b.

6.3.3.4.2 Group 2 FLDs and FLDs_1-15

This section examines the RADARSAT-1 backscatter trends across Group-2 FLDs and all fields (FLD_1-15) as a function of within field variability (and between field variability) defined by late season NDVI (SP98_ND_27). Backscatter trends per DOY are presented in Figure 6.25, and regression coefficients are presented in Tables C7-C8, (Appendix C).

No significant backscatter trends were evident early in the growing season (DOY 149 to 163) for the Group-2 FLDs. With the inclusion of Group-1 FLDs, DOY 156 and 163 showed strong negative trends (high backscatter over low biomass), $r^2 = 0.98$ and 0.95 respectively, with backscatter ranges 2.60 and 2.01 dB respectively. Considering that the soils were relatively wet early in the season, the negative backscatter trend may be indicative of high backscatter from the soil surface over low biomass areas.

On DOY 173 to 187 backscatter trends over Group-2 FLDs and FLDs_1-15 were positive, but the range of backscatter was generally less than 1 dB (0.35 - 0.99) for Group-2 FLDs and marginally higher for FLDs_1-15 (0.35 - 1.23 dB).

The backscatter trends from DOY 197 to 204 were very poor. The strongest end of year trends occurred on DOY 211 ($r^2 = 0.80 - 0.89$) yet the range in backscatter averaged over NDVI zones differed by no more that 0.98 dB for Group-2 FLDs and 0.96 dB over all the canola fields (FLD_1-15).

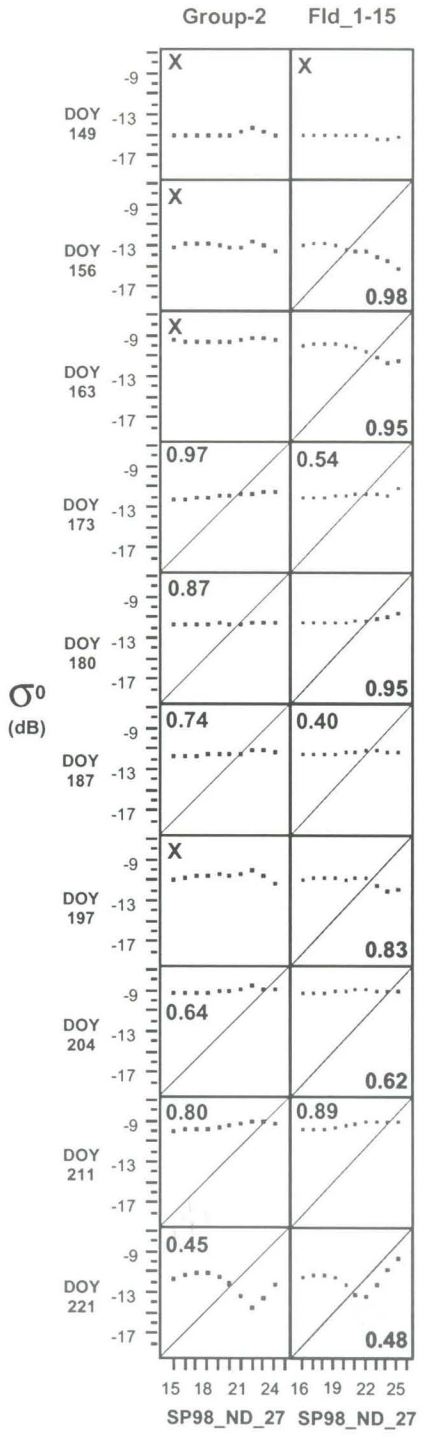

Adjusted R^2

Linear
0.65
0.83
2nd order Poly.

X = no signif. (0.05)

Group-2
Backscatter Statistics over SP98_ND_27

DOY	Mean	Range
149	-14.63	1.02
156	-12.71	1.09
163	-9.23	0.51
173	-11.66	0.99
180	-11.39	0.35
187	-11.18	0.79
197	-10.40	1.48
204	-8.82	0.98
211	-9.23	1.24
221	-12.17	3.53
Mn	**-11.14**	**1.20**

Fld_1-15
Backscatter Statistics over SP98_ND_27

DOY	Mean	Range
149	-14.97	0.59
156	-13.43	2.60
163	-10.16	2.01
173	-11.60	1.21
180	-11.13	1.23
187	-11.16	0.57
197	-10.81	1.55
204	-8.90	0.65
211	-9.12	0.96
221	-11.48	3.97
Mn	**-11.28**	**1.53**

Figure 6.25. RADARSAT-1 backscatter per DOY over Group-2 FLDS and FLDs_1-15 as a function of SP98_ND_27.

Since the DOY 211 regression coefficients are comparable for Group 2 and FLD_1-15 data, mapped results are shown for the latter. Inverting the regression in Figure 6.27a, the predicted in-field variation over FLD_1-15 as a function of mean backscatter per NDVI zone, is mapped in Figure 6.28b. The two maps are highly correlated ($r^2 = 0.87$) with in-field and between field variations being for the most part consistent.

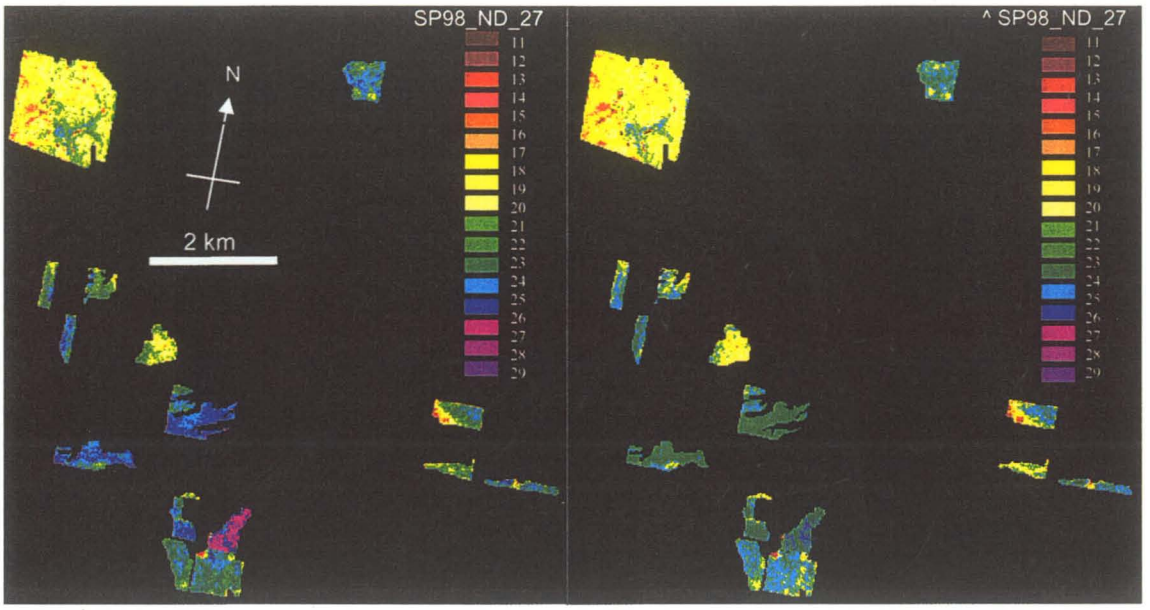

a) b)

Figure 6.26 FLDs_1_15 (area means). a) Observed NDVI classes for SP98_ND_27 (DOY208); b) predicted (^) variation based inversion of the regression relationship in Figure 6.25a.

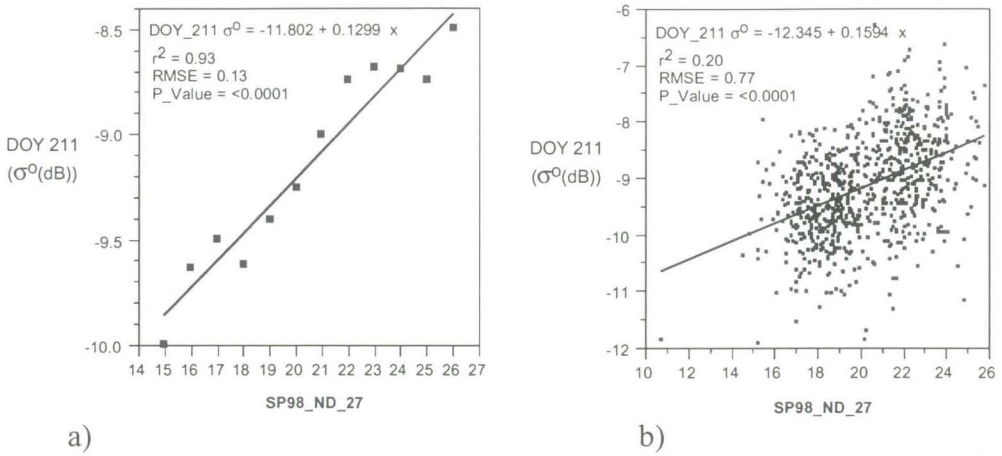

Figure 6.27 FLD_1_15 a) SP98_ND_27 vs. DOY 211 backscatter averaged over NDVI zones; b) SP98_ND_27 vs. DOY 211 backscatter averaged over 11x11 grid cells.

The more realistic potential of RADARSAT-1 data is represented by Figure 6.28b, where within field variation as defined by SP98_ND_27 is poorly related to the observed backscatter (r^2 = 0.20, RMSE = 0.77). Inverting the regression (in Figure 6.27b) results in a map that bears little resemblance to the estimated within field variation as represented by SP98_ND_27 (r^2 = 0.13, RMSE 2.26).

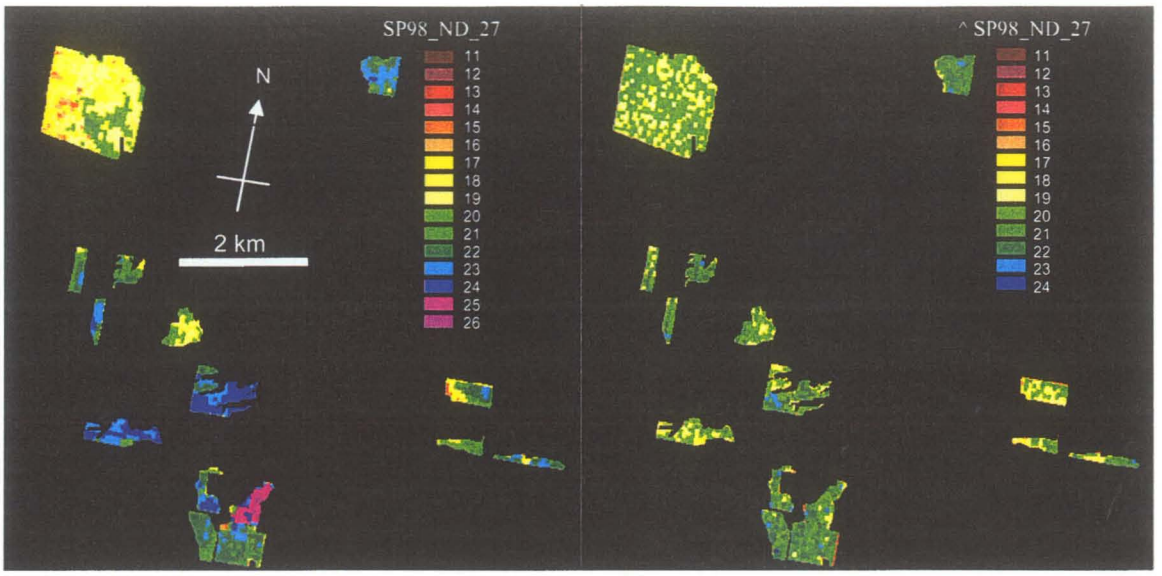

a) b)

Figure 6.28 FLDs-1-15 (11x11 means), a) observed variation based on SP98_ND_27, b) predicted variation based inversion of the regression relationship in Figure 6.29b.

6.4 Conclusions

This chapter examined within field variability using seasonal and inter-annual NDVI and weekly RADARSAT-1 data. It was shown that the optical data (CASI and SPOT) provided a relatively consistent seasonal and inter-annual representation of within field variability as defined by NDVI. The 1998 SPOT data showed that variations in NDVI are directly a function of crop canopy characteristics. The mid-season NDVI were more a function of green leaf area, but later in the season these were more directly related to areal ($m^2 \cdot m^{-2}$) variations of stem and pods. It was also shown that variations in green

biomass were strongly related to the magnitude and distribution of gravimetric moisture within the component parts of the canopy, a fact that is of particular significance in regards to microwave backscatter since it relates to variations in the dielectric properties of the canopy.

The seasonal backscatter profiles plotted for each of the 15 fields revealed two distinct profiles. The two groups of profiles may be indicative of different canopy architecture (perhaps related to variety), but ground confirmation data are insufficient to suggest the exact nature of the variation. In addition, Group-2 profiles had an early season spike in backscatter, which may be a function of canopy architecture enhanced by `canopy_ground` interaction due to increased soil wetness from a rain event 2 days prior to the acquisition. This would be an item for further investigation.

The ability of RADARSAT-1 data to discriminate variations in biomass per DOY over relative productivity zones as defined by mid- and late-season NDVI (SP98_ND_12 & 27) was very poor. This was initially demonstrated in FLD_1 using the mean backscatter values extracted using the 11x11 grid. The best correlation relative to mid-season NDVI was on DOY 173 (canola stage 2.5-2.6), $r^2 = 0.35$, the best correlation using late season NDVI to define within field variation was $r^2 = 0.26$.

When backscatter was averaged over NDVI zones within FLD_1 the correlations improved significantly, e.g., DOY 221, SP98_ND_27 vs. σ^o (dB), $r^2 = 0.99$. Therefore having a priori knowledge of within field zones (e.g., inter-annual yield monitor data, detailed soil survey data (generally not available at the scales needed) or NDVI data) mean backscatter per zone can reveal subtle variations related to within field biomass. The range in mean backscatter across late season NDVI over FLD_1 on average varied

no more than 1.5 dB seasonally, the backscatter range on DOY 221 (SP98_ND_27) was 2.55 dB. The range in mean backscatter across NDVI integrated across all fields (FLDs 1-15) was comparable (1.53 dB).

Without a priori knowledge of within field productivity zones, RADARSAT-1 data cannot be used to meaningfully map in-field variation as it relates to canola biomass or productivity as revealed by the 11x11 grid data of 1998. The results suggest the that longer wavelength MW data (L or P-band) be evaluated to monitor canola due to its ability to penetrate the canopy more effectively and thus potentially provide a better characterization of in-field biomass variation (move to Chapter 7).

Chapter 7: Summary and Conclusions

7.1 Conclusions

In Chapter 2 background information was provided regarding the phenological development of wheat and canola, along with and some key factors affecting growth and development of crop canopies, specifically soil moisture, soil fertility and air temperature. It was shown that whatever the source of stress within the growth cycle, the potential productivity of a canopy was expressed in the magnitude and duration of green leaf area and biomass and thus the ability of the plant to absorb photosynthetically active radiation and convert it into salable biomass. Optical data and, in particular vegetation indices were shown to be highly correlated to LAI and green biomass and therefore an effective tool in assessing crop condition and yield potential.

From a review of previous research it was shown that microwave backscatter from crop canopies was closely related to volumetric moisture, plant geometry (size and orientation) of the component parts of the canopy, and soil volumetric moisture. Factors independent of crop condition, such as row orientation and spacing, and environmental parameters such as dew and rain events also significantly affected backscatter from agricultural surfaces. To maximize microwave backscatter from canopies and minimize potential soil background contributions, previous research often relied on higher frequency data (>8 GHz) and VV polarizations to seasonally monitor phenological development. These parameters were chosen to maximize canopy contributions and minimize soil background contributions to backscatter. Early volumetric moisture models (Ulaby and Bush, 1976; Attema and Ulaby 1978) showed that canopy volumetric

moisture (M_v) was highly related to seasonal backscatter. These models were subsequently modified to incorporate two layers within the canopy (e.g., heads versus leaf layer for wheat) to take into account variations in crop geometry. The results of this research suggested that a more detailed vertical characterization of canopies may be appropriate to modeling backscatter. Research related to the use of C-band HH data to seasonally monitor wheat and canola was generally lacking, especially as it related to the use of RADARSAT-1 data.

In Chapter 3, a detailed (4 layer) physical characterization of wheat canopies was provided from emergence to harvest. This data was used to develop a new multi-layer volumetric moisture model for wheat. The model was used as a tool to understand the physics of EM interactions from RADARSAT-1 and wheat. This more detailed multi-layer approach was unique, and provided a more effective method of assessing microwave extinction during sensitivity trials. The model generated a measure referred to as the TMc (total effective volumetric moisture), which was correlated to RADARSAT-1 backscatter. Canopy inputs into the model included volumetric soil moisture (Ms), normalized volumetric moisture (nMv) of leaves per layer ($nMv_{i,j,k}$), heads (nMv_l), and weeds (nMv_m).

Results from the model suggested a relatively high two-way extinction coefficient (B = 0.0038) within high biomass canopies. Manipulation of the extinction coefficient for the low biomass canopy had no effect due to insufficient biomass. Seasonal backscatter at the low biomass site was primarily related to soil moisture ($r^2 = 0.86$). Backscatter over the high biomass sites was highly correlated to the observed TMc ($r^2 = 0.73$-0.96). Model results showed that early season backscatter was dominated by soil contributions and

subsequently by the green leaf portion of the canopy (DOY 163-187). Head volumetric moisture dominated the TMc on DOY 197-211; on DOY 221 the model suggested significant soil backscatter contributions. RADARSAT-1 backscatter from wheat had a bimodal distribution associated with green leaves early in the season and heads later in the season. Row direction effects were most significant (±2 dB) early in the season. The rain event on DOY 187 increased backscatter by an estimated 2-3 dB. The seasonal backscatter range over wheat as observed by RADARSAT was 6-7 dB.

Chapter 4 examined a series of objectives functionally similar to those in Chapter 3, namely: 1) to provide a detailed weekly vertically stratified (4 layer) characterization of the component parts of a canola canopy from emergence to harvest and, 2) to adapt the multi-layer volumetric moisture model for canola. Canopy inputs into the model included volumetric soil moisture (Ms), normalized volumetric moisture (nMv) of leaves (nMv_{L1-3}), pods (nMv_{p2-4}), flowers ((nMv_{fl}),), and stems (nMv_{st1-4}) per canopy layer.

The model assumed a high extinction coefficient (B = 0.0038) and a significantly reduced soil moisture weighting (C=100). The model results generated for FLD_1 were highly correlated for Sites 1 and 2 (r^2 = 0.79 and 0.90, respectively), but more poorly correlated over Site 3 the high biomass site (r^2 = 0.67). When the model results were integrated over all three sites, it became apparent that a volumetric moisture characterization of the canola surface did not adequately take into account the effect of canopy structure. Later in the season when pods dominated the canopy, the volumetric model worked much better (r^2 = 0.94). The model results (FLD_1) suggest that soil background moisture may not play a significant role in backscatter from DOY 173 to 221. This was further evidenced by the lack of a backscatter response to the rain event on DOY

187. The seasonal backscatter plots revealed a clear relationship with crop phenology coinciding with green leaf portion early in the season and the emergence of pods later in the season. To effectively model early season backscatter, a scattering model based on leaf geometry should be incorporated.

Chapter 5 assessed the ability of RADARSAT-1 to detect within field and between field variations of wheat biomass. The objectives were to: 1) examine the nature of in-field variability within the intensively sampled field (FLD_100) to quantify the relationships between soil texture, organic matter (OM), and yield and relate these to inter-annual and seasonal NDVI; and 2) to assess RADARSAT-1s ability to identify within field variation based on "productivity zones" defined by relative NDVI. In support of objective 2, biomass data was also examined in FLD_100-120 vis-à-vis NDVI to provide further support / rationale for using NDVI as a variable to delineate zones of variation in FLDs_130-240 where physical ground confirmation was not available.

The results for objective 1 showed that seasonal and inter-annual NDVI were highly correlated to soil texture (r^2 = 0.66 - 0.87), organic matter (r^2 = 0.70 - 0.82) and yield in FLD_100 (r^2 = 0.74 - 0.94). Physical data further supported the fact that NDVI were significantly related to variations in green leaf area and duration, and leaf, head, and stem gravimetric moisture. NDVI were also indicative of other crop canopy variables such as plant height and number of tillers per plant. These findings were significant in that: 1) they supported the use of NDVI to delineate relative productivity zones within fields where ground confirmation data were lacking or absent, and 2) variations in NDVI were indicative of crop canopy parameters that have bearing on MW backscatter (canopy moisture, plant density and height).

The results for objective 2 showed that RADARSAT-1 backscatter was related to soil texture (FLD_100) and NDVI zones (FLDs_100-240) (where backscatter was extracted using area means per zone of variability). Texture_1 was positively correlated to backscatter on DOY 149-156 (r^2 = 0.70 - 0.85), as was Texture_2 (r^2 = 0.91 - 0.92). The positive trends were likely indicative of early season soil moisture variation across soil texture zones. Negative correlations were detected on DOY 180 and 187 (r^2 = 0.53 - 0.73), and positive trends towards the end of the season on DOY 211 to 221 (r^2 = 0.79 - 0.93).

In terms of backscatter versus NDVI for FLD_100, significant negative trends were evident on DOY 180 (booting), r^2 = 0.85 - 0.94, and on DOY 187 (heading), r^2 = 0.77 - 0.88. As the wheat senesced (DOY 221) strong positive trends were evident (r^2 = 0.82 - 0.87). When backscatter was averaged per NDVI zone over all the wheat fields, the correlations became much stronger, e.g., on DOY 180-187 (r^2 = 0.92-0.95, dynamic range of σ^o = 1.96 -2.48 dB) and DOY 221 (r^2 = 0.98 - 0.99, dynamic range of σ^o = 3.99 - 4.77dB).

Whereas spatially averaging backscatter over soil texture or NDVI zones is useful in establishing backscatter trends per DOY, the resulting coefficients of determination do not truly represent of the variation inherent in RADARSAT backscatter per productivity zone. Using the 11x11 grid data the coefficients of determination dropped considerably but were nevertheless promising. For example, using backscatter versus SP98_ND_27 over all fields on DOY 187 and DOY 221 resulted in r^2 = 0.49 and 0.60 respectively. When the inverse relationships were exploited between these two dates (DOY 187/221), the backscatter versus SP98_ND_12 and SP98_ND_27 correlations were significantly higher, (r^2 = 0.64 and 0.72 respectively). The results indicated the potential for using

RADARSAT-1 to map relative variations in biomass. The results also indicated a synergy between SAR data and optical data. Crop canopy parameters that affect the optical properties of a canopy (e.g., green leaf area and duration, biomass) are also directly, or indirectly related to variables that determine the nature of radar backscatter. For example, green leaf area and duration are indicative of variations in leaf, stem and head volumetric moisture, crop density, and plant height parameters that also determine the magnitude and nature of backscatter.

Chapter 6, the suitability of RADARSAT-1 data to detect within field and between field variations of canola biomass was assessed. The objectives were the same as those in Chapter 5. The first objective was to determine the nature of in-field variability. Seasonal and inter-annual NDVI were examined including biomass data. It was shown that the seasonal NDVI and inter-annual variability were highly correlated. The ground confirmation data showed that in-field variation was associated with soil texture and that NDVI were indicative of significant variations in biomass as expressed by green leaf, stem and pod area ($m^2 \cdot m^{-2}$), gravimetric moisture ($gm \cdot m^{-2}$) and canopy height.

Backscatter trends as a function of NDVI within FLD_1 were generally non-existent. When backscatter was averaged over NDVI zones, the highest correlations consistently occurred during the latter part of the growing season. The seasonal backscatter trends were positive with the exception of DOY 187. The dynamic range in backscatter (σ^o (dB)) over NDVI zones was on average 1.30 - 1.50 dB, the maximum backscatter range was 2.55 dB on DOY 221 (SP98_ND_27, $r^2 = 0.99$). The same relationship for DOY 221 using the 11x11 grid data over FLD_1 resulted in a coefficient of determination of 0.24. The scattering properties of the canopy combined with the

inability of C-band HH to penetrate the canopy sufficiently enough to detect variations in biomass renders RADARSAT-1 data ineffectual for mapping biomass variations within canola. If one has prior knowledge of productivity zones within the field, mean average backscatter per zone will mimic NDVI during that latter part of the season. The extent to which this can be exploited remains questionable.

RADARSAT-1 backscatter profiles extracted per canola field as a function of SP98_ND_27 classes, revealed two distinct backscatter profiles (Group_1 and Group_2 FLDs). The unique profiles may be a function of different canopy architectures due to canola variety, or as a function of differences related to phenological development. Further information is required to assess the exact nature of the variation. These results are promising in that RADARSAT-1 shows a potential for mapping phenological development of canola.

7.2 Summary

The results of this research have contributed significantly to our understanding of the physical properties of wheat and canola vis-à-vis optical and microwave interactions with wheat and canola.

1) Modeling Results

- The detailed physical characterizations of the wheat and canola canopies are unique due their detail and temporal coverage. These data were fundamental to the analysis of the nature of RADARSAT-1 backscatter.

- The multi-layer model, which was developed, provided an effective tool by which to assess the seasonal nature of RADARSAT-1 backscatter. The results it provided showed that backscatter from the vegetative canopy was not necessarily indicative of the total volumetric moisture within the canopy as demonstrated by the relatively high extinction coefficients.

The model results for wheat also showed that soil contributions to backscatter were most significant early and very late in the season, while for the remainder of the year backscatter was driven by the wheat canopy (although modulated by rain events). These results also showed a strong bimodal backscatter profile associated with leaves early in the season and heads late in the season.

Model results for canola showed that soil volumetric moisture played a significant role in early season backscatter and was thereafter an insignificant interaction term. Mid-season growth was dominated by green leaf contributions to total backscatter. A backscatter minima observed on DOY 197 marked the transition from leaves to pods as the dominant canopy element driving backscatter. Canola had a distinct bimodal seasonal backscatter profile, with the second and higher peak associated with pod development and senescence. There appears, however, to be a limitation to using a purely volumetric model to examine seasonal backscatter especially in broad leaf canopies where the leaf size is comparable to the wavelength (5.6 cm). In this case leaf geometry plays a more significant role than purely volumetric moisture early in the season.

- Both the wheat and canola backscatter profiles are unique and point to the potential of deriving crop phenological information from RADARSAT data.

2) In-field Variability

- The optical data showed that both mid- and late-season NDVI were highly correlated to soil texture, organic matter and yield. Based on the physical data, it was also effectively demonstrated that NDVI are indicative of green leaf area and duration and indirectly indicative of variations in stem, head, and leaf moisture, plant density (number of tillers) and canopy height. Each of these parameters are significantly related to microwave backscatter.
- Significant backscatter trends related to in-field biomass were evident within the wheat fields at the booting and heading. These trends are inversely related to mid- and late-season NDVI. Backscatter profiles extracted using NDVI zones over all wheat fields showed that backscatter is representative of biomass for a significant portion of the growing season. During the early part of the year backscatter versus NDVI trends are negative (high backscatter = low NDVI). Toward the end of the season they are strongly positive.

  Mid- and late-season backscatter trends can be exploited using ratios to map biomass variation. The seasonal trends also effectively show a synergy between optical data and microwave data that should be explored further.
- Mapping in-field variability for canola is not possible using C-band HH polarized data. Although it may be possible to effectively determine crop phenology, this

requires further validation. The monitoring of canola for crop assessment purposes will require lower frequency microwave data (e.g., L-band) to better penetrate the canopy and thus more effectively characterize variability within and between fields.

7.3 Recommendations

The results of the current research suggest some potential for using RADARSAT-1 data to monitor wheat. The data suggest that the booting to heading stage may be the most appropriate period during which to conduct crop condition assessment. Towards the end of the season, variation within and between fields was very evident, but it is unclear as to what extent late season backscatter can be exploited for assessing yield potential. The data suggest that between field variations towards the end of the season are more a function of crop phenology. The extent to which RADARSAT-1 data can be used operationally is still very questionable given the dynamic range of the data and the variability of the data per DOY.

The following questions /observations point to areas of further research:

- Whereas optical data are highly related to green leaf area, MW backscatter can vary significantly at any given LAI due to crop geometry. This observation leads to a number of questions: 1) To what extent are seasonal backscatter profiles unique to a wheat variety? 2) To what extent are the seasonal backscatter profiles of wheat unique when compared to other cereal grains such as barley, rye and oats?

- To what extent are inter-annual backscatter profiles indicative of yield potential?
- To what extent do spatially heterogeneous rain events complicate information extraction as related to: 1) crop phenological development and 2) potential productivity on a regional basis, both seasonally and inter-annually?
- Are backscatter trends at booting and heading always strongly negative and to what extent does background soil moisture enhance mid-season backscatter trends?
- To what degree does the incident angle affect MW backscatter especially as it relates to phenological stage? To what extent are seasonally adjusted corrections required?
- To what extent will RADARSAT-2 or ENVISAT ASAR data enhance crop information extraction? These satellites will provide multi-polarimetric data. From recent research in cooperation with the Canada Centre for Remote Sensing (CCRS) (McNairn et al., 2002a) results have shown that the HH polarized data was poorest in differentiating wheat biomass. Both VV and HV polarizations were superior to HH. HV data showed the greatest potential for mapping within field biomass variations. Multi-polarized data will also provide opportunity to explore various polarization ratios. Initial results suggest a greater potential for crop condition monitoring using multi-polarized data. Even so, most if not all of the questions posed above remain relevant.

Literature Cited

Aase, J.K. and F.H. Siddoway, 1981, Spring Wheat Yield Estimates from Spectral Reflectance Measurements. *IEEE Transactions on Geoscience and Remote Sensing*, GE-19, No. 2, pp. 78 - 84

Ahlrichs, J.S. and M.E. Bauer (1983). Relation of Agronomic and Multispectral Reflectance Characteristics of Spring Wheat Canopies. *Agronomy Journal.* 75:987 - 993.

Allen, C.T., and Ulaby, F.T. (1984). Characterization of the Microwave Extinction Properties of Vegetation Canopies, University of Michigan, College of Engineering, Radiation Laboratory, Ann Arbor, MI 48109.

Anderson, P.M., E.A. Oelke, and S.R. Simmons. (1985). Growth and Development Guide for Spring Barley. *University of Minnesota Agricultural Extension Folder AG-FO-2548.*

Asrar, G., E.T. Kanemasu and M. Yoshida (1985). Estimates of Leaf Area Index from Spectral Reflectance of Wheat under Different Cultural Practices and Solar Angle. *Remote Sensing of Environment,* 17:1 - 11.

Attema E.P.W. and F. Ulaby (1978). Vegetation modeled as a water cloud. *Radio Science.* Vol. 13, No. 2, pp. 357-364

Barnett, T.L. and D.R. Thompson (1982). The use of large area spectral data in wheat yield estimation. *Remote Sensing of Environment.* 12:509-518.

Bauer, A., A. B. Frank and A. L. Black. (1984). Estimation of spring wheat leaf growth rates and anthesis from air temperature. *Agronomy Journal.* 76: 829-835

Benedetti, R. and Paolo Rossini. 1993. "On the use of NDVI Profiles as a Tool for Agricultural Statistics: The Case Study of Wheat Yield Estimate and Forecast in Emilia Romagna, *Remote Sensing of Environment,* Vol. 45, pp. 311 - 326.

Bouman, Bas. A.M., and Henk W.J. van Kasteren (1990). Ground-based X band (3-cm wave) radar backscattering of agricultural crops. II. Wheat, barley, and Oats; the impact of canopy structure. *Remote Sensing of the Environment.* 34:107-118.

Brisco B., Brown R.J., Hirose T., McNairn H., Staenz K. (1998). Precision Agriculture and the Role of Remote Sensing: A Review; *Canadian Journal of Remote Sensing*, Vol. 24, No 3 , 1998 , pp. 315-327.

Brisco, B., Bedard, D., Naunheimer, J. and Brown, R.J. (1993). Environmental Effects on Radar Data of Agricultural Areas, *Proceedings 16th Canadian Symposium on Remote Sensing, Sherbrooke, Quebec*, pp.283-288

Brisco, B., R.J. Brown, J.G., Gairns and B. Snider, 1992, Temporal ground-based scatterometer observations of crops in western Canada. *Canadian Journal of Remote Sensing*, 18, 14.

Campbell, C.A. and H.R. Davidson (1979). Effect of Temperature, nitrogen fertilization and moisture stress on growth, assimilate distribution and moisture use efficiency by Manitou spring wheat. *Canadian Journal of Plant Science.* 59: 603-626.

Campbell, C.A., H.R. Davidson and G.E. Winkleman (1981). Effect of nitrogen, temperature, growth stage and duration of moisture stress on yield components

and protein content of manitou spring wheat. *Canadian Journal of Plant Science.* 61: 549-563.

Cihlar, J., D. Manak and N, Voisin (1992). AVHRR bidirectional reflectance effects and compositing. *Canada Centre for Remote Sensing, Unpublished,* pp. 1-33.

Colwell, J.E. (1974). Vegetation canopy reflectance. *Remote Sensing of Environment* (3). pp. 175 - 183.

Crist, E. P. (1984). Effects of Cultural and Environmental Factors on Corn and Soybean Spectral Development Patterns. *Remote Sensing of Environment.* 14: 3 - 13.

Daughtry, C.S.T., M. E. Bauer, D. W. Crecelius, and M. M. Hixson (1980). Effects of Management Practices on Reflectance of Spring Wheat Canopies. *Agronomy Journal,* Vol. 72, pp. 1055 - 1060.

Dobson, M. C. and F.T. Ulaby (1986). Microwave backscatter dependence on rough surfaces, soil moisture and soil texture. Part III - Soil tension. *IEEE Transactions on Geoscience and Remote Sensing*, Vol. GE-19 No.1, pp 51-61.

Dobson, M. Craig and F.T. Ulaby (1986). Active Microwave Soil Moisture Research. *IEEE Transactions on Geoscience and Remote Sensing*, Vol. GE-24 No.1, pp., 23-36.

Dobson, M.C. F.T. Ulaby, M.T. Hallikainen and M.A. El Rayes (1985). Microwave dielectric behaviour of wet soil - Part II: Empirical models and experimental observations. *IEEE Transactions on Geoscience and Remote Sensing*, Vol. GE-23, No.1, pp. 35-46.

Doraiswamy, P., Hart, G., Craig, M.E., Cook, P.W. (1994) "The Anomalous '93 Growing Season - How USDA Used AVHRR Data," *1994 ASPRS/ACSM Convention Technical Papers, Volume One*, pp. 144-151.

Elachi, C. (1987). Introduction to the Physics and Techniques of Remote Sensing. John Wiley and Sons. New York. pp. 411.

Gauer, E., C.f. Shaykewich and E.H. Stobbe (1982). Soil temperature and soil water under zero tillage in Manitoba. *Canadian Journal of Soil Science*. 62: 311-325.

Gausman, H.W. (1973). The leaf mesophylls of twenty crops, their light spectra, and optical and geometrical parameters. *Agricultural Research Service, United States Department of Agriculture, Technical Bulletin No. 1465*. Washington DC. p. 59.

Gausman, H.W. and W.A. Allen (1973). Optical parameters of leaves of 30 plant species. *Plant Physiology*, Vol. 52, pp. 57 - 62.

Gillespie, T.J., Brisco, B., Brown, R.J., and Sofko, G.J. (1990). Radar Detection of a Dew Event in Wheat. R*emote Sensing of Environment*, 33:151-156.

Goward, S. N., B. Markham, D.G. Dye, W. Dulaney, and Jingli Yang, 1991, Normalized difference vegetation index measurements from the Advanced Very High Resolution Radiometer. *Remote Sensing of Environment*, 35: 257.

Grant, L. (1987). Diffuse and specular characteristics of leaf reflectance. *Remote Sensing of Environment.* 22:309 - 322.

Griguolo, Silvio and Massimo Mazzanti. (1996) Establishment of an Operational Satellite Remote Sensing System to Support Agricultural Production and Desert Locust Monitoring and Forecasting (ARTEMIS Phase III). ADDAPIX Pixel-by-Pixel

Classification for Zoning and Monitoring. Rome: *UN FAO Technical Report SD:GCP/INT/578/NET.*

Gutman G.G., 1991, Vegetation indicies from AVHRR: An update and future prospects. *Remote Sensing of Environment.* 35: 121.

Guyot, G. (1990). Optical properties of vegetation canopies. In: Steven, M.D. and J.A. Clark, *Applications of Remote Sensing in Agriculture*, Butterworths, and Toronto. pp. 19 - 43.

Haun, J. R. (1973). Visual quantification of wheat development. *Agronomy Journal.* 65:116-119

Hay, R.K.M. and A.J. Walker (1989). *An Introduction To The Physiology Of Crop Yield*, John Wiley and Sons, Inc. New York. pp. 291.

Hinzman, L. D. , M. E. Bauer, and C.S.T. Daughtry (1986). Effects of nitrogen fertilization on growth and reflectance characteristics of winter wheat. *Remote Sensing of Environment.* 19:47 - 61.

Hochheim, K.P. and D.G. Barber (1998). Spring wheat yield estimation for western Canada using NOAA NDVI data. *Canadian Journal of Remote Sensing.* Vol. 24, No. 1, 17-27.

Hochheim, K.P. and D.G. Barber, (2003). The seasonal backscatter of Wheat and Canola as observed by RADARSAT-1. *International Journal of Remote Sensing.* (In prep.)

Hoekman, D.H., L. Krul, E.P.W. Attema, 1982, A multi-layer model for radar backscattering from vegetation canopies. *Digest, 2nd Annual International*

Geoscience and Remote Sensing Symposium, Vol. 11, Munich, West Germany, 1-4 June, p. 4.1.

Holben B. N. and R. S. Fraser, (1984). Red and near-infrared sensor response to off-nadir viewing. *International Journal of Remote Sensing.* Vol. 5, No. 1, 145 - 160.

Holben, B. N., C.J. Tucker and Cheg-Jeng Fan (1980). Spectral assessment of soybean leaf area and leaf biomass. *Photogrammetric Engineering and Remote Sensing*, Vol. 46, No. 5, pp. 651 - 656.

Holben, B. N., Dan Kimes and R. S. Fraser (1986). Directional reflectance response in AVHRR red and near-IR bands for three cover types and varying atmospheric conditions. *Remote Sensing of Environment.* 19:213 - 236.

Huete, A.R. (1987). Soil-dependent spectral response in a developing plant canopy. *Agronomy Journal.* Vol. 79, pp. 61 - 68.

Huete, A.R. and R.D., Jackson (1988). Soil and atmosphere influences on the spectra of partial canopies. *Remote Sensing of Environment.* 25:89 - 105.

Jackson, R.D., P.J. Pinter, Jr., S.B. Idso, and R. J. Reginato (1979). Wheat spectral reflectance:interactions between crop configuration, sun elevation, and azimuth angle. *Applied Optics.* Vol. 18, No. 22, pp. 3730 - 3732.

Jackson, R.D., P.N. Slater, and P.J. Pinter, JR. (1983). Discrimination of growth and water stress in wheat by various vegetation indices through clear and turbid atmospheres. *Remote Sensing of Environment.* 13:187 - 208.

Jordon, C.F. (1969). Derivation of leaf area index from quality of light on the forest floor. *Ecology.* 50:633 -666.

Kimes, D.S. (1983). Dynamics of directional reflectance factor distributions for vegetation canopies. *Applied Optics*. Vol. 22, No. 9, pp. 1364 - 1372.

Kleman, J. and E. Fagerlund, (1987). Influence of different nitrogen and irrigation treatments on the spectral reflectance of barley. *Remote Sensing of Environment*. 21:1-14.

Knipling, E.B. (1970), Physical and physiological basis for the reflectance of visible and near-infrared radiation from vegetation. *Remote Sensing of Environment.* 1:155-159.

Korporal, K.D., R. Dubbins and N.M. Hillary (1989). The Statistics Canada crop condition assessment program. *IGARSS '89 - 12th Canadian Symposium on Remote Sensing. An Economic Tool for the Nineties, July 10-14th Vancouver, Canada*, Vol. 4., pp. 1972-1974.

Large, E.C. (1954). Growth stages in cereals, illustration of the feekes scale. *Plant Pathology*, 3:128-129

Le Toan, T., A. Lopes and M Huete (1984). On the relationship between radar backscattering coefficient and vegetation canopy characteristics. *Proceedings of IGARSS '84 Symposium*, pp. 155-160.

McNairn H, Deguise J.-C. , Pacheco A. (2002). Remote sensing derived products for precision farming; *CCRS Report on Results from Clinton '99* , Canada Centre for Remote Sensing, Natural Resources Canada, pp. 5.

McNairn, H., K. Hochheim and N. Rabe (2002a). Applying polarimetric radar imagery for mapping the productivity of wheat crops, *Canadian Journal of Remote sensing*. (in press).

Michalyna, W., Glenn Podolsky, and E.S.T. Jacques, 1988, Soils *Report No. D60. Soils of the Rural Municipalities of Grey, Dufferin, Roland, Thompson and Part of Stanley*. (Canada Manitoba Soil Survey).

Miller, J.R., H. McNairn, E. Cloutis E. Pattey and N. Tremblay (2002). *User Requirement Report for Agriculture. Canadian Hyperspectral Users and Science Advisory Team*. Canadian Space Agency. Pp. 60.

Moore, R. (1976). Active Microwave Systems, in: *Remote Sensing of Environment*. (Ed.) J. Lintz Jr. and D.S. Simonett. Addison-Wesley Publishing Co. pp.694.

Moran, M.S., Y. Inoue and E.M. Barnes (1997). Opportunities and limitations for image-based remote sensing in precision crop management. *Remote Sensing of Environment*. 61:319-346.

Murphy, D.P., E. Schnug anf S. Haneklaus (1995). Yield mapping – a guide to improved techniques and strategies. In: Robert, P.C., R.H Rust, and W.E.Larson. (Eds.) Proceeding of Site Specific Management for Agricultural systems, Second International Conference., March 27-30, 1994. American Society of Agronomy. pp. 33-47

Myers, V.I. (Ed.). (1983). Remote sensing applications in agriculture. In: Colwell, R.N., J.E. Estes and G.A. Thorley. (Eds.). *Manual of Remote Sensing, Volume 2, Interpretation and Applications (2nd ed.)*. Falls Church, Virginia: American Society of Photogrammetry. pp. 2111-2228.

Paris, J.F. (1986). The effect of leaf size on the microwave backscattering by corn. *Remote Sensing of Environment*. 19:81-95.

Pearson, G.R.L. and L.D. Miller (1972). Remote Mapping of standing crop biomass for estimation of the productivity of the short grass prairie, Eighth *International Symposium on Remote Sensing of Environment, University of Michigan, Ann Arbor, Mich.*, pp. 1357 - 1381.

Raddatz, R.L., C.F. Shaykewich and P.R. Bullock (1994). Prairie crop yield estimates from modelled phenological development and water use. *Canadian Journal of Plant Science.* 47: 429-436.

Reichart, G. C. and David Caissy (2002). A reliable Crop Condition Assessment Program (CCAP) incorporating NOAA AVHRR data, a geographic information system and the internet. *ESRI User Conference, July 8-12, San Diego.* pp.9.

Rouse, J.W., R.H. Haas, J.A. Schell and D.W. Deering (1973). Monitoring vegetation systems in the Great Plains with ERTS; *3rd ERTS Symposium*, NASA SP=351, I: 309:317.

Rouse, J.W., R.H. Haas, J.A. Schell, D.W. Deering and J.C. Harlan. (1974). Monitoring the vernal advancement and retroradiation (greenwave effect) of natural vegetation. *NASA/GSFC Type III Final Report.* Greenbelt MD. pp. 371.

Rudorff, B. F. T. and G. T. Batista (1990). Yield estimation of sugarcane based on agrometeorological-spectral models. *Remote Sensing of Environment.* 33:183 - 192.

Rudorff, B. F. T. and G. T. Batista (1990a). Spectral response of wheat and its relationship to agronomic variables in the tropical region. *Remote Sensing of Environment.* 31:53 - 63.

Sinclair, T.R., R. M. Hoffer, and M. M. Schreiber (1971). Reflectance and internal structure of leaves from several crops during a growing season. *Agronomy Journal,* 63:864 - 868.

Skriver H., M.T. Svendsen, and A.G. Thomsen, (1999), Multitemporal C- and L- band polarimetric signatures of crops. *IEEE Transactions on Geoscience and Remote Sensing*, 37, 2413.

Sofko, G.J., Sloboshan, J., McKibben, M., Koehler, J., and Brisco, B. (1989). Variation of microwave radar cross-section of wheat during the early hours of a rainfall, *IGARSS 89, 12th Canadian Symposium on Remote Sensing, Vancouver, B.C.* pp. 1191-1194.

Taconet, O., M. Benallegue, D. Vidal-Madjar, L. Prevot, M. Dechambre, and M. Normand, 1994, Estimation of soil and crop parameters for wheat from airborne radar backscattering data in C and X bands. *Remote Sensing of Environment*, 50, 287.

Thomas, P. (1984) Canola Growers Manual. Canola Council of Canada.

Toure', A., K.P.B. Thomson, G. Edwards, R.J. Brown and B. Brisco (1994). Adaptation of the MIMICS backscattering model to the agricultural context - Wheat and Canola at L and C Bands. *IEEE Transactions on Geoscience and Remote Sensing*, Vol. GE-32 No.1, pp 47-61.

Tucker, C. J., B.N. Holben, J. H. Elgin, Jr., and J. E. McMurtrey III, 1980, Relationship of spectral data to grain yield variation. *Photogrammetric Engineering and Remote Sensing.* 46, 657.

Tucker, C. T. and P. J. Sellers (1986). Satellite remote sensing of primary production. *International Journal of Remote Sensing*. Vol. 7, No. 11, pp.1395 - 1416.

Tucker, C.T., J.H. Elgin Jr., and J.E. McMurtrey III. (1979). Temporal spectral measurements of corn and soybean crops. *Photogrammetric Engineering and Remote Sensing*. Vol. 45, No. 5, pp. 643 - 653.

Tucker, C.T., J.H. Elgin Jr., J.E. McMurtrey III and C.J. Fan. (1979a). Monitoring corn and soybean crop development with hand-held radiometer spectral data. *Remote Sensing of Environment*. 8:237 - 248.

Ulaby, F.T. (1975). Radar response to vegetation. *IEEE Transactions on Geoscience and Remote Sensing*, Vol. AP-23, No.1, pp.36-45.

Ulaby, F.T. and M.A. El-Rayes (1987). Microwave dielectric spectrum of vegetation-Part II: Dual dispersion model. *IEEE Transactions on Geoscience and Remote Sensing*, Vol. GE-25, No.5, pp., 550-557.

Ulaby, F.T. and T.F. Bush (1976). Corn growth as monitored by radar. *IEEE Transactions on Antennas and Propagation*, Vol. AP-24, No. 6, pp. 819-828.

Ulaby, F.T., A. Aslam and M.C. Dobson (1982). Effects of vegetation cover on the radar sensitivity to soil moisture. *IEEE Transactions on Geoscience and Remote Sensing*, Vol. GE-20, No.4, pp., 476-481.

Ulaby, F.T., and R.P. Jedlicka (1984). Microwave dielectric properties of plant materials. *IEEE Transactions on Geoscience and Remote Sensing*, Vol. GE-22 No.4, pp 406-415.

Ulaby, F.T., C.T. Allen, G Eger III and E. Kanemasu (1984). Relating the microwave backscattering coefficient to leaf area index. *Remote Sensing of the Environment.* 14: 113-133.

Ulaby, F.T., K. Sarabandi, K. McDonald, M. Whitt and M.C. Dobson. (1990). Michigan Microwave canopy scattering model. *International Journal of Remote Sensing.* Vol., 11, No. 7, pp. 1223-1253.

Ulaby, F.T., R.K. Moore, and A.K. Fung, (1982). *Microwave Remote Sensing: Active and Passive: Volume II: Radar Remote Sensing and Surface and Emission Scattering Theory.* Addison-Wesley Publishing Company, Massachusetts.

Wiegand, C. L. and A. J. Richardson (1990). Use of spectral vegetation indicies to infer leaf area, evapotranspiration and yield: I. Rationale. *Agronomy Journal*, Vol. 82, pp.623-629.

Wiegand, C. L., A. J. Richardson, and E. T. Kanemasu (1979). Leaf Area Index Measurements for wheat from Landsat and their implications for evapotranspiration and crop modeling. *Agronomy Journal,* 71:336 - 342.

Wiegand, C. L., S.J. Mass, J, K. Aase, J.L. Hatfield, P.J. Pinter, R.D. Jackson, E.T. Kanemasu, and R.L. Lapitan (1993). Multi-site analyses of spectral-biophysical data for wheat. *Remote Sensing of the Environment.* 42: 1-21.

Wood, D. McNairn, H. Brown, R.J., Dixon R.G. (2002). The effect on the use of RADARSAT-1 for crop monitoring choosing between ascending and descending orbits. *Remote Sensing of Environment*, Vol. 80. 2002, pp. 241-247.

Zadoks, J. C., T. T. Chang and B. F. Konzak. (1974). A decimal code for the growth stages of cereals. *Weed Research.* 14:415-421.

Appendices

Appendix A

Growth and Development Scales for Wheat and Canola

Table A-1. Condensed summary of the Zadoks two-digit code system for growth staging in wheat with corresponding Feekes code (FC), and Haun code (HC).

Zadoks code	Description	FC	HC
	Germination		
00	Dry kernel		
01	Start of imbibition (water absorption)		
05	Radicle emerged		
07	Coleoptile emerged		
09	Leaf just at coleoptile tip		
	Seeding development		
10	First leaf through coleoptile	1	1
11	First leaf at least 50% emerged		
12	Second leaf at least 50% emerged		1.+
13	Third leaf at least 50% emerged		2.+
14	Fourth leaf at least 50% emerged		3.+
15	Fifth leaf at least 50% emerged		4.+...
...19	Nine or more leaves		
	Tillering		
20	Main shoot only		
21	Main shoot plus 1 tiller visible	2	
22	Main shoot plus 2 tillers		
23	Main shoot plus 3 tillers		
24	Main shoot plus 4 tillers		
25	Main shoot plus 5 tillers	3	
...29	Main shoot 9 or more tillers		
	Stem elongation		
30	Pseudostem erection (leaf sheaths erect)	4-5	
31	1st node detectable	6	
32	2nd node detectable	7	
33	3rd node detectable		
...36	6th node detectable		
37	Flag leaf just visible	8	
39	Flag leaf collar just visible	9	

ZC		FC	HC
	Boot		
41	Flag leaf sheath extending		8-9
43	Boot just beginning to swell		
45	Boot swollen	10	9.2
47	Flag leaf sheath opening		
49	First awns visible		10.1
	Head emergence		
50	First spikelet of head just visible	10.1	10.2
53	One-fourth of head emerged	10.2	
55	One-half of head emerged	10.3	10.5
57	Three-fourths of head emerged	10.4	10.7
59	Head emergence complete	10.5	11.0
	Flowering		
61	Beginning of flowering	10.51	11.4
65	Half of florets have flowered	10.52	11.5
69	Flowering complete		11.6
	Milk development in kernel		
71	Kernel watery ripe	10.54	12.1
73	Early milk		13.0
75	Medium milk	11.1	
77	Late milk		
	Dough development in kernel		
83	Early dough		14.0
85	Soft dough	11.2	
87	Hard dough, head losing green colour		15.0
89	Approximate physiological maturity		
	Ripening		
91	Kernel hard (difficult to divide with thumbnail)	11.3	
92	Kernel cannot be dented by thumbnail, harvest ripe	11.4	16.0

Table A2 Summary of growth stages for canola.

Stage	Description of Main Raceme
0	Pre-emergence
1	Seedling
2	Rosette
2.1	First true leaf expanded
2.2	Second true leaf expanded
2.3 etc.	for each additional leaf
3	Bud
3.1	Flower cluster visible at centre of rosette
3.2	Flower cluster raised above level of rosette
3.3	Lower buds yellowing
4	Flower
4.1	First flower open
4.2	Many flowers opened, lower pods elongating
4.3	Lower pods starting to fill
4.4	Flowering complete, seed enlarging in lower pods
5	Ripening
5.1	Seeds in lower pods full size, translucent
5.2	Seeds in lower pods green
5.3	Seeds in lower pods green-brown or green-yellow, mottled
5.4	Seeds in lower pods yellow or brown
5.5	Seeds in all pods brown, plant dead

Appendix B

Regression Coefficients for RADARSAT Backscatter versus NDVI

Tables B1 - B25

Table B1. Regression Coefficients for Texture_1 versus RADARSAT-1 backscatter (11x11 Grid).

Linear				Reg. Coef.		Polynomial (2nd order)					Reg. Coef.		
DOY	R2	RMSE	P_Value	Intercept	B1	R2	RMSE	P_Value	P_Val B1	P_Val B2	Intercept	B1	B2
149	**0.38**	0.50	**0.0010**	-16.973	0.247	0.39	0.50	0.0027	0.0687	0.2448	-17.761	0.635	-0.041
156	0.05	0.92	0.1641	-16.210	0.171	0.08	0.90	0.1605	0.1206	0.1887	-17.832	0.970	-0.085
163	-0.02	0.91	0.4992	-13.606	0.081	-0.07	0.93	0.7707	0.6928	0.7860	-13.944	0.247	-0.018
173	0.01	0.60	0.3024	-13.301	-0.081	0.03	0.59	0.2935	0.1781	0.2401	-12.358	-0.545	0.049
180	**0.24**	0.72	**0.0096**	-12.073	-0.264	0.24	0.72	0.0254	0.7354	0.3721	-12.941	0.163	-0.045
187	0.08	0.88	0.1029	-11.889	-0.194	0.08	0.88	0.1707	0.2101	0.3380	-10.749	-0.755	0.059
197	**0.17**	0.65	**0.0277**	-16.148	0.199	0.13	0.67	0.0927	0.7868	0.8593	-15.991	0.121	0.008
201	0.10	0.77	0.0741	-15.320	0.187	**0.23**	0.72	0.0296	**0.0242**	**0.0502**	-17.294	1.159	-0.103
210	-0.03	0.80	0.5069	-15.203	0.070	**0.17**	0.72	0.0564	**0.0184**	**0.0227**	-17.541	1.220	-0.122
221	0.15	0.97	0.0387	-18.248	0.277	**0.39**	0.82	0.0027	**0.0023**	**0.0063**	-21.561	1.907	-0.173

Indicates significance at 95%

Table B2 Regression coefficients for Texture_2 versus RADARSAT-1 backscatter (11x11 Grid).

Linear				Reg. Coef.		Polynomial (2nd order)					Reg. Coef.		
DOY	R2	RMSE	P_Value	Intercept	B1	R2	RMSE	P_Value	P_Val B1	P_Val B2	Intercept	B1	B2
149	**0.31**	0.53	**0.0035**	-17.138	0.227	0.32	0.53	0.0083	0.1122	0.2623	-18.369	0.721	-0.044
156	0.09	0.90	0.0834	-16.687	0.212	**0.34**	0.77	0.0063	**0.0040**	**0.0079**	-21.267	2.052	-0.164
163	0.01	0.89	0.2959	-13.995	0.124	-0.02	0.91	0.4922	0.459	0.5578	-15.091	0.565	-0.039
173	0.03	0.59	0.2207	-13.100	-0.097	-0.01	0.60	0.4217	0.7570	0.6116	-13.727	0.155	-0.022
180	0.11	0.78	0.0641	-12.195	-0.197	0.16	0.76	0.0685	0.2749	0.1605	-14.425	0.699	-0.080
187	0.07	0.88	0.124	-11.716	-0.184	0.02	0.91	0.311	0.6839	0.8681	-11.408	-0.308	0.011
197	**0.13**	0.67	**0.0491**	-16.270	0.181	0.10	0.68	0.1274	0.3745	0.5609	-17.079	0.506	-0.029
204	0.21	0.73	0.0163	-15.936	0.246	**0.42**	0.62	0.0018	**0.0032**	**0.0088**	-19.600	1.718	-0.131
210	-0.02	0.80	0.4923	-15.306	0.072	**0.26**	0.68	0.0201	**0.0060**	**0.0074**	-19.412	1.722	-0.147
221	**0.26**	0.91	**0.0076**	-19.056	0.348	0.34	0.86	0.0062	0.0301	0.0768	-22.290	1.647	-0.116

Table B3 Regression coefficients for OM versus RADARSAT-1 backscatter (11x11 Grid)

Linear				Reg. Coef.		Polynomial (2nd order)					Reg. Coef.		
DOY	R2	RMSE	P_Value	Intercept	B1	R2	RMSE	P_Value	P_Val B1	P_Val B2	Intercept	B1	B2
149	0.11	0.60	0.0633	-16.72	0.24	0.18	0.58	0.0555	0.0684	0.1244	-18.92	1.36	-0.13
156	-0.01	0.95	0.3889	-16.05	0.17	0.11	0.89	0.127	0.053	0.0684	-20.11	2.23	-0.25
163	-0.03	0.91	0.6081	-13.61	0.10	-0.07	0.93	0.7887	0.7117	0.6444	-12.58	-0.42	0.06
173	0.12	0.56	0.0571	-12.70	-0.23	0.08	0.57	0.1638	0.9663	0.7701	-13.10	-0.03	-0.02
180	0.10	0.78	0.0803	-12.18	-0.30	0.11	0.78	0.1226	0.1719	0.2764	-10.12	-1.34	0.12
187	0.07	0.88	0.1197	-11.62	-0.30	0.12	0.86	0.1129	0.1021	0.1622	-8.66	-1.80	0.18
197	0.03	0.70	0.1947	-15.94	0.19	0.04	0.70	0.2697	0.2381	0.3278	-17.60	1.04	-0.10
204	0.03	0.80	0.2161	-15.25	0.21	0.13	0.76	0.1011	0.0558	0.0825	-18.54	1.89	-0.20
210	0.00	0.79	0.3146	-15.57	0.17	0.04	0.77	0.2482	0.1413	0.1850	-18.08	1.44	-0.15
221	**0.28**	0.89	**0.0052**	-19.31	0.58	0.32	0.87	0.0081	0.0619	0.1613	-22.29	2.09	-0.18

Table B4. Regression coefficients for SP98_12_ND versus RADARSAT-1 backscatter (11x11 Grid).

Linear				Reg. Coef.		Polynomial (2nd order)					Reg. Coef.		
DOY	R2	RMSE	P_Value	Intercept	B1	R2	RMSE	P_Value	P_Val B1	P_Val B2	Intercept	B1	B2
149	**0.23**	0.56	**0.0113**	-18.63	0.15	0.33	0.52	0.0076	0.0963	0.0639	-6.19	-1.22	0.04
156	-0.02	0.95	0.4512	-16.69	0.07	-0.05	0.97	0.6341	0.5211	0.5548	-23.71	0.84	-0.02
163	-0.05	0.92	0.864	-12.86	-0.02	0.04	0.88	0.2606	0.1054	0.1071	5.07	-1.99	0.05
173	0.13	0.56	0.0535	-11.53	-0.11	0.10	0.57	0.1421	0.713	0.6100	-15.09	0.28	-0.01
180	**0.33**	0.68	**0.0026**	-9.04	-0.22	0.29	0.69	0.0121	0.6935	0.8727	-7.68	-0.37	0.00
187	**0.25**	0.79	**0.0087**	-8.50	-0.22	0.24	0.80	0.0243	0.301	0.4008	-0.23	-1.13	0.02
197	0.12	0.67	0.0626	-17.63	0.13	0.14	0.66	0.0846	0.2731	0.2176	-7.44	-1.00	0.03
204	0.00	0.82	0.3284	-15.88	0.08	-0.05	0.84	0.6235	0.8553	0.9095	-17.04	0.21	0.00
210	-0.01	0.79	0.3858	-16.18	0.07	0.02	0.78	0.3291	0.2069	0.2281	-27.95	1.36	-0.03
221	**0.27**	0.90	**0.0063**	-22.02	0.26	0.24	0.92	0.0244	0.8633	0.7020	-17.72	-0.21	0.01

☐ Indicates significance at 95%

Table B5. Regression coefficients for SP98_27_ND versus RADARSAT-1 backscatter (11x11 Grid).

Linear				Reg. Coef.		Polynomial (2nd order)					Reg. Coef.		
DOY	R2	RMSE	P_Value	Intercept	B1	R2	RMSE	P_Value	P_Val B1	P_Val B2	Intercept	B1	B2
149	**0.21**	0.57	**0.017**	-17.158	0.107	0.21	0.57	0.038	0.5178	0.3256	-15.31	-0.207	0.012
156	-0.03	0.96	0.6158	-15.785	0.035	-0.04	0.96	0.5536	0.3117	0.3390	-18.81	0.550	-0.020
163	-0.05	0.92	0.9381	-13.243	0.005	0.07	0.87	0.1943	0.078	0.0740	-7.99	-0.888	0.035
173	0.13	0.56	0.0494	-12.540	-0.084	0.10	0.57	0.1418	0.9167	0.7096	-13.23	0.033	-0.005
180	**0.28**	0.70	**0.0055**	-11.266	-0.157	0.28	0.70	0.0139	0.1659	0.3107	-8.93	-0.554	0.016
187	**0.33**	0.75	**0.0025**	-10.271	-0.187	0.31	0.76	0.0095	0.2995	0.5389	-8.74	-0.447	0.010
197	0.07	0.69	0.1259	-16.210	0.080	0.02	0.71	0.3	0.8862	0.7277	-15.41	-0.056	0.005
204	-0.01	0.82	0.4128	-15.012	0.050	-0.06	0.84	0.6908	0.6948	0.7724	-15.80	0.184	-0.005
210	-0.02	0.80	0.4757	-15.424	0.042	0.01	0.79	0.3503	0.1837	0.2113	-18.69	0.597	-0.022
221	**0.37**	0.84	**0.0013**	-19.966	0.226	0.36	0.84	0.0046	0.7391	0.4166	-17.72	-0.157	0.015

Table B6 Regression coefficients for Texture_1 versus RADARSAT-1 backscatter (σ^o averaged per Texture_1 zone), FLD_100.

	Linear			Reg. Coef.		Polynomial (2nd order)					Reg. Coef		
DOY	R2	RMSE	P_Value	Intercept	B1	R2	RMSE	P_Value	P_Val B1	P_Val B2	Intercept	B1	B2
149	**0.70**	0.27	**0.0058**	-16.550	0.177	0.84	0.20	0.0043	0.0143	0.0546	-17.127	0.523	-0.039
156	0.62	0.32	0.0127	-16.379	0.173	**0.85**	0.20	0.0035	**0.0069**	**0.0223**	-17.127	0.622	-0.050
163	0.00	0.28	0.3619	-13.478	0.042	0.18	0.25	0.2598	0.1420	0.1839	-13.921	0.308	-0.030
173	0.33	0.28	0.0781	-13.337	-0.090	0.57	0.22	0.0514	0.0475	0.0911	-12.803	-0.410	0.036
180	**0.72**	0.28	**0.0050**	-12.500	-0.189	0.86	0.20	0.0034	0.2703	0.0474	-13.112	0.178	-0.041
187	**0.73**	0.31	**0.0042**	-11.735	-0.215	0.85	0.23	0.0039	0.0154	0.0640	-11.095	-0.599	0.043
194	**0.64**	0.35	**0.0108**	-16.077	0.194	0.79	0.26	0.0083	0.2631	0.0642	-15.364	-0.233	0.048
201	**0.47**	0.37	**0.0359**	-15.135	0.152	0.70	0.28	0.0220	0.0287	0.0676	-15.883	0.601	-0.050
211	0.18	0.72	0.1600	-16.040	0.178	**0.89**	0.27	0.0019	**0.0010**	**0.0016**	-17.955	1.326	-0.128
221	0.56	0.71	0.0200	-18.755	0.342	**0.92**	0.29	0.0007	**0.0009**	**0.0028**	-20.607	1.454	-0.123

Indicates significance at 95%

Table B7 Regression coefficients for Texture_2 versus RADARSAT-1 backscatter. (σ^o averaged per Texture_2 zone), FLD_100.

	Linear			Reg. Coef.		Polynomial (2nd order)					Reg. Coef.		
DOY	R2	RMSE	P_Value	Intercept	B1	R2	RMSE	P_Value	P_Val B1	P_Val B2	Intercept	B1	B2
149	0.73	0.29	0.0086	-16.919	0.231	**0.91**	0.17	0.0038	**0.0118**	**0.0323**	-18.188	0.835	-0.060
156	0.80	0.31	0.0039	-17.154	0.299	**0.92**	0.20	0.0031	**0.0153**	**0.0497**	-18.454	0.918	-0.062
163	0.23	0.32	0.1579	-13.763	0.102	0.46	0.27	0.1305	0.1055	0.1512	-14.866	0.627	-0.053
173	0.10	0.32	0.2541	-13.349	-0.077	-0.04	0.34	0.4769	0.7254	0.5866	-13.811	0.142	-0.022
180	**0.61**	0.26	**0.0240**	-12.425	-0.156	0.64	0.25	0.0573	0.5633	0.2898	-13.115	0.172	-0.033
187	**0.53**	0.36	**0.0392**	-11.697	-0.188	0.46	0.38	0.1310	0.8918	0.5837	-12.220	0.062	-0.025
197	0.27	0.40	0.1320	-16.034	0.136	0.11	0.44	0.3550	0.6119	0.7960	-16.314	0.270	-0.013
204	0.35	0.52	0.0952	-15.509	0.203	0.67	0.37	0.0471	0.0437	0.0705	-17.582	1.190	-0.099
211	0.30	0.82	0.1170	-16.479	0.294	**0.79**	0.45	0.0198	**0.0151**	**0.0240**	-20.147	2.041	-0.175
221	0.78	0.49	0.0054	-19.419	0.438	**0.93**	0.28	0.0024	**0.0093**	**0.0283**	-21.598	1.475	-0.104

Table B8 Regression coefficients for OM versus RADARSAT-1 backscatter (σ^o averaged per OM zone), FLD_100

	Linear			Reg. Coef.		Polynomial (2nd order)					Reg. Coef.		
DOY	R2	RMSE	P_Value	Intercept	B1	R2	RMSE	P_Value	P_Val B1	P_Val B2	Intercept	B1	B2
149	0.06	0.47	0.3188	-16.269	0.127	0.05	0.47	0.4314	0.3322	0.3973	-17.583	0.810	-0.076
156	0.47	0.27	0.0789	-16.063	0.154	0.46	0.28	0.1832	0.2798	0.4095	-16.815	0.544	-0.043
163	-0.23	0.45	0.8119	-13.269	0.028	-0.31	0.47	0.6975	0.4736	0.4492	-12.112	-0.573	0.067
173	**0.67**	0.23	**0.0286**	-12.946	-0.185	0.84	0.16	0.0284	0.0536	0.1011	-11.892	-0.733	0.061
180	0.25	0.41	0.1778	-12.633	-0.161	0.67	0.27	0.0875	0.0657	0.0896	-10.716	-1.156	0.111
187	0.77	0.30	0.0140	-11.528	-0.295	**0.95**	0.13	0.0049	**0.0120**	**0.0271**	-9.982	-1.098	0.089
197	**0.69**	0.14	**0.0251**	-15.653	0.118	0.74	0.13	0.0612	0.1499	0.2753	-16.140	0.370	-0.028
204	0.24	0.25	0.1864	-14.806	0.097	0.56	0.19	0.1335	0.1031	0.1383	-15.898	0.664	-0.063
211	0.41	0.55	0.1022	-16.271	0.278	0.43	0.54	0.2015	0.2585	0.3666	-17.905	1.127	-0.094
221	**0.88**	0.30	**0.0039**	-18.793	0.435	0.96	0.17	0.0036	0.0173	0.0527	-20.297	1.216	-0.087

Table B9 Regression coefficients for SP98_ND_12 versus RADARSAT-1 backscatter (σ^o averaged per SP98_ND_12 zone), FLD_100

	Linear			Reg. Coef.		Polynomial (2nd order)					Reg. Coef.		
DOY	R2	RMSE	P_Value	Intercept	B1	R2	RMSE	P_Value	P_Val B1	P_Val B2	Intercept	B1	B2
149	**0.56**	0.33	**0.0050**	-18.053	0.116	0.63	0.30	0.0074	0.0806	0.1293	-23.514	0.743	-0.017
156	0.28	0.45	0.0551	-17.326	0.095	0.22	0.47	0.1495	0.6756	0.5650	-14.309	-0.251	0.010
163	-0.05	0.31	0.4702	-12.893	-0.023	-0.17	0.33	0.7792	0.9688	0.9261	-13.235	0.017	-0.001
173	0.21	0.48	0.0902	-16.185	0.087	0.13	0.50	0.2338	0.5628	0.6545	-18.692	0.374	-0.008
180	**0.94**	0.19	**<.0001**	-9.057	-0.224	0.94	0.18	<.0001	0.0592	0.2646	-6.729	-0.491	0.007
187	**0.88**	0.31	**<.0001**	-10.865	-0.255	0.87	0.32	0.0001	0.1761	0.4253	-7.983	-0.586	0.009
197	0.20	0.43	0.0932	-16.681	0.077	**0.68**	0.27	0.0041	**0.0070**	**0.0049**	-5.499	-1.205	0.036
204	**0.32**	0.42	**0.0401**	-12.031	-0.096	0.31	0.42	0.0938	0.4916	0.3909	-16.147	0.376	-0.013
211	0.14	0.47	0.1397	-16.422	0.072	0.14	0.47	0.2280	0.4181	0.3550	-11.492	-0.493	0.016
221	**0.82**	0.47	**<.0001**	-22.835	0.308	0.80	0.50	0.0006	0.5825	0.9462	-23.206	0.350	-0.001

Indicates significance at 95%

Table B10. Regression coefficients for SP98_ND_27 versus RADARSAT-1 backscatter, (σ^o averaged per SP98_ND_27 zone), FLD_100.

	Linear			Reg. Coef.		Polynomial (2nd order)					Reg. Coef.		
DOY	R2	RMSE	P_Value	Intercept	B1	R2	RMSE	P_Value	P_Val B1	P_Val B2	Intercept	B1	B2
149	0.33	0.38	0.0228	-16.752	0.074	**0.77**	0.22	0.0003	**0.0004**	**0.0009**	-20.349	0.678	-0.023
156	**0.35**	0.33	**0.0195**	-16.506	0.067	0.49	0.29	0.0142	0.0398	0.0748	-18.514	0.403	-0.013
163	-0.07	0.32	0.6816	-13.465	0.010	-0.11	0.33	0.6901	0.4313	0.4569	-14.349	0.158	-0.006
173	**0.25**	0.44	**0.0460**	-12.880	-0.074	0.23	0.45	0.1075	0.5934	0.4211	-14.186	0.145	-0.008
180	0.79	0.29	<.0001	-11.402	-0.145	**0.85**	0.24	<.0001	**0.0062**	**0.0346**	-9.364	-0.487	0.013
187	**0.77**	0.40	**<.0001**	-10.067	-0.194	0.82	0.36	<.0001	0.0172	0.0801	-7.636	-0.602	0.016
197	**0.54**	0.28	**0.0027**	-16.350	0.080	0.62	0.25	0.0031	0.2193	0.0917	-14.710	-0.195	0.011
204	-0.03	0.39	0.4245	-14.872	0.024	0.09	0.36	0.2464	0.1267	0.1483	-16.851	0.356	-0.013
211	0.14	0.57	0.1127	-15.933	0.073	0.06	0.60	0.3021	0.8781	0.9603	-15.827	0.055	0.001
221	**0.87**	0.44	**<.0001**	-20.843	0.292	0.85	0.46	<.0001	0.4752	0.7433	-20.302	0.202	0.003

Table B11. Regression coefficients for RADARSAT-1 backscatter versus SP98_ND_12 classes, FLD_100.

	Linear			Reg. Coef.		2nd order Polynomial					Reg. Coef.		
DOY	R2	RMSE	P_Value	Intercept	B1	R2	RMSE	P_Value	P_Val B1	P_Val B2	Intercept	B1	B2
149	**0.56**	0.33	**0.0050**	-18.05	0.12	0.63	0.30	0.0074	0.0806	0.1293	-23.51	0.74	-0.02
156	0.28	0.45	0.0551	-17.33	0.09	0.22	0.47	0.1495	0.6756	0.5650	-14.31	-0.25	0.01
163	-0.05	0.31	0.4702	-12.89	-0.02	-0.17	0.33	0.7792	0.9688	0.9261	-13.24	0.02	0.00
173	0.21	0.48	0.0902	-16.19	0.09	0.13	0.50	0.2338	0.5628	0.6545	-18.69	0.37	-0.01
180	**0.94**	0.19	**<.0001**	-9.06	-0.22	0.94	0.18	<.0001	0.0592	0.2646	-6.73	-0.49	0.01
187	**0.88**	0.31	**<.0001**	-7.86	-0.26	0.87	0.32	0.0001	0.1761	0.4253	-7.98	-0.59	0.01
197	0.20	0.43	0.0932	-16.68	0.08	**0.68**	0.27	0.0041	**0.0070**	**0.0049**	-5.50	-1.20	0.04
204	**0.32**	0.42	**0.0401**	-12.03	-0.10	0.31	0.42	0.0938	0.4916	0.3909	-16.15	0.38	-0.01
211	0.14	0.47	0.1397	-16.42	0.07	0.14	0.47	0.228	0.4181	0.3550	-11.49	-0.49	0.02
221	**0.82**	0.47	**<.0001**	-22.84	0.31	0.80	0.50	0.0006	0.5825	0.9462	-23.21	0.35	0.00

Indicates significance at 95%

Table B12. Regression coefficients for RADARSAT-1 backscatter versus SP98_ND_12 classes, FLD_110.

	Linear			Reg. Coef.		2nd order Polynomial					Reg. Coef.		
DOY	R2	RMSE	P_Value	Intercept	B1	R2	RMSE	P_Value	P_Val B1	P_Val B2	Intercept	B1	B2
149	-0.11	0.33	0.5946	-14.821	0.028	-0.31	0.36	0.8465	0.7697	0.7919	-16.86	0.281	-0.008
156	-0.14	0.41	0.7254	-13.726	0.023	0.45	0.29	0.097	0.0401	0.0414	-29.85	2.016	-0.060
163	-0.15	0.44	0.8059	-10.209	0.018	**0.61**	0.26	0.042	**0.0161**	**0.0165**	-29.10	2.352	-0.071
173	-0.10	0.36	0.5763	-13.507	0.033	-0.24	0.38	0.7337	0.6026	0.5808	-8.85	-0.542	0.017
180	**0.71**	0.30	**0.0053**	-8.775	-0.195	0.75	0.28	0.0139	0.3246	0.2289	-16.59	0.772	-0.029
187	**0.83**	0.31	**0.0010**	-9.516	-0.285	0.81	0.33	0.0067	0.4191	0.6124	-5.87	-0.736	0.014
197	-0.16	0.26	0.8866	-11.853	-0.006	-0.10	0.25	0.5479	0.2971	0.2998	-8.88	-0.745	0.022
204	-0.02	0.15	0.3924	-12.441	-0.021	0.23	0.13	0.2268	0.1610	0.1477	-17.05	0.548	-0.017
211	-0.14	0.38	0.7127	-13.383	0.023	-0.31	0.41	0.8449	0.6455	0.6594	-17.36	0.514	-0.015
221	**0.87**	0.16	**0.0004**	-19.084	0.174	0.87	0.17	0.0028	0.2669	0.4401	-21.94	0.526	-0.011

Table B13 Regression coefficients for RADARSAT-1 backscatter versus SP98_ND_12 classes, FLD_120.

	Linear			Reg. Coef.		2nd order Polynomial					Reg. Coef.		
DOY	R2	RMSE	P_Value	Intercept	B1	R2	RMSE	P_Value	P_Val B1	P_Val B2	Intercept	B1	B2
149	**0.87**	0.23	**0.0135**	-6.795	-0.374	0.94	0.15	0.0279	0.1323	0.1540	31.915	-4.077	0.088
156	0.65	0.57	0.0632	-3.388	-0.517	0.86	0.35	0.069	0.1286	0.1400	95.647	-9.992	0.226
163	**0.86**	0.48	**0.0155**	4.572	-0.765	0.80	0.58	0.1024	0.7050	0.7798	26.263	-2.840	0.049
173	**0.76**	0.32	**0.0339**	-5.504	-0.381	0.83	0.27	0.0825	0.2407	0.2667	42.825	-5.005	0.110
180	**0.85**	0.33	**0.0170**	-1.973	-0.508	0.92	0.24	0.0382	0.1604	0.1843	53.173	-5.784	0.126
187	**0.84**	0.23	**0.0190**	-5.231	-0.343	0.77	0.28	0.1146	0.6726	0.7406	4.134	-1.526	0.028
197	-0.22	0.18	0.6327	-15.511	0.031	-0.41	0.20	0.7031	0.5129	0.5194	-33.355	1.738	-0.041
204	0.18	0.21	0.2626	-15.487	0.093	0.16	0.22	0.4213	0.4565	0.4407	8.790	-2.230	0.055
211	**0.84**	0.28	**0.0176**	-4.022	-0.422	0.87	0.26	0.0649	0.2935	0.3332	33.952	-4.055	0.087
221	0.60	0.41	0.0776	-22.433	0.342	0.90	0.21	0.0516	0.0976	0.0898	53.325	-6.906	0.173

Table B14. Regression coefficients for RADARSAT-1 backscatter versus SP98_12_ND classes, FLD_100-120.

	Linear			Reg. Coef.		2nd	order	Polynomial			Reg. Coef.		
DOY	R2	RMSE	P_Value	Intercept	B1	R2	RMSE	P_Value	P_Val B1	P_Val B2	Intercept	B1	B2
149	0.02	0.34	0.2919	-14.131	-0.036	**0.54**	0.23	0.0191	**0.0133**	**0.0109**	-22.433	0.916	-0.026
156	**0.37**	0.47	**0.0268**	-12.058	-0.118	0.56	0.39	0.0152	0.0874	0.0592	-21.263	0.938	-0.029
163	0.62	0.61	0.0025	-6.861	-0.242	**0.90**	0.32	<.0001	**0.0022**	**0.0010**	-24.078	1.732	-0.055
173	**0.51**	0.31	**0.0079**	-11.314	-0.102	0.53	0.31	0.0204	0.4123	0.2892	-15.077	0.330	-0.012
180	0.92	0.22	<.0001	-8.387	-0.224	**0.97**	0.14	<.0001	**0.0392**	**0.0057**	-14.130	0.434	-0.018
187	**0.96**	0.19	**<.0001**	-6.563	-0.294	0.96	0.21	<.0001	0.2148	0.8556	-6.148	-0.342	0.001
197	0.03	0.25	0.2749	-15.509	0.027	0.33	0.20	0.0821	0.0668	0.0559	-10.610	-0.535	0.016
204	0.45	0.26	0.0138	-12.215	-0.075	**0.75**	0.17	0.0015	**0.0147**	**0.0086**	-18.613	0.659	-0.020
211	0.08	0.33	0.2027	-12.868	-0.044	0.06	0.34	0.3142	0.4443	0.3881	-16.162	0.334	-0.010
221	**0.83**	0.27	**<.0001**	-19.671	0.183	0.86	0.25	0.0002	0.3135	0.1311	-15.227	-0.327	0.014

☐ Indicates significance at 95%

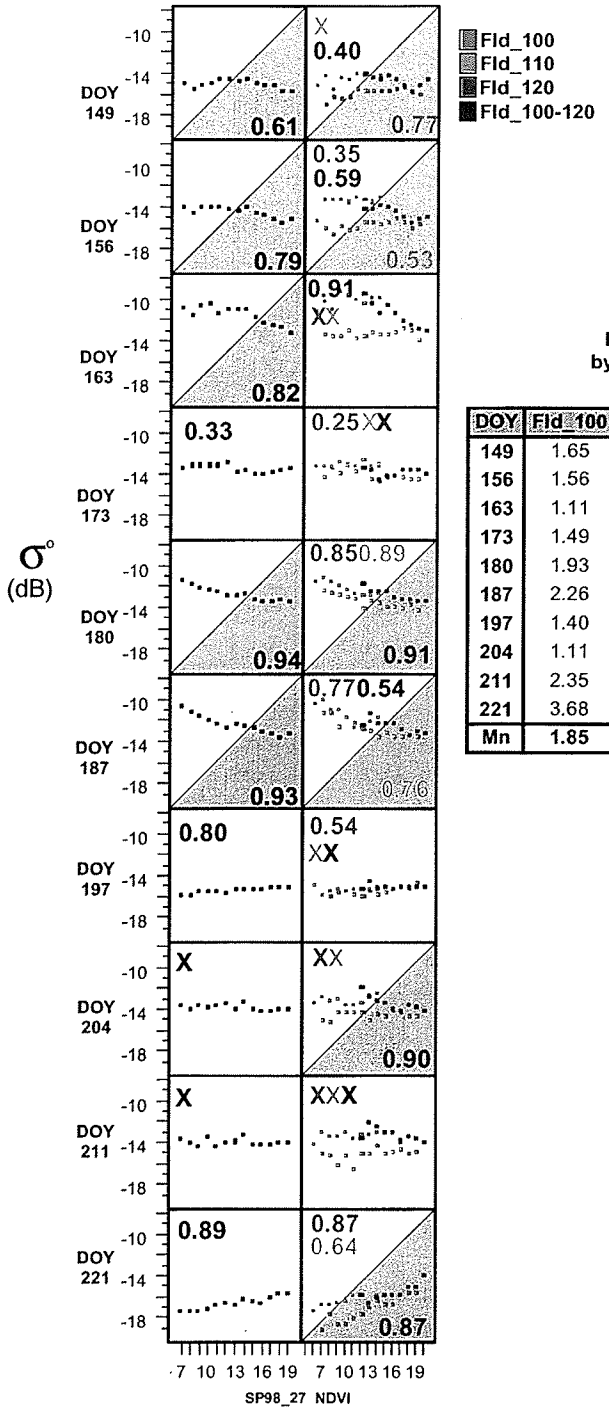

Backscatter Range by SP98_27_ND class per DOY

DOY	Fld_100	Fld_110	Fld_120	Fld_100-120
149	1.65	1.40	1.67	1.25
156	1.56	2.38	1.77	1.71
163	1.11	1.81	3.71	2.80
173	1.49	1.29	1.25	1.35
180	1.93	2.09	1.68	2.17
187	2.26	2.46	2.01	2.91
197	1.40	0.87	0.95	0.94
204	1.11	1.27	2.25	1.16
211	2.35	1.17	1.91	1.34
221	3.68	1.78	2.60	1.86
Mn	**1.85**	**1.65**	**1.98**	**1.75**

Figure B1. RADARSAT-1 backscatter trends per DOY for FLDs_100-120 as defined by SP98_ND_27 zones, Tables B15-B18.

Table B15. Regression coefficients for RADARSAT-1 backscatter versus SP98_ND_27 classes, FLD_100.

	Linear			Reg. Coef.		2nd order Polynomial					Reg. Coef.		
DOY	R2	RMSE	P_Val	Intercept	B1	R2	RMSE	P_Value	P_Val B1	P_Val B2	Intercept	B1	B2
149	**0.33**	0.38	**0.0228**	-16.75	0.07	**0.77**	0.22	**0.0003**	**0.0004**	**0.0009**	-20.35	0.68	-0.02
156	**0.35**	0.33	**0.0195**	-16.51	0.07	0.49	0.29	0.0142	0.0398	0.0748	-18.51	0.40	-0.01
163	-0.07	0.32	0.6816	-13.47	0.01	-0.11	0.33	0.6901	0.4313	0.4569	-14.35	0.16	-0.01
173	**0.25**	0.44	**0.0460**	-12.88	-0.07	0.23	0.45	0.1075	0.5934	0.4211	-14.19	0.15	-0.01
180	0.79	0.29	<.0001	-11.40	-0.15	**0.85**	0.24	**<.0001**	**0.0062**	**0.0346**	-9.36	-0.49	0.01
187	**0.77**	0.40	**<.0001**	-10.07	-0.19	0.82	0.36	<.0001	0.0172	0.0801	-7.64	-0.60	0.02
197	**0.54**	0.28	**0.0027**	-16.35	0.08	0.62	0.25	0.0031	0.2193	0.0917	-14.71	-0.19	0.01
204	-0.03	0.39	0.4245	-14.87	0.02	0.09	0.36	0.2464	0.1267	0.1483	-16.85	0.36	-0.01
211	0.14	0.57	0.1127	-15.93	0.07	0.06	0.60	0.3021	0.8781	0.9603	-15.83	0.06	0.00
221	**0.87**	0.44	**<.0001**	-20.84	0.29	0.85	0.46	<.0001	0.4752	0.7433	-20.30	0.20	0.00

Indicates significance at 95%

Table B 16 Regression coefficients for RADARSAT-1 backscatter versus SP98_ND_27 classes, FLD_110.

	Linear			Reg. Coef.		2nd order Polynomial					Reg. Coef.		
DOY	R2	RMSE	P_Value	Intercept	B1	R2	RMSE	P_Value	P_Val B1	P_Val B2	Intercept	B1	B2
149	0.15	0.41	0.1441	-15.16	0.07	0.21	0.40	0.1828	0.1921	0.2508	-17.39	0.53	-0.02
156	0.01	0.70	0.3332	-14.18	0.08	**0.44**	0.53	0.0529	**0.0247**	**0.0304**	-20.48	1.38	-0.06
163	0.19	0.52	0.1175	-10.99	0.10	0.21	0.51	0.1816	0.2302	0.3039	-13.52	0.62	-0.02
173	-0.05	0.34	0.4662	-12.52	-0.03	0.33	0.27	0.1036	0.0631	0.0520	-15.37	0.56	-0.03
180	**0.89**	0.24	**<.0001**	-9.71	-0.22	0.88	0.24	0.0002	0.1053	0.4138	-8.79	-0.41	0.01
187	**0.60**	0.55	**0.0051**	-8.94	-0.23	**0.76**	0.43	0.0029	**0.0186**	**0.0422**	-4.26	-1.19	0.05
197	0.08	0.25	0.2130	-15.39	0.04	0.26	0.22	0.1422	0.1715	0.1298	-13.71	-0.31	0.02
204	0.07	0.40	0.2336	-13.63	0.06	0.20	0.37	0.1923	0.2237	0.1744	-11.12	-0.46	0.02
211	-0.01	0.33	0.3590	-13.42	0.04	0.08	0.32	0.3091	0.1940	0.2270	-15.30	0.42	-0.02
221	**0.64**	0.33	**0.0032**	-17.81	0.15	0.62	0.34	0.0141	0.2761	0.5032	-18.89	0.37	-0.01

Table B17 Regression coefficients for RADARSAT-1 backscatter versus SP98_ND_27 classes, FLD_120.

	Linear			Reg. Coef.		2nd order Polynomial					Reg. Coef.		
DOY	R2	RMSE	P_Value	Intercept	B1	R2	RMSE	P_Value	P_Val B1	P_Val B2	Intercept	B1	B2
149	**0.40**	0.43	**0.0389**	-12.28	-0.14	0.42	0.42	0.0812	0.2465	0.3115	-5.63	-0.99	0.03
156	**0.59**	0.39	**0.0091**	-11.49	-0.18	0.54	0.42	0.0422	0.9295	0.7536	-13.44	0.07	-0.01
163	**0.91**	0.39	**<.0001**	-4.24	-0.45	0.90	0.41	0.0005	0.4034	0.7684	-2.43	-0.68	0.01
173	-0.14	0.42	0.8756	-13.72	0.01	-0.08	0.41	0.5277	0.2874	0.2820	-6.88	-0.87	0.03
180	0.83	0.25	0.0004	-9.41	-0.20	**0.91**	0.18	0.0003	**0.0176**	**0.0381**	-2.61	-1.07	0.03
187	**0.54**	0.42	**0.0142**	-9.56	-0.18	0.50	0.44	0.0532	0.7054	0.5601	-13.41	0.32	-0.02
197	-0.14	0.31	0.8926	-14.70	-0.01	-0.32	0.33	0.9656	0.8186	0.8250	-13.62	-0.14	0.00
204	0.71	0.40	0.0027	-9.64	-0.23	**0.90**	0.23	0.0004	0.0054	0.0098	2.76	-1.82	0.05
211	0.33	0.53	0.0626	-10.49	-0.15	0.30	0.54	0.1419	0.4976	0.4139	-17.22	0.71	-0.03
221	0.70	0.41	0.0030	-19.20	0.24	**0.87**	0.27	0.0009	**0.0347**	**0.0184**	-6.87	-1.35	0.05

Table B18. Regression coefficients for RADARSAT-1 backscatter versus SP98_ND_27 classes, FLD_100-120.

	Linear			Reg. Coef.		2nd	order	Polynomial			Reg. Coef.		
DOY	R2	RMSE	P_Value	Intercept	B1	R2	RMSE	P_Value	P_Val B1	P_Val B2	Intercept	B1	B2
149	0.06	0.41	0.2138	-14.29	-0.04	**0.61**	0.26	0.0038	**0.0037**	**0.0023**	-17.98	0.58	-0.02
156	0.63	0.35	0.0008	-12.74	-0.12	**0.79**	0.27	0.0002	**0.0481**	**0.0124**	-15.53	0.35	-0.02
163	0.66	0.51	0.0004	-9.03	-0.19	**0.82**	0.37	<.0001	**0.0347**	**0.0075**	-13.26	0.52	-0.03
173	**0.33**	0.36	**0.0231**	-12.32	-0.07	0.27	0.37	0.0857	0.6763	0.9126	-12.17	-0.09	0.00
180	0.88	0.24	<.0001	-10.31	-0.17	**0.94**	0.17	<.0001	**0.0004**	**0.0051**	-8.22	-0.52	0.01
187	0.91	0.26	<.0001	-9.41	-0.21	**0.93**	0.22	<.0001	**0.0033**	**0.0482**	-7.66	-0.50	0.01
197	**0.80**	0.13	**<.0001**	-15.90	0.06	0.80	0.13	0.0001	0.0772	0.2984	-16.38	0.14	0.00
204	0.14	0.32	0.1103	-13.08	-0.04	0.14	0.32	0.1924	0.4830	0.3621	-14.14	0.14	-0.01
211	-0.06	0.39	0.5573	-13.43	-0.02	-0.16	0.41	0.8473	0.9904	0.9524	-13.52	0.00	0.00
221	**0.89**	0.21	**<.0001**	-18.25	0.15	0.88	0.21	<.0001	0.5643	0.5515	-17.80	0.07	0.00

☐ Indicates significance at 95%

Table B19. Regression coefficients for RADARSAT-1 backscatter versus SP98_ND_27, FLD_130

	Linear			Reg. Coef.		2nd order Polynomial					Reg. Coef.		
DOY	R2	RMSE	P_Value	Intercept	B1	R2	RMSE	P_Value	P_Val B1	P_Val B2	Intercept	B1	B2
149	**0.65**	0.25	**0.0054**	-14.199	-0.127	0.69	0.23	0.0128	0.3188	0.2197	-19.332	0.491	-0.018
156	0.27	0.48	0.0891	-12.765	-0.123	0.22	0.50	0.2024	0.4134	0.4798	-6.702	-0.854	0.021
163	**0.61**	0.27	**0.0081**	-9.751	-0.126	0.55	0.29	0.0386	0.6080	0.7637	-8.299	-0.301	0.005
173	-0.08	0.18	0.5518	-13.009	-0.015	-0.17	0.19	0.6760	0.5410	0.5163	-15.136	0.241	-0.008
180	**0.54**	0.26	**0.0145**	-11.273	-0.109	0.48	0.28	0.0600	0.5733	0.7065	-9.499	-0.323	0.006
187	0.12	0.27	0.1928	-12.674	-0.050	0.41	0.22	0.0885	0.0696	0.0812	-5.305	-0.937	0.026
197	0.14	0.24	0.1694	-15.675	0.048	0.13	0.25	0.2793	0.4371	0.3858	-11.986	-0.396	0.013
204	0.30	0.31	0.0714	-15.065	0.086	0.44	0.28	0.0743	0.1233	0.1524	-22.514	0.983	-0.026
211	**0.80**	0.35	**0.0007**	-18.460	0.260	0.79	0.36	0.0041	0.7282	0.4896	-14.181	-0.256	0.015
221	0.42	0.47	0.0354	-17.492	0.157	**0.77**	0.29	0.0051	**0.0202**	**0.0142**	-1.337	-1.789	0.057

Indicates significance at 95%

Table B20. Regression coefficients for RADARSAT-1 backscatter versus SP98_ND_27, FLD_140

	Linear			Reg. Coef.		2nd order Polynomial					Reg. Coef.		
DOY	R2	RMSE	P_Value	Intercept	B1	R2	RMSE	P_Value	P_Val B1	P_Val B2	Intercept	B1	B2
149	**0.71**	0.40	**0.0027**	-18.343	0.231	0.66	0.43	0.0166	0.6654	0.9802	-18.415	0.245	-0.001
156	**0.66**	0.36	**0.0046**	-17.025	0.191	0.65	0.37	0.0184	0.6975	0.4421	-15.045	-0.190	0.017
163	**0.49**	0.48	**0.0211**	-13.959	0.185	0.44	0.51	0.0724	0.7499	0.5537	-11.893	-0.213	0.018
173	0.13	0.29	0.1848	-13.507	0.055	**0.53**	0.21	0.0447	**0.0303**	**0.0391**	-17.178	0.762	-0.032
180	0.14	0.26	0.1731	-11.395	-0.051	0.28	0.24	0.1578	0.2234	0.1756	-13.798	0.411	-0.021
187	**0.73**	0.35	**0.0020**	-9.675	-0.214	0.80	0.30	0.0036	0.2750	0.1266	-13.162	0.457	-0.031
197	-0.08	0.49	0.5302	-14.889	0.042	-0.25	0.53	0.8336	0.9230	0.9706	-15.022	0.068	-0.001
204	-0.14	0.31	0.8746	-12.012	0.007	-0.26	0.32	0.8417	0.5781	0.5862	-13.227	0.240	-0.011
211	0.39	0.57	0.0420	-15.669	0.183	**0.72**	0.39	0.0091	**0.0377**	**0.0226**	-7.996	-1.293	0.067
221	0.36	0.44	0.0518	-18.597	0.133	0.34	0.45	0.1234	0.5508	0.4167	-16.056	-0.356	0.022

Table B21. Regression coefficients for RADARSAT-1 backscatter versus SP98_ND_27, FLD_150

	Linear			Reg. Coef.		2nd order Polynomial					Reg. Coef.		
DOY	R2	RMSE	P_Value	Intercept	B1	R2	RMSE	P_Value	P_Val B1	P_Val B2	Intercept	B1	B2
149	0.90	0.29	0.0008	-12.202	-0.397	**0.96**	0.18	0.0007	**0.0181**	**0.0416**	-5.383	-1.679	0.058
156	0.85	0.19	0.0021	-12.600	-0.207	**0.96**	0.10	0.0008	**0.0106**	**0.0212**	-7.898	-1.092	0.040
163	**0.59**	0.20	**0.0264**	-10.221	-0.118	0.63	0.19	0.0605	0.2106	0.2840	-7.223	-0.681	0.026
173	**0.62**	0.05	**0.0213**	-12.298	-0.034	0.56	0.06	0.0851	0.7760	0.6135	-12.707	0.043	-0.003
180	**0.71**	0.25	**0.0109**	-9.899	-0.188	0.70	0.26	0.04	0.5698	0.4065	-12.928	0.381	-0.026
187	**0.91**	0.17	**0.0005**	-8.782	-0.265	0.91	0.18	0.0038	0.2349	0.4730	-6.954	-0.609	0.016
197	**0.71**	0.13	**0.0107**	-15.591	0.098	0.77	0.12	0.0238	0.1391	0.2081	-17.836	0.520	-0.019
204	**0.54**	0.27	**0.0372**	-13.019	0.142	0.65	0.23	0.0547	0.1357	0.1815	-17.812	1.044	-0.041
211	0.07	0.26	0.2844	-14.374	0.059	-0.02	0.27	0.4584	0.5367	0.4856	-11.718	-0.441	0.023
221	**0.88**	0.10	**0.0010**	-18.276	0.133	0.93	0.08	0.0023	0.2528	0.1134	-16.174	-0.262	0.018

Table B22. Regression coefficients for RADARSAT-1 backscatter versus SP98_ND_27, FLD_160

	Linear			Reg. Coef.		2nd	order	Polynomial			Reg. Coef.		
DOY	R2	RMSE	P_Value	Intercept	B1	R2	RMSE	P_Value	P_Val B1	P_Val B2	Intercept	B1	B2
149	0.46	0.29	0.0572	-16.524	0.135	0.32	0.33	0.2044	0.8363	0.9771	-16.628	0.157	-0.001
156	-0.16	0.45	0.6918	-14.692	-0.036	-0.45	0.51	0.9315	0.9344	0.9585	-14.398	-0.097	0.003
163	-0.19	0.37	0.8834	-10.696	0.011	-0.13	0.36	0.5657	0.3155	0.3190	-15.023	0.912	-0.045
173	**0.75**	0.32	**0.0070**	-9.493	-0.267	0.88	0.22	0.006	0.1153	0.0620	-15.420	0.968	-0.062
180	**0.80**	0.31	**0.0041**	-8.615	-0.290	0.86	0.25	0.0082	0.2639	0.1413	-13.454	0.718	-0.050
187	0.81	0.35	0.0038	-8.091	-0.340	**0.95**	0.18	**0.0012**	**0.0399**	0.0180	-15.464	1.196	-0.077
197	**0.55**	0.21	**0.0344**	-12.932	-0.113	0.57	0.20	0.084	0.4541	0.3387	-15.249	0.370	-0.024
204	-0.18	0.21	0.7864	-10.875	0.011	-0.46	0.23	0.941	0.8395	0.8227	-10.297	-0.109	0.006
211	0.91	0.16	0.0005	-15.265	0.238	**0.94**	0.13	**0.0014**	**0.0450**	0.1132	-17.929	0.793	-0.028
221	0.87	0.25	0.0015	-19.036	0.298	**0.93**	0.18	**0.002**	**0.0322**	0.0699	-23.564	1.241	-0.047

Indicates significance at 95%

Table B23 Regression coefficients for RADARSAT-1 backscatter versus SP98_ND_27, FLD_170

	Linear			Reg. Coef.		2nd	order	Polynomial			Reg. Coef.		
DOY	R2	RMSE	P_Value	Intercept	B1	R2	RMSE	P_Value	P_Val B1	P_Val B2	Intercept	B1	B2
149	0.48	0.32	0.0517	-13.475	-0.156	**0.81**	0.20	0.0168	**0.0282**	**0.0372**	-4.183	-1.749	0.066
156	**0.85**	0.17	**0.0019**	-12.771	-0.195	0.83	0.19	0.0135	0.4144	0.6333	-11.289	-0.450	0.011
163	0.19	0.66	0.1826	-8.710	-0.192	0.51	0.51	0.1058	0.1260	0.1063	-24.870	2.578	-0.115
173	**0.89**	0.24	**0.0009**	-8.902	-0.318	0.91	0.22	0.0037	0.4224	0.2204	-13.750	0.513	-0.035
180	**0.79**	0.37	**0.0044**	-7.622	-0.347	0.83	0.34	0.0133	0.1500	0.2352	-0.315	-1.599	0.052
187	**0.56**	0.53	**0.0325**	-8.801	-0.293	0.65	0.47	0.0529	0.2626	0.1971	-19.846	1.600	-0.079
197	-0.08	0.35	0.4963	-14.059	-0.049	**0.83**	0.14	0.0123	**0.0055**	**0.0059**	-2.773	-1.984	0.081
204	0.27	0.41	0.1303	-9.578	-0.140	0.68	0.27	0.0455	0.0664	0.0537	-20.810	1.786	-0.080
211	-0.09	0.67	0.5080	-14.130	0.090	-0.05	0.65	0.4869	0.3155	0.3342	-25.104	1.971	-0.078
221	-0.11	0.50	0.5538	-15.005	-0.060	-0.39	0.56	0.8566	0.9639	0.9945	-14.943	-0.070	0.000

Table B24. RADARSAT-1 Backscatter versus SP98_ND_12, FLDs_100-240.

	Linear			Reg. Coef.		2nd order Polynomial					Reg. Coef.		
DOY	R2	RMSE	P_Value	Intercept	B1	R2	RMSE	P_Value	P_Val B1	P_Val B2	Intercept	B1	B2
149	**0.47**	0.17	**0.0059**	-15.190	-0.043	0.42	0.18	0.0253	0.5150	0.7034	-14.651	-0.102	0.002
156	**0.84**	0.16	**<.0001**	-13.362	-0.096	0.86	0.15	<.0001	0.3860	0.1297	-15.315	0.118	-0.006
163	0.23	0.31	0.0550	-10.943	-0.050	**0.60**	0.23	0.0042	**0.0121**	**0.0076**	-16.801	0.592	-0.017
173	0.46	0.30	0.0066	-11.663	-0.075	**0.83**	0.17	<.0001	**0.0011**	**0.0005**	-18.279	0.650	-0.019
180	0.76	0.34	<.0001	-9.281	-0.160	**0.92**	0.20	<.0001	**0.0037**	**0.0008**	-16.632	0.645	-0.021
187	**0.92**	0.26	**<.0001**	-7.899	-0.220	0.95	0.21	<.0001	0.2074	0.0263	-12.084	0.238	-0.012
197	0.03	0.24	0.2576	-14.474	-0.022	**0.48**	0.18	0.0147	**0.0113**	**0.0087**	-18.993	0.473	-0.013
204	0.01	0.58	0.3116	-13.559	0.046	**0.56**	0.39	0.0069	**0.0028**	**0.0034**	-25.107	1.311	-0.033
211	0.15	0.34	0.1037	-14.725	0.045	0.07	0.36	0.277	0.9392	0.8254	-14.097	-0.024	0.002
221	0.94	0.33	<.0001	-21.985	0.332	**0.98**	0.19	<.0001	**0.0166**	**0.0006**	-14.784	-0.456	0.021

☐ Indicates significance at 95%

Table B25. RADARSAT-1 Backscatter versus SP98_ND_27, FLDs_100-240.

	Linear			Reg. Coef.		2nd order Polynomial					Reg. Coef.		
DOY	R2	RMSE	P_Value	Intercept	B1	R2	RMSE	P_Value	P_Val B1	P_Val B2	Intercept	B1	B2
149	0.37	0.20	0.0074	-15.559	-0.033	**0.56**	0.16	0.0018	**0.0072**	**0.0188**	-14.465	-0.201	0.006
156	**0.79**	0.18	**<.0001**	-14.189	-0.076	0.80	0.18	<.0001	0.9653	0.2771	-14.704	0.003	-0.003
163	**0.81**	0.21	**<.0001**	-10.501	-0.091	0.80	0.22	<.0001	0.1980	0.7897	-10.355	-0.113	0.001
173	**0.77**	0.22	**<.0001**	-11.814	-0.085	0.77	0.22	<.0001	0.0701	0.3455	-11.276	-0.168	0.003
180	**0.92**	0.20	**<.0001**	-10.352	-0.141	0.92	0.19	<.0001	0.0073	0.2179	-9.728	-0.237	0.003
187	0.93	0.22	<.0001	-9.905	-0.166	**0.95**	0.18	<.0001	**0.0002**	**0.0151**	-8.652	-0.358	0.007
197	0.44	0.23	0.0032	-14.170	-0.044	**0.70**	0.17	0.0001	**0.0008**	**0.0027**	-12.641	-0.279	0.008
204	0.52	0.40	0.0010	-11.036	-0.090	**0.63**	0.35	0.0006	**0.0115**	**0.0388**	-9.019	-0.400	0.011
211	-0.03	0.54	0.4614	-14.079	0.022	**0.45**	0.39	0.0077	**0.0041**	**0.0029**	-10.511	-0.525	0.019
221	0.95	0.33	<.0001	-19.659	0.301	**0.99**	0.15	<.0001	**0.0426**	**<.0001**	-16.841	-0.131	0.015

Appendix C

Regression Coefficients for RADARSAT Backscatter versus NDVI

Tables C1 - C8

Table C1 RADARSAT-1 backscatter versus field variability as expressed by SP98_ND_12, (11x11 grid), FLD_1.

	Linear			Reg. Coef		2nd order Polynomial					Reg. Coef		
DOY	R2	RMSE	P_Value	Intercept	B1	R2	RMSE	P_Value	P_Val B1	P_Val B2	Intercept	B1	B2
149	**0.08**	0.83	**0.0311**	-19.996	0.283	0.11	0.81	0.0228	0.1065	0.0866	13.34	-4.534	0.173
156	**0.09**	0.66	**0.0210**	-18.075	0.241	0.07	0.67	0.0686	0.6834	0.7627	-22.81	0.925	-0.025
163	0.19	0.85	0.0009	-18.633	0.461	**0.25**	0.82	0.0004	**0.0477**	**0.0326**	23.60	-5.641	0.219
173	**0.35**	0.75	**<.0001**	-20.351	0.592	0.36	0.74	<.0001	0.2369	0.1580	4.60	-3.013	0.130
180	0.04	0.63	0.0934	-12.624	0.164	0.02	0.63	0.233	0.6637	0.7196	-17.96	0.936	-0.028
187	**0.24**	0.68	**0.0002**	-4.791	-0.418	0.23	0.69	0.0011	0.7502	0.8895	-2.55	-0.742	0.012
197	0.04	0.71	0.0882	-9.225	-0.188	0.05	0.70	0.1184	0.2733	0.2405	-28.74	2.632	-0.101
204	**0.06**	0.62	**0.0478**	-11.328	0.194	0.04	0.63	0.144	0.8939	0.9657	-11.96	0.286	-0.003
211	-0.02	0.61	0.6630	-8.900	0.041	0.02	0.60	0.2627	0.1128	0.1168	-31.38	3.288	-0.117
221	-0.01	0.85	0.4298	-12.306	0.104	0.00	0.85	0.3826	0.2419	0.2559	-35.20	3.411	-0.119

Indicates significance at 95%

Table C 2 RADARSAT-1 backscatter versus field variability as expressed by SP98_ND_27, (11x11 grid), FLD_1.

	Linear			Reg. Coef		2nd order Polynomial					Reg. Coef		
DOY	R2	RMSE	P_Value	Intercept	B1	R2	RMSE	P_Value	P_Val B1	P_Val B2	Intercept	B1	B2
149	-0.01	0.87	0.4411	-18.257	0.104	-0.01	0.87	0.4414	0.3201	0.3084	29.22	-4.301	0.102
156	0.01	0.69	0.2116	-17.600	0.134	-0.01	0.69	0.4338	0.6943	0.7230	-30.73	1.352	-0.028
163	0.00	0.95	0.3657	-15.007	0.133	-0.03	0.96	0.6672	0.9706	0.9929	-15.46	0.176	-0.001
173	**0.08**	0.89	**0.0268**	-18.855	0.313	0.07	0.90	0.0763	0.5429	0.5900	-44.73	2.713	-0.056
180	-0.02	0.65	0.9196	-10.502	0.010	-0.01	0.64	0.4528	0.2111	0.2120	-53.59	4.008	-0.092
187	**0.15**	0.72	**0.0034**	-3.211	-0.340	0.14	0.72	0.0106	0.3872	0.4408	26.50	-3.097	0.064
197	0.02	0.71	0.1733	-8.544	-0.151	0.07	0.69	0.0739	0.0743	0.0677	-77.57	6.253	-0.148
204	-0.02	0.65	0.6007	-9.724	0.052	-0.03	0.65	0.6703	0.4598	0.4695	-34.95	2.393	-0.054
211	0.01	0.60	0.2543	-10.693	0.107	0.01	0.60	0.3052	0.2836	0.2994	-44.31	3.226	-0.072
221	**0.26**	0.73	**0.0001**	-21.316	0.472	0.24	0.74	0.0006	0.7682	0.6720	-4.58	-1.081	0.036

Table C3. RADARSAT-1 backscatter versus field variability as expressed by SP98_ND_12, (11x11 grid), FLD_1.

	Linear			Reg. Coef		2nd order Polynomial					Reg. Coef		
DOY	R2	RMSE	P_Value	Intercept	B1	R2	RMSE	P_Value	P_Val B1	P_Val B2	Intercept	B1	B2
149	**0.53**	0.18	**0.0239**	-17.095	0.082	0.55	0.17	0.057	0.4008	0.3090	-14.01	-0.354	0.015
156	0.01	0.38	0.3427	-15.755	0.061	-0.09	0.40	0.5322	0.4870	0.5243	-20.07	0.671	-0.021
163	**0.87**	0.32	**0.0005**	-16.765	0.340	0.84	0.36	0.0045	0.6151	0.9174	-17.38	0.427	-0.003
173	**0.48**	0.60	**0.0345**	-15.719	0.251	0.63	0.50	0.0355	0.0910	0.1204	-30.55	2.349	-0.072
180	**0.49**	0.20	**0.0312**	-11.695	0.088	0.70	0.16	0.0208	0.0528	0.0715	-17.33	0.885	-0.027
187	**0.62**	0.58	**0.0120**	-6.102	-0.316	0.69	0.53	0.0239	0.1430	0.2008	6.16	-2.050	0.060
197	-0.15	0.19	0.7637	-11.750	-0.009	-0.38	0.20	0.9599	0.9899	0.9950	-11.77	-0.006	0.000
204	**0.83**	0.15	**0.0011**	-10.539	0.132	0.80	0.16	0.0074	0.4007	0.6118	-11.87	0.320	-0.006
211	**0.84**	0.19	**0.0008**	-11.000	0.181	0.84	0.19	0.0046	0.6456	0.4038	-8.23	-0.210	0.013
221	0.32	0.33	0.0852	-12.471	0.104	**0.72**	0.21	0.0182	**0.0213**	**0.0271**	-22.79	1.564	-0.050

Indicates significance at 95%

Table C4. RADARSAT-1 backscatter versus field variability as expressed by SP98_ND_27, (11x11 grid), FLD_1.

	Linear			Reg. Coef		2nd order Polynomial					Reg. Coef		
DOY	R2	RMSE	P_Value	Intercept	B1	R2	RMSE	P_Value	P_Val B1	P_Val B2	Intercept	B1	B2
149	0.02	0.25	0.3375	-14.860	-0.050	-0.08	0.26	0.52	0.5311	0.5075	-23.90	0.819	-0.021
156	-0.19	0.19	0.8473	-14.981	0.007	0.61	0.11	0.0684	0.0285	0.0288	-32.48	1.689	-0.040
163	-0.03	0.44	0.4096	-13.722	0.075	-0.28	0.49	0.7305	0.8998	0.8751	-9.79	-0.303	0.009
173	**0.55**	0.43	**0.0347**	-17.250	0.234	0.70	0.35	0.0396	0.1116	0.1317	-48.82	3.269	-0.072
180	**0.50**	0.15	**0.0462**	-12.103	0.075	0.66	0.12	0.0508	0.1185	0.1377	-22.96	1.118	-0.025
187	**0.80**	0.35	**0.0042**	-3.458	-0.325	0.89	0.26	0.0055	0.0651	0.0876	24.16	-2.979	0.063
197	-0.10	0.24	0.5247	-11.310	-0.031	-0.07	0.24	0.5097	0.3609	0.3489	-23.41	1.132	-0.028
204	-0.14	0.28	0.6389	-9.185	0.027	-0.38	0.31	0.8511	0.7240	0.7366	-14.54	0.542	-0.012
211	0.65	0.39	0.0179	-14.178	0.258	**0.96**	0.13	0.0007	**0.0024**	**0.0030**	-54.19	4.104	-0.092
221	**0.99**	0.11	**<.0001**	-20.066	0.415	0.98	0.12	0.0001	0.7341	0.7153	-17.83	0.200	0.005

Table C5. RADARSAT-1 backscatter versus field variability as expressed by SP98_ND_12, (area means), Group-1 fields.

	Linear			Reg. Coef		2nd	order	Polynomial			Reg. Coef		
DOY	R2	RMSE	P_Value	Intercept	B1	R2	RMSE	P_Value	P_Val B1	P_Val B2	Intercept	B1	B2
149	0.15	0.54	0.1684	-17.996	0.107	**0.56**	0.39	0.0348	**0.0388**	**0.0318**	-0.74	-1.971	0.061
156	-0.07	0.54	0.5158	-14.785	-0.048	0.04	0.51	0.368	0.2098	0.2229	-3.68	-1.385	0.039
163	-0.14	0.58	0.9253	-12.960	0.007	0.49	0.39	0.057	0.0217	0.0213	6.44	-2.329	0.069
173	-0.13	0.48	0.8131	-11.930	0.015	-0.13	0.48	0.6013	0.3536	0.3454	-4.03	-0.937	0.028
180	-0.09	0.22	0.5831	-10.780	0.016	0.37	0.16	0.1079	0.0533	0.0494	-4.28	-0.767	0.023
187	0.42	0.21	0.0348	-9.870	-0.070	**0.93**	0.07	0.0001	**0.0002**	**0.0003**	-1.46	-1.083	0.030
197	0.17	0.21	0.1510	-11.401	-0.044	**0.77**	0.11	0.0054	**0.0039**	**0.0048**	-3.53	-0.992	0.028
204	-0.07	0.33	0.5021	-8.745	-0.030	0.07	0.31	0.3443	0.1953	0.2081	-1.72	-0.876	0.025
211	-0.03	0.25	0.4002	-9.442	0.029	-0.19	0.27	0.7197	0.9794	0.9371	-9.08	-0.014	0.001
221	**0.91**	0.25	**<.0001**	-15.180	0.285	0.89	0.27	0.0005	0.7572	0.8260	-14.20	0.167	0.003

☐ Indicates significance at 95%

Table C6 RADARSAT-1 backscatter versus field variability as expressed by SP98_ND_27, (area means), Group-1 fields.

	Linear			Reg. Coef		2nd	order	Polynomial			Reg. Coef		
DOY	R2	RMSE	P_Value	Intercept	B1	R2	RMSE	P_Value	P_Val B1	P_Val B2	Intercept	B1	B2
149	**0.51**	0.39	**0.0281**	-19.953	0.174	0.74	0.29	0.0153	0.0693	0.0557	7.66	-2.306	0.055
156	-0.08	0.18	0.5166	-15.931	0.019	-0.30	0.20	0.826	0.9897	0.9685	-15.61	-0.009	0.001
163	0.39	0.44	0.0593	-16.288	0.159	0.51	0.39	0.0711	0.1966	0.1691	8.20	-2.041	0.049
173	0.04	0.62	0.2997	-13.862	0.108	**0.73**	0.33	0.0169	**0.0113**	**0.0102**	37.00	-4.461	0.102
180	0.75	0.13	0.0033	-12.611	0.095	**0.91**	0.08	0.0011	**0.0300**	**0.0203**	-2.29	-0.832	0.021
187	0.12	0.25	0.2138	-9.796	-0.053	-0.06	0.27	0.4952	0.8850	0.9274	-8.79	-0.144	0.002
197	0.23	0.24	0.1263	-13.566	0.066	0.48	0.20	0.0856	0.1246	0.1100	1.40	-1.278	0.030
204	**0.65**	0.19	**0.0094**	-11.600	0.110	0.74	0.16	0.015	0.1848	0.1438	-0.58	-0.880	0.022
211	0.82	0.22	0.0012	-13.323	0.193	**0.95**	0.12	0.0003	**0.0066**	**0.0104**	-31.24	1.802	-0.036
221	**0.94**	0.29	**<.0001**	-20.766	0.462	0.93	0.31	0.0006	0.6138	0.9144	-22.13	0.584	-0.003

Table B.7. RADARSAT-1 backscatter versus within field variability as expressed by SP98_ND_27 (area means), Group-2 FLDs.

	Linear			Reg. Coef		2nd	order	Polynomial			Reg. Coef		
DOY	R2	RMSE	P_Value	Intercept	B1	R2	RMSE	P_Value	P_Val B1	P_Val B2	Intercept	B1	B2
149	0.17	0.29	0.1336	-15.682	0.054	0.06	0.31	0.3352	0.6948	0.7672	-17.24	0.217	-0.004
156	0.09	0.29	0.2106	-11.854	-0.044	0.14	0.28	0.2471	0.2993	0.2640	-17.45	0.543	-0.015
163	0.17	0.14	0.1286	-9.754	0.027	0.13	0.15	0.2522	0.5135	0.4517	-7.84	-0.173	0.005
173	**0.97**	0.06	**<.0001**	-13.914	0.116	0.97	0.06	<.0001	0.9340	0.3372	-12.89	0.009	0.003
180	**0.87**	0.04	**<.0001**	-12.151	0.039	0.87	0.04	0.0003	0.7182	0.4048	-11.51	-0.029	0.002
187	**0.74**	0.13	**0.0009**	-12.642	0.075	0.70	0.14	0.0062	0.7962	0.9678	-12.55	0.065	0.000
197	-0.11	0.42	0.7911	-10.651	0.013	0.43	0.30	0.0581	0.0212	0.0217	-24.96	1.513	-0.038
204	**0.64**	0.19	**0.0033**	-10.536	0.088	0.63	0.20	0.0131	0.3078	0.4292	-13.20	0.367	-0.007
211	**0.80**	0.18	**0.0003**	-11.659	0.124	0.79	0.19	0.0019	0.3633	0.5724	-13.50	0.317	-0.005
221	**0.45**	0.90	**0.0207**	-6.585	-0.286	0.37	0.97	0.0836	0.8853	0.9812	-6.97	-0.246	-0.001

Indicates significance at 95%

Table B.8. RADARSAT-1 backscatter versus within field variability as expressed by SP98_ND_27, (area means), FLDs_1-15.

	Linear			Reg. Coef		2nd	order	Polynomial			Reg. Coef		
DOY	R2	RMSE	P_Value	Intercept	B1	R2	RMSE	P_Value	P_Val B1	P_Val B2	Intercept	B1	B2
149	0.26	0.17	0.0767	-14.194	-0.038	0.28	0.17	0.1331	0.3623	0.3064	-17.51	0.292	-0.008
156	0.84	0.33	0.0001	-8.155	-0.257	**0.98**	0.13	<.0001	**0.0009**	**0.0003**	-23.73	1.293	-0.038
163	0.79	0.36	0.0004	-5.422	-0.231	**0.95**	0.18	<.0001	**0.0034**	**0.0014**	-21.42	1.361	-0.039
173	**0.54**	0.23	**0.0091**	-13.389	0.087	0.53	0.23	0.0289	0.5042	0.3912	-9.55	-0.295	0.009
180	0.79	0.18	0.0004	-13.510	0.116	**0.95**	0.09	<.0001	**0.0028**	**0.0012**	-5.41	-0.690	0.020
187	**0.40**	0.14	**0.0285**	-11.981	0.040	0.46	0.13	0.0466	0.1656	0.2109	-15.19	0.360	-0.008
197	0.51	0.39	0.0126	-7.982	-0.138	**0.83**	0.23	0.0009	**0.0080**	**0.0051**	-24.56	1.512	-0.040
204	0.34	0.17	0.0443	-9.796	0.044	**0.62**	0.13	0.0143	**0.0268**	**0.0352**	-15.69	0.630	-0.014
211	**0.89**	0.13	**<.0001**	-11.688	0.125	0.88	0.14	0.0003	0.3304	0.6017	-13.06	0.262	-0.003
221	-0.10	1.21	0.6831	-12.639	0.057	**0.48**	0.84	0.0427	**0.0174**	**0.0164**	34.44	-4.629	0.114